New regolith mapping approaches for old Australian landscapes

John Richard Wilford

University of Adelaide/Geoscience Australia, Canberra; john.wilford@ga.gov.au

Australian regolith
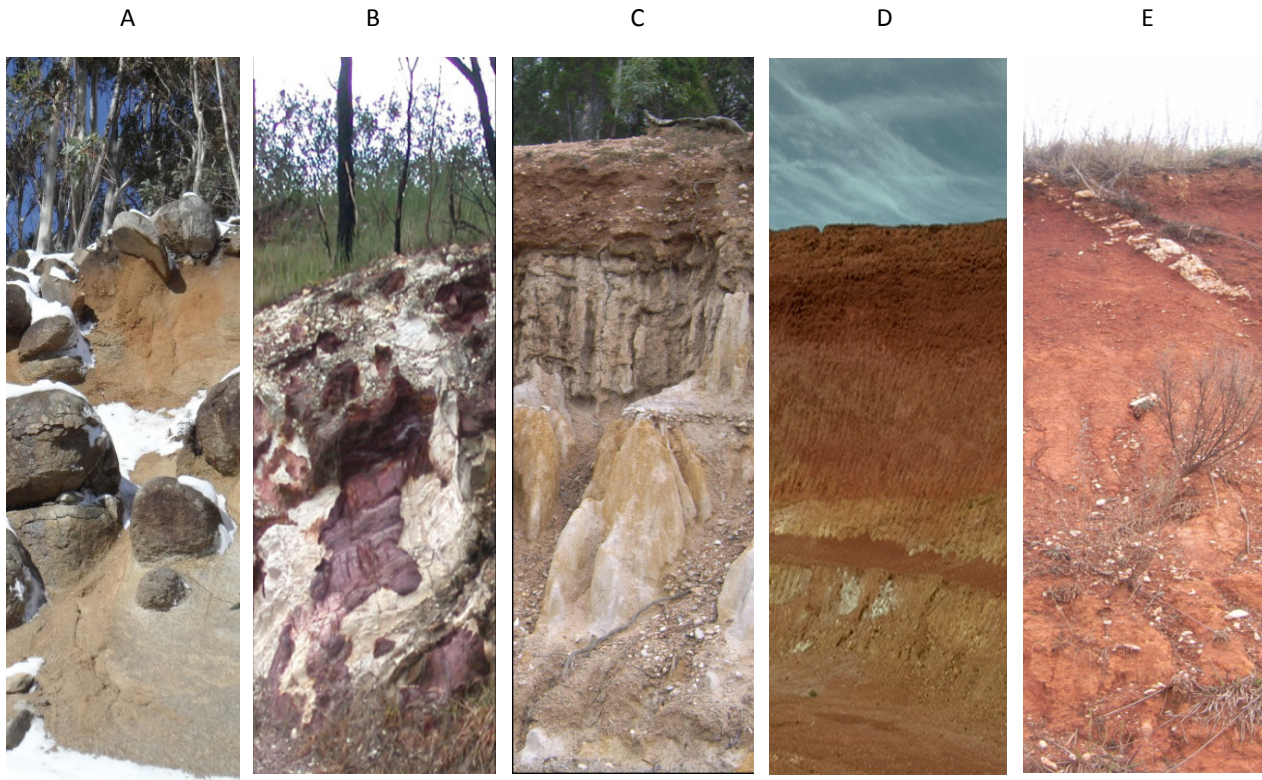
Australian regolith profiles. A – Highly weathered saprolite (gruss) with granitic core stones party covered with snow, Snowy Mountains NSW (vertical height (VH) 4m); B – Mega mottling, Adelaide Hills, South Australia (VH 2.8m); C – Floodplain sediments over very highly weathered bedrock, central West NSW (VH 4.2m); D – highly ferruginous saprolite, Tanami gold fields central Northern Territory (VH 42m) and E – ferruginous saprolite (in situ weathering as indicated by the quartz vein) largely weathered to residual clay (VH 2.5m), central West NSW.

Dedication

For Anna and Sarah in the words of the great Albert Einstein "Learn from yesterday, live for today, hope for tomorrow. The important thing is to not stop questioning."

Table of contents

List of Figures

List of tables

Thesis Declaration

This work contains no material which has been accepted for the award of any other degree or diploma in any university or other tertiary institution to John Richard Wilford and, to the best of my knowledge and belief, contains no material previously published or written by another person, except where due reference has been made in the text.

I give consent to this copy of my thesis when deposited in the University Library, being made available for loan and photocopying, subject to the provisions of the Copyright Act 1968.

The PhD consists of 3 published journal research papers and one that is currently in review. Two of the research papers are co-authored. Statements of the contributions from the jointly authored papers are detailed in the next two pages.

The author acknowledges that copyright of published works contained within this thesis (as listed below) resides with the copyright holder(s) of those works. However in accordance with Australian Government policy these papers have been published under Creative Commons Attribution 3.0. I also give permission for the digital version of my thesis to be made available on the web, via the University's digital research repository, the Library catalogue, and also through web search engines, unless permission has been granted by the University to restrict access for a period of time.

Wilford, J., 2009. Using airborne geophysics to define the 3D distribution and landscape evolution of Quaternary valley-fill deposits around the Jamestown area, South Australia, Australian Journal of Earth Sciences, 56, S67-S88.

Wilford, J., 2012. A weathering intensity index for the Australian continent using airborne gamma-ray spectrometry and digital terrain analysis, Geoderma, 183-184, 124-142.

Wilford, J and Thomas, M. 2013. Predicting regolith thickness in the complex weathering setting of the central Mt Lofty Ranges, South Australia. Geoderma, 206, 1-13.

Wilford, J., Caritat, P. de and Bui, E., 2014. Digital mapping of regolith carbonate in the Australian regolith using environmental covariates. In review – AGU Earth Surface Processes.

Statement of Authorship

Published: Wilford, J and Thomas, M. 2013. Predicting regolith thickness in the complex weathering setting of the central Mt Lofty Ranges, South Australia. Geoderma, 206, 1-13.

John Wilford

Led the conceptual thinking and research direction. Implemented all aspects of the cubist modelling and evaluation including compilation of site datasets and environmental covariates. I wrote 90% of the manuscript including background, aims, objectives, methods, results, discussion and conclusions. Acted as corresponding author.

Mark Thomas

Shared in project conceptualisation, fieldwork and some writing

Statement of Authorship

Wilford, J., Caritat, P. de and Bui, E., 2014. Digital mapping of regolith carbonate in the Australian regolith using environmental covariates. In review – AGU Earth Surface Processes.

John Wilford

Developed the ideas and conceptual thinking that underpins the study. I wrote the manuscript and ran the cubist models. Compiled all datasets for modelling including site and environmental covariates. I interpreted the results within the context of existing maps and discussed strengths and limitations of the modelling approach. Acted as corresponding author.

Dr Patrice de Caritat

Calculated normative calcium carbonate abundances, assisted with statistical analysis and modelling strategy

Dr Elisabeth Bui

Guided running of Cubist for modelling; helped with interpretation of results.

Acknowledgements

Executive Summary

The regolith, or 'critical zone', forms a discontinuous layer that covers large areas of Earth's terrestrial surface. It is a dynamic zone that forms and changes through time in response to interactions between air, rocks (minerals), water and biota. Knowledge of regolith is critical because of its key role in supporting terrestrial life, through physical, chemical and biological processes that operate at mineral-water interaction scales up to the regional scale through geological and tectonic activity.

There are many disciplines or areas of applied integrated research that rely on an improved understanding of regolith formation and information on surface and sub-surface regolith properties at appropriate spatial scales. These areas of study include; agriculture, land use sustainability, hydrology, salinity management, ecology, mineral exploration, natural hazard risk assessment and civil engineering. Furthermore, mapping regolith is critical in understanding the origin and evolution of regolith through space and time.

Mapping the regolith and formulation of associated robust process models are in their infancy compared with geological and soil mapping, which have had a long history of development and refinement. Regolith mapping can be seen as a hybrid approach combining elements from the existing mapping disciplines of geology, soil and geomorphology. The regolith-landform approach, used extensively in Australia, is broadly similar to soil-landscape mapping where landforms are used as the principal surrogate to map regolith. Regolith-landform and soil-landscape mapping are inherently empirical and qualitative. However, in the last ten years there has been a move from the qualitative land resource survey (i.e. soil-landscape mapping) approaches to quantitative, digital survey underpinned by statistical methods. These new quantitative approaches are enabling the prediction of specific soil properties with associated estimates of model confidence or uncertainty not possible using traditional approaches.

The aim of the thesis is to demonstrate and assess the application of quantitative soil mapping approaches in predicting regolith properties. Four case studies are presented that illustrate the application of quantitative mapping approaches in predicting regolith across a range of spatial scales and within different landscape settings. These four investigations include:

1. A continent-wide prediction of weathering intensity using a step-wise multiple regression-based model using airborne gamma-ray imagery and terrain relief;

2. A continent-wide prediction of near-surface secondary carbonate using environmental correlation and regolith geochemistry;

3. A regional-scale prediction of soil-regolith thickness over the Mt Lofty Ranges in southern South Australia using environmental correlation, drilling and legacy data, and

4. A regional-scale 3D regolith-landscape evolution model of valley-fill deposits from the Jamestown area in South Australia based on dataset integration, regression analysis and optically stimulated luminescence dating.

The investigations are interpreted within a landscape evolutionary framework and future research directions are discussed.

Digital regolith mapping shows considerable potential in predicting regolith properties over different landscape scales. This mapping is also important for understanding the complex interaction of environmental factors that control regolith formation, removal and preservation. Addressing gaps in predictive datasets that describe or reflect properties within the sub-surface (i.e. 5–100 m depth interval) and systematic collection of quantitative regolith attributes such as weathering depth and geochemistry will greatly enhance the future applications of digital regolith mapping in Australia.

Chapter 1

Introduction

1 Introduction

1.1 Background

1.1.1 The regolith

The regolith encompasses the zone between fresh rock and fresh air (Pain et al., 2007). The word comes from the Greek 'rhegos' meaning blanket and 'lithos' meaning stone – hence a blanket of material covering stone. Merrill (1897) defined regolith as unconsolidated materials that mantle the Earth's surface. Ollier (1984) described the regolith as the entire mantle of weathered material. This weathered zone includes the soil, which may constitute the whole of the regolith profile or represent only its upper part. The pedolith describes the zone where pedological processes have destroyed the original bedrock structure principally through the weathering of primary bedrock minerals and the formation and re-distribution of secondary materials (e.g. clays, oxides) within the profile. The pedolith or soil can develop on in-situ or transported materials (e.g. alluvium, colluvium). The saprolith refers to the zone where the bedrock fabric is weathered but still preserved (Figure 1). Preservation of bedrock fabric implies that weathering has been largely isovolumetric and in-situ (Eggleton et al., 2001). The saprolith includes saprolite and saprock. Saprolite or weathered bedrock has more than 20% of its minerals altered, whereas saprock has less than 20% minerals weathered and therefore has a closer affinity both compositionally and texturally to unweathered bedrock. In places the pedolith and or the saprolith may exhibit secondary induration. Common induration types include silica, iron, aluminium and carbonate. The base of the regolith is defined by the weathering front which may form a sharp or gradational boundary over many 10s of metres to unweathered bedrock (Figure 1). The weathering front therefore denotes the boundary between the regolith and the unweathered bedrock at depth. The degree to which the characteristics of the regolith diverge from the unweathered bedrock widens with increasing weathering intensity. Many of these changes are reflecting re-equilibration of high temperate/pressure minerals in the rock to near-surface environmental conditions and are driven by interactions between air, minerals, water and biota. Regolith therefore includes all weathered materials, either in-situ (weathered in place) and/or transported (e.g. alluvium, colluvium, aeolian sediments). The composition and thickness of the regolith is often highly variable, both spatially and vertically, reflecting differences in bedrock type, weathering processes (including physical, chemical and biogeochemical processes) and geomorphic processes operating through time.

Important hydrological and biogeochemical cycles operate within the regolith, including the infiltration and storage of near-surface water and nutrient cycles involving elements such as carbon, nitrogen, oxygen, phosphorus and sulphur, necessary to support life. Biological agents within the weathered zone are important in mineral weathering both physical and chemical, cycling nutrients and physical bioturbation of the regolith. Geochemical and biogeochemical processes within this zone are invariably complex and occur across diverse spatial and temporal scales.

Northern hemisphere researchers use the term 'critical zone' to describe this life-sustaining environment (Brantley et al., 2006). Brantley et al. (2007) describes the critical zone as the fragile skin of the planet from the outermost vegetation layer to the lower limit of groundwater.

Critical zone research involves integrated studies of water with soil, air and biota in the near-surface terrestrial environment (Brantley et al., 2006; Lin 2010). The regolith therefore reflects reactions and inter-reactions of the biosphere, hydrosphere, atmosphere and lithosphere (Taylor and Eggleton, 2001; Figure 2). Therefore, understanding processes occurring within the weathered zone and the nature and origin of regolith materials draws on a range of often interrelated scientific disciplines including pedology, geochemistry, hydrology, geomorphology, biology and geology.

1.1.2 Regolith - the Australian context
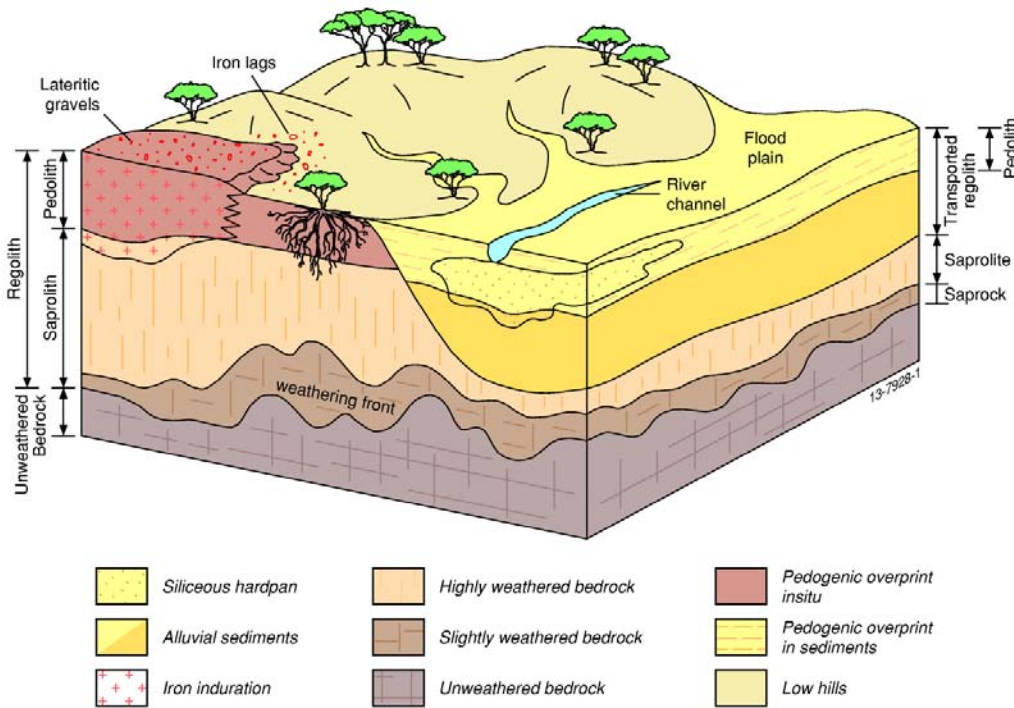
Figure 1 Idealised regolith profiles developed on in-situ and transported materials. Iron induration shown – other common induration types include silica, aluminium and carbonate.

Knowledge of the nature and distribution of regolith materials within the Australian landmass is particularly important because the regolith blankets most of the continent. Unweathered to slightly weathered rocky exposures account for less than 15% of the 7.7 million km^2 of the Australian continent; the rest is regolith cover, which can be over 100 m thick (Pain, 2001). Within a mineral exploration context the regolith can also include sedimentary cover which might be lithified into rock. Here the combined weathered zone and the sedimentary rock can be several kilometres thick. The preservation and accumulation of weathered materials in Australia reflects the continent's overall low-relief and slopes (e.g. average slope for the entire continent based on the space shuttle DEM is 1.4 degrees), geological stability and more recent arid climate (Figure 3 and 4). These factors contribute to low erosion rates compared with processes that lead to weathering and accumulation or retention of regolith materials at or near to the surface. Rocks over the Australian continent have been exposed to surface weathering for hundreds of millions of years (Pillans, 2001). In places burial and later exhumation of ancient landforms has led to preservation of old highly weathered landforms (Pillans, 2001). Ollier (2001) argues that the landscape evolution of Australia is on the same time scale as global tectonics and biological evolution. Australia's rich and diverse flora and fauna is largely an expression of the continent's climatic and regolith variability and palaeo-history.

The regolith has been significant in shaping our nation. Deeply weathered Australian landscapes tend to have soils that are low in fertility, and are fragile. Many of the soils in these highly weathered landscapes are deficient in phosphorus, potassium and nitrogen and can limit growth in agricultural productivity (McKenzie et al., 2004). The Australian regolith in many places contains high concentrations of salt which has a significant influence on how we manage current and future agricultural landscapes. The regolith also has a close connection with mineral exploration. The regolith either contains minerals in economic concentrations, or is seen as a barrier to the discovery of minerals at depth. Therefore, from both an agricultural and mining perspective, the regolith has had and continues to have a major influence on the development of Australia, its prosperity and the way people live (Pain et al., 2012).
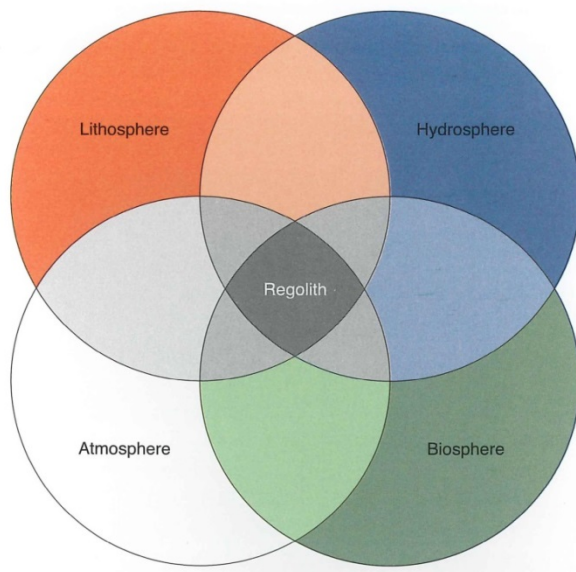
Figure 2 The influence of different interactions on regolith. The regolith also occupies in all areas where the lithosphere overlaps with the other spheres (Taylor and Eggleton, 2001).

1.1.3 Mapping regolith - an Australian perspective

Regolith mapping can be seen as a hybrid of soil, geomorphological and surface geology mapping. Regolith mapping has the greatest affinity to soil mapping. This is reflected in the fact that the landscape classification and terminology used in most regolith maps is based on the soil mapping classification scheme of McDonald et al. (1990). Regolith landform mapping builds on the concepts and relationships that underpin land system and soil-landscape mapping. A land system is defined by Christian and Stewart (1953) as an area of land throughout which recurring patterns of topography, soils and vegetation can be recognised. Soil-landscape mapping is largely based on landform patterns and geology (Atkinson, 1993). In both mapping approaches landforms are the principle surrogate in defining soil unit boundaries. As with soil mapping, regolith maps are largely based on a classification of terrain to predict the distribution of the weathered materials due to the close spatial and genetic association between landforms and regolith. The relationships between soil and landscapes have been known for many decades (Hall and Olson, 1991). The close connection between soils and landforms are exemplified by the catena concept (Latin for chain) that describes sequences of soil along a slope (Milne 1935). Similar relationships are described by Dalrymple et al. (1968) with their nine unit landscape model. Pain (2001) used the term toposequences to describe repeating associations of landform types and regolith.

Figure 3 Extensive sheet-flood colluvial plains and lacustrine plains – Gawler South Australia.

Figure 4 Meandering river system, lined by trees, dissects the arid and flat Lake Eyre Basin between Oodnadatta and William Creek, South Australia. The descriptions flat and red are synonymous for Australian landscapes (source: Blewett, 2012). © Getty Images [J Edwards]

Landforms and regolith are therefore inextricability linked and it is not uncommon to see feedback processes where weathering is the primary control on landscape morphology, as illustrated by karst and inverted relief landforms.

However, there are some fundamental differences between soil and regolith maps. Regolith maps differ from soil maps in that the whole of the weathering profile is described with considerably more emphasis on how the regolith and associated landscapes has evolved through time. Relict-landforms and associated regolith are identified and often studied in detail because they can provide insights into past weathering and geomorphic processes. Residual weathering features provide information on environmental change and relative ages of exposed surfaces, palaeosurfaces, and sediments (Turkington et al., 2005). Regolith maps are compiled within the context of long-term landscape evolution models which not only involve mapping regolith materials but also incorporate drainage analysis (e.g. river capture, drainage reversals, superimposed drainage), regolith dating, slope and fluvial process models and identification of geomorphic features such as erosional scarps that provide information on denudation processes and relative land surface age. Ollier and Pain (1996) argue that effective regolith mapping needs to be underpinned with a sound understand of the basic principles behind landform and regolith development. Soils, particularly in Australia, are an expression of present environmental conditions and associated processes within material (regolith) that is often considerably older. Understanding regolith and landscapes through time is a critical component of regolith mapping and more broadly regolith geoscience. This involves understanding different patterns and periods of the processes influencing the regolith including additions, removals, transformations and translocation of materials over potentially long time scales (McKenzie et al., 2004). Recognising that the regolith in many regions of Australia reflects more recent or present-day processes superimposed on inherited weathered materials is the bridge between soil pedology and regolith geoscience.

The study of regolith as a discipline is relatively new (Ollier and Pain, 1996) compared with soil science which dates back to the late eighteen hundreds based on the pioneering work of Vasily Dokuchaev –

commonly regarded as the father of pedology (http://en.wikipedia.org/wiki/Vasily_V._Dokuchae). In Australia, early maps showing relationships between regolith materials and landforms were produced by Butler et al. (1973), Hays (1967) and Mulcahy (1967). Woodall (1981) compiled a simple regolith map of Australia showing the distribution of deep weathering profiles. Chan et al. (1986) compiled the first regolith terrain map of Australia at 1:5 000 000 scale. Since that time many maps have been published at various scales and over contrasting Australian landscapes (Pain and Kilgour, 2003). Early regolith maps were based on landform delineation using aerial photography. Associations of landforms and regolith materials were described within regolith landform units (RLU) and in places geological maps were used to identify different styles of weathering pertaining to specific parent material types. Regolith maps and models of landscape evolution were largely driven by the need of the mineral exploration industry to explore deeply weathered terrains more effectively (Butt et al., 2000; Butt et al., 2008). The regolith also contains economic deposits such as bauxite, heavy mineral sands, lateritic gold and nickel and placer deposits. Over the last 30 years regolith maps were improved with the inclusion and interpretation of remotely sensed imagery (e.g. Landsat TM, SPOT, airborne geophysics), and in particular airborne radiometrics (Dickson and Scott, 1997; Wilford et al., 1997; Martelet et al., 2013). These datasets were useful in mapping variations of regolith materials within the landform derived RLUs. Regolith maps were used to help plan and interpret geochemical surveys by showing the distribution of in-situ and transported materials, geochemical sampling medium (e.g. Fe and Ca lags and nodules) as well as providing a landscape evolution framework to better understand geochemical dispersion processes (Craig, 2001; Pain, 2008). Thematic maps that incorporated regolith information with airborne magnetic imagery and mineral deposits were generated to aid exploration in highly weathered terrains of Western Australia (Craig and Wilford, 1995). Customised geochemical sampling strategy maps were compiled by integrating regolith sample materials, surface flow dispersion vectors, airborne magnetic imagery (highlighting buried litho-structural elements) and enhanced Landsat TM to support geochemical exploration and interpretation (Wilford, 2002; Wilford and Butrovski, 2000).

From the late 1990s to the present day, regolith maps became increasingly important in natural resource management. This utility stems from the fact that the regolith plays an important role in the hydrologic cycle; providing a storage, medium controlling water flow (rate and direction), and the interface through which drainage occurs into the deeper groundwater tables or aquifers. Existing hydro-geological frameworks were largely based on geological mapping (Coram et al., 2000; Walker et al., 2003). Regolith mapping, in conjunction with hydrological analysis has been used to enhance these largely geological frameworks by identifying salt stores, and fresh and saline discharge sites which are controlled by the nature and distribution of the regolith (Gibson 2003; Lawrie et al., 2004; Wilford, 2004). Electromagnetic methods were used to generate 3D conductivity maps of regolith and bedrock materials (Lane et al., 2000). Airborne electromagnetic (AEM) datasets calibrated by drilling extended regolith maps into a vertical dimension, where they were used to build hydrogeological models to support salinity and groundwater management (Lawrie, et al 2000; Lawrie et al., 2010; Munday et al., 2004; Dent et al., 2002). Where these AEM datasets are available they have the potential to significantly improve our understanding of the processes controlling the distribution of salts and their mobilisation pathways, as well as generating spatially explicit maps to target salinity remediation actions.

Over the last 10 years we have seen an increase in the sophistication of regolith mapping approaches with the integration of digital terrain analysis, airborne geophysical datasets including radiometrics, magnetics and AEM, and satellite remote sensing, together with the more traditionally used aerial photographic interpretation. However, most of these maps are still largely empirically derived. Many customised thematic regolith maps that were used to address specific client needs (e.g. mineral exploration, natural resource management) were compiled by adding together or superimposing complementary thematic datasets.

While regolith mapping was evolving through integrative, qualitative regolith-landform frameworks, a significant transition was occurring in the approaches used to map and predict soil properties. That transition reflected a move from empirical, qualitative land resource survey (i.e. soil-landscape mapping) approaches to quantitative, digital survey underpinned

by geostatistical methods (Webster and Oliver, 1990; Hengl, 2009). The evolution of soil mapping in Australia provides the background framework that underpins the rationale of the thesis.

1.1.4 Soil Mapping – from qualitative to quantitative

In Australia there has been a significant shift away from traditional, qualitative, soil survey based on soil-landscape mapping to a quantitative soil survey approach, also known as digital soil mapping (DSM) or predictive/pedometric soil modelling. This shift is in response to perceived limitations in the traditional methods including the lack of explicit models, unrepeatability of the method and inability to harness landscape/soil knowledge collected by the soil surveyor. Digital soil mapping to a large degree addresses these limitations. Digital soil mapping also provides a mechanism to handle the huge amount of covariate information that currently exists, future datasets obtained by new satellite and airborne platforms, as well as assessing the uncertainty in soil attributes prediction. Digital soil mapping essentially involves linking field, laboratory, and proximal soil observations with quantitative methods to predict soil characteristics (either soil classes or properties) across various spatial and temporal scales (Grunwald, 2010). Digital soil mapping includes a broad spectrum of geostatistical approaches as reviewed by McBratney et al. (2003) and Lagacherie and McBratney (2007). The development and implementation of DSM has increased significantly over the last 20 years reflecting advances in computing, software, geographic information systems and the ever increasing availability of digital thematic datasets to support both local and global scale mapping (e.g. DEMs, satellite remote sensing).

Australian scientists have been at the forefront in the development and implementation of DSM (Bui, 2007). Predictive statistical based modeling of soil properties flourished in the late eighties and nineties including McKenzie and Austin (1993), Moore et al. (1993), Odeh et al. (1994), Gessler et al. (1995), McKenzie and Ryan (1999). Skidmore et al. (1996) developed a GIS expert system approach for mapping forest soils and O'Connell et al. (2000) demonstrated the use of DSM to map temperate forest soils. Minasny and McBratney (2002) used artificial neural networks to predict soil properties. More recently Thomas et al. (2009) used an expert systems approach to predict salinity

characteristics and different soil types. Viscarra Rossel et al. (2010) and Viscarra Rossel (2011) used DSM to predict soil properties over the Australian continent. Software developments and associated covariate datasets for use in soil prediction provided the framework to facilitate the early implementation of DSM in Australia. Software included ANUDEM (Hutchinson, 1989) and TAPES-G (Gallant and Wilson, 1996) for generating DEMs and terrain derivatives, and ANUCLIM software for generating climatic surfaces (Houlder et al., 1999). These datasets or derivations from them are used extensively today as predictive covariates in DSM.

A key component or sub-branch of DSM is environmental correlation. Environmental correlation uses environmental covariates representing soil-forming factors coupled with statistical methods for correlation and regression to predict soil properties or classes (McKenzie and Grundy, 2008; Minasny et al., 2008). The soil forming factors are described in Jenny (1941) and include climate, relief, parent material organisms and time. These soil forming factors have been adapted for digital soils mapping as describe by the 'SCORPAN' term (McBratney et al., 2003).

$S = f(s, c,o,r,p,a,n)$, where

S = soil classes or attributes (to be modeled)

s = soil; other or previously measured properties of the soil at a point

c = climate; climatic properties of the environment at a point

o = organisms; including land cover and natural vegetation or fauna or human activity

r = topography; landscape attributes

p = parent material; lithology

a = age; the time factor

n = spatial or geographic position

In Australia predictive relations between quantitative environmental covariates and soil properties have been used to model soil characteristics from local to national scales (Mckenzie and Austin, 1993; Gessler et al., 1995; Odeh et al., 1995; Cook et al., 1996; Mckenzie and Ryan, 1999; Mckenzie and Gallant, 2007; Henderson et al., 2005; O'Connell et al., 2000). Key to many of these studies has been the use of terrain attributes, gamma-ray radiometric and climatic surfaces as environmental variables for soil property prediction. The environmental correlation approach described in these studies broadly under-pins the approaches used to predict properties of the regolith described in Chapters 2 to 5.

1.2 Rationale and aims

Advances in geostatistical modelling, analytical methods and the availability of geo-referenced thematic digital datasets that capture key components involved in soil formation is leading to a substantial shift away from traditional soil survey to quantitative DSM. Soil is part of the regolith and therefore it is reasonable to assume that the advantages argued for DSM will equally apply to regolith mapping. These include:

1. Cost - potentially significantly cheaper than traditional regolith-landform mapping, particularly when predicting regolith attributes at the national scale.
2. Generates an explicitly stated model with degrees of confidence or uncertainty in terms of the statistical model.
3. Accommodates both abrupt and gradual changes in regolith properties across the landscape.
4. Models are repeatable with existing data and have the flexibility to be readily updated or revised with new information.
5. Provides a mechanism to capture and understand models of regolith formation and the controls on regolith distribution.
6. Allows an integration and synthesis of many environmental covariate datasets that would otherwise not be possible in traditional methods.

The aim of this thesis is to demonstrate the application of quantitative digital soil mapping approaches in predicting regolith properties over different spatial

scales and within different landscape settings. Digital soil mapping approaches are largely concerned with predicting standard soil properties (e.g. pH, texture, cation exchange capacity (CEC) organic carbon) within the upper 1 m of the weathering profile or the upper part of the regolith profile. This thesis will examine attributes important in understanding the nature of regolith materials within a landscape evolution context (e.g. weathering depth, weathering intensity). Specifically, the use of environmental correlation will be evaluated for predicting regolith attributes. Surprisingly little work has been published on the use of environmental correlation in the prediction of regolith materials, a notable exception is Laffan and Lees (2004). Therefore, there is considerable scope to explore the value of DSM for regolith mapping.

1.3 Thesis structure and connectivity

This thesis consists of six Chapters. Following this introductory Chapter, the middle four Chapters are peer-reviewed journal-published papers covering specific aspects and approaches in mapping regolith across different spatial scales. The research papers and hence Chapters are ordered from national or continental scale mapping applications in Chapters 2 and 3 to more local or district scale studies in Chapters 4 and 5 (Figure 5). The regolith mapping case study described in Chapter 4 includes a mixed erosional and depositional landscape, whereas Chapter 5 describes methods to model and predict regolith materials in a largely depositional setting. Finally, Chapter 6 includes a discussion and summary of the complementary research themes, and future research directions. Supplementary and related work associated with the research themes are documented in Appendix 1.

Chapter 2

The degree to which the regolith is weathered (or its weathering intensity) is intrinsically linked to the factors involved in soil formation including parent material, climate, topography, biota and time. The degree to which the bedrock or sediments are weathered has a significant effect on the nature and distribution of regolith materials. There is commonly a strong correlation between the degree of weathering intensity and the degree of soil development. With

changes in weathering intensity we see changes in the geochemical and physical character of the bedrock, ranging from essentially unweathered parent materials through to intensely weathered and leached regolith, where all traits of the original bedrock are either strongly overprinted or lost altogether. Degree of weathering is an important attribute to describe in regolith-landform mapping and is a critical component in developing models of landscape evolution. With increasing weathering intensity we typically see mineral and geochemical convergence to more resistant secondary weathered materials including, clay, quartz, and various oxides.

This Chapter describes a method to predict the degree of surface weathering by generating a weathering intensity index for the Australian continent using gamma-ray spectrometry and digital terrain analysis. These attributes are combined and modelled using a stepwise multiple regression analysis. The weathering intensity prediction is evaluated with surface geochemistry and previous regolith-landform mapping. Weathering intensity is a fundamental property of the regolith and the weathering intensity index has potential broad application within a range of different disciplines including natural resource management, ecological studies, mineral exploration and engineering.

Chapter 3

This Chapter demonstrates the application of environmental correlation in mapping the near-surface distribution of regolith carbonate over the Australian continent. Regolith carbonate or secondary carbonate is a key component of the regolith, particularly in many arid and semi-arid regions of Australia. The presence of carbonate in soil can affect a range of soil properties including pH, texture, structure and consequently water infiltration. Calcareous soils have a high 'buffering capacity,' and the presence of carbonate can promote aggregation of soil colloids. From a mineral exploration perspective regolith carbonates are associated with some Uranium deposits and can be a useful geochemical sampling medium for mineral exploration, particularly gold (Lintern and Butt, 1993). Geochemical databases are used in the analysis because carbonate is typically not recorded quantitatively in soil survey.

The model produces a continuous, quantitative prediction of regolith carbonate abundance in surficial regolith with associated estimates of model uncertainty. The carbonate model is compared to existing thematic coverage of soil and regolith carbonate distribution. The methodology described has the potential to be used in other carbonate-rich landscapes globally. The Chapter also highlights the strengths and weakness of the environmental correlation method to predict regolith carbonate and future research directions to improve the model are discussed.

Chapter 4

Thickness of the regolith profoundly affects groundwater interactions and subsoil water movement, water storage and nutrient availability. There is often a positive correlation between regolith thickness or depth and weathering intensity. Regolith thickness (including soil thickness) has an important bearing on land use, and the viability of land-based industries dependent on rooting depth, e.g. agriculture and forestry. In addition, from a mineral exploration perspective, the surface geochemical expression of buried deposits is often intrinsically linked to the nature and thickness of the regolith cover. Thickness estimates also have direct application in seismic risk assessment. Existing soil and regolith landform maps do not capture regolith thickness as a continuous variable across the landscape.

This Chapter describes the use of the environmental correlation approach in predicting regolith thickness over the complexly weathered landscapes of the central Mt Lofty Range in South Australia. The results are interpreted within a long term landscape evolution model that reflects variable rates of weathering, uplift and erosion processes potentially dating back to the Mesozoic. Key issues facing future research in predicting regolith depth are discussed.

Chapter 5

This Chapter describes the construction of a 3D architectural and landscape evolution model of valley-fill deposits around the township of Jamestown in South Australia. The 3D model is based on modelling, interpretation and integration of airborne electromagnetics (AEM), airborne gamma-ray spectrometry (AGRS) and magnetics, a digital elevation model, drilling, OSL dating of the valley fill deposits and surface geochemistry and textural analysis. A sediment isopach (line or surface of equal thickness) map generated from the AEM dataset and calibrated through drilling reveals the 3D structure of the valley-fill deposits. Regression analysis using airborne potassium and laboratory measured soil texture were used to model surface texture over the depositional landforms. The airborne magnetics identified buried 'magnetic channels' which differed markedly from present day streams that are largely ephemeral and interrupted. These thematic datasets were then combined and constrained by OSL dating of the valley-fill sediments to construct a palaeo-environmental and landscape evolution model for the area.

Chapter 6

The final Chapter brings together results and methods described within the individual chapters and discusses future research direction.
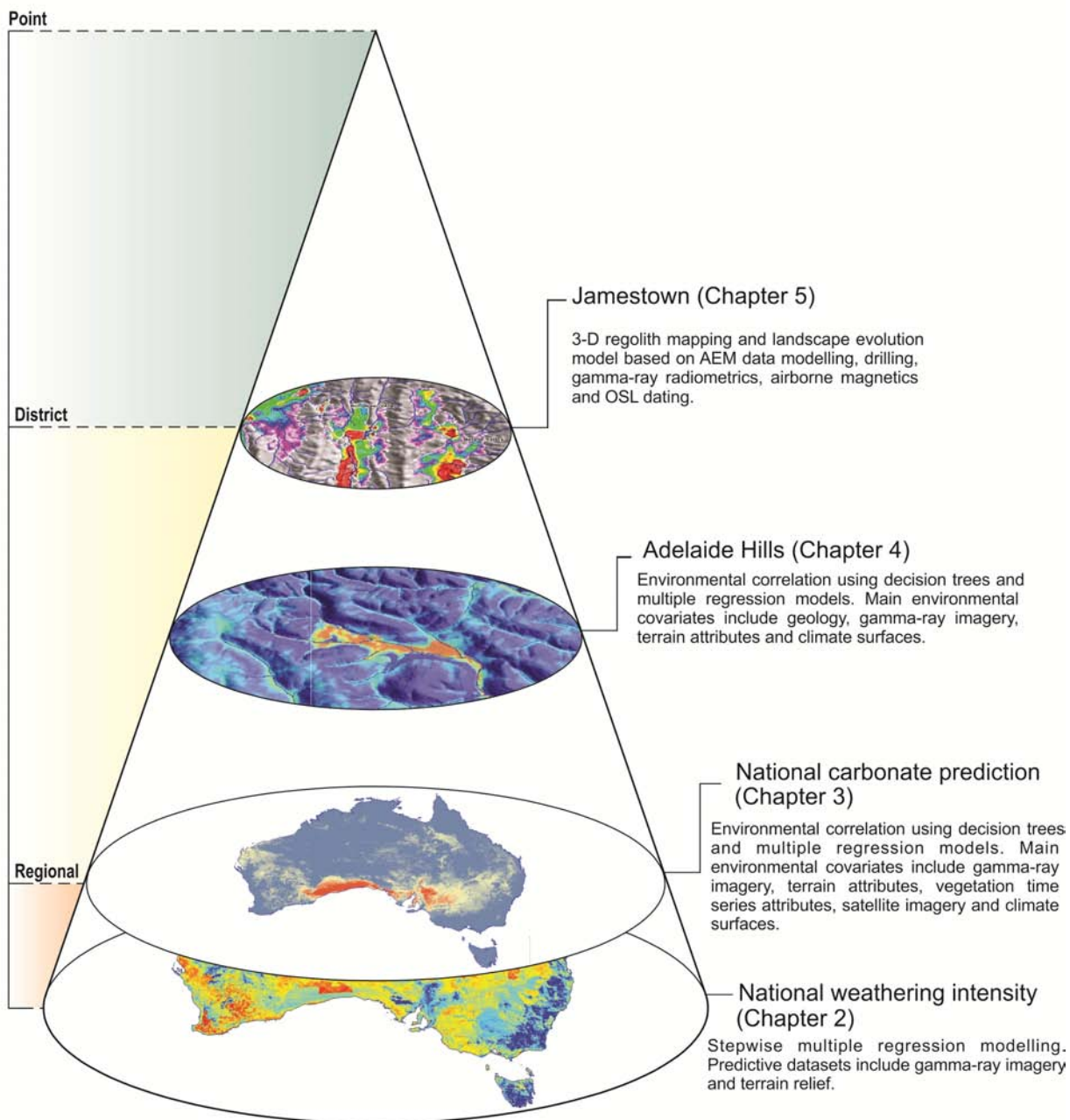
Figure 5 Summary of digital regolith mapping research investigations from district to national scale regolith predictions.

Chapter 2

A weathering intensity index for the Australian continent using gamma-ray spectrometry and digital terrain analysis

2 A weathering intensity index for the Australian continent using gamma-ray spectrometry and digital terrain analysis

Contrasting regolith-landscapes in central North Victoria. A – Slightly weathered granitic landforms with protruding tors and B – very highly weathered and bleached granitic saprolite. The weathering intensity index separates these contrasting regolith landscapes based on relative proportion of K, Th, U and terrain relief. Areas of more intense weathering are recognised by low K and relief and the retention of U and Th in the upper part of the weathering profile.

Summary

Weathering intensity largely controls the degree to which primary minerals are altered to secondary components including clay minerals and oxides. As weathering intensity increases there are changes in the hydrological, geochemical and geophysical characteristics of the regolith. Thus, once calibrated, weathering intensity can be used to predict a range of regolith properties. A weathering intensity index (WII) over the Australian continent has been developed at a 100 m resolution using regression models based on airborne gamma-ray spectrometry imagery and the Shuttle Radar Topography Mission (SRTM) elevation data. Airborne gamma-ray spectrometry measures the concentration of three radioelements — potassium (K), thorium (Th) and uranium (U) at the Earth's surface. The total gamma-ray flux (dose) is also calculated based on the weighted additions of the three radioelements. Regolith accounts for over 85% of the Australian land area and has a major influence in determining the composition of surface materials and in controlling hydrological and geomorphological processes. The weathering intensity prediction is based on the integration of two regression models. The first uses relief over landscapes with low gamma-ray emissions and the second incorporates radioelement distributions and relief. The application of a stepwise forward multiple regression for the second model generated a weathering intensity index equation of: WII=6.751+−0.851 K+−1.319 Relief+2.682 Th/K+−2.590 Dose. The WII has been developed for erosional landscapes but also has the potential to inform on deposition processes and materials. The WII correlates well with site based geochemical indices and existing regolith mapping. Interpretation of the WII from regional to local scales and its application in providing more reliable and spatially explicit information on regolith properties are described.

2.1 Introduction

Weathering involves chemical and mechanical processes associated with the break down or alteration of rocks and minerals in response to environmental conditions at or near to the Earth's surface. Weathering is a prerequisite for material to be eroded and it is the interplay between weathering and erosional processes, across different temporal and spatial scales that is fundamental in understanding the nature and evolution of landscapes. Soil is an important product of weathering and therefore soil genesis is intrinsically linked with weathering processes and products.
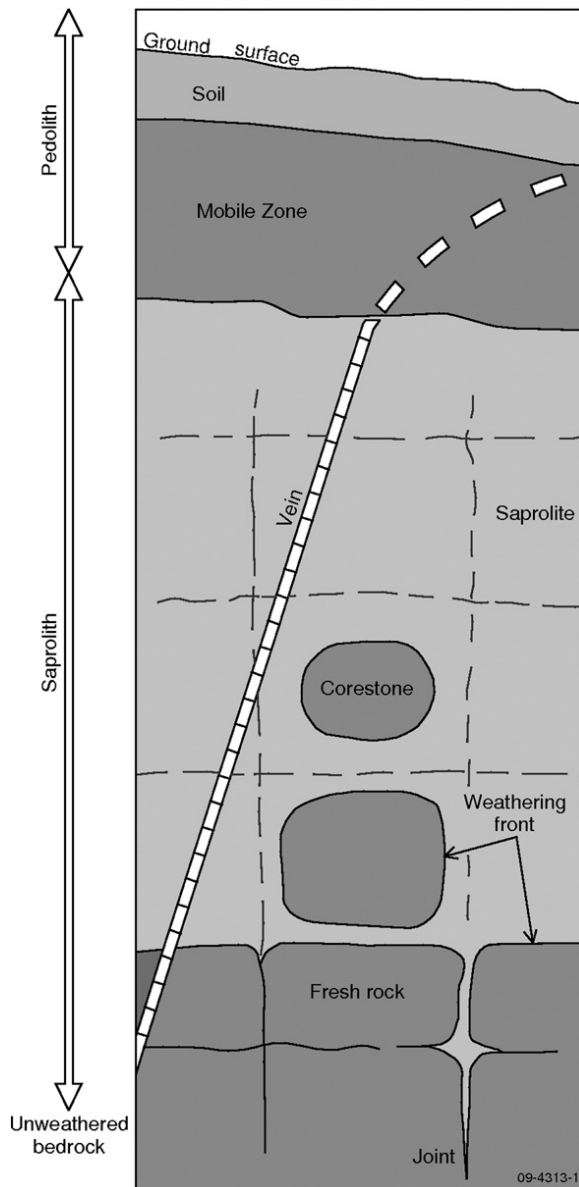
Figure 6 A typical regolith profile showing the pedolith (mobile zone) and saprolith (in situ weathered bedrock). Indurated (e.g., iron duricrust) zones can develop in the pedolith and/or saprolith (modified from Ollier 1984).

The regolith includes soils and more broadly all weathered materials above fresh bedrock. Soil in this context is seen as the upper part of a continuum that includes the whole weathering profile. In Australia regolith profiles can be up to several hundred metres thick. The lower boundary of the regolith profile is defined by the weathering front, which may be abrupt or transitional to the unweathered bedrock at depth (Figure 6). Geomorphologists, geologists, soil scientists, biologists and civil engineers all investigate or describe the regolith differently reflecting the nature of their particular discipline (Ehlen, 2005). Nevertheless an

understanding of regolith is common to each discipline and contributes directly to key activities including agriculture, engineering and mineral exploration (Ollier and Pain, 1996).

The five key factors that play a role in soil formation apply equally to the regolith, and include p = parent material, cl = external climate, r = topography, o = biotic potential and t = time (Jenny, 1941). These factors influence to varying degrees the weathering intensity or the degree of weathering. Weathering intensity has a major control on the degree to which the primary mineralogy of the bedrock is altered to secondary minerals including clays and oxides. The nature and distribution of the regolith are strongly influenced by parent material and weathering intensity. Given similar parent materials and climatic conditions, increasing weathering intensity is reflected in a change of the nature and proportions of these secondary minerals. As weathering increases, clays such as illite and smectite change to more stable clays such as kaolinite. With extreme leaching, iron and silicon can be removed leaving an aluminium rich gibbsite residuum (Eggleton, 1998; Summerfield, 1991). In many cases the regolith profile is not uniform but exhibits distinctive zones reflecting changes in colour, fabric and composition, mineralogy and geochemistry. In general, zonation is likely to become more distinctive as weathering progresses. Furthermore, there is generally an increase in regolith depth with increasing weathering intensity until a dynamic equilibrium is established (Ahnert, 1987).

Factors leading to the development of intensely weathered regolith include:

1. Landscapes that have been exposed to weathering agents for a considerable time. This situation usually infers that the rates of erosion are relatively low compared with rates of accumulation;

2. Bedrock that contains highly weatherable minerals; and,

3. Where the environmental conditions, e.g., rainfall, temperature and biota, promote rapid rates of weathering.

High weathering rates are not essential as long as denudation rates are relatively low and there is sufficient time to weather the bedrock.

This is particularly relevant to palaeo-landscapes in Australia where the regolith owes its character to a long history of weathering (Gale, 1992; Ollier, 2001). Many of these highly weathered landscapes are not in equilibrium with present day climatic conditions that are generally drier now than in the past. Here, landscape preservation is a critical factor governing the distribution of intensely weathered bedrock. This highlights the need to adopt a long term landscape perspective when assessing the degree of weathering. In this context the analysis of landforms can be used to delineate areas where geomorphic process rates are low. Low process rates leading to the preservation or retention of weathered materials are likely to be associated with landscapes with low relief and low slope angles. Landscape position (Jenness, 2006) and hydrological indices such as the Topographic Wetness Index (Beven and Kirkby, 1979) can also provide further constraints on likely areas where higher rates of leaching (both lateral and vertical) may occur. However, these terrain-derived predictions are based on present day surface morphology that may not adequately explain or predict geomorphic processes associated with palaeo-landscapes that have since been modified by more recent landscape processes. This explains why we can develop relatively young soils on much older and intensely weathered substrates (Pain and Ollier, 1996).

Weathering intensity can also be determined by measuring changes in the mineralogy or chemistry of the parent material as it weathers. For example, geochemical weathering indices have been used widely to describe weathering profiles and assess the degree of bedrock weathering (Chittleborough, 1991; Nesbitt and Young, 1982; Parker, 1970; Price and Velbel, 2003). These indices are based on chemical changes, often ratios of stable vs. mobile elements, from sample points through a weathering profile. Geochemical weathering indices are based on site measurements, such as geochemical composition, that cannot be easily extrapolated across the landscape without an appropriate surrogate.

In this paper, such a surrogate is described using geochemical variations of radioelements potassium (K), thorium (Th) and uranium (U), measured from airborne gamma-ray spectrometry surveys, together with terrain attributes from a digital elevation model. These datasets, together with training sites that describe the degree of weathering, are used to generate a weathering intensity index (WII). The technique has been developed for erosional landscapes that are described here as areas where hill slope processes dominate and where regolith materials are associated with residual or locally derived materials. The WII is generated over the Australian continent at a resolution of 100 m. Background information on gamma-ray spectrometry, specifically the distribution of radioelements in bedrock and regolith materials, is presented, followed by the methodology used to generate the WII. The WII is evaluated and assessed with regolith geochemistry, existing regolith maps and soil/regolith field site attributes. The reliability of the approach and its potential use in complementing traditional soil/regolith mapping and quantitative soil survey methods is then discussed in light of providing a framework to better understand weathering and geomorphic processes across a range of landscape scales.

2.2 Background — gamma-ray spectrometry

Airborne gamma-ray spectrometry measures the natural gamma-ray flux emitted from soils and bedrock to a depth of approximately 40 cm. Sampling depths will vary according to the soil density. For example, gamma-rays measured from low-density organic-rich soils are thought to emanate from up to one meter depth (Rawlins et al., 2009). Almost all gamma radiation detected near or at the Earth's surface results from the radioactive decay of K, Th and U. Potassium abundance is measured by gamma-ray photons emitted when ^{40}K decays to argon (^{40}Ar). Uranium and Th abundances are measured from daughter nuclides in their respective decay chains. Distinct emission peaks associated with bismuth (^{214}Bi, a daughter product in the ^{238}U decay series) and thallium (^{208}Tl, a daughter product in the ^{232}Th decay series) are used to estimate the concentrations of U and Th respectively (Minty, 1997). As a result U and Th concentrations are normally expressed in units of "equivalent" parts per million; eU and eTh. The estimation of U and Th assumes that their respective radioactive decay series are in equilibrium (Minty, 1997).

Gamma-rays emitted from the Earth's surface relate largely to the mineralogy and geochemistry of the bedrock and weathered materials. Gamma-ray survey data was used initially for uranium exploration and geological mapping but in the last two decades has been used more broadly in conjunction with other datasets for mapping soils and regolith (Wilford and Minty, 2007). Once calibrated with field data, gamma-ray imagery can often provide information on quite specific soil/regolith properties (Bierwirth, 1996; Cattle et al., 2003; Cook et al., 1996; Dauth, 1997; Dickson and Scott, 1997; Gessler et al., 1995; Lahti and Jones, 2003; Martz and de Jong, 1990; McKenzie and Ryan, 1999; Rawlins et al., 2009, 2007; Ryan et al., 2000; Roberts et al., 2002; Taylor et al., 2002; Thomas et al., 2009; van Egmond et al., 2010; Wilford et al., 1997) and in understanding erosion and weathering processes (Erbe et al., 2010; Pickup and Marks, 2000; Wilford, 1995).

2.3 Distribution of radioelements in the weathered environment

2.3.1 Potassium

Potassium is a highly incompatible element during magma melting and as a result higher K concentrations occur with increasing fractionation of igneous rocks (Figure 7). Potassium is most abundant in felsic plutonic igneous rocks and their volcanic equivalents. Common K-rich rocks include granite, rhyolite, syenite, nephelinite and pegmatite (Figure 7). Potassium-rich minerals associated with these rocks include orthoclase and microcline feldspars, muscovite, biotite, alunite, leucite, phlogopite and some amphiboles. Mafic minerals and associated rocks such as basalts, dunites and peridotites have little K in comparison.

The concentration of K generally decreases with increasing weathering because K is highly soluble and, given sufficient time, leaches from the weathering profile (Curtis, 1976; Taylor and Eggleton, 2001). However, during the early stages of weathering, the K content can increase as a result of the preferential removal or dissolution of more soluble mafic minerals (Dickson and Scott, 1997). Potassium can persist for some time in the regolith where it is adsorbed onto the surfaces of clay minerals to partially satisfy substitutions of silicon (Si^{+4}), aluminium (Al^{+3}), iron (Fe^{+2}) and magnesium (Mg^{+2}). Potassium is also associated with organic matter (Martz and De Jong, 1990) where it can be recycled in the upper part of the soil profile.
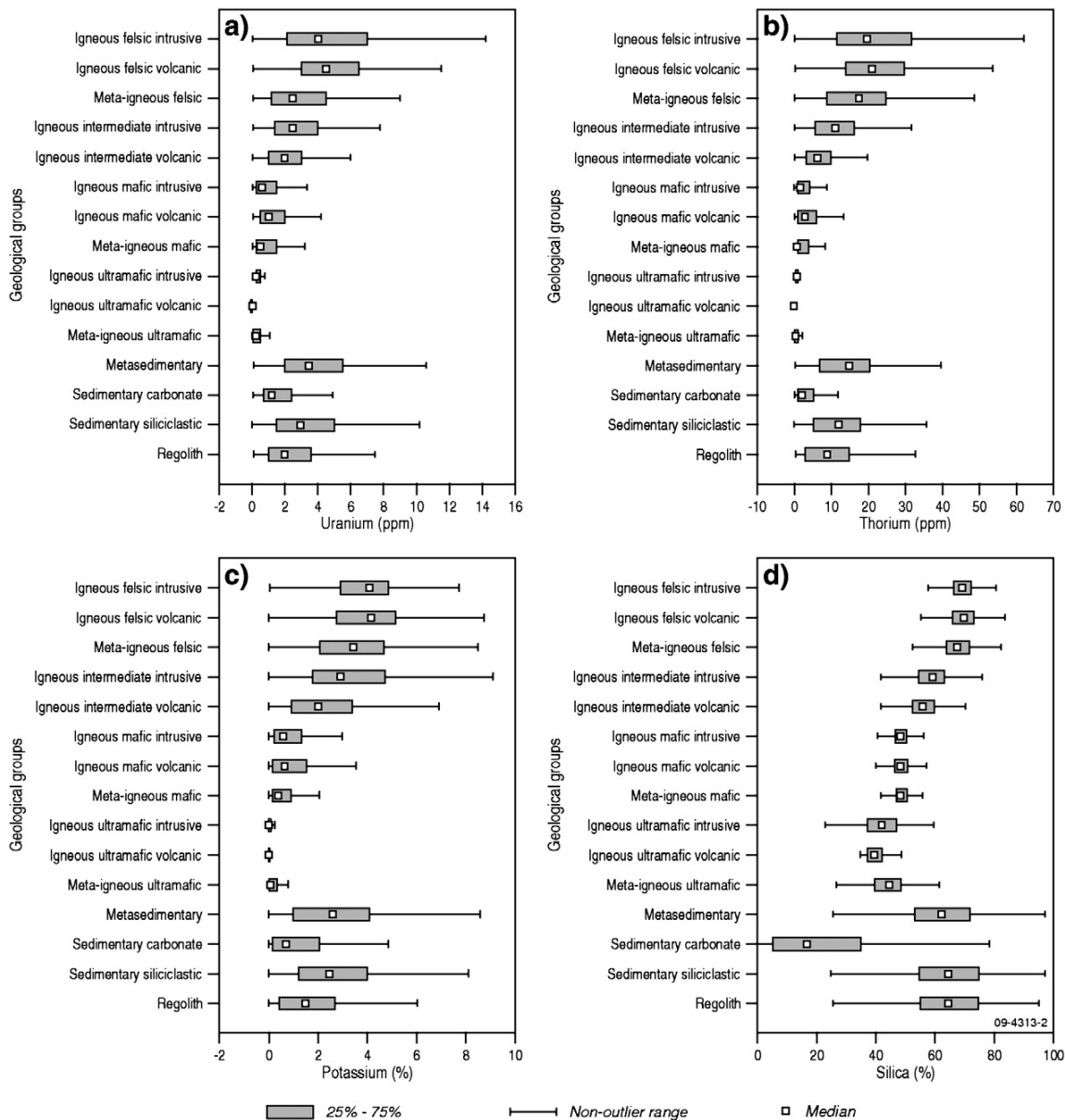
Figure 7 Distribution of potassium, thorium and uranium in Australian rocks and regolith based on 30,000 samples from the OZCHEM whole rock geochemistry database (Geoscience Australia www.ga.gov.au). The concentration of K, Th and U increases with higher silica content (D) in igneous and volcanic rocks.

2.3.2 Thorium

Thorium occurs in minerals or as a tetravalent Th^{4+} ion. Thorium ions readily form complexes in solution with chloride, fluoride, nitrate, sulphate, carbonate, phosphate, hydroxide, silicate, citrate, oxalate, tartrate, acetate and organic materials (Mernagh and Miezitis, 2008). Thorium associated with organic complexes is more easily transported into solution with pH below 8.0 (Langmuir and Herman, 1980). Thorium occurs in minerals such as thorianite, monazite, cheralite, huttonite and thorite (Krishnaswami, 1999) and can also occur in small quantities in major rock-forming minerals such as quartz and feldspar. Thorium-bearing minerals precipitate late in the igneous crystallisation sequence and therefore an association of Th with other incompatible elements including U, K, rubidium (Rb) and rare earth elements is often observed. Thorium is most abundant in felsic igneous rocks (e.g. granite, rhyolite, gneiss) (Figure 7).

Thorium released during bedrock weathering is readily adsorbed onto clay minerals, Fe and Al oxyhydroxides and organic matter in the regolith. Thorium can persist in weathering profiles where it is associated with

accessory and resistate minerals (minerals not readily weathered by chemical and physical processes) such as zircon, titanite, apatite, allanite, xenotime, monazite and epidote. Therefore, due to its association with clays, oxides and resistate minerals, Th is typically retained in the weathering profile compared with more soluble elements such as K. Very highly weathered materials such as Fe duricrust and bauxitic soils typically exhibit high-Th responses.

2.3.3 Uranium

As with K and Th, U-bearing minerals precipitate late in the igneous crystallisation sequence (Galbraith and Saunders, 1983). There is a general increase in U concentration with increasing silica content in plutonic igneous and volcanic rocks (Figure 7). Uranium is most common in granitic and felsic volcanic rocks and least common in ultramafic rocks. Uranium occurs as traces in major rock-forming minerals such as quartz, biotite, hornblende and feldspars, but is most abundant in accessory minerals including allanite, apatite, epidote, betafite, huttonite, monazite, titanite, xenotime, zircon, thorianite, uraninite, thorite and uranothorite (Wedepohl, 1969). The most common U mineral is uraninite (UO_2–U_3O_8), which is sometimes referred to as pitchblende.

The mobility of U isotopes is complex and largely depends on pH and oxidation state (Wedepohl, 1969). Uranium can be leached from soluble minerals under oxidising conditions and precipitated in reducing conditions. Uranium, like Th, is associated with relatively stable constituents in the soil profile. Uranium released during weathering is readily adsorbed onto clay minerals, oxides (Fe and Al) and organic matter. Uranium can also be retained in soils as resistate minerals such as zircon and monazite — these minerals are often preferentially concentrated in highly weathered regolith materials. Unlike Th, the oxidised form of U as the soluble uranyl ion allows it to be more readily mobilised in the weathering environment. Uranium can show an initial increase in concentration as the bedrock weathers due to its retention in clays and oxides. Leaching of U and Th in topsoil and precipitation lower in the soil profile has been described by Greenman et al. (1999) and Taboada et al. (2006). In advanced stages of weathering and under favourable conditions, U can be leached from the profile relative to Th (Harriss and Adams, 1966). The presence of specific bacteria including, for example, sulphate-reducers, can also influence the re-distribution of U in the regolith (Adbelouas et al., 2000; Chan et al., 2007). The mobility and re-distribution of U and Th in the regolith is therefore often highly complex.
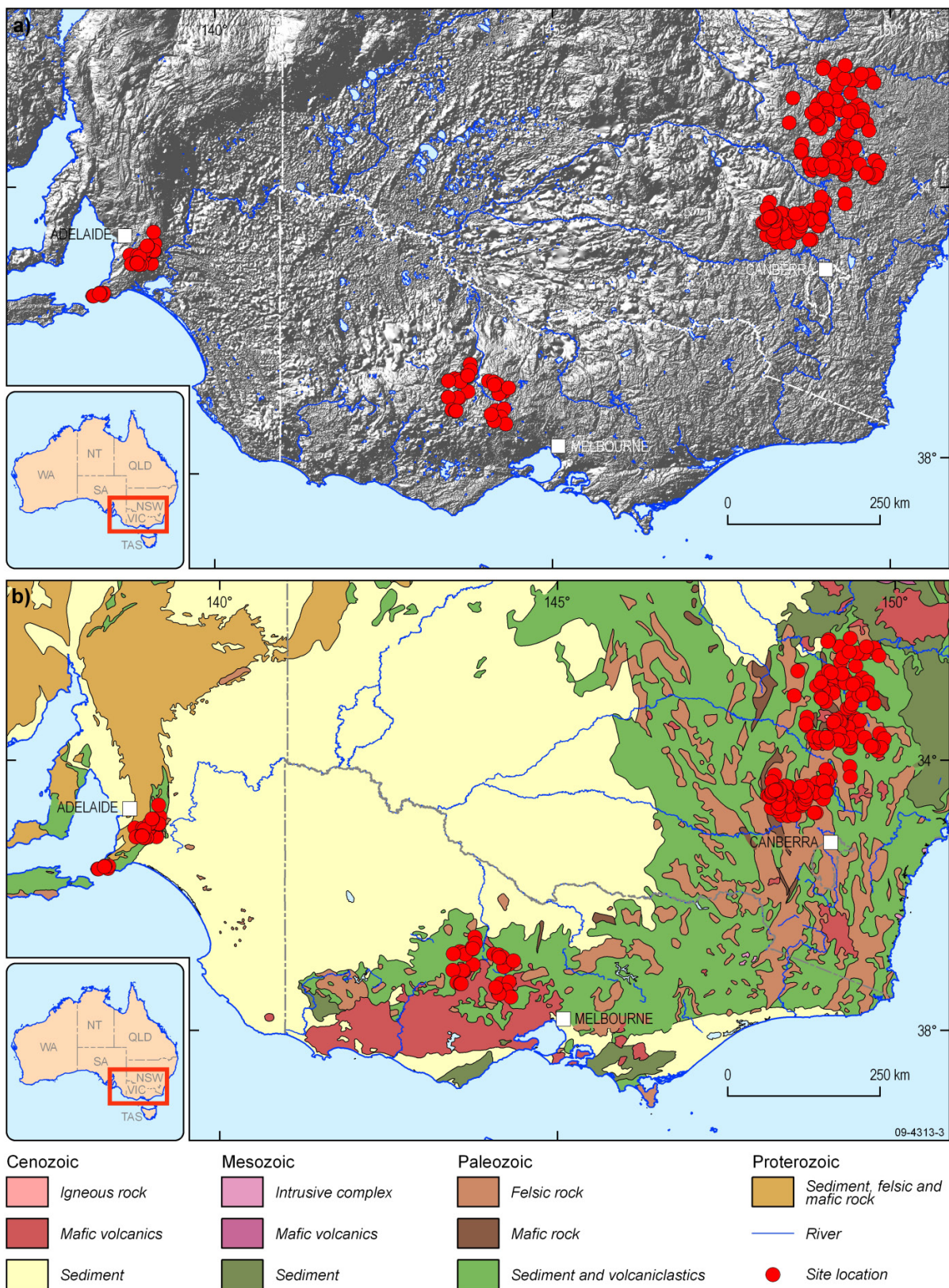
Figure 8 a — Hill shaded DEM with field site locations. b — Simplified geology. Study areas as indicated by the cluster of sample sites from left to right include, the Lofty Ranges, central Victoria and Central West New South Wales.
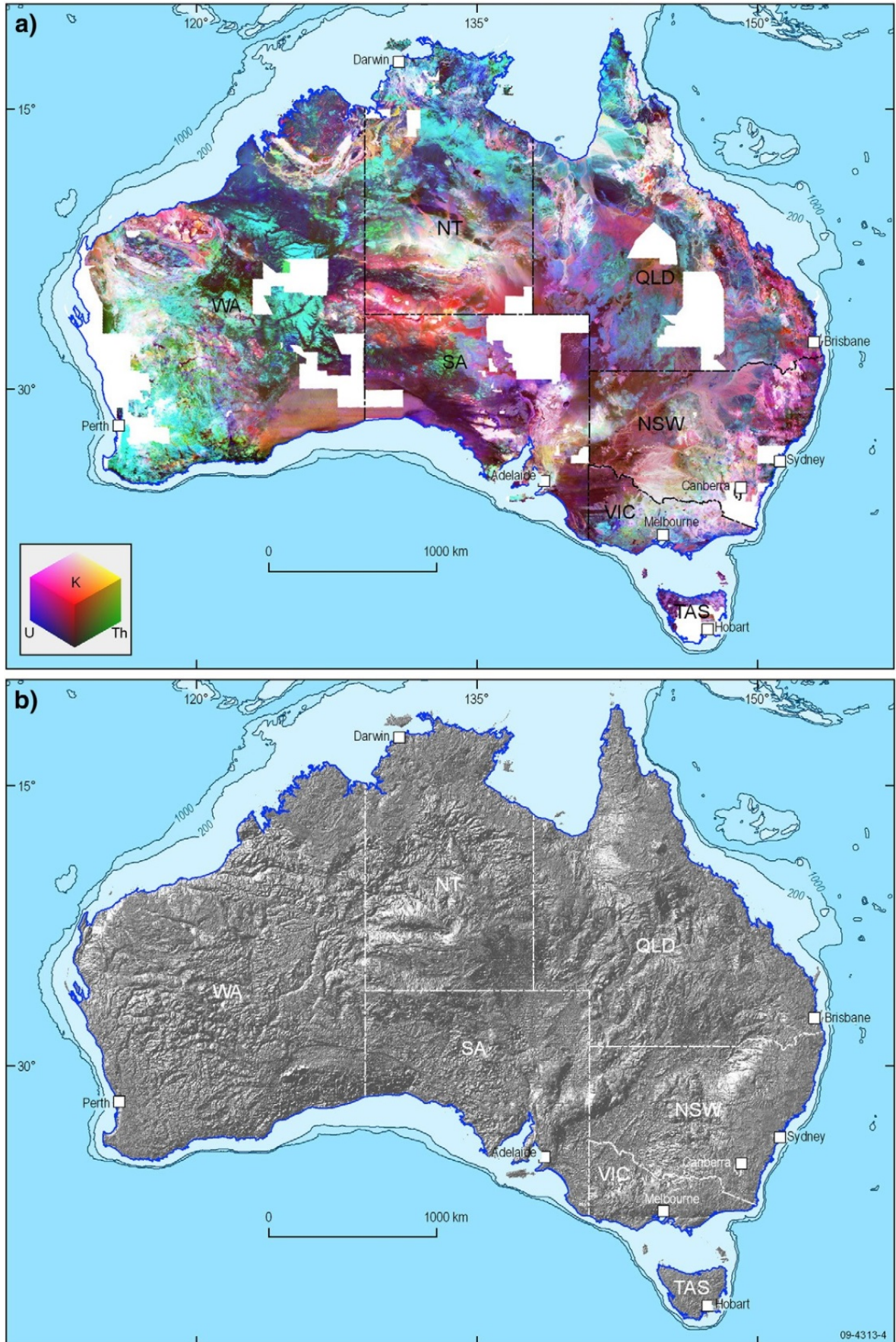
Figure 9 a — Radiometric map of Australia ternary image with K in red, eTh in green and eU in blue. b — Hill shaded 90 m SRTM DEM image with NW sun illumination.

2.4 Materials and methods

2.4.1 Study areas, geology and landforms

The study areas are the central west slopes of NSW, central north Victoria and the central Mount Lofty Ranges in South Australia (Figure 8a). Landforms range from low relief erosional and depositional plains (<9 m, relief) to rises (9–30 m relief) and hills (30–300 m relief). Field investigations and regolith sampling were carried out within these areas to establish relationships between weathering intensity, radioelement response and terrain relief. The relationships between weathering intensity and the explanatory variables were used to generate a weathering index prediction over the Australian continent. This index was then compared with surface soil geochemistry and regolith datasets (e.g., maps and site observations).

The central west of NSW and Victorian study areas include rocks of the Lachlan Fold Belt (Figure 8b) consisting of Paleozoic metavolcanics, metasediments and granites (Brown et al., 1982; Gray, 1997). Rocks in the NSW central west area are partially covered by Cenozoic basalts and colluvial and alluvial sediments. Sub-horizontal Permian to Triassic sedimentary rocks of the Gunnedah and Sydney basins cover older Paleozoic rocks over the northern and western parts of the study area. Extensive Paleogene/Neogene basalts and associated eruptive cones are a characteristic feature of the central Victorian highlands (Figure 8b). Rocks in the central Lofty Ranges are older and consist of Proterozoic and Cambrian gneisses, schists, feldspathic sandstones, meta-siltstones, quartzites and dolomites. These sediments were folded and metamorphosed during polyphase deformation associated with the Late Cambrian Delamerian Orogeny (Drexel and Preiss, 1995).

The study areas exhibit a range of weathering characteristics from fresh to intensely weathered bedrock. The most intensely weathered profiles are usually preserved on palaeo-landforms that have been exposed and weathered during at least the Paleogene/Neogene (Bourman, 2007; Chan, 1998; Joyce, et al., 2003; Milnes et al., 1985; Twidale, 1976) and continue to be weathered and modified to the present day. These regolith-landform characteristics are therefore ideal in assessing weathering and corresponding radioelement responses over a range of contrasting bedrock types with differing landscape histories.

2.4.2 Datasets — gamma-ray spectrometry, DEM and geology

Gamma-ray grids of K, eTh, eU and dose rate were obtained from the recently compiled radiometric map of Australia (Figure 9a), which integrates over 540 surveys at a 100 m resolution (Minty et al., 2009). Potassium is expressed in percent and Th and U in parts per million. The dose rate or total count is expressed in nanoGrays per hour (nGy/h) and is calculated from weight additions of K, eU and eTh using the formula 13.078 K (%) + 5.67 U (ppm) + 2.49 Th (ppm). The radiometric map of Australia is a levelled database and is consistent with the International Atomic Energy Agency's (IAEA 2003) Global Radioelement Datum. This enables quantitative comparison of radiometric signatures reflecting bedrock and regolith materials across the Australian continent.

The Shuttle Radar Topography Mission (SRTM) elevation data, collected by the Space Shuttle Endeavour during an 11-day mission in February of 2000, was used in this study (Figure 9b). The 3 arc second resolution data (~ 90 m) version of the data was used to generate a relief surface for the continent. The relief surface provided a key input variable to the regression modelling. The relief surface was calculated using a migrating circular kernel that determined the maximum elevation range within a 270 m radius window. The size of the window was chosen to broadly correlate with the gamma-ray 'foot print' based on an average 400 m flight-line-spacing survey.

A 1:1,000,000 scale digital surface geology map of Australia (http://www.ga.gov.au/resources/maps/minerals/geological-maps.jsp) was used to delineate unconsolidated transported materials from erosional bedrock dominated landscapes. The map is largely compiled from 1:250,000, and in places 1:100,000 and 1:50,000, geological mapping and as a result has sufficient detail and accuracy to be used at sub-regional scales.

2.4.3 Field classification and measurements

The degree of bedrock weathering was assessed using a 6-level, field-based classification scheme. The scheme is largely based on visual characteristics such as presence/absence criteria (e.g., outcrop—present or not, preservation or not of bedrock structures/fabrics),

relative proportion of clay, degree of mottling and ferruginisation. It is a qualitative classification with a degree of subjectivity implicit in each of the groupings. However the scheme provided a rapid assessment and classification of bedrock weathering over a range of landscape and bedrock types. At one end of the spectrum, level 1 describes largely unweathered landscapes with a high proportion of fresh bedrock exposed at the surface. At the other end of the spectrum, level 6 describes extremely weathered landscapes where the bedrock is completely weathered to secondary minerals (e.g., clays and oxides). The criteria used to define each of the 6 weathering classes are shown in Table 1. The classification scheme draws some of its definitions from degree of weathering criteria proposed by Eggleton (2001), Melton (1965) and Ollier (1965). The classes are not just based on weathered profiles, but take into account the broader landscape characteristics, such as the proportion of outcrop. Field sites with highly variable weathering characteristics that change over local scales (e.g., tens of metres) were excluded from the training set. Where there was some local variability an average weathering intensity value was estimated and recorded. This is because the radiometrics 'sees' or records information from a broad 'foot print' on the ground. For example, at 100m height (a common flying height for many surveys), about 80% of recorded gamma radiation originates from a 600 m diameter circle below the aircraft.

Surface regolith samples from previous field mapping projects were used to assess the relationships between the weathering index and soil geochemistry. Major and trace element compositions of soil samples were determined using inductively coupled plasma mass spectrometry (ICP-MS) at Geoscience Australia.

2.4.4 Regression models and exploratory analysis

Regression modelling is used to predict weathering intensity from airborne radioelement channels K, Th, U, Th/K, dose and a DEM-derived 'relief' image. The Th/K ratio was used in the analysis in addition to the other radioelement channels because it was known to be useful for delineating weathered materials (Dauth, 1997). These datasets provided the independent environmental variables and the ground based field site weathering classes provided the dependent variable (Table 2). The model therefore mixes continuous data (airborne and terrain attributes) with discrete or categorical classes. However, the weathering classes used in the analysis are ordered and represent intervals along a weathering continuum. Class 1 transitions through class 2 and finally through to class 6. Weathering intensity by its nature is continuous and therefore the regression approach is compatible with the inherent characteristics of the prediction variable.

Two regression models were used and combined to generate the final weathering intensity prediction. This is because some rocks (e.g., ultramafics, some sandstones and carbonates) (Figure 2) contain little or no gamma-emitting radioelements. These rocks exhibit little change in their radioelement distribution during weathering due to their low primary radioelement content. In this circumstance the gamma-ray imagery is not effective in detecting changes due to weathering. Instead, relief is used as a surrogate for estimating weathering intensity based on the assumption that landscapes with high relief are likely to have or maintain thin soil and slightly weathered bedrock. Low relief landscapes, in contrast, are likely to accumulate and preserve weathered materials (i.e., palaeo-surfaces) with corresponding higher weathering intensities. Rocks with low radioelement content are identified where total gamma-ray emissions are ≤25 nGy/h. The 25 nGy/h value was obtained empirically by selecting a dose value that delineated mafic from intermediate and felsic rocks using geological map units from the study areas. This 25 nGy/h threshold effectively identifies quartzite, siliceous sandstones and mafic/ultramafic bedrock in the study areas. Intersecting field site classes with the relief image and within areas where total gamma-ray emissions are ≤25 nGy/h generated the data to develop the first regression model (Table 2). Where dose emissions are ≥25 nGy/h, a second multiple regression model was used. The second regression model uses dose, K, Th/K, relief, U and Th as its prediction variables. Over 90% of the rocks in the study areas have gamma-ray emission >25 nGy/h, and therefore the second regression model largely determines the weathering intensity prediction (Table 2).

Two sets of field site data across the 6 weathering intensity classes were used to develop the regression correlations for each of the models. The relief-based and multiple regression models used 79 and 229 field site observations, respectively. Table 3 shows the exploratory data summary statistics for each dataset.

2.4.4.1 Relief based model

There is a systematic decrease in relief with increased weathering over bedrock and regolith materials with low gamma-ray emissions (< 25 nGy/h) (Figure 10). The range and average value of relief decreases with increasing weathering intensity (R = -0.57). Relief values are not normally distributed and were log (Ln) transformed with a subsequent improvement in the fit of the regression line to R = -0.71. The log transformed data formed the basis of the first regression model.

Table 1 Rock material weathering classification

Level	Degree of bedrock weathering	Definitions
1	Unweathered bedrock	Rock shows no sign of decomposition or staining, and bedrock outcrop exceeds soil cover. Outcrop very common (>70%).
2	Slightly weathered	Rock is slightly discoloured, may be diffusely mottled or iron stained. Overall bedrock fabric very well preserved. Soils are typically lithosols. Bedrock outcrop common (20–70%). Slight weathering of feldspars; primary minerals largely preserved.
3	Moderately weathered	Residual clays and sands are common in the upper part of the weathering profile. Bedrock partly decomposed but still cohesive, mottling common. Most feldspars partly weathered; primary minerals still dominate with smectite, kaolin ± iron oxides present. Minor outcrop (<20%) or absent.
4	Highly weathered	Residual clays or sands are common in the upper part of the weathering profile. Bedrock structure and fabric only weakly preserved. Saprolite commonly mottled and ferruginous. The material can be broken apart in the hand. Most primary minerals (e.g. feldspars) are weathered. Mineralogy dominated by clays, silica and oxides. Minor outcrop — where present usually highly weathered.
5	Very highly weathered	Residual clays and sands are common in the upper part of the weathering profile; mineralogy is dominated by clays, oxides with or without residual quartz; other primary minerals in low abundance or absent. Profile commonly mottled with the primary bedrock structure typically lost. Saprolite soft and weakly cohesive (easily be broken by hand) — although can be indurated by iron and silica. Usually no outcrop — where present typically highly weathered.
6	Intensely weathered	Residual clays and sands are common in the upper part of the weathering profile. Weathered profile usually intensely mottled or leached. Iron lags and ironstone gravels not uncommon. Saprolite soft with the primary mineralogy completely weathered to clays or oxides. However, resistate quartz veins may still remain. Quartz is the only remaining primary mineral. Usually no outcrop — where present typically completely weathered and indurated by oxides or silica.

2.4.4.2 Multiple regression correlations and stepwise regression

Table 2 Basic statistics and regression data

Relief data

Signal	N	Mean	Minimum	Maximum	Std.Dev	Skewness
Relief	79	32.76	3.14	123.43	29.37	1.36

Pearson correlation coefficients: natural log (ln) transformed signal data

Signal	WC[a]	Relief
WC[a]	1.00	−0.84
Relief		1.00

Multiple regression data

Signal	N	Mean	Minimum	Maximum	Std.Dev	Skewness
Relief	229	23.13	4.53	127.77	22.37	2.40
Total count	229	62.86	32.85	143.10	20.64	1.38
K	229	1.27	0.17	4.02	0.81	0.84
Th	229	14.23	4.53	34.32	4.45	1.42
U	229	1.82	0.44	5.71	0.79	1.44
Th/K	229	17.95	2.02	111.74	16.82	2.41

Pearson correlation coefficients: natural log (ln) transformed signal data

Signal	WC	Relief	Dose	K	Th	U	Th/K
WC	1.00	−0.74	−0.58	−0.90	−0.03	−0.31	0.83
Relief		1.00	0.57	0.68	0.22	0.35	−0.55
Dose			1.000	0.61	0.71	0.72	−0.30
K				1.00	0.06	0.27	−0.91
Th					1.000	0.50	0.33
U						1.00	−0.05
Th/K							1.00

[a] Weathering class.

Table 3 Summary of stepwise regression.

	Variables included	Multiple R	Multiple R-squared	F – to Ent/rem	p-level
K	1	0.904713	0.81850	1023.731	0.000000
Relief	2	0.921038	0.848312	44.407	0.000000
Th/K	3	0.923548	0.852941	7.083	0.008342
Dose	4	0.927162	0.859630	10.674	0.001257

The histograms of all six variables were slightly to moderately right-skewed (Table 2) and consequently the data was log (Ln) transformed. The Pearson correlation matrices (Table 2) indicated that K (R = −0.90), Th/K ratio (R = 0.83) and relief (R = -0.74) were well correlated to the weathering index classes. Dose rate (R = -0.58) was moderately well correlated and Th (R = -0.03) and U (R = -0.31) were not or weakly correlated (Figure 10). A forward stepwise regression is used to progressively add terms to the regression

model. This approach firstly identifies the independent variable that explains the most variation in the dependent variable. A second variable is then chosen that explains the most residual variation and the regression coefficients are re-calculated until no variables 'significantly' explain the residual variation. Correlations between some of the environmental variables are therefore accommodated in this regression model approach. The stepwise regression (Table 3) ranks K as the most significant predictive parameter (R^2 = 0.82) with relief, Th/K and dose rate providing incremental improvements to a final R^2 of 0.86. All four independent variables in the regression model that are statistically significant (p values <0.01) were used to generate the weathering index prediction grid by the equation:

Regression model 2 = 6.75180 + −0.85103*K +
    −1.31944*Relief+ 2.68282*Th/K + −2.59011* Dose.

2.4.4.3 Combining the regression models

The final weathering intensity prediction was generated by combining the relief grid (model 1) and multiple regression derived grid (model 2). To avoid boundary discontinuities when combining the two prediction grids a simple linear weighting function was developed. This facilitated a smooth transition between the two predictions and removed any abrupt boundary effects in the final grid.
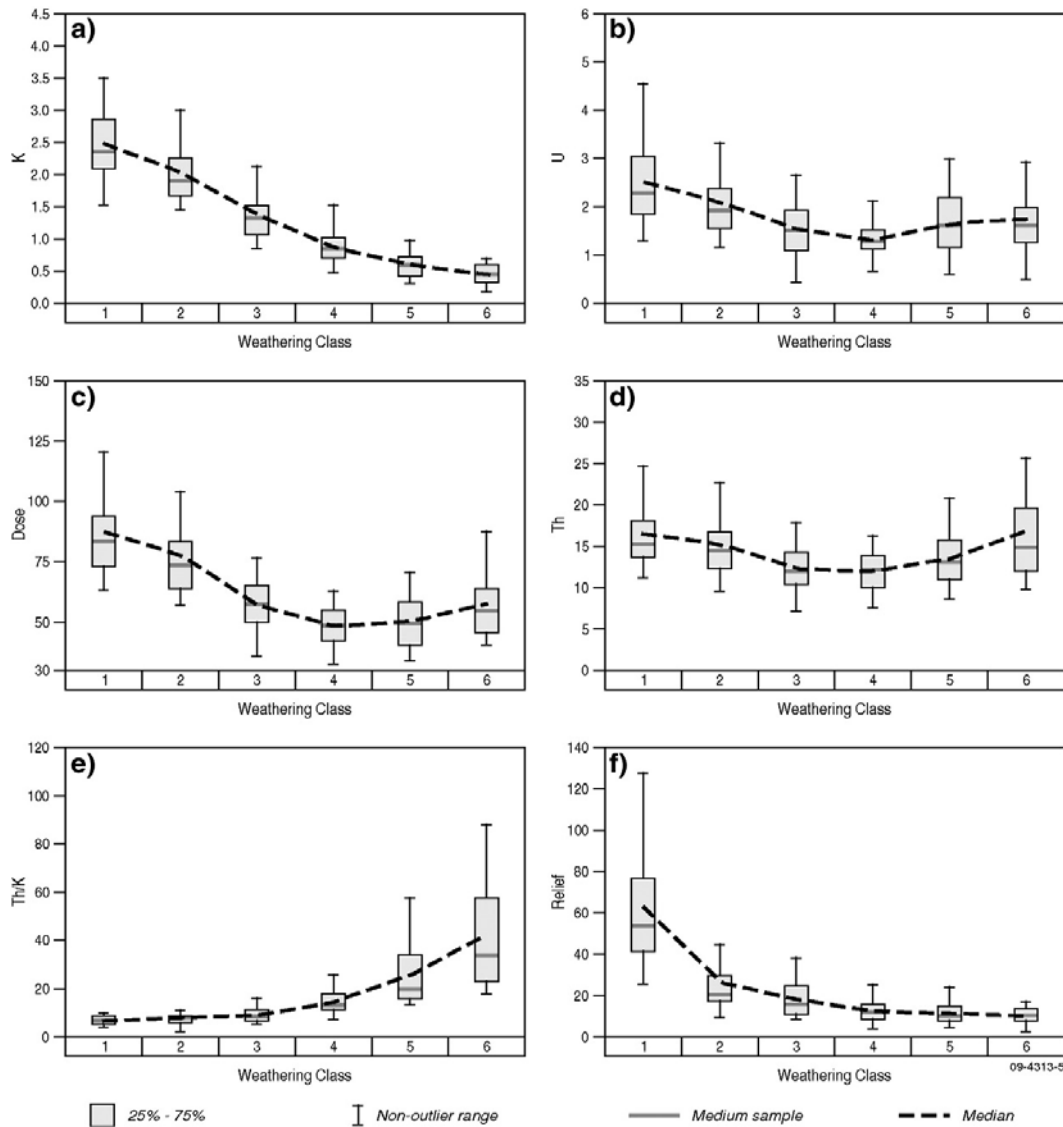
Figure 10 Whisker and box plots for each of the environmental variables. Whiskers showing data range with outliers removed. Boxes show the 75th and 25th percentiles. The middle line identifies the medium sample value and the connected line intersects the mean value.

The weighting function involved rescaling all dose values ≤ 18 nGy/h to 0 and all values ≥ 33 nGy/h to 1. Where values are 0 and 1 the result from the first and second regression models are applied, respectively. Values between 0 and 1 are used to add weighted percentages of the two regression models (e.g., 0.5 = equal weighting for the two regression models). The weighting function is shown diagrammatically in Figure 11.
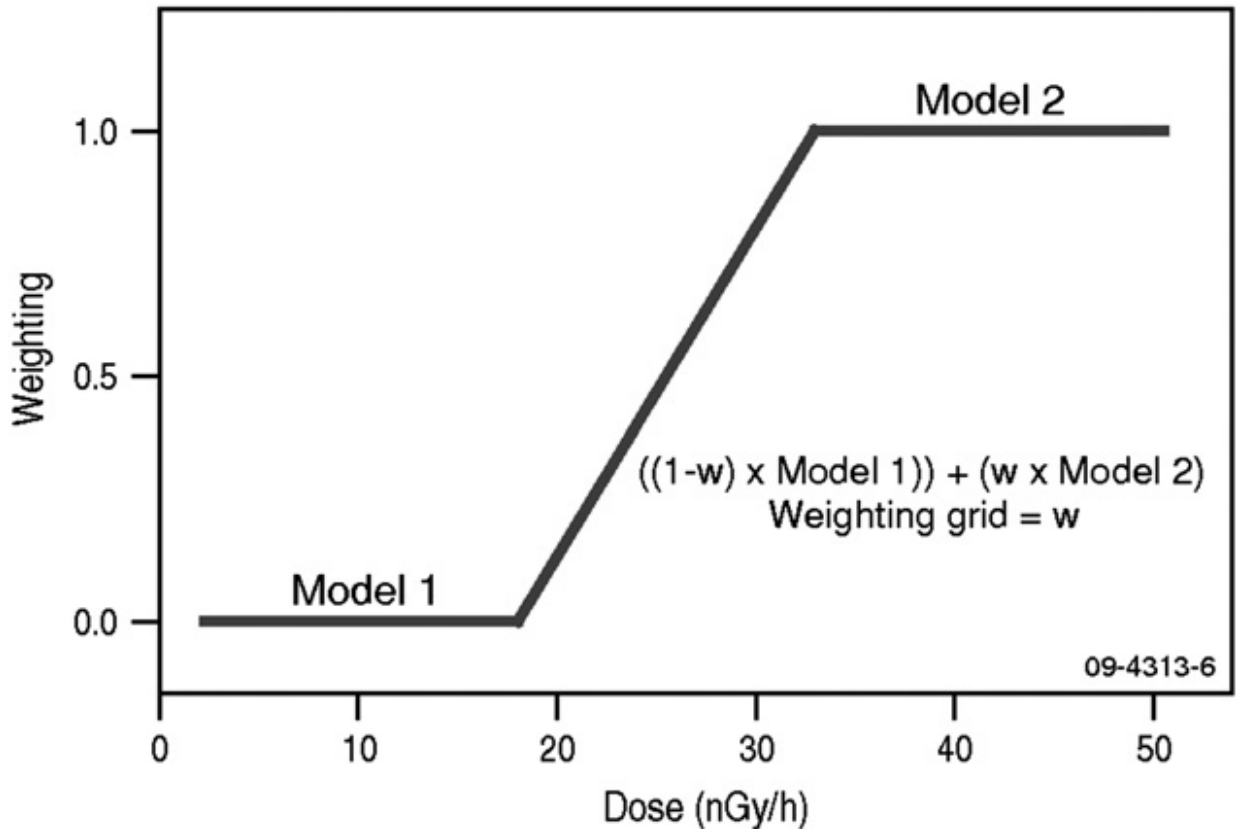
Figure 11 Weighting function using the dose grid to combine the two regression models.

2.4.5 Prediction accuracy and uncertainly

Interpretations should be made within the context of the overall uncertainties in the weathering predictions. Uncertainty is associated with the statistical model, the training sets used to derive the model, scale issues related to input dataset resolution and the underlying geomorphic and weathering assumptions on which the modelling relies.

The prediction accuracy as measured by the root-mean-square error (RMSE) of 0.643 indicates a degree of spread within the residuals but its average variation is within the range of one weathering class and is considered relatively small. Nevertheless, there is a component of in-class and to a lesser extent between-class variations that may not reflect weathering responses, but changes in bedrock chemistry. The model predictions are likely to be more accurate in lithologies that show marked changes in radioelement chemistry during weathering. Although low emittance rocks and regolith (dose <25 nGy/h) are accommodated using the relief-based regression model, weathered materials just above this threshold

might be difficult to resolve due to subtle differences in bedrock and weathering signatures.

The repeatability or robustness of the regression model was also assessed using the training and validation splitting method (Massart et al., 1996). This involved randomly subdividing the data into two groups. This first group is used to generate a prediction (i.e., calculating the regression model) and the second group is used to independently assess the prediction performance. The prediction and validation groups were then swapped to assess the robustness of the regression model. The R^2 and the standard RMSE were generated for both conditions (Table 4). The R^2 for both models is high and the RMSE relatively low. The R^2 values for both groups are consistent, suggesting a high degree of stability within the model. This is likely to reflect the high number of training set observations and low number of significant prediction variables that are used to drive the model.

An important consideration when interpreting the weathering index is the resolution or scale of the prediction. The spatial resolutions of the DEM and gamma-ray imagery are 90 and 100 m, respectively.

Using the index at spatial scales less than 100 m is therefore not supported by the inherent resolution of the input variables. Furthermore, although the gamma-ray imagery was gridded to 100 m pixels its actual resolution will depend on the flight line spacing and flying height of the survey. To honour the data recorded along the flightline, most surveys are only gridded to one fifth the flightline spacing. Flight line spacing for the national radiometric grid mainly included 400 m surveys but surveys with 1.5 km flight spacing were also used in places (Minty et al., 2009). Therefore the resolution of the airborne data is variable despite all the surveys being gridded to 100 m and consequently the accuracy of the weathering prediction will vary accordingly. The other factor to consider is the size of the gamma-ray footprint. For example, at 100 m flying height about 80% of the recorded gamma-rays would originate from a circular radius of approximately 600 m below the aircraft. The gamma-ray pixels are therefore based on averages over relatively large areas and as a result may not resolve local scale outcrop and soils patterns. This is the reason that training classes were based on 'average' regolith characteristics over several hundred metres. Weathering profiles exposed in pits or road cuttings were only used if they were thought to represent the wider local area. Field areas that exhibited a high degree of local variability in weathering intensity were avoided when selecting calibration training sites.

Another potential source of error can be caused by disequilibrium in the radioactive decay chain for estimating U. Uranium disequilibrium occurs when daughter products above the measured bismuth isotope (214Bi) for estimating U in the decay chain are either enriched or depleted, thereby giving either over-estimates or under-estimates of U. Since the WII does not use U in the formula, potential U anomalies in the data are avoided in this approach.

2.5 Results

The weathering intensity image generated using the twin multiple regression method is shown in Figure 12a. Prediction of weathering intensity where there are gaps in the radioelement image (see Figure 9a) is based solely on the relief-based model. Regional patterns observed in the image broadly correspond with major geological and physiographic areas. For example, the south eastern highlands are less weathered than low relief, highly weathered landscapes in central and north eastern Western Australia. The WII shows significant variation in weathering intensity across a range of landform types over the Australian continent (Figure 12b). This variation is reflecting surface materials developed on depositional and erosional landscapes with different parent materials and weathering histories.

2.5.1 Regional scale observations

Brief descriptions from selected regions in Australia (Figure 12a) provide insights into the relationships between the weathering index, regolith materials and landscape processes.

2.5.1.1 Weipa bauxites

Table 4 Prediction capability of the regression analysis based on model 1 and model 2 datasets and their reciprocal training set validation.

	R^2	RMSE
Prediction model 1 vs. Training 1	0.84	0.684
Prediction model 2 vs. Training 2	0.85	0.643

The weathering intensity highlights extremely weathered, bauxite-rich soils associated with the Weipa Plateau. The bauxite has developed on the Cretaceous Rolling Downs Group and the Paleogene Bulimba Formation. The bauxite profiles reflect extreme weathering and consist largely of Fe and Al oxides, quartz and kaolinite (Taylor et al., 2008). Deep Red Kandosols (Orthiplinthic Ferrasol) are the dominant soil group. All soils are classified using the Australian Soil Classification (Isbell, 1996) and their equivalent to the world reference base is shown in brackets. The WII values are in the 5.5 to 6 range, i.e., completely weathered regolith.

2.5.1.2 Eastern Australia uplands

The eastern uplands of Australia consist of mountain ranges, hills and rises, plateaus, and escarpments. The uplands form the Great Dividing Range that separates rivers flowing east to the Pacific Ocean from westward flowing rivers that form part of the Murray–Darling Basin. Regolith in the area is highly variable but overall is less weathered compared to other parts of Australia due to relatively high rates of erosion. Bedrock types include mainly Paleozoic granites, volcanic and meta-sedimentary rocks and Mesozoic sediments. The WII is predicting slight to moderately weathered regolith (WII values = 1–3) over large areas of the uplands. In areas of high relief the gamma-ray imagery is reflecting the geochemistry and mineralogy of the exposed bedrock or thin soils developed on bedrock.

2.5.1.3 Ashburton surface

The Ashburton surface has developed across steeply dipping Proterozoic rocks and contains terraced fluvial sediments of Cambrian age. This suggests that the surface is of Cambrian age or older (Stewart et al.,

1986). It was thought to be one of the oldest continually exposed land surfaces in the world, although, based on apatite fission track data, Belton et al. (2004) suggested that it represents an exhumed surface from Mesozoic time. A major erosional scarp advancing SW is progressively removing highly weathered regolith associated with the old surface and exposing less weathered materials at the base of the scarp. Deep Kandosols and Vertosols (Orthiplinthic Ferrasol, Geric Ferrasol, Vertic Solonchak) commonly occur above the scarp edge with less weathered and differentiated Rudosols (Epileptic Regosol) below the scarp. These soils are highlighted in red (highly weathered) and blue (less weathered) hues, respectively. The WII values on the Ashburton Surface range between 5 and 6 while less weathered bedrock below the scarps typically have ranges between 3 and 4.

2.5.1.4 Victorian Basalts

The WII highlights variations in weathering over the western volcanic plains of Victoria. Basaltic lava flows in the area range in age from 5 to less than 1 Ma with corresponding changes in weathering intensity and depth (Joyce, 2003). The oldest flows and associated regolith consist of pallid kaolinitic profiles with mottles and ferruginous nodules compared with the youngest flows that have thin regolith and preservation of primary bedrock fabrics and mineralogy (Joyce, 2003). The oldest flows are preferentially enriched in Th and U due to their affinities with clays and iron oxides whereas the youngest flows typically contain some K associated with volcanic glass in the rock matrix. Highly weathered basalts have WII values between 4 and 5.5, compared with less weathered flows in the range of 2.0 and 3.0.
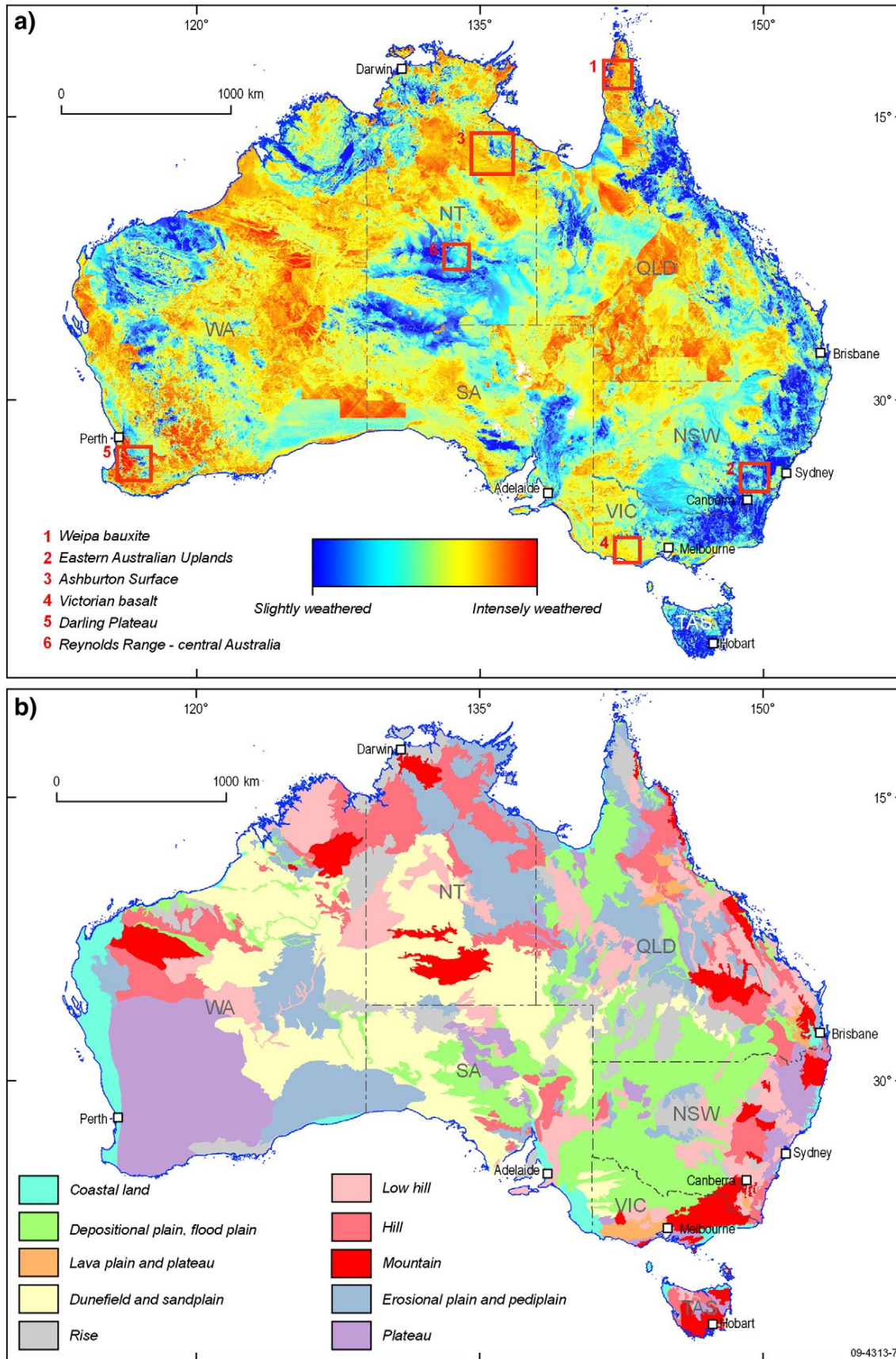
Figure 12 a — Weathering intensity index. b — Major landforms (based on the 1:5,000,000 scale Regolith Terrain Map: Chan, 1986).

2.5.1.5 Darling Plateau

Deep weathering on the Darling Plateau is associated with in situ and locally reworked ferrosols developed mainly on granitic parent materials. The ferruginous layer overlies a well developed mottled and pallid zone consisting of sandy loams and clays (Sadlier and Gilkes, 1976). The Darling Scarp forms a sharp break between the highly weathered regolith on the uplifted block and less weathered rocks (blue) exposed along the base of the Scarp. Soils developed on this deeply weathered substrate include Chromosols (Orthiplinthic Luvisol). The WII over the Plateau is in the range of 5.2 and 6.0 and is therefore consistent with the highly weathered nature of the regolith observed in the area.

2.5.1.6 Reynolds Range Central Australia

Reynolds Range in the Northern Territory forms part of the Arunta Block. Rocks include actively eroding granite, schist, gneiss, phyllite, shale, siltstone, quartzite and minor mafic intrusives. The felsic intrusive rocks are rich in K-bearing minerals like K-feldspar and K-mica. Landforms include N–W trending strike ridges, low hills, colluvial footslopes and sand plains. Rocks are well exposed and relatively fresh. The WII is mainly within the 0.5 to 3.0 range, indicating unweathered to slightly weathered bedrock.

2.5.2 Local scale observations

The index has a spatial resolution of 100 m and can therefore potentially provide information on weathering intensity and variability down to local district scales (e.g., 1:100,000). To illustrate this, two examples are given where the index can be used to improve and/or extrapolate 1:100,000 regolith-landform mapping and where it can be used to delineate hydrological and other soil attributes at local sub-catchment scales.

2.5.2.1 Correlations with existing regolith-landform maps

Regolith-landform maps describe the distribution and characteristics of weathered materials including sediments and in situ weathered profiles (e.g., saprolite). In erosional landscapes regolith maps generally classify weathered materials based on the degree to which the bedrock is weathered (e.g., slightly through to completely weathered) and the nature of the weathered materials (e.g., residual clay over highly weathered bedrock).

The classification criteria used on many regolith-landform maps (Pain et al., 2001) are similar to those described in this paper. A comparison of a regolith-landform map over the Bathurst area in central NSW (Chan, 1998) with the WII is shown in Figure 13a and b. The map was largely based on interpretation of aerial photography with field site calibration. Local relief extracted from the aerial photographs was used as the principal surrogate to describe the degree of bedrock weathering. The WII image broadly correlates with regolith map-derived weathering classes. Furthermore, boundaries between the weathering classes often correspond to erosional scarps delineated on the regolith map. The scarps have developed at different elevations and are progressively removing a highly weathered palaeo-surface in the area (Chan, 1998). Erosional scarps highlight boundaries between less weathered materials at the base to more weathered materials above the scarp as seen by a topographic cross-section through the area (Figure 14).

The WII was also compared to field site descriptions used in the compilation of broad scale regolith-landform mapping in the Northern Territory (Robertson et al., 2006). These site descriptions were classified into weathering index classes based on the criteria shown in Table 1. A significant correlation was found between classified site descriptions and the modelled weathering intensity prediction (Figure 15). Correlations are most clear between the slightly and highly weathered classes, whereas more subtle changes in the highly weathered components were less well resolved. The correlation is seen as only a guide due to the inherent subjectivity involved in interpreting the field site observations in terms of weathering intensity.

2.5.2.2 Hydrological applications and predicting specific soil attributes

As weathering increases we typically see systematic changes in the porosity and permeability in the developing regolith. The degree to which the bedrock is weathered has a major control in how water moves through the landscape and the capacity of the landscape to store salts (George and Conacher, 1993; Johnston et al., 1980). In the central west region of NSW the WII identifies deeper and more highly weathered bedrock associated with a partially preserved palaeo surface (Figure 16). The weathered materials are clay-rich and, as a result, the

groundwater and interflow pathways are sluggish, which leads to water-logging and salt scalding. Most of the areas affected by water-logging and salt scalding are associated with more weathered landscapes identified by the WII (Figure 16).

A more direct link between the WII and clay rich substrates is found when comparing the index with detailed field soil profile descriptions. A strong positive correlation was found between the clay content at 0.8–1.70 m depth and the WII over variably weathered felsic rocks near Mount Narayen, Queensland (Figure 17). This trend is reflecting the breakdown of primary minerals in the bedrock to secondary components (e.g., clay and oxides). The field site attributes were extracted from the CSIRO national soil database (http://www.asris.csiro.au/index_ie.html) and the correlation highlights the potential of the index to predict specific soil properties. The model is based only on the WII and geology, and further constraints and improvement to the prediction are likely when additional information (e.g., landscape position criteria) is incorporated into the model.

Other examples include delineating highly leached soils in North Queensland and differing degree of regolith development controlled by recent fault movements in central Victoria. The WII effectively maps highly leached sandy soils developed on granite bedrock in the Cape York Peninsula (Figure 18). Intense leaching of the bedrock leaves behind a thick layer of residual quartz sand that is very low in organic carbon and exchangeable cations (Isbell and Gillman, 1973). Due to the low gamma-ray emission of these sandy soils the WII is largely utilising the first regression model based on relief as the covariant to predict weathering intensity. In central Victoria, active movement associated with the Whitelaw Fault (Cherry and Wilkinson 1994) is clearly visible in the WII image (Figure 19) with deeper and more intensely weathered regolith preserved on the down-faulted eastern side of the fault compared to the uplifted western side.

2.5.2.3 Correlation with field based geochemical weathering indices

The weathering index was compared with weathering indices derived from the geochemical analyses of surface (0–30 cm) regolith samples collected over the Central West region of NSW (data sourced from Geoscience Australia geochemical database —

http://www.ga.gov.au/gda/index.jsp). The geochemical analyses were then used to generate two weathering indices — the chemical index of alteration (CIA) developed by Nesbitt and Young (1982) and the weathering index of Parker (WIP) (Parker, 1970). Both indices use ratios of considered immobile and mobile elements, and their formulas are;

$$CIA = \{Al_2O_3 / (Al_2O_3 + CaO + Na_2O + K_2O)\} * 100$$

$$WIP = \{2Na_2O / 0.35 + (MgO/0.9) + 2K_2O/0.25) + (CaO/0.7)\} * 100$$

These ground-based weathering indices were compared to the modelled WII predictions. The results show a moderate correlation between the CIA (R^2 = 0.45) and a significant correlation between the WIP (R^2 = 0.80) and the modelled WII (Figure 20).

The high correlation (R^2 = 0.8) between the WII and the soil-based geochemical weathering index, using the Parker formula, provides a quantitative and objective validation of the WII. The high correlation reflects the fact that K is measured directly in gamma-ray surveys and that the other cations in the Parker formula will generally decrease with decreasing K concentration (i.e., increased leaching). Correlations between the WII and the CIA index are, however, relatively weak (R^2 = 0.45). The CIA assumes that Al remains immobile during weathering. However, work by Chittleborough (1991) demonstrated that elluvial processes in many Australian soils and palaeosols can result in the mobilisation of Al to lower parts of the profile. Aluminium mobility in the regolith might therefore explain the weaker correlation between the WII and the soil-based CIA. The Parker index is based on the proportions of alkali and alkaline earths including sodium (Na), K, magnesium (Mg) and calcium (Ca) and does not rely on the assumption that Al remains immobile during weathering.

Furthermore, individual mobilities of these elements are accommodated in the formula with weightings based on their bond strengths with oxygen (Parker, 1970). Price and Velbel (2003) assessed commonly used chemical weathering indices for characterising weathering profiles developed on heterogeneous felsic and metamorphic parent rocks and also found the weathering index of Parker (WIP) to be the most reliable. This work supports that conclusion.
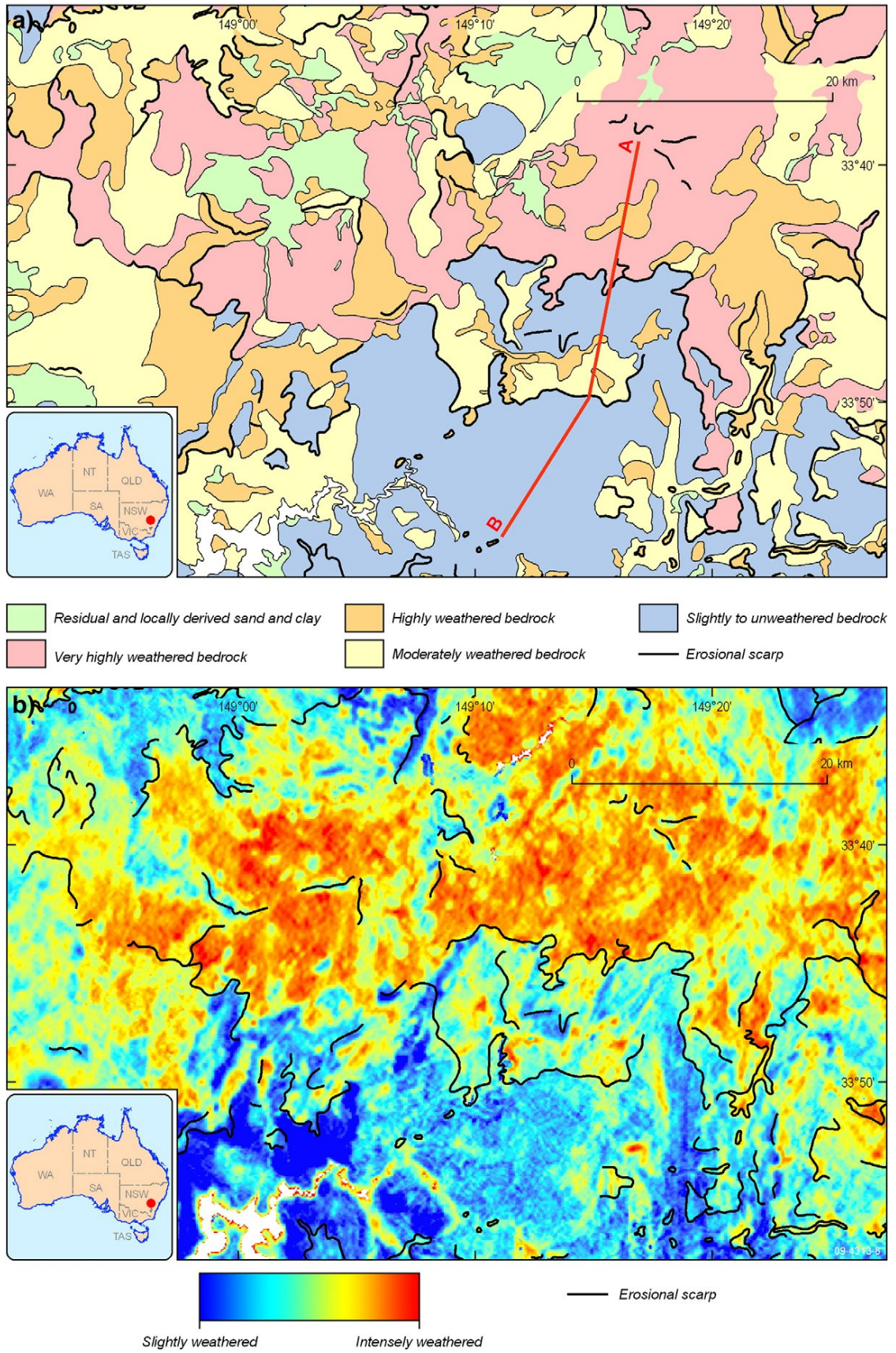
Figure 13 a — Subset of the regolith-landform map over the Bathurst 1:250,000 map sheet area (Chan, 1998). b — Corresponding WII image with erosional scarps.
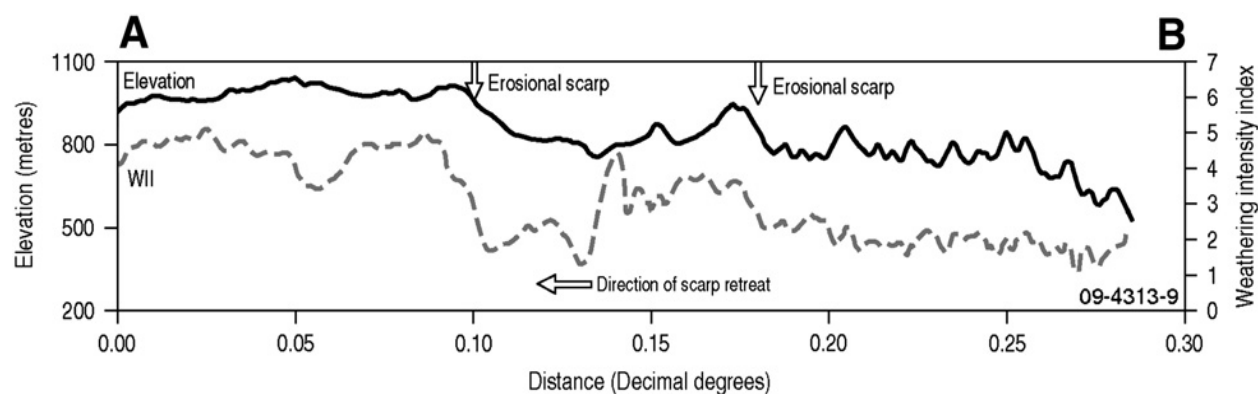
Figure 14 Topographic cross-section A–B (refer to Figure 13) through a series of erosional scarps (vertical arrows). Weathering intensity index values are shown with the dashed line. More weathered regolith is preserved above the scarp edge associated with the palaeo-surface than below the erosional scarps in this setting.

2.5.2.4 Weathering index over depositional landscapes

Although the regression models have been based on field data from erosional landscapes, the prediction of weathering intensity also has the potential to provide insights into weathering and geomorphic processes across depositional landscapes. Depending on the provenance and geochemical characteristics of the regolith source rocks, the WII can highlight active and less active depositional systems and the degree to which the sediment has been weathered. Active alluvial fans with geochemical compositions similar to their source rocks can be differentiated from more intensely weathered fan sediments (Figure 21).

2.6 Discussion

2.6.1 Radioelement trends during weathering

The strong negative correlation of K with increasing weathering is expected. Preferential leaching of K from K-bearing minerals such as K-feldspar and the retention of Th within resistate minerals and weathering products including oxides and clays has been observed in many studies (e.g., Dickson and Scott, 1997; Koons et al., 1980; Wilford et al., 1997). Potassium shows a steady linear decrease in concentration with a smaller variance as weathering progresses. Mean bedrock concentrations range from 2.38 wt. % in unweathered or slightly weathered bedrock to around 0.5 wt. % in completely weathered profiles. The relatively high variance within the

unweathered and slightly weathered classes is likely to reflect variations in the primary geochemistry and mineralogy of the bedrock. The Th/K ratio has a similar but inverse trend (Figure 10). Bedrock Th/K ratio values are relatively low with a small variance, whereas highly weathered bedrock has higher ratio values with higher variance. This trend reflects the relative loss of K compared to less mobile Th. The wide variance of Th/K ratio values in the highly weathered classes is likely to reflect changes in Th which shows significant variations in concentration across different weathering classes (Figure 10). The distribution of Th and U is complex; both show an initial decline in concentration and then a slight increase in the highly weathered regolith. Dose also has a similar trend (Figure 10). Since dose is calculated by the weighted addition of the three radioelement elements its distribution will reflect the combined influence for each of the radio-elements. Paralleling trends in K, Th and U, dose also shows a steady decline with increasing weathering as radioelements within primary minerals are lost or redistributed within the profile. The decline in dose and associated radioelements during weathering is likely to reflect reduction in bulk density as primary minerals weather to less dense secondary minerals. Dickson and Scott (1997) recorded losses of up to 60% of both K and Th with the development of saprolite. The relative increase in dose values within the very highly weathered classes is likely to reflect elevated Th and, to a lesser degree, U associated with resistant minerals, clays and oxides in the regolith.
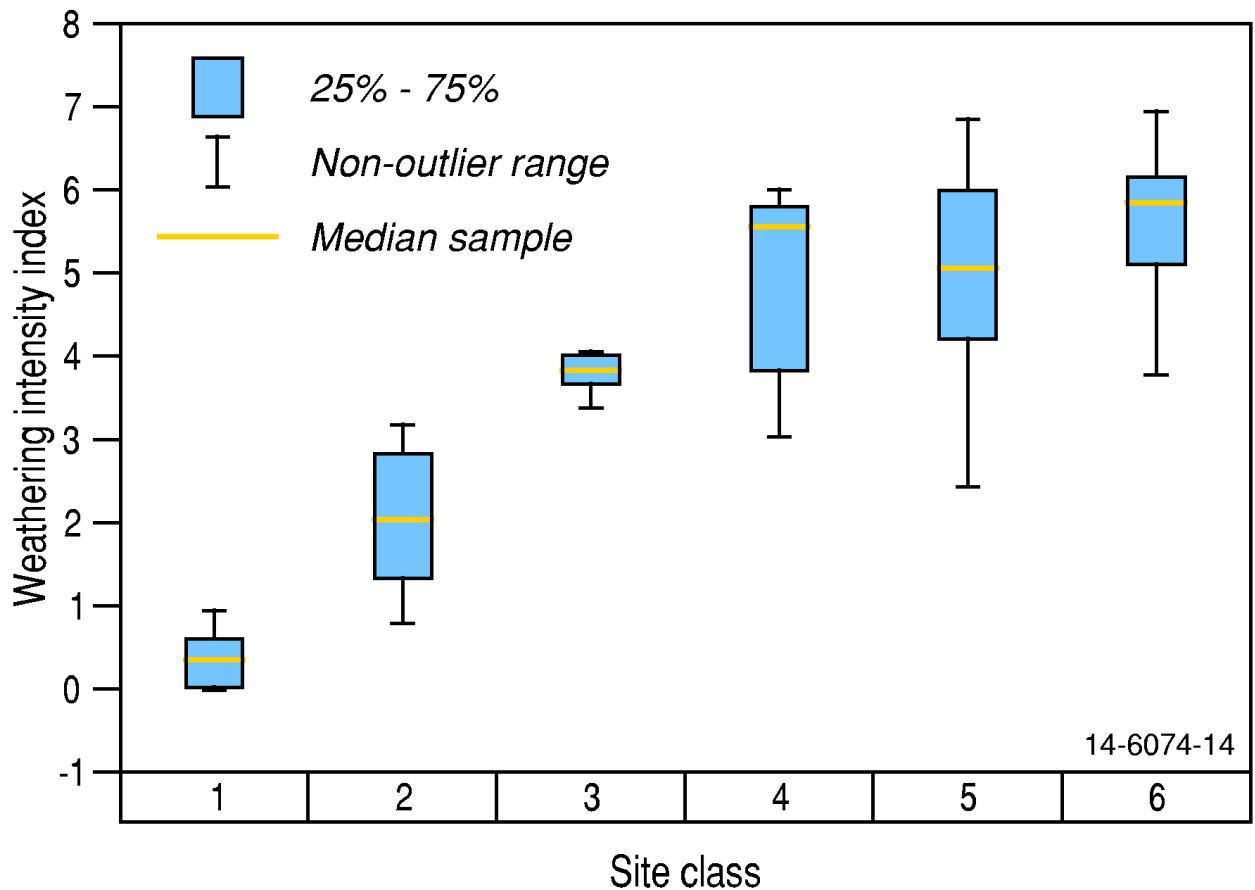
Figure 15 Correlation between interpreted weathering classes from field site descriptions over parts of the Northern Territory (Robertson et al., 2006) and the corresponding WII predictions.

The distribution of Th and U was highly variable across a range of weathering intensities. The concentration and mobilisation of these elements during weathering appears to be highly complex. The concentration, retention and loss of U and Th in the regolith is likely to vary according to the primary mineralogy of the parent material, proportion and nature of secondary clays and oxides, rock fabric and structure, geochemical and biochemical weathering conditions and pedological processes. Uranium and Th are typically associated with the silt and clay fractions of soils (Dickson and Scott, 1997) and as a consequence their distribution can be modified in the soil profile by translocation processes (e.g., illuviation/elluviation). Other studies have shown a decline in U and Th content during advanced stages of weathering as a result of desorption from oxyhydroxides (Scheepers and Rozendaal, 1993). The precipitation of U and Th in weathered volcanic and granitic bedrock in Hong Kong was shown to be highly localised and controlled by the amount of oxyhydroxides, the oxygen content of the groundwater, the rate of groundwater percolation and the presence of organic matter and bacteria within interstitial pore spaces and fractures in the weathered profile (Chan et al., 2007).
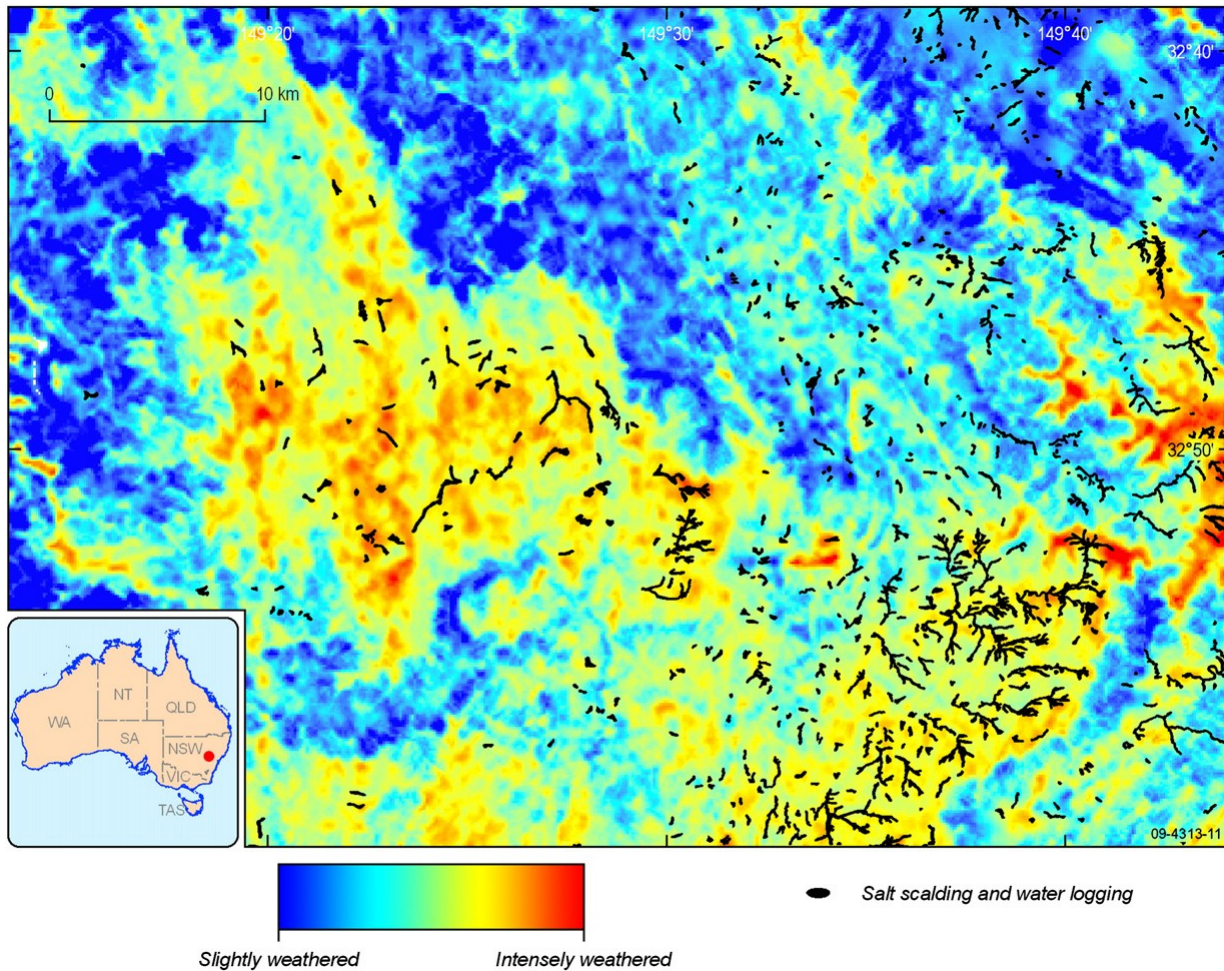
Figure 16 Correlation between high WII (reddish hues) with salt scalding and water-logging (black).

As might be expected, there is a correlation between increasing weathering intensity and decreasing relief. Relief is important in controlling soil formation through its influence in determining rates of potential soil loss vs. soil accumulation. The in-class variability of relief is relatively high, particularly at the less weathered end of the weathering spectrum. This is likely to reflect the fact that relief is only 1 of the 5 principle factors determining soil formation. The accumulation and retention of weathered materials on slopes will also depend on the cohesion strength of the regolith (Selby, 1982). Furthermore, local relief might reflect present day processes but not necessarily palaeo-landscape processes. For instance, partial incision of an old weathered surface may have similar relief characteristics to more contemporary landscapes mantled by slightly weathered bedrock. In addition, low relief will not always equate to more weathered; low relief erosional pediments with exposed bedrock near to the surface can have a similar morphology to relict flat-lying, deeply weathered palaeo-surfaces. The strength of this

technique is that the WII predictions are based on both geochemical and terrain attributes for most locations.

In considering the uncertainties in the WII it is probably more useful to interpret the data as a relative index rather than an absolute measure of weathering intensity. The model was based on training sets in eastern Australia. The extrapolated WII model assumes that these observations are representative over the whole of the continent. Weathering intensity predictions are likely to change from region to region due to changes in geology, landform and weathering histories. Customisation and calibration of the model based on local field site observations have the potential to fine tune the prediction of weathering intensity to accommodate these regional differences.

Nevertheless, preliminary interpretation of the index at both regional and local scales reveals a high degree of coherence and consistence with geomorphological principles, existing mapping, field site observation and

quantitative field measurements (e.g., geochemical weathering indices). From a statistical perspective the predictive trends are strong and robust with a relatively high degree of accuracy. The high correlation (R^2 = 0.8) between the WII and the soil-based geochemical weathering index using the Parker formula provides a quantitative and objective validation of the WII.
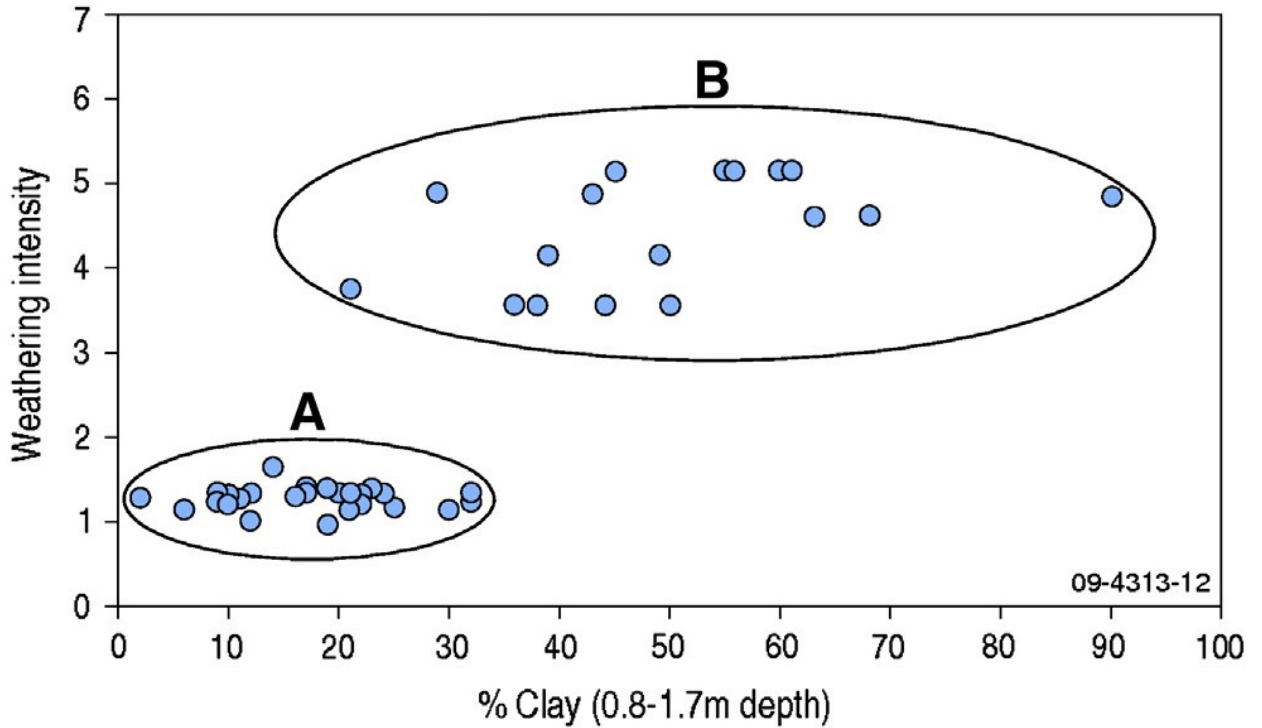
Figure 17 Correlation between the weathering intensity index and % clay in the B horizon. A — Low weathering intensities correlate with <30% clay in the subsoil; B — relative high weathering intensities correlate with >30% clay in the subsoil.
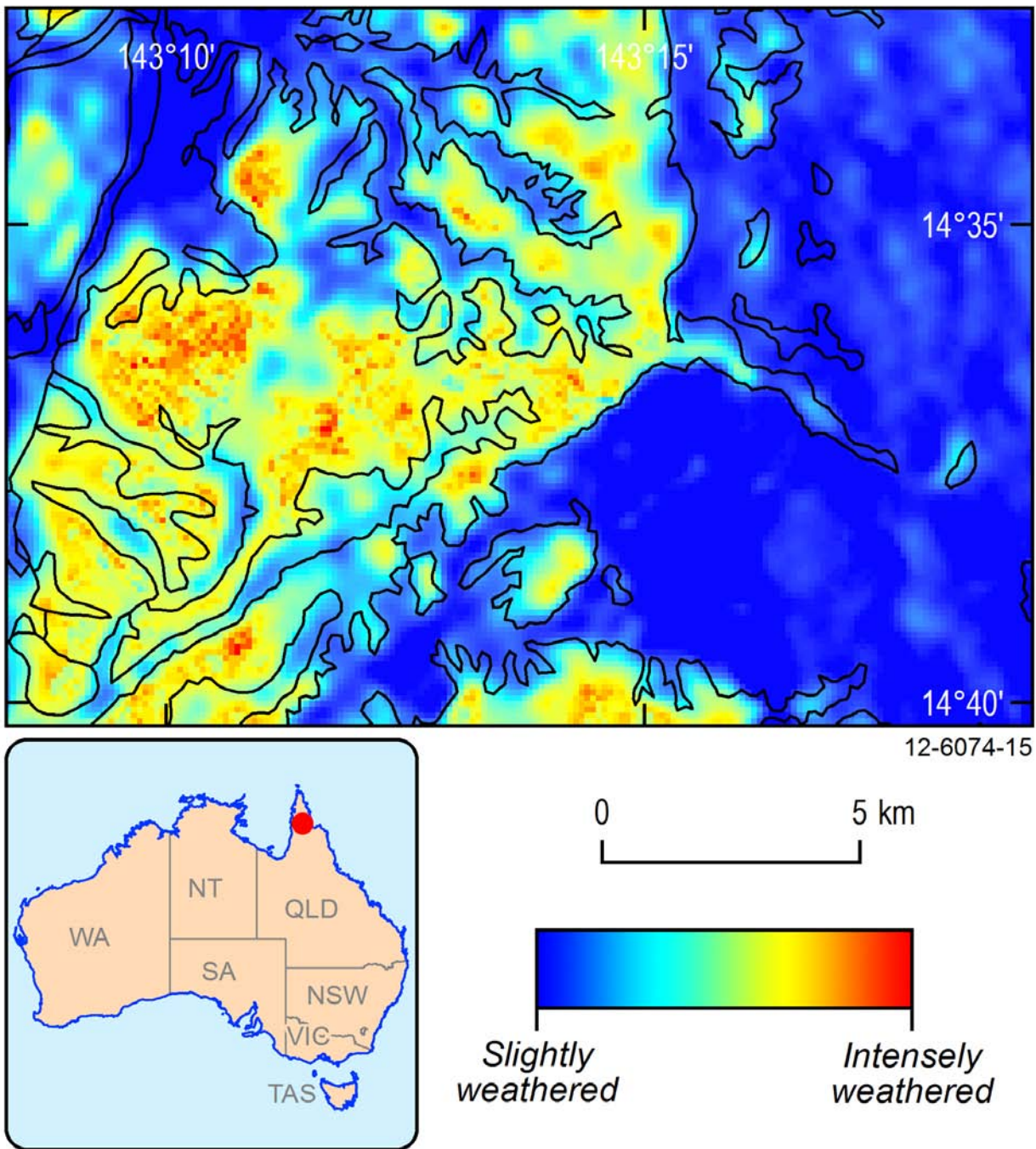
Figure 18 Highly leached sandy soils (WII red and yellow hues) developed on granitic landscapes in Cape York Peninsula. The WII prediction is largely based on the relief-based regression model.
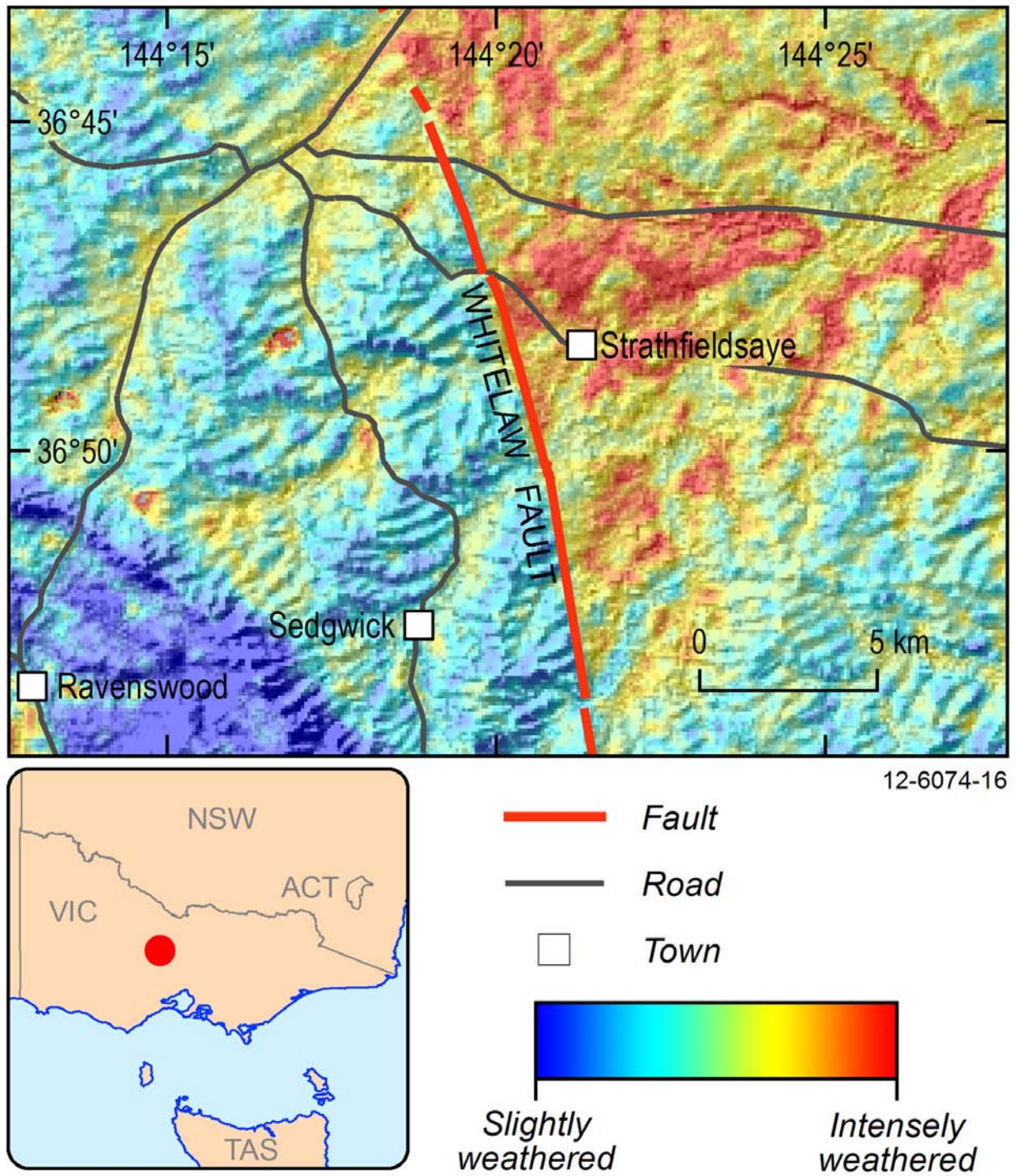
Figure 19 Weathering intensity index highlighting differences in regolith either side of the Whitelaw Fault (Cherry and Wilkinson, 1994). The active fault scarp exposes less weathered regolith on the uplifted western and more weathered regolith preserved on the lower eastern side of the fault scarp.

$y=4.0686x + 62.017$
$R^2 =0.4477$

$y=898.49x+ 4878.9$
$R^2 =0.814$
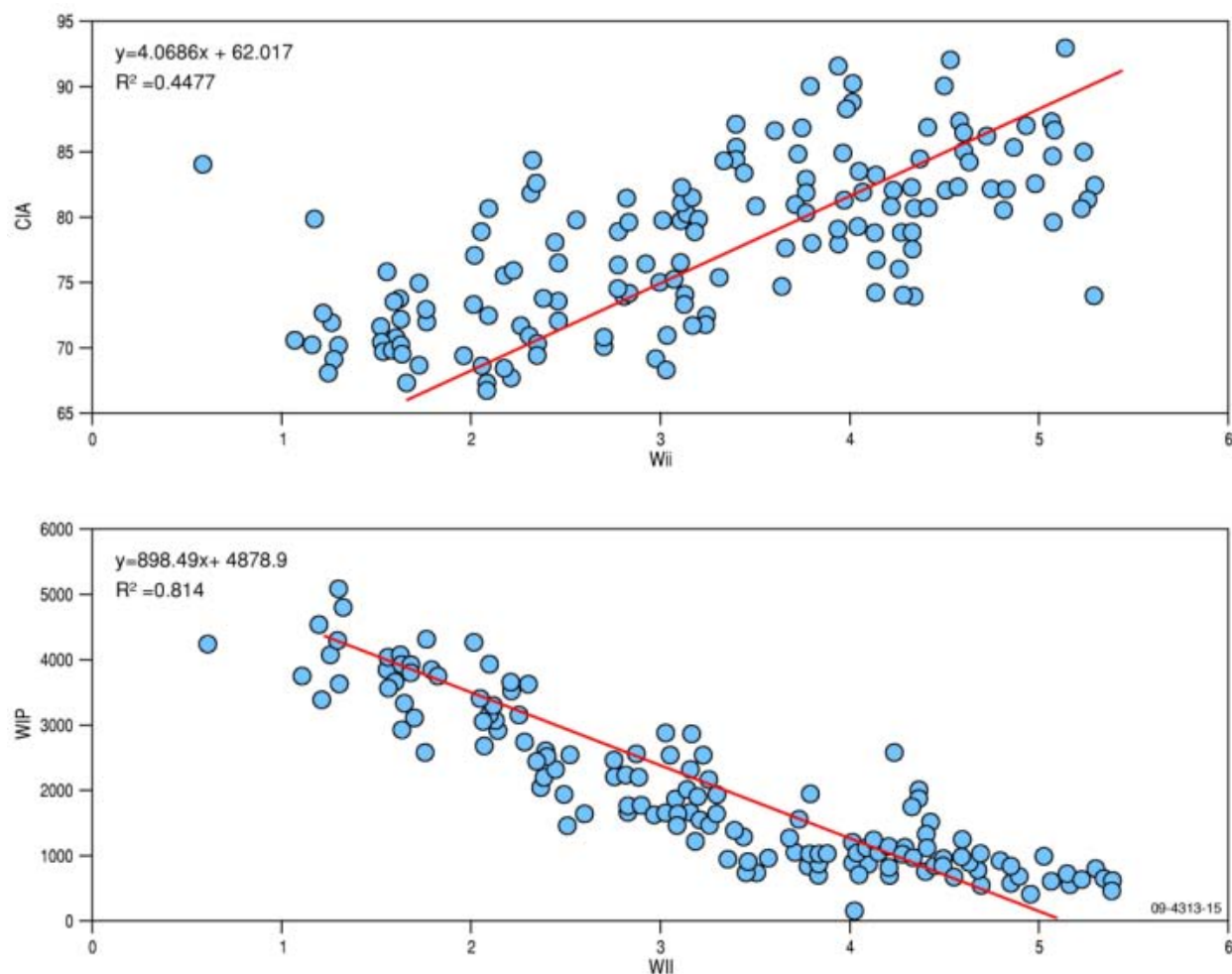
Figure 20 Correlations between the WII and the CIA index (a) and the WIP index (b).

2.6.2 Weathering intensity index a proxy for regolith thickness

Although regolith thickness was not part of the criteria used in defining the weathering intensity classes, the two components are likely to be correlated. Regolith thickness will tend to increase with increasing weathering intensity. Highly weathered landscapes predicted by the index are likely to have thicker regolith than landscapes mantled by exposed bedrock. In this sense the WII can be used as a proxy for relative regolith thickness. The controls on regolith depth are complex and relate to subsurface as well as surface weathering processes. Accurate prediction of regolith depth is unlikely from this approach, which only measures the geochemistry from the top 30–40 cm of exposed bedrock and soil. Wilford et al. (2004a) demonstrated that leaching of airborne-measured K in soils over the Central Lofty Ranges in South Australia could be used to delineate deeply weathered regolith

as measured by drilling and ground based geophysical survey. This suggests that the upper part of the weathering profile can be diagnostic of deeper characteristics like weathering depth. Correlations between the WII and clay content in the lower B horizon of soils described earlier (Figure 19) illustrate this point. Perhaps the top 30–40 cm of earth material is representative of the deeper profile characteristics due to pedoturbation processes operating within the upper part of the regolith (Wilkinson et al., 2009). The relationships between surface geochemistry and mineralogy and the nature of the underlying regolith warrants further investigation.

2.6.3 Applications

Deeply weathered regolith is a characteristic feature of the Australian landscape that in part reflects the overall low relief (i.e., high preservation potential) and lack of any substantial glaciation since the Permian that may have otherwise removed the weathered layer

and exposed bedrock at the surface. The highly weathered nature of the Australian landscape exerts a significant control on soil type and is a major factor explaining low fertility soils in Australia (McKenzie et al., 2004). In this context the WII has the potential to improve our understanding of landscape processes as well as predicting specific properties of the regolith. The value of the WII in geomorphic and pedogenetic studies, natural resource management and mineral exploration are now briefly discussed.

2.6.3.1 Geomorphic studies and pedogenesis

The Australian landscape reflects its history of weathering, erosion, burial and exhumation over long time scales (Gale, 1992; Ollier, 2001; Pillans, 2005). The WII provides information on landscape processes across different spatial scales and, when constrained by dating, across different temporal scales. The WII can be used to assess chemical and physical denudation processes, and the relative rates of regolith formation and removal. Since the weathering intensity will reflect the interplay of the 5 factors in soil formation, holding four of these factors constant will provide insights into the influence of individual factors on soil formation. For example, isolating areas with similar parent material, climate, topography and biota, but exhibit differences in weathering intensity, can be used to better understand and quantify the influence of time on soil formation. Many upland landscapes in Australia show juxtaposition of old and young geomorphic elements associated with recent and palaeo-weathering processes. This variability in many cases reflects older landscape elements that are in the process of being modified by more recent erosional processes associated with tectonic events, such as uplift, sub-continental scale warping and faulting (Sandiford et al., 2009), basin base-level changes and climate. The WII can be used to identify these different landscape elements across a range of differing landscape scales to assist in unravelling the interplay between landscape evolution, neotectonics, erosional and weathering processes (Figure 19).
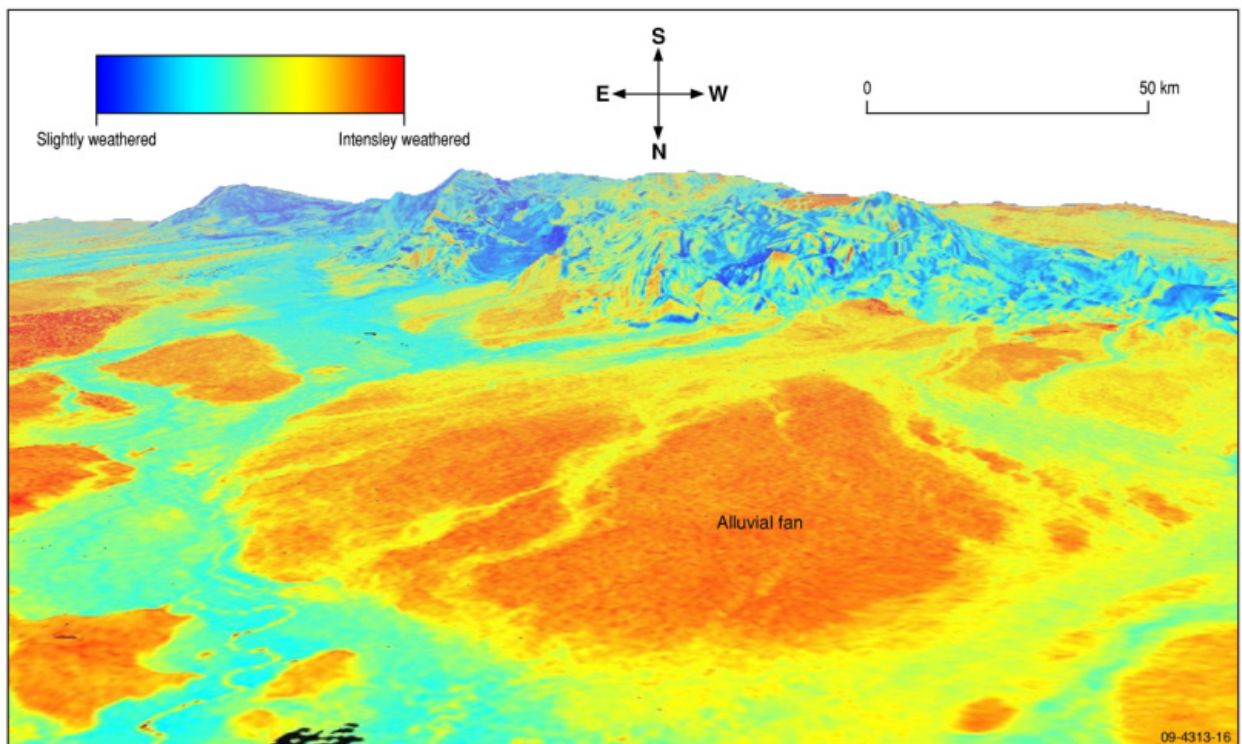
Figure 21 Foreground — inactive and highly weathered floodplain and alluvial fan systems in reddish hues: active fluvial systems in light blue hues — retaining their source rock geochemistry. Background — variably weathered hilly terrain consisting of well exposed Proterozoic rocks associated with the Mt Isa Inlier.

2.6.3.2 Digital soil mapping and natural resource management

The WII can be integrated with other datasets in conventional compilations of soil-landscape and regolith-landform maps and in developing improved quantitative methods to predict more specific soil characteristics. The latter underpins the broader discipline of digital soil mapping (DSM) which involves linking field, laboratory and environmental covariates with quantitative statistical methods to predict soil properties (Grunwald, 2009; Lagacherie et al., 2007; Henderson et al., 2005; McBratney et al., 2003; McKenzie and Ryan, 1999; Bui et al., 2006). The WII has the potential to be a key covariate in DSM.

Variation in the degree of weathering together with climate, geology, topography and vegetation all influence the distribution and movement of water in the near-surface. Specifically, the WII improves our understanding of, and our ability to reliably predict, hydropedological processes and characteristics within different landscapes. For example, the degree of weathering has a major control on the permeability and porosity characteristics of the soil and underlying saprolite, which in turn influences the manner in which water and solutes move via groundwater and interflow pathways (Acworth,1987). Prediction of regolith-water characteristics is pivotal to better understanding a broad range of natural resource issues including erosion, salinisation, water-logging, crop production, contamination and acidification (McKenzie and Jacquier, 1997). In Australia, deeply weathered landscapes often contain significant salt stores that can lead to soil salinity and saline discharge (Evans, 1998; Jenkin and Dyson 1983; Tsykin and Slessar, 1985). The WII can rapidly delineate fractured bedrock hydrological systems from more weathered regolith-controlled hydrological systems. More generally the index can be used to characterise and understand processes occurring in the regolith where life supporting hydrological and biogeochemical cycles operate (Lin, 2010) — since interactions between soil, water, air and biota within the near-surface terrestrial environment are likely to change with increasing weathering intensity.

2.6.3.3 Mineral exploration

The WII provides better insights into the modification of mineralised bedrock by weathering and leaching processes. Weathering can dilute or enrich pathfinder elements at the surface. Information on the degree of weathering should be used in refining the interpretation of and/or the planning of geochemical exploration surveys for mineral exploration. The WII, in combination with regolith mapping tailored for geochemical exploration (Craig, 2001), can be used to improve our understanding of the distribution and origin of regolith materials and their geochemical characteristics. The index allows surface geochemical surveys to be interpreted in the context of variably weathered and leached landscapes. It also has the potential to provide information on secondary enrichment processes that involve the leaching and redistribution of elements within the regolith (e.g., palaeo-channel U-bearing calcrete deposits).

2.6.3.4 The global context

Australia is fortunate to have an extensive and well calibrated gamma-ray coverage at moderate to high resolution (Minty et al., 2009), without which this type of continental-scale analysis would not have been possible. Data acquisition in Australia was driven initially for mineral exploration, particularly U, and more generally for geological mapping. These drivers are likely to be similar in other countries, since most of the gamma-ray datasets reside in national geological surveys. However, globally, with few exceptions, gamma-ray survey data is either not available, or where it has been acquired it has limited spatial coverage or is of poor resolution. For example, there is a national coverage over the United States but the data has been collected at broad 1.6–10 km flight-line spacing (Duval, 1990). In Australia it was not until the mid-1990s that the value of gamma-ray data for soil mapping became widely recognised. The benefits of gamma-ray data for soil mapping, understanding earth surface processes and natural resource management including environmental geochemistry, together with its traditional use in mineral exploration, are all considered in prioritising funding for data acquisition. Gamma-ray imagery is now a critical covariate in predicting soil characteristics using digital soil mapping approaches in Australia. Similar uses of the data are being demonstrated from pilot airborne gamma-ray surveys in Europe (Rawlins et al., 2007, 2009). Broader applications of the gamma-ray data need to be argued to facilitate greater acquisition in other countries.

2.7 Conclusions and future work

A WII has been developed for landscapes over the Australian continent based on the distribution of radioelements measured from airborne gamma-ray spectrometry and a terrain relief model based on the SRTM DEM. Weathering intensity is a fundamental property of the regolith that reflects changes in the geochemical, physical and hydrological characteristics as the bedrock transitions from unweathered through to intensely weathered and leached bedrock. The WII, therefore, has broad application in understanding weathering and geomorphic processes across a range of spatial and temporal landscape scales and in mapping specific regolith properties. However, the use of the WII should be predicated by the potential limitations of the technique both in terms of the inherent characteristics of the input datasets and the statistical model. The use of other geostatistical techniques such as regression kriging and decision tree analysis with additional covariates such as landscape position and climate has the potential to improve predictive power of the WII.

Future work will explore the integration of the WII with other complementary datasets for digital soil/regolith mapping. Refinements to the model prediction taking into account more subtle changes in bedrock geochemistry will be investigated.

The Australian continent exhibits a range of landscapes with differing ages and with varied climates. The effective use of the WII in Australia suggests that it has broader application globally. Evaluation of the index within more youthful glaciated landscapes of North America and Europe warrants further investigation.

Acknowledgements

Chapter 3

Digital mapping of regolith carbonate in the Australian regolith using environmental covariates

3 Digital mapping of regolith carbonate in the Australian regolith using environmental covariates

John Wilford[1], Patrice de Caritat[1], Elisabeth Bui[2]

[1]Geoscience Australia, GPO Box 378, Canberra ACT 2611, Australia

[2]CSIRO Land and water, Christian Laboratory, Clunies Ross Street Black Mountain ACT 2601 Australia

Low relief and carbonate rich landscapes of the Gawler region in South Australia, approximately 110km north-west of Tarcoola. Photographs illustrate the close geo-botanical associated between vegetation and regolith carbonates. Blue bushes (Maireana sedifolia sp) are associated with alkaline rich soils. B-Carbonate nodules and granules are a typical of the soils in the region. Chapter 3 describes a method to map near-surface carbonate through establishing correlations between climate, landform, regolith, geology and vegetation.

Summary

Regolith carbonate, or secondary carbonate is a key component of the regolith, particularly in many arid and semi-arid regions of Australia. Regolith carbonate influences major soil attributes and is an important component of inorganic carbon soil stores. Regolith carbonate is also an important sampling medium in mineral exploration, particularly for gold. National maps of regolith carbonate distribution have been compiled from regional soil, regolith and geological mapping with varying degrees of confidence and consistency. Here we apply a piecewise linear decision tree approach to model and map the near-surface regolith carbonate concentration at the continental scale in an internally consistent manner. The model is based on relationships established from the 1311 field sites of the National Geochemical Survey of Australia (NGSA) and 49 national environmental covariate datasets, including rainfall, slope, and airborne gamma-ray spectrometric response. Regolith carbonate concentration (weight percent) was averaged from the <2 mm grain size-fractions of samples taken from two depth ranges (0-10 cm and ~60-80 cm) at each NGSA site. The final model is based on the average of twenty runs generated by randomly selecting 90% training and 10% validation splits of the input data. Results present an average coefficient of determination (R^2) of 0.56 on the validation dataset. The covariates used in the prediction are consistent with our understanding of the controls on the sources (inputs), preservation and distribution of regolith carbonate within the Australian landscape. The model produces a continuous, quantitative prediction of regolith carbonate abundance in surficial regolith with associated estimates of model uncertainty. The model-derived map is broadly consistent with our current knowledge of the distribution of carbonate-rich soil and regolith in Australia. Thus this methodology allows the rapid generation of an internally consistent and continuous layer of geoinformation that may be applicable to other carbonate-rich landscapes globally. Identified inconsistencies between model prediction and prior knowledge require further investigation and field validation. Future sampling across toposequences and different bedrock types would improve the prediction at the local landscape scale.

3.1 Introduction

In contrast to primary carbonate, which is associated with carbonate-bearing rocks (e.g. limestone, marble), secondary carbonate accumulates in the regolith (i.e. the regolith comprises all weathered material above fresh bedrock, including soil) through a process of calcification (Lal and Kimble, 2000; Schaetzl and Anderson, 2005). The carbonate concentration influences soil pH and a range of other regolith properties including texture, porosity, permeability, hydraulic conductivity, soil structure, and cation exchange capacity (Peverill et al., 2001). In terms of global carbon accounting and modelling the amount of carbon contained in regolith carbonate is similar to that stored in the atmosphere (Dart et al., 2007). Accordingly, regolith carbonate forms a key part of the terrestrial pool of inorganic carbon. The stable isotopic composition of secondary carbonates in soils has been used to reconstruct palaeoclimatic fluctuations and changes in C3/C4 vegetation patterns (e.g. Cerling, 1984; Schlesinger and Pilmanis, 1998). Secondary carbonate also plays an important role in mineral exploration where it can be used as a geochemical sampling medium for locating areas of potential gold

mineralisation (McQueen et al., 1999; Lintern et al., 2006) and copper, zinc, nickel, and cobalt (McQueen, 2006). Groundwater-related carbonate deposits are also known to act as a trap for uranium mineralisation (e.g. U-calcrete deposits; Butt et al., 1977).

Carbonate in the regolith can appear as either finely disseminated powder not visible to the naked eye or as visible carbonate accumulations; either way its presence can be detected or confirmed using various field and laboratory techniques (e.g. acid effervescence, X-Ray Diffraction, X-Ray Fluorescence). Caliche, travertine, kunkar and calcrete are all terms used to describe secondary carbonate accumulations in the weathered zone. Of these, calcrete is probably the most widely used term referring to regolith carbonate accumulations that are composed dominantly of calcite ($CaCO_3$) but which can also include Mg-substituted calcite and dolomite (Milnes and Hutton, 1983; Bui et al., 1990; Eggleton, 2001). Here we use the term regolith carbonate (Hill et al., 1999) to encapsulate all forms of secondary carbonate. Regolith carbonates are broadly divided into two main genetic types: (1) pedogenic and (2) groundwater carbonates. Pedogenic carbonates are associated with soil-forming processes related to the movement of air

and water through the soil profile, such as eluviation/illuviation processes, waterlogging (e.g. wetting and drying cycles), and biological activity (e.g. root respiration).

The chemical reactions involved in the precipitation and dissolution of carbonate within the soil profile are expressed by the following series of general reactions (e.g. Schaetzl and Anderson, 2005):

Water combines with atmospheric and soil carbon dioxide to form weak carbonic acid (H_2CO_3):

$$H_2O + CO_2 \leftrightarrow H_2CO_3 \qquad \text{Eqn. (1)}$$

Carbonic acid reacts with calcium carbonate ($CaCO_3$) to produce mobile calcium (Ca^{2+}) and bicarbonate (HCO_3^-) ions:

$$H_2CO_3 + CaCO_3 \leftrightarrow Ca^{2+} + 2HCO_3^- \qquad \text{Eqn. (2)}$$
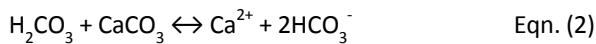
Under favourable conditions (decreasing moisture and carbon dioxide or increasing pH) secondary carbonate precipitates; opposite conditions leads to dissolution:

$$Ca^{2+} + 2HCO_3^- - H_2O \leftrightarrow CaCO_3 + CO_2 \qquad \text{Eqn. (3)}$$

Pedogenic carbonates form in the unsaturated (vadose) zone of the regolith profile or in perched watertables when they become saturated with respect to carbonate minerals (e.g. in E-horizons). In contrast, groundwater carbonate forms where carbonate-rich groundwater precipitates carbonate minerals and is typically associated with valley floors and groundwater discharge sites. Groundwater carbonate is common within the axis of palaeo-channel systems in semi-arid central and Western Australia where groundwater becomes saturated with respect to carbonate minerals. These carbonates typically form narrow sinuous deposits often referred to as 'valley calcretes' (Butt et al., 1977; Mann and Horwitz, 1979; Arakel, 1986; Chen et al., 2002).

A necessary condition for calcite to precipitate is that its saturation index (SI) must approach or exceed zero, where SI is defined as:

$$SI = \log[(a_{Ca2+} \times a_{HCO3-}) / K_{sp}] \qquad \text{Eqn. (4)}$$

and a_i is the activity of species i, and K_{sp} is the solubility product of calcite. Other conditions also need to be fulfilled for nucleation to occur, and kinetics have to be favourable (Schaetzl and Anderson, 2005).

At any given temperature, K_{sp} is fixed, so in order for a dilute solution to approach calcite saturation (increase SI) the activity of Ca^{2+}, the activity of HCO_3^-, or both must increase (Eqn. 4). The activity of Ca^{2+} can increase through either *in situ* dissolved calcium production by dissolution of calcium-rich minerals from parent rocks, cation exchange and desorption/leaching of surface-bound Ca^{2+}, or via calcium input from external (usually atmospheric) sources, such as dust, sea-spray or rainfall (Monger and Gallegos, 2000). For the activity of HCO_3^- to increase, CO_2 from the atmosphere must combine with water to form carbonic acid (Eqn. 1), which then readily dissociates to produce HCO_3^- and H^+. Extensive Cenozoic limestone associated with the Nullarbor Plain (Eucla Basin, Figure 22 – straddling the border between Western Australia and South Australia) is a major source of secondary regolith carbonate (Miller et al., 2012). External atmospheric sources of calcium are also significant in Australia. Strontium (Sr), like calcium, is an alkaline earth cation that can substitute for calcium in calcite and other carbonates. Strontium isotope ($^{87}Sr/^{86}Sr$) studies in Australia and elsewhere have indicated a predominantly marine source for strontium (and by inference, calcium) found in regolith carbonates (Quade et al., 1995; Capo and Chadwick, 1999; Chiquet et al., 1999; Naiman et al., 2000; Dart et al., 2007).

Regolith carbonate is found across approximately 21% (Chen et al., 2002) to 50% (Fitzpatrick and Merry 2000) of the Australia continent and is most abundant in Mediterranean, arid, and semi-arid regions where average annual rainfall is low (< 400mm) and evaporation significantly exceeds precipitation. Soil, regolith and geological maps are currently the main source of information characterising the distribution of regolith carbonate in Australia. National coverages are produced only at low resolution (> 1:1 million scale), whereas more accurate information associated with 1:100 000 and 1:50 000 scale mapping has limited spatial coverage. The continental map compiled by Fitzpatrick and Merry (2000) was derived by re-interpretation of the Northcote et al. (1960-1968) map published at 1:2 million scale. Inconsistency in capturing carbonate attributes during map compilation

has led to mismatches between adjoining map sheets (Chen et al., 2002). Earth scientists with different backgrounds and expertise place different degrees of emphasis on recording or mapping regolith carbonate. For example, the regolith carbonate map produced by Chen et al. (2002) underestimates carbonate extent because it was produced essentially by geologists focused on calcrete whereas the pedogenic carbonate map produced by Fitzpatrick and Merry (2000), that showed the distribution of soils that are calcareous throughout the upper one meter (30% of continent) as well as those with calcareous subsoils (19% of continent), was derived by pedologists. Nevertheless soil maps can underestimate the distribution of regolith carbonate; for example, the presence of carbonate in red-brown hard-pans, that frequently contain very finely dispersed calcium carbonate in partly silicified and ferruginous matrices is not always recorded in soil-landscape descriptions. Red-brown hard-pans are believed to be a more recent material developed in alluvium and colluvium in the lower parts of ferricrete-mantled landscapes and to be restricted to environmental conditions that favour the accumulation and formation of certain iron, silica, and carbonate compounds in high base-status weathering environments of hot and dry climates (Fitzpatrick, 1988; Wright, 1984).
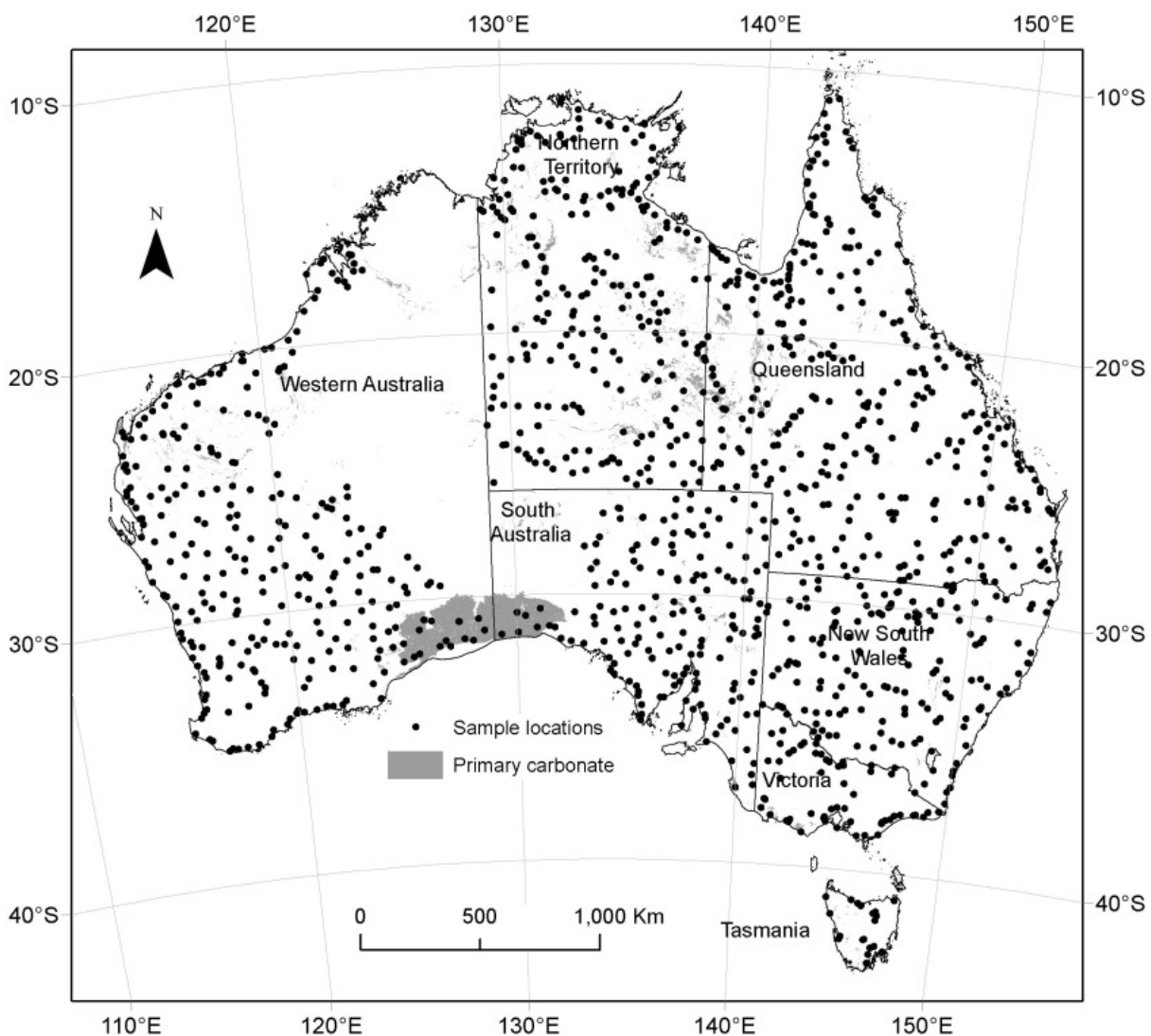
Figure 22 Location of NGSA samples used in the model (Caritat and Cooper 2011) and distribution of primary carbonate bedrock (shaded).

Over the last 10-15 years a number of advances in technology and data availability have facilitated a rapid development in quantitative modelling of soil/regolith, generally termed Digital Soil Mapping (DSM) (McBratney et al., 2003). DSM is a quantitative approach that predicts individual soil properties with statistically determined accuracy and precision (McBratney et al., 2003). Environmental correlation is an DSM approach that establishes predictive relationships at specific locations between a soil or regolith property and variables derived from other covariate datasets such as terrain (e.g. slope, relief) and climate (e.g. rainfall, temperature) (McKenzie and Ryan, 1999). In this paper we apply an environmental correlation approach to predict and map the distribution of regolith carbonate with the aims of: (1) addressing inconsistencies and gaps in the existing national map coverages of regolith carbonate, and (2) improving our understanding of the environmental controls on regolith carbonate spatial distribution. The modelled spatial distribution of regolith carbonate presented herein is discussed in the context of our current knowledge of carbonate formation and distribution from existing soil and geological mapping.

3.2 Methods

3.2.1 Modelling approach

Relationships between regolith carbonate distribution and environmental covariates (e.g. rainfall, parent material, terrain, vegetation) are explored using the machine learning decision tree software 'Cubist' (www.rulequest.com). 'Cubist' has been used effectively in predicting soil properties at the national scale in previous studies (Henderson et al., 2005; Bui et al., 2009). The 'Cubist' model structure consists of a decision-based component coupled with multiple piecewise linear regression models. Continuous and categorical variables can be used in the decision tree to split the data into more homogeneous sub-regions. Splits in the decision tree are based on recursive partitioning of the prediction variable to minimise the standard deviation across all potential splits (Henderson et al., 2005). Predictions within these sub-regions are then explained using linear regression models. This nested modelling approach enables local linear segments of the data to be captured from an otherwise poorly correlated dataset or one that exhibits non-linearity. The 'Cubist' model rule-set is expressed as paired conditional statements and associated linear models as shown in the example below (where c1, c2 and c3 are constants).

1. If (conditional statement; decision tree splits)

    Relief < 50 m
        Gamma-ray K > 2.1 %
        Lithology = (siltstone, sandstone, metasediment)

2. Then (linear model)

    Property = c1 * rainfall + c2 * slope + c3 *gamma-
        ray K

Being explicitly expressed, rules can be evaluated with expert knowledge and compared with conceptual models of landscape and soil development. Where more than one rule explains the prediction response the average of the rule predictions is used for the final model.

3.2.2 Environmental correlation

Two types of datasets are used: (1) environmental explanatory variables or covariates for prediction, and (2) site data used to train and establish correlations between the covariates and the target variable, in this case regolith carbonate in wt %. Accurate, consistent and representative measurement of regolith carbonate is critical in developing robust predictive models. For this study we rely on existing geochemical data, as quantitative mineralogical information on carbonate concentration is generally not recorded in soil databases. In this study the recently released National Geochemical Survey of Australia (NGSA; Caritat and Cooper, 2011) was used to derive estimates of near-surface regolith carbonate concentration. Other available geochemical databases from mining companies and government agencies were not included due to differences in sampling procedures and analytical methods. The covariates used in the model and the characteristics of the site data, including the procedure to convert measured calcium concentration to estimated calcite abundance, are described below.

3.2.3 Covariates

The covariates are selected to broadly represent the soil-forming factors described by Jenny (1941) through the following formula:

$$S = f\,(cl,o,r,p,t)$$

where the soil in its current state (S) is a function (f) of soil forming factors representing climate (cl), biological organisms (o), relief (r), parent material (p) and time (t). This equation was modified by McBratney et al., (2003) to include spatial position where the soil (S) property or class is a function of climate (C), organisms/vegetation (O), relief (R), parent material (P), age (A) and spatial position (N) (i.e. SCORPAN). A set of environmental covariates were then compiled to represent (act as proxies) these SCORPAN soil formation factors, and more specifically to this study, the accumulation and preservation of regolith carbonate in the landscape. The age (time) component is difficult to assess, particularly over large areas. However, a weathering intensity covariate (Table 5) provides a relative measure of the degree to which the surface is weathered, which will, in part, relate to surface age or the relative rates of regolith formation versus removal (Wilford, 2012). The major covariate themes used in the model prediction are briefly summarised below and are detailed further in Table 5.

3.2.4 Soil and geological maps

A digital version of the Atlas of Australian Soils at 1:2 million scale (Northcote et al., 1960-1968) was used to define major soil types re-classified at the Soil Order level of the Australian Soil Classification (ASC, Isbell et al., 1997). The 1:1 million Surface Geology of Australia provides information on parent material type (Raymond, 2012). Geological units were classified into consolidated (bedrock) and unconsolidated materials (e.g. colluvium and alluvial sediments). Further sub-divisions were based on the silica content of the bedrock and textural and compositional criteria.

3.2.5 Climate

A series of climate variables (e.g. average annual rainfall, annual mean radiation and temperature: Table 5) were generated using the ANUCLIM program (Xu and Hutchinson, 2011). The ANUCLIM model interpolates as series of climatic surfaces based on long-term weather station observations (daily records and monthly averages) and a 9 arc second resolution digital elevation model (Hutchinson et al., 2008). Climate variables were gridded to 250 m.

3.2.6 Vegetation

Information on vegetation was derived from Landsat Thematic Mapper (TM) and Moderate Resolution Imaging Spectro-radiometer (MODIS) satellite imagery. Landsat TM bands 1 and 3 correspond to absorption features related to chlorophyll pigments, while bands 2 and 4 correspond to green vegetation reflection peaks. We included MODIS imagery that was processed to derive 12 coefficients based on Enhanced Vegetation Index (EVI) time-series data from 2000 to 2008 (Tan et al., 2009; Lymburner et al., 2011). These coefficients relate to a range of phenological parameters and include EVI statistics including mean, standard deviation, flatness, rate of rise, rate of drop, global minimum, average length of the growing cycle, global maximum, maximum ratio, mean of the timing of the maximum, standard deviation of the timing of the maximum and annual minimum greenness (Table 5). These EVI coefficients have been used to identify different vegetation communities (Lymburner et al. 2011). The time series coefficients also have the potential to highlight relationships between vegetation and soils. For example, the rate of greenness decline reflected in the rate of drop coefficient will relate to climate and vegetation type and also to the water holding capacity of the soil.

3.2.7 Terrain

Terrain attributes were derived from an improved version of the 3 arc second (90 m) Shuttle Radar Topographic Mission (SRTM) digital elevation model. The improved version has vegetation features removed and is smoothed to reduce noise (Gallant et al., 2011) and was used to generate several terrain covariates (Table 5) that capture variations in surface morphology.

3.2.8 Remotely-sensed mineralogy and geochemistry

Multi-spectral Landsat Thematic Mapper (TM) imagery and airborne gamma-ray spectrometric imagery provided information on surface and near-surface

mineralogy and geochemistry (http://landsat. gsfc.nasa.gov/; Wilford and Minty, 2007). Landsat TM bands 1-4 correspond to various diagnostic iron spectral features. Band 5 corresponds to maximum reflectance responses for most soils and rocks, while band 7 covers the absorption region of Al-OH and Mg-OH bearing minerals, including clays. Airborne gamma-ray spectrometric data measures the surface concentration of three gamma-ray emitting radioelements including potassium (K), thalium (the equivalent of thorium - eTh) and bismuth (the equivalent of uranium - eU) (Wilford and Minty, 2007). The distribution of these elements varies in response to bedrock type and secondary weathering processes and soil formation (Wilford, 2012). Individual and ratio grids for K, eTh and eU were compiled from the radiometric map of Australia (Minty et al., 2009). Gaps in the radiometric map were filled by inclusion of gridded data from the Australia-Wide Airborne Geophysical Survey (AWAGS; http://www.ga.gov.au/ ausgeonews/ausgeonews200812/radiometrics.jsp).

Table 5 Environmental covariate predictive variables used in the calcite model, their contributions, key references and sources.

Theme	Covariate name	Description	Pedogenic/geomorphic contribution and key soil forming factors (cl=climate, o=organisms, r=relief, p=parent material, and t=time)	Source data / reference
Geology, soils, surface geochemistry	Geology	Re-classification of units based on silica content and texture	Parent materials and sediments (p)	Geoscience Australia (Raymond, 2012)
	Soil class	Australian Soil Classification (ASC)	Major soil types (pre-existing soil knowledge)	1:2 m soil mapping (Northcote et al., 1960-1968)
	Rad K	Airborne gamma-ray derived K %	Surface mineralogy and geochemistry, degree of weathering. (p, t)	Modified from Minty et al. (2009)
	Rad Th	Airborne gamma-ray derived thallium-208 to infer Th ppm	Surface mineralogy and geochemistry, degree of weathering. (p, t)	Modified from Minty et al. (2009)
	Rad U	Airborne gamma-ray derived bismuth-214 to infer U ppm	Surface mineralogy and geochemistry, seepage zones (p, t)	Modified from Minty et al. (2009)
	Rad Total	Airborne total count :weighted total of K, Th and U	Surface mineralogy and geochemistry, degree of weathering (p, t)	Modified from Minty et al. (2009)
	Ratio Th/K	Ratio of airborne thorium / potassium	Freshness and degree of weathering (p, t)	Modified from Minty et al. (2009)
	Ratio U/K	Ratio of airborne uranium / potassium	Freshness and degree of weathering (p, t)	as above Modified from Minty et al. (2009)
	WII	Weathering intensity index	Degree of weathering and leaching (p,t)	Wilford, 2012
Climate	Aus20	Annual mean radiation. The mean of all the monthly radiation surfaces	Soil temperate, evaporation rates and weathering rates (cl, o)	Xu and Hutchinson (2011)
	Aus12	Mean annual precipitation	Soil wetness; weathering rates (cl, o)	Xu and Hutchinson (2011)
	Aus01	Mean temperature	Soil temperature, weathering rates (cl, o)	Xu and Hutchinson (2011)
	Aus44	Precipitation minus potential evaporation	Annual water deficit, weathering rates (cl, o)	Xu and Hutchinson (2011)

Theme	Covariate name	Description	Pedogenic/geomorphic contribution and key soil forming factors (cl=climate, o=organisms, r=relief, p=parent material, and t=time)	Source data / reference
	Aus43	Total annual evaporation (pan evaporation)	Annual water deficit, weathering rates (cl, o)	Xu and Hutchinson (2011)
	Prescott	Prescott Index or leaching index	Water balance, weathering rates (cl o)	CSIRO (Prescott, 1948)
	Aus40	Autumn & winter rainfall totals	Water balance, weathering rates (cl, o)	Xu and Hutchinson (2011)
	Aus41	spring & summer rainfall totals	Water balance, weathering rates (cl, o)	Xu and Hutchinson (2011)
	Aus42	Ratio (spring & summer rainfall/autumn & winter rainfall)	Water balance, weathering rates (cl, o)	Xu and Hutchinson (2011)
	Aus28	Annual mean moisture index	Water balance, weathering rates (cl, o)	Xu and Hutchinson (2011)
	Aus30	Lowest period moisture index	Water balance, weathering rates (cl, o)	Xu and Hutchinson (2011)
	Aus06	The minimum temp of the coldest period	Soil temperate, water balance, weathering rates (cl, o)	Xu and Hutchinson (2011)
	Aus29	Highest period moisture index	Water balance, weathering rates (cl, o)	Xu and Hutchinson (2011)
	Aus13	Precipitation of the wettest period.	Water balance, weathering rates (cl, o)	Xu and Hutchinson (2011)
	Aus31	Moisture index seasonality	Water balance, weathering rates (cl, o)	Xu and Hutchinson (2011)
Vegetation	MODIS 1	Mean	Vegetation, biota (o, cl, p)	Tan et al. (2009), Lymburner et al. (2011)
	MODIS 2	Standard deviation	Vegetation, biota (o, cl, p)	Tan et al. (2009), Lymburner et al. (2011)
	MODIS 3	Flatness	Vegetation, biota (o, cl, p)	Tan et al. (2009), Lymburner et al. (2011)
	MODIS 4	Rate of rise	Vegetation, biota (o, cl, p)	Tan et al. (2009), Lymburner et al. (2011)
	MODIS 5	Rate of drop	Vegetation, biota (o, cl, p)	Tan et al. (2009), Lymburner et al. (2011)
	MODIS 6	Global minimum	Vegetation, biota (o, cl, p)	Tan et al. (2009), Lymburner et al. (2011)
	MODIS 7	Avg. Length of a cycle	Vegetation, biota (o, cl, p)	Tan et al. (2009), Lymburner et al. (2011)
	MODIS 8	Global maximum	Vegetation, biota (o, cl, p)	Tan et al. (2009), Lymburner et al. (2011)
	MODIS 9	Max ratio	Vegetation, biota (o, cl, p)	Tan et al. (2009), Lymburner et al. (2011)
	MODIS 10	Mean of the timing of the maximum	Vegetation, biota (o, cl, p)	Tan et al. (2009), Lymburner et al. (2011)
	MODIS 11	Standard deviation of the timing of the maximum	Vegetation, biota (o, cl, p)	Tan et al. (2009), Lymburner et al. (2011)

Theme	Covariate name	Description	Pedogenic/geomorphic contribution and key soil forming factors (cl=climate, o=organisms, r=relief, p=parent material, and t=time)	Source data / reference
	MODIS 12	Annual minimum	Vegetation, biota (o, cl, p)	Tan et al. (2009), Lymburner et al. (2011)
Terrain	Elevation	90 m Shuttle Radar Topographic Mission (SRTM) digital elevation model	Climate, temperature, rainfall; vegetation (o, r)	Gallant (2011)
	MrVBF	Identifies locally low-lying landscape zones, i.e. valley floors	Zones of deposition and erosion (r)	Gallant and Dowling (2003)
	Aspect	Aspect derived from the 90 m SRTM	Micro climate, vegetation type; (cl,o)	Gallant (2011)
	Relief	Elevation range within a 270 m radius – using 90m SRTM	Rates of erosion and deposition (r,)	Gallant (2011)
	Median relief	Median relief over a 300m radius circle	Erosional and depositional processes (r)	Gallant (2011)
	Slope	Rate of elevation fall. Using the 90 m SRTM	Surface flow acceleration; rates of mass wasting (r, o)	Gallant .(2011)
	TPI	Topographic position index Using the 90 m SRTM	Landscape position – upper – mid slopes and valleys floors	Geoscience Australia
Multispectral satellite	TM1-TM6	Landsat Thematic Mapper (TM) Bands 1-6	Surface mineralogy and vegetation (p, o)	Geoscience Australia

3.2.9 Site data - sampling and analytical methods

The National Geochemical Survey of Australia (Caritat and Cooper, 2011) collected both a surface (0-10 cm depth range) and sub-surface (60-80 cm depth range) regolith sample from each sampling site. The sampling medium was catchment outlet sediments, i.e. floodplain or similar landforms, which in most cases correspond to fine-grained overbank alluvial sediments. The samples are referred to as the top outlet sediment (TOS) and bottom outlet sediment (BOS) respectively. The NGSA collected a total of 1315 samples from 1186 catchments across Australia (including field duplicates), equating to an average sample density of 1 site per 5200 km^2 (Figure 22). In the present study geochemical data for TOS and BOS samples from only 1311 sites are utilised, due to two sites missing covariate data and a further two sites missing the relevant analytical data.

Collection and preparation of the NGSA samples is described in Caritat et al. (2009). In this study we only use the <2 mm rather than the finer (< 75 microns) grain-size fraction, as the coarser split is more likely to represent the bulk composition of the sample. We also combine and averaged the TOS and BOS sample data to estimate carbonate in the near-surface zone (i.e. the upper 80 cm). The suite of elements for which the NGSA samples were analysed and the various digestion and analytical methods used are described by Caritat et al. (2010).

3.2.10 Normative carbonate calculation

The total calcium oxide (CaO) concentration recorded by X-Ray Fluorescence (XRF) in the NGSA geochemical database was used to calculate a normative abundance of calcite in the samples based on the linear programming code 'LPNORM' (Caritat et al., 1994). Two Ca-bearing minerals were explicitly included in the calculation: gypsum (CaSO$_4$.2H$_2$O) and calcite (CaCO$_3$).

The abundance of gypsum, the only S-bearing mineral considered, was calculated from the measured S concentration, with the 'remaining' CaO stoichiometrically attributed to normative calcite (hereafter referred to as *cal**). Furthermore if Loss on Ignition (LOI; a proxy for CO_2) was not high enough for the amount of *cal**, then the latter was reduced to be consistent with LOI. Although we are specifically predicting calcium carbonate in the regolith, where Mg is soluble in the soil, Mg carbonates could be present.

A characteristic feature of carbonate-rich soils is that they are highly alkaline, with pH values between 8 and 9.5, although some highly leached sandy soils and gradational clay loams with calcareous lower horizons can have pH values around 6.5 in the upper part of the profile (Hall et al., 2009). Using the field-recorded soil pH values from the NGSA database (Caritat et al., 2011), calcite abundances associated with average ([TOS + BOS]/2) soil pH of pH $\leq$ 4.75 were rescaled to the detection limit of 0.002 wt% CaO. It was assumed that any calcium detected in these samples reflected primary calcium-bearing minerals such as Ca-feldspars and not secondary calcite.

Final screening and weighting of calcite abundance was then determined using effervescence reaction tests (McDonald et al., 1990). Effervescence test results ranging from 'no reaction' to 'very highly reactive' were recorded for each NGSA sample (Cooper et al., 2010). We observed a notable increase in effervescence in samples with pH >7. Samples with average (TOS and BOS) pH <7 were considered increasingly likely to contain silicate-bound Ca, rather than calcite-hosted Ca, as pH decreased. Therefore a scaled penalty was applied to the *cal** values for samples with the most acid pH. The results of this methodology were tested as described below.

3.2.11 Validating cal* against quantitative mineralogical results

Results from the normative calculations described above were validated against quantitative mineralogy determined by X-Ray Diffraction (XRD) for a subset of ten samples that represented low through to high calcite values. The XRD data was processed with the 'SIROQUANT' program (www.siroquant.com) to calculate the abundance of calcite and other minerals. The ten selected samples had a range of calcite abundances between 0 and 80 wt%. The 'SIROQUANT' and *cal** data were found to be highly correlated, with a coefficient of determination (R^2) of 0.96 (Figure 23). Based on this, we had confidence that the normative *cal** values were representative of the real abundances of calcite in the other NGSA samples.

$R^2 = 0.9645$
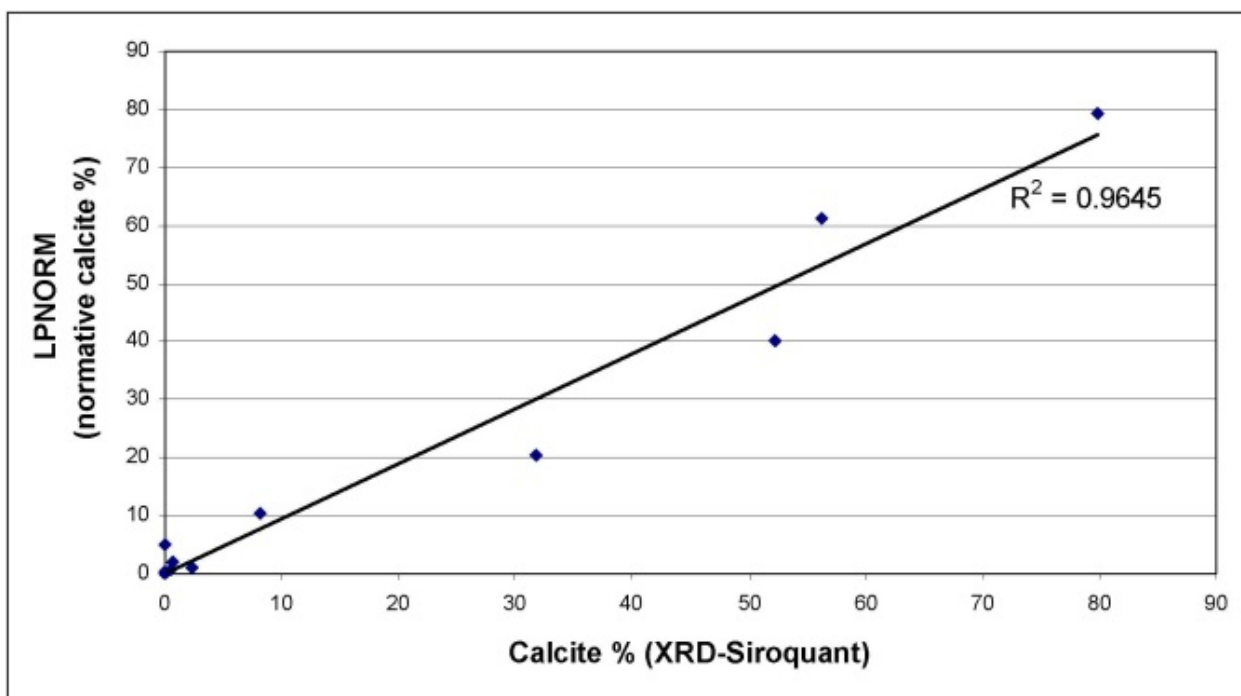
Figure 23 Scatterplot and least-squares regression of calcite abundance estimates by XRD ('SIROQUANT') versus normative calculation ('LPNORM').

Table 6. Descriptive statistics for raw wt. % and log_{10}-wt % transformed calcite (cal*) values.

	Count	Mean	Median	Minimum	Maximum	Std.Dev	Skewness
cal*(wt%)	1311	2.3807	0.2557	0.002	90.2767	8.1062	6.2999
cal* (log10 wt. %)	1311	-0.6254	-0.5922	-2.6989	1.9556	1.0226	-0.1811

3.2.12 Statistical modelling

Due to the highly skewed distribution of the raw Ca concentration population towards low concentrations the calcite predictions were modelled based on log(10)-transformed cal* values (Table 6; Figure 24). Training and validation data were split into 90%:10% subsets. Twenty 'Cubist' models were run, each based on a randomly selected 90% of the data, with the remaining 10% providing a validation data set. Each model produces slightly different rules and hence yields slightly different predictions of calcite abundance. The correlations of measured and predicted values from the training and validation components of each of the 20 models run were recorded (Table 7). Repeated model runs using different training sets allows an assessment of prediction uncertainty (Bui and Moran, 2003) and is akin to 'bagging' (Breiman, 1996). A final averaged modelled prediction grid was generated from the 20 individual models. For each grid cell (90 X 90m) the relative standard deviation of the 20 predictions provided an estimate of the model uncertainty. The log-scaled values were back-transformed to weight % calcite for mapping, interpretation and evaluation against complementary data sets.
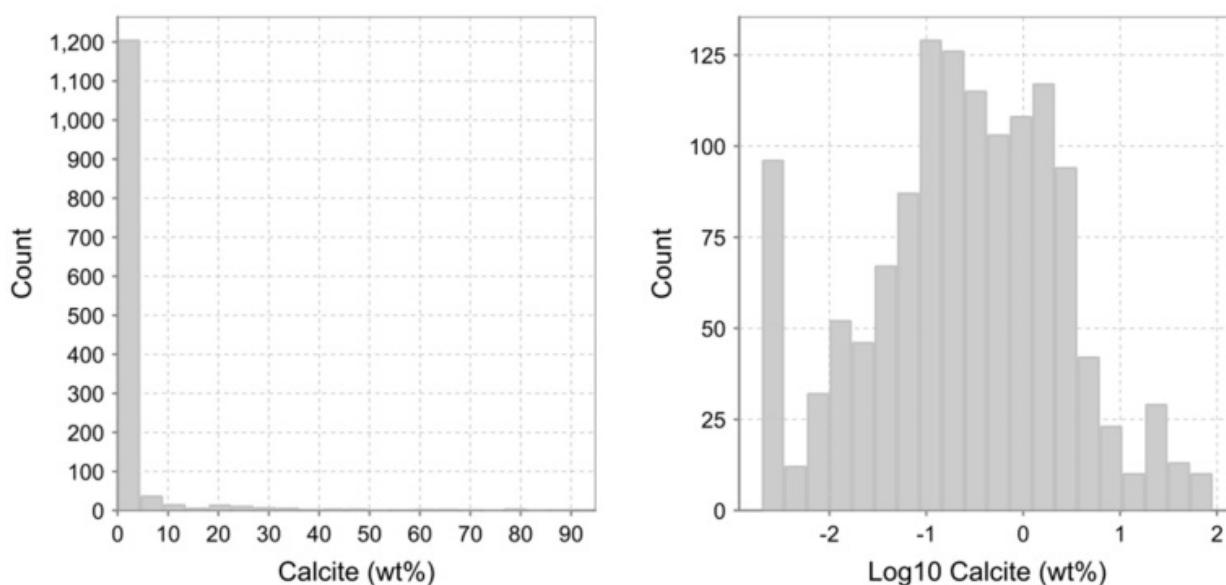
Figure 24. Histograms of calcite concentration in (a) raw wt % and (b) log_{10}-wt transformed values.

Table 7 Correlation coefficients (r) for training and validation subsets for each of the 20 model runs.

	Correlation Coefficient (r)	
Cubist model	Training	Validation
Model 1	0.75	0.70
Model 2	0.73	0.71
Model 3	0.74	0.69
Model 4	0.76	0.72
Model 5	0.74	0.70
Model 6	0.76	0.73
Model 7	0.76	0.73
Model 8	0.76	0.70
Model 9	0.76	0.71
Model 10	0.77	0.73
Model 11	0.75	0.76
Model 12	0.77	0.75
Model 13	0.74	0.70
Model 14	0.78	0.72
Model 15	0.75	0.71
Model 16	0.74	0.70
Model 17	0.75	0.73
Model 18	0.74	0.73
Model 19	0.77	0.68
Model 20	0.78	0.70
Average	0.75	0.71

3.3 Results and discussion

The average of all training datasets produced a correlation coefficient (R) of 0.75 (R^2 = 0.56) with the 10 % validation sample yielding an average r of 0.71 (R^2 = 0.50). The average of the 20 regression tree models is used to predict surface calcite distribution across the continent (Figure 25a) while the relative standard deviations provide an estimate of uncertainty (Figure 25b). Higher uncertainties are associated with predictions of low calcite abundance whereas very low and high calcite abundances were predicted with more certainty.
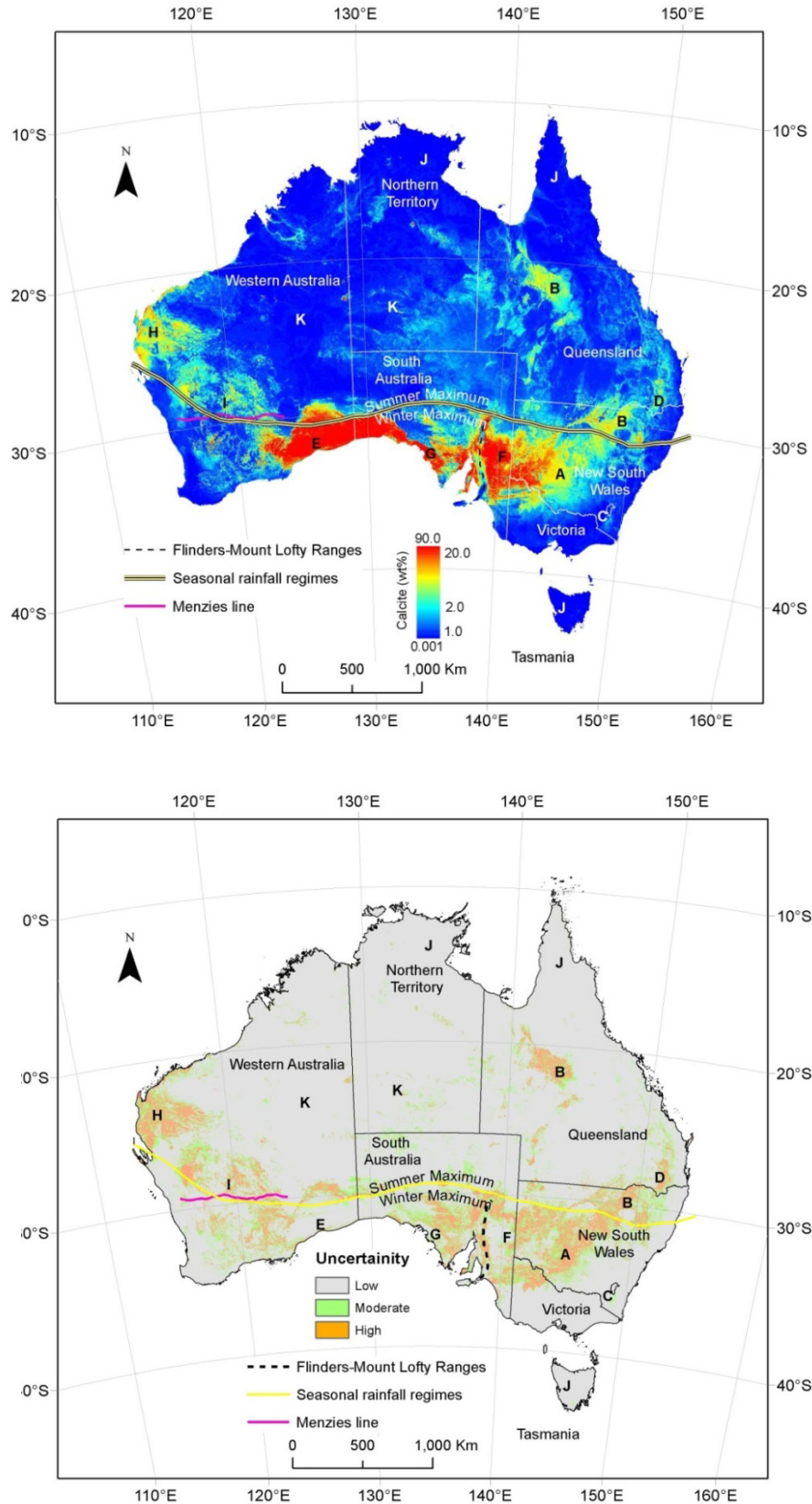
Figure 25. a) Australia-wide prediction of near-surface regolith carbonate. A – Aeolian derived carbonate, B – Ca rich vertosols, C – Monaro region, D – Main Range Volcanics, E -Nullarbor Plain, F – Ca regolith east of the Flinders-Mount Lofty Ranges, G – Eyre Peninsula carbonates, H – coastal carbonates, I – Yilgarn region, J - high rainfall areas and K – arid interior away from marine influences. b). Model uncertainity based on the relative standard deviation of the twenty regression models. Seasonal rainfall regime line derived from Hill et al., 1999.
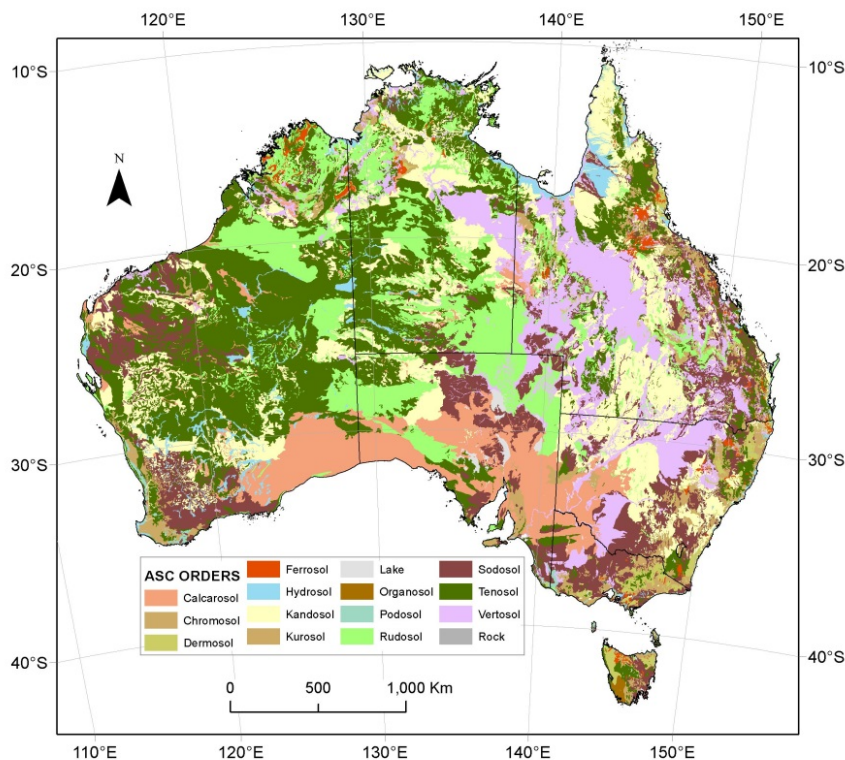
Figure 26 Australian Soil Classification (ASC) soil orders (Northcote et al., 1960-1968; Isbell et al., 1997).

The resulting map of calcite abundance over Australia (Figure 25a) is generally consistent with the distribution of certain soil orders that have dominant calcareous features (see Figure 26 - the regolith carbonate map of Chen et al. (2002; Figure 27)) and the soil carbonate map of Fitzpatrick and Merry (2000: Figure 28). Clear correlations are observed between the distribution of Calcarosols and the map of near surface regolith carbonate from the calcite prediction model (compare Figure 25a and Figure 26). This is not surprising since the ASC was an important conditional covariate in the model (Table 8).

In western New South Wales the distribution of calcareous regolith extends further east than the mapped extent of Calcarosols (see 'A' on Figure 25a). The modelled distribution is consistent with the observations of Butler (1956) and McQueen et al. (1999) who recognised a much broader blanket of regolith carbonate due largely to aeolian accession across the region ('parna'). The dispersion east and north-east of known areas of Calcarosols is also consistent with Australian dust paths (Hesse et al., 2003; Dart et al., 2007). Vertosols in arid and semi-arid regions of New South Wales and Queensland are delineated by the model with relatively low

concentrations of near-surface regolith carbonate ('B' on Figure 25a). These soils form extensive black, cracking clay plains and are known to contain variable amounts of carbonate, particularly in the upper B horizon (McKenzie et al., 2004). Similar associations are found with many Sodosols, which are characterised by a sharply-defined, textured B horizon with carbonate accumulation typically in the B and BC soil horizons (McKenzie et al., 2004).

The model was sensitive enough to delineate sightly elevated regolith carbonate in a pocket of the Eastern Highlands in southeast Australia ('C' on Figure 25a). This area, known as the Monaro Plains, lies in a rain shadow of the Great Dividing Range, and is characterised by extensive basaltic lava fields with many of the soils exhibiting secondary carbonate overprints and calcretisation within the regolith profile (Taylor and Roach, 2005). Moderately high regolith carbonate also correlates with basalts associated with the Main Range Volcanics (Stevens, 1965) in northern NSW and Southern QLD ('D' on Figure 25a).

The highest predicted concentration of near-surface regolith carbonate corresponds to shallow, highly calcareous sandy loams over the Nullarbor Plain in the

Eucla Basin ('E' on Figure 25a). Boulder, nodular and pisolitic calcrete and karstic landforms dominate this region (Chen et al. 2002; Miller et al., 2012), which has formed on the Mio-Pliocene Nullarbor Limestone (Lowry, 1970). High regolith carbonate values occur east of the Flinders-Mount Lofty ranges and extend into the western Murray-Darling Basin ('F' on Figure 25a), and correlate well with mapped Calcarosol distribution (Figure 26). High regolith carbonate concentrations occur over the Eyre Peninsula in South Australia ('G' on Figure 25a).

However, upon closer examination, the model appears to be underestimating regolith carbonate over the Eyre Peninsula (South Australia) compared to the known mapped calcareous soils (Hall et al., 2009). Areas mapped in this region as containing >20 % regolith carbonate correspond to model prediction ranges between 6 and 15 % calcite. This discrepancy might indicate preferential removal of coarse, carbonate-rich material (e.g. nodules, pisolites, which are common) during sample preparation (i.e. sieving) leading to lower measured calcite compared to the bulk composition of the soil. Alternatively these regolith carbonates might have a high Mg content that is not being detected because we are only mapping calcite.

The modelled regolith carbonate map highlights highly calcareous soils and calcrete over the coastal plain of northwest Western Australia ('H' on Figure 25a), although this area has a relatively high degree of uncertainty (Figure 25b) in the prediction and therefore warrants further field validation. Moderately high regolith carbonate correlates with the occurrence of red-brown hardpans in Western Australia (see Fitzpatrick, 1988). Calcareous soils, pedogenic and groundwater carbonates known from the Yilgarn region of Western Australia (Anand and Pain, 2002) ('I' on Figure 25a) are also identified. Regolith carbonate is generally rare to absent in high rainfall regions, including much of the eastern margin of the continent, southwest Western Australia, Tasmania and the Northern Tropics north of 20°S (e.g. 'J' on Figure 25). The majority of the relationships identified and described above are broadly consistent with the existing national carbonate maps (Chen et al., 2002; Fitzpatrick and Merry, 2000) (Figure 27 and Figure 28).
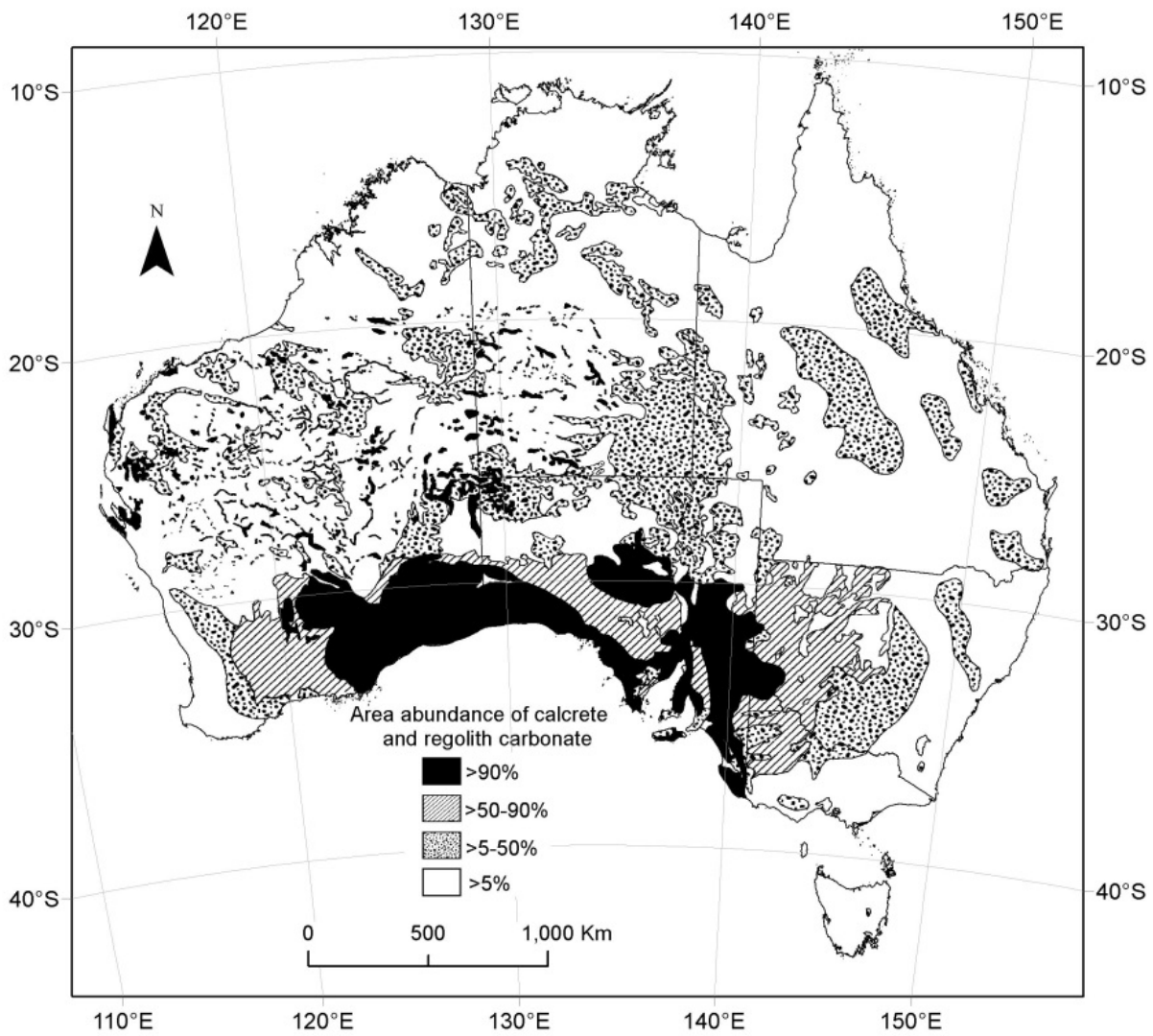
Figure 27 Interpretative map of the distribution of Australian calcrete and regolith carbonates based largely on soil and geological mapping (from Chen et al., 2002).
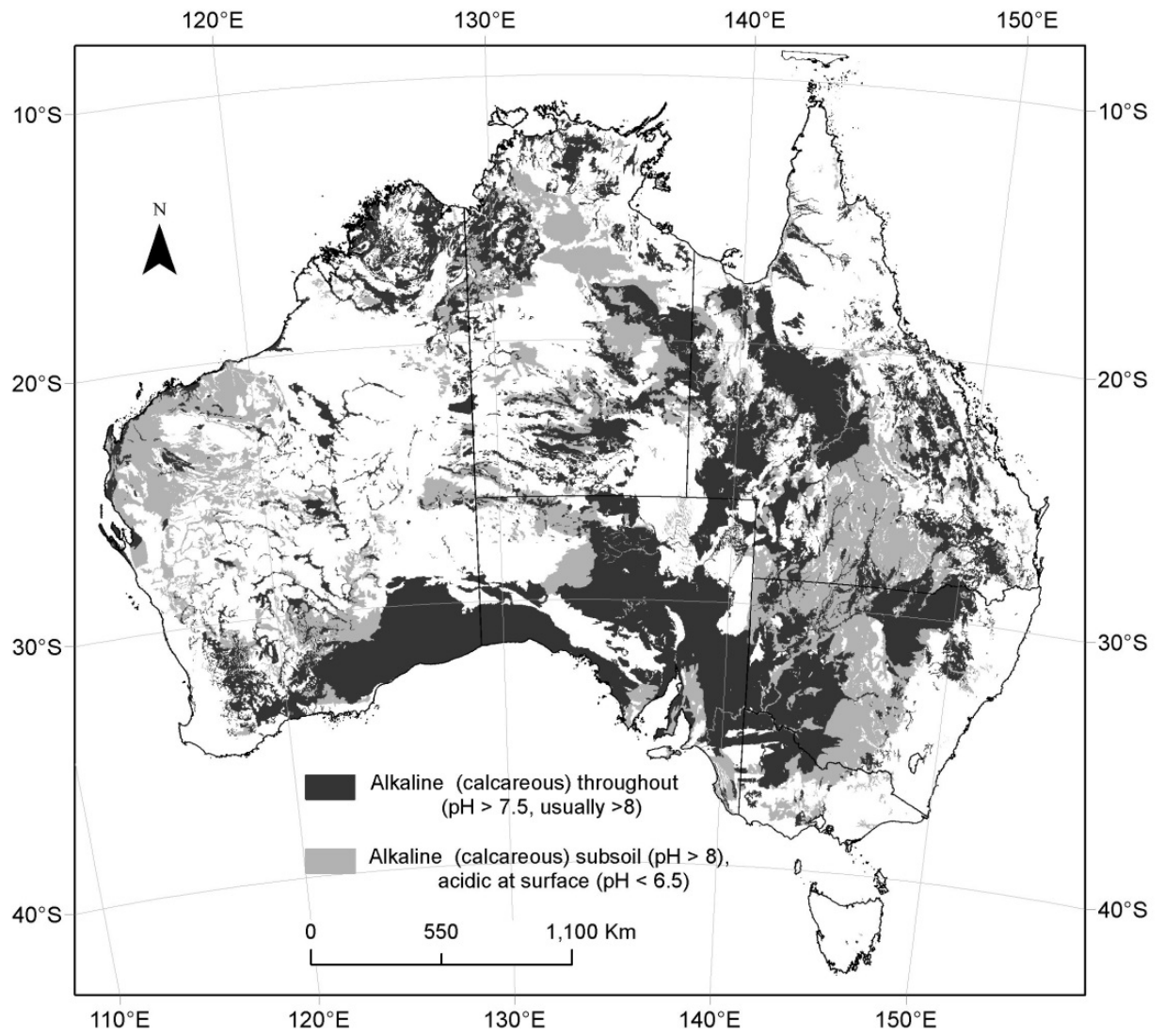
Figure 28 Distribution of alkaline soils (Fitzpatrick and Merry, 2000).

a)
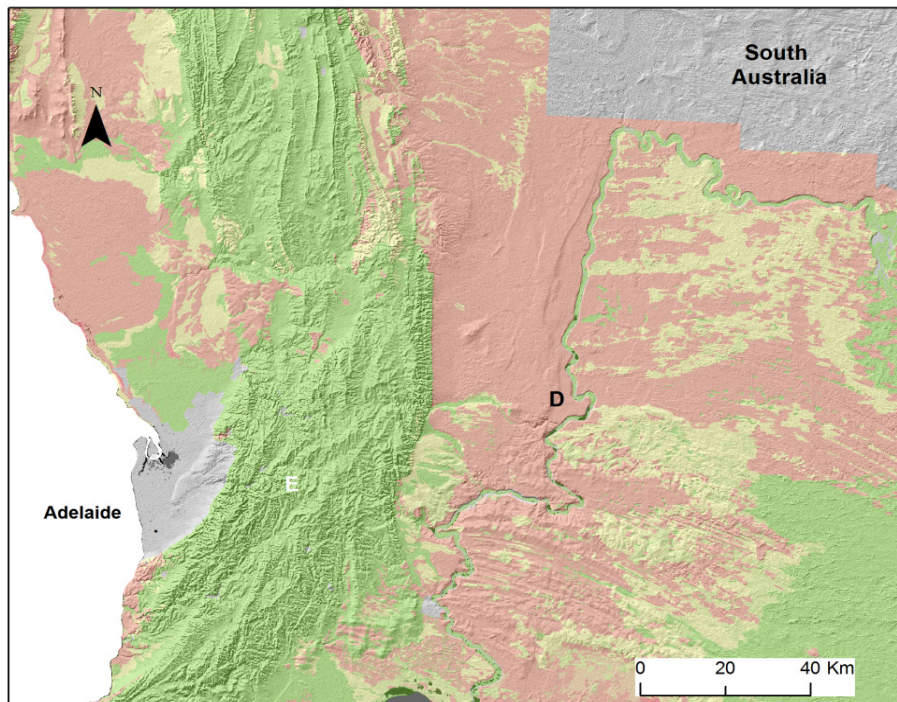
b)
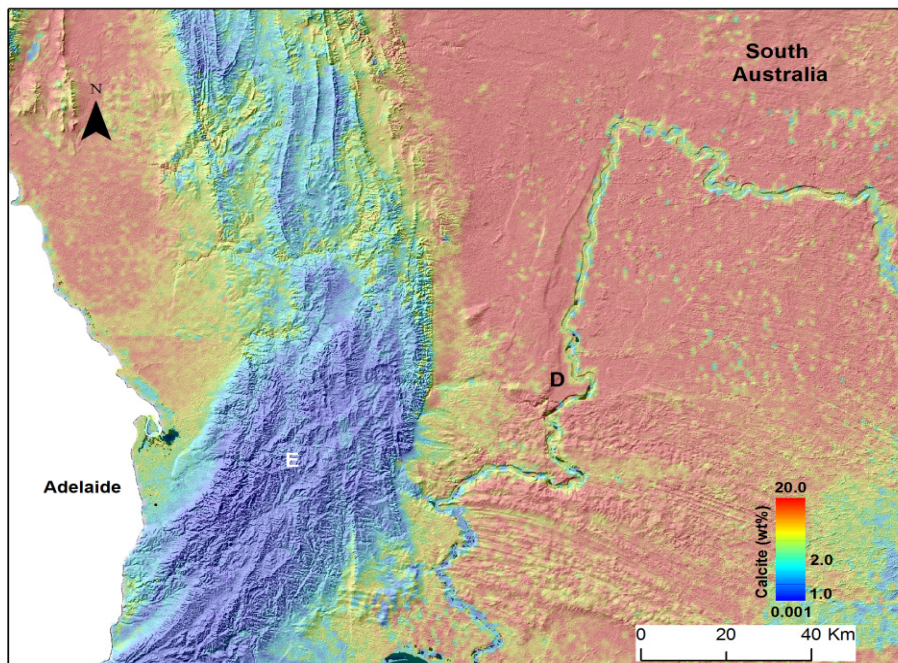
Figure 29. A – Proportion of carbonate within mapped soil-landscape units of Mt Lofty Ranges erosional landforms (E) and the Murray Basin depositional plains (D). Grey = no data, green = negligible; yellow = 30-60% and reddish orange > 60% (Land and Soil Spatial Data for Southern South Australia –GIS CD. 2007). B –Soil calcium carbonate prediction model shows calcite concentration up to and greater than 20%.

Table 8 Usage of covariates in the condition and regression components of the model.

Conditional covariates – decision tree splits	Usage in %
Mean annual precipitation	45.40
Mean annual radiation	40.90
ASC (soil classes)	39.40
Mean annual temperature	26.50
MODIS vegetation - Flatness	20.45
Model covariates – linear regressions	
Potassium	69.90
RatioTh/K	68.10
Precipitation - potential evaporation	64.75
Prescott (leaching index)	63.35
Annual evaporation	60.95
Thorium	59.90
Total Count	53.20
Uranium	52.15
Mean moisture index	51.25
Highest period moisture index	45.60
Spring + summer rainfall	45.30
Precipitation of the wettest period	44.00
Mean temperature	41.85
MODIS vegetation - standard deviation	36.30

3.3.1 Relationships between covariates and calcite

The key covariates used in the conditional part of the model include mean annual precipitation, mean annual radiation, ASC soil groups, mean annual temperature, and the MODIS vegetation coefficient of flatness (Table 8). High flatness values correlate with low EVI values over the MODIS 2000 to 2008 time-series. The use of the major soil groups captures our existing knowledge of the distribution of calcareous soils over Australia. The climatic covariates are consistent with the strong control that low rainfall and high evapo-transpiration has on the accumulation and preservation of carbonate in many landscapes. The climate covariates in the regression component of the model (Table 8) largely reflect the moisture regime or water balance and the degree of hydrolysis and leaching in the regolith. Minimal leaching associated

with low rainfall, high temperature and evaporation will lead to the retention of atmospherically-sourced calcium including that from rainfall, sea-spray aerosols and aeolian dust. Carbonate dissolved by rainwater will translocate lower into the profile. The depth of translocation typically corresponds to the depth of the wetting front, which is broadly controlled by the amount of rainfall. Since 90% of the calcium in Australian regolith carbonates is attributed to external marine sources (Dart et al., 2007) climate has a first order control on regolith carbonate accession and distribution. The importance of climate is evident in the model through the use of climatic covariates in both the condition and regression parts of the prediction.

Climate, however, is not the sole mechanism controlling regolith carbonate distribution. For example, in central Australia there are large areas that are characterised by low rainfall and high evapo-transpiration, but which possess little to no regolith carbonate ('K' on Figure 25a). Proximity to the coast and the path of dominant weather systems are also important factors controlling the distribution of regolith carbonate. A prominent regional feature of the Australian landscape is an east-west zone or boundary at approximately 30°S latitude that separates pedogenic regolith carbonates to the south from predominantly local groundwater regolith carbonates to the north, with the latter tending to be confined to lower slopes and valley floors. In Western Australia this division coincides with the 'Menzies line' (Figure 25a), which has been previously recognised as a boundary delineating a change in soil type, vegetation, groundwater chemistry and climate (Butt et al., 1977). A continuation of the boundary extends eastwards through South Australia and into western and central New South Wales (Hill et al., 1999). The boundary closely matches a division of rainfall seasonality between predominantly summer rainfall in the north and winter dominated rainfall in the south (Hill et al., 1999; Figure 25a). Winter rains in southern Australia are largely sourced from the Indian and Southern Oceans which are rich in calcium and magnesium (Keywood et al., 1995; McQueen et al., 1999), compared with the summer (monsoonal) rains that lose their marine signatures due to the distance from the northern coastline. Regolith carbonates tend to be more widely distributed in the south compared to the northern side of the Menzies line and its continuation

into South Australia and New South Wales (the west-east climate boundary). The differences related to rainfall seasonality appear to be captured with the inclusion of the spring and summer rainfall surface in the regression component of the model (Table 8 covariate Aus41; Table 5).

The west-east climatic boundary (Figure 25a) also marks a distinct change in vegetation composition with mulga (*Acacia aneura*) dominant in the north and mallee (*Eucalyptus sp*.) communities dominant in the south (Specht, 1981; Hill et al., 1999). Vegetation is an important covariate in predicting regolith carbonate with the coefficients of flatness (MODIS 3) and standard deviation in the timing of the maximum or peak (MODIS 11) (Table 5) used in the condition and regression components of the model, respectively. The flatness vegetation coefficient highlights extended periods of non-photosynthetic activity where greenness is absent or at a low constant level through time. High flatness values correlate with calcareous soils because many of these soils occur in arid or semi-arid areas where variation in greenness is relatively low. Low standard deviations of EVI values over the time-series are characterised by "narrow high" amplitude green peaks that decline rapidly to a bare soil signature. This trend is typical of grasslands and treeless plains. Low to moderate standard deviations are associated with regolith carbonate-related vegetation consisting of saltbush (*Atriplex sp*.), bluebush (*Maireana sedifolia*) and some mallee woodlands and shrublands on Calcarosols of the Nullarbor Plain and tussock grasslands on Vertosols of the black soil plains. Both of these MODIS coefficients indicate relatively low overall biological activity with local scale seasonal variations. Soil biology has a strong influence on regolith carbonate distribution through transpiration and CO_2 production. Roots can extract water leaving behind pore water reaching saturation with respect to carbonate minerals. This is a particularly important process in drying climate cycles where available soil moisture is extracted by plant roots. Regolith carbonate can precipitate in pore spaces or in voids or channels left by decaying roots, forming karst pseudomorphs (Klappa, 1980). The concentration of soil $pCO_2(g)$, through its control on bicarbonate ions (HCO_3^-) and protons (H^+), will also favour regolith carbonate dissolution and translocation to positions lower in the profile. Soil CO_2 is associated with respiration of plant roots, decaying organic matter

and microbial activity. There is also evidence that organisms play a more direct role in regolith carbonate accumulation by acting as catalysts for regolith carbonate precipitation (Goudie, 1996). Monger et al. (1991) concluded that soil micro-organisms actively precipitate regolith carbonate. Calcified fungal hyphae and other biological materials suggest a close relationship between regolith carbonate and biogenic processes (Kahle, 1977). Potential links between MODIS vegetation coefficients and the complex interactions associated with biological processes that influence carbonation and precipitation require further investigation.

Airborne-measured regolith geochemistry is also used extensively in the models (Table 8). Relationships between surface airborne geochemistry and the distribution of regolith carbonate are complex. Potassium (K) in calcrete is generally low with average concentrations at 0.3 wt % (Dickson and Scott, 1997). However, slightly elevated K values are noted in association with Calcarosols and Vertosols. Potassium can be contained in or associated with 2:1 secondary clay minerals such as illite, vermiculite and smectite (Taylor and Eggleton, 2001). Very low K and total count values delineate highly siliceous, relatively low regolith carbonate soils associated with dune fields and sandy alluvial sediments in central Australia. Thorium and the ratio of Th/K are used to map highly ferruginous soils associated with highly weathered landscapes in Western Australia, the Northern Territory and North Queensland. These soils generally have lower calcite values.

Landsat TM bands and terrain covariates were not strong predictors in the model. Vegetation and surface mineralogical information from the Landsat TM imagery was probably better explained using MODIS vegetation coefficients and airborne geochemistry, respectively. The lack of usage of the terrain attributes was expected due to the fact that the target variable only sampled floodplains on low relief depositional landforms.

3.3.2 Model limitations

The model appears to capture the main regional to national-scale controls on regolith carbonate distribution, namely rainfall and temperature and their seasonality. However, there are numerous local factors not accounted for that also exert controls on regolith

carbonate mobilisation and precipitation, including topography, parent material and interaction with carbonate-bearing groundwaters. Topography influences the local moisture regime and soil biological activity, which in turn can control regolith carbonate distribution (e.g. Harrison et al., 2003). Hill et al. (1999) demonstrated a strong toposequence control associated with erosional and depositional processes on the lateral distribution and morphology of regolith carbonate. Regolith carbonates also occur in non-arid areas where they are associated with Ca-rich bedrock including, for example, primary carbonate, mafic rocks and coastal calcarenite dune complexes (e.g. Hill et al., 1999). Near-surface regolith carbonate can be associated with upward capillary transport of Ca^{2+} ions from shallow groundwater and in perched watertables (e.g. in E-horizons), precipitating within the unsaturated zone of the regolith profile during wetting and drying cycles. The ability to capture these local controls is limited due to sampling of only overbank flood plain sediments. Future sampling across toposequences and different bedrock type will likely improve the prediction of regolith carbonate over erosional landscapes. However, we did find a broad correlation between the distribution of soil carbonate over erosional landscapes based on detailed soil-landscape mapping and the carbonate predictive model (Figure 29), despite the fact that the carbonate model was trained only using sites on floodplain landscapes. This is likely to reflect that the principal drivers controlling carbonate accumulation particularly at the regional scale are largely independent of landscape type – in this case depositional and erosional landscapes. At the regional scale, accumulation and retention of secondary carbonate is controlled largely by climate (low rainfall and high evapotranspiration), proximity to coast and prevailing wind regimes. Landscape morphology is therefore likely to exert more local scale controls on carbonate distribution.

3.4 Conclusions

The environmental modelling approach employed in this study has produced a national regolith carbonate map (Figure 25) that is generally in agreement with existing soil and geological maps (Figure 27 and Figure 28), despite being based on relatively few site measurements compared to the size of the Australian continent. Whether inconsistencies reflect limitations in our existing maps or in the modelling approach

requires further investigation. The covariates used in the prediction are broadly consistent with our understanding of the controls on the source (inputs), preservation and distribution of regolith carbonate across the landscape. The model produced a continuous, quantitative prediction of regolith carbonate with associated degrees of model uncertainty. Unlike existing maps of carbonate distribution this approach is quantifying the concentration of carbonate in the upper regolith. Robust and accurate predictions using this approach rely on strong correlations between measured regolith carbonate and the environmental covariates. Of equal importance, however, is the need for the site data to adequately sample the distribution of regolith carbonate and the range of factors that controls its distribution. Although the NGSA covers a large geographic area, its bias towards samples from floodplain locations meant that more local landscape and parent material controls on regolith carbonate distribution were not well explained by the model.

In addition, the model strictly predicts regolith carbonate distribution based on the calcium oxide concentration, subject to geochemical constraints, in the <2 mm fraction of the soil over the average of two near-surface sample depths. Preliminary results suggest that the <2 mm fraction might under-estimate the total amount of regolith carbonate, particularly in highly calcareous soils that are likely to contain a high proportion of carbonate aggregates (e.g. nodules, pisoliths and cemented calcareous sands).

Key advantages of this type of modelling approach include flexibility, internal consistency, scalability, and transparency. The map of regolith carbonate that we have produced is consistent with our current knowledge of regolith carbonate formation and distribution, and even with a relatively sparse point validation data set, the product highlights the potential of this type of approach to characterise and map regolith materials at the continental scale. Incorporation of new and targeted site measurements to capture local landscape control on regolith carbonate distribution has the potential to improve future model predictions.

Acknowledgements

Chapter 4

Predicting regolith thickness in the complex weathering setting of the central Mt Lofty Ranges, South Australia

4 Predicting regolith thickness in the complex weathering setting of the central Mt Lofty Ranges, South Australia

J. Wilford

Geoscience Australia, Canberra, ACT, 2601, Australia

M. Thomas

CSIRO Land and Water, PMB 2, Glen Osmond, Adelaide, SA 5064, Australia

The push core drilling rig used to measure regolith depth in the Adelaide Hills, South Australia. A combination of existing site data, new drilling and field measurements (e.g. road cuttings and gullies) were used to develop a predictive model of weathering depth in the region.

Summary

We describe a model to predict regolith thickness in a 128 000 ha study area in the central Mt Lofty Ranges in South Australia. The term regolith encompasses soil (A and B horizons) and highly weathered bedrock (C horizon). The thickness of the regolith has a major control on water holding capacity for plant growth and movement of water through the landscape, and as such is important in hydrogeological modelling and in evaluating land suitability, e.g. for forestry and agriculture. Thickness estimates also have direct application in mineral exploration and seismic risk assessment. Geology and landscape evolution within the study area is complex, reflecting the variable nature of bedrock materials, and the partial preservation of deeply weathered profiles as a consequence of weathering processes dating to the Cenozoic, or possibly older. These characteristics, together with strong climatic gradients, make the study area an ideal location to understand environmental and landscape evolution controls on weathering depth. The area also features weathered landscape analogues to many parts of southern Australia. We use a digital soil mapping rules based approach to develop a model to predict regolith thickness. This model uses statistically-based relationships established between 714 regolith thickness measurements and 29 geographic environmental covariates including geology, geochemistry, terrain and climate themes, and with a ground resolution of 10 m. Accuracy testing based on a 75:25% training:test data split on the resulting map established a correlation R^2 of 0.64. This result is encouraging and is a significant advance over regolith depth mapping by traditionally-based regolith-landscape mapping methods. Finally, it leads the way towards a nationally consistent regolith thickness map for landscape scale environmental simulation modelling and decision support.

4.1 Introduction

Regolith encompasses all weathered materials in the zone between the Earth's surface and fresh bedrock at depth (Figure 30). This zone is covered in Australian pedological terminology (National Committee on Soil and Terrain, 2009) by the A, B and C master horizons, whereas in United States terminology (Schoeneberger et al., 2002) it is covered by the A, E, B and C master horizons. Using the Australian system, the A and B horizons—the solum—have undergone strong pedogenesis by chemical, physical and biological action to such a degree that the material retains none or little of the fabric of the hard rock below, i.e. the presumed parent material of an in situ soil profile. The C horizon is a mineral layer below the A and B horizons that retains at least some of the rock fabric due to variable degrees of in situ weathering. The composition and fabric of the C horizon can range from almost complete mineral alteration to secondary minerals (e.g. Fe-oxides and clays) with only the most resistant minerals (e.g. quartz) being retained, to moderately weathered material retaining much of the primary mineralogy and fabric of the bedrock. Deeper still is the R horizon, which consists of a continuous mass of hard rock that may have undergone minor weathering only along fractures and bedding/cleavages. The A, B and C horizons broadly equate with completely, highly, moderately and slightly weathered bedrock zones in an in situ weathering profile (Figure 30). Here, we apply the term regolith to encompass the A, B, and C horizons.

The nature and depth of regolith varies considerably in response to soil forming factors, and in particular landscape history and preservation. In areas of colluvial and alluvial cover we measure the combined thickness of the sediments to the base of the highly weathered bedrock. The thickness of regolith may be negligible in areas of exposed bedrock to many tens of metres in highly weathered or buried landscapes.
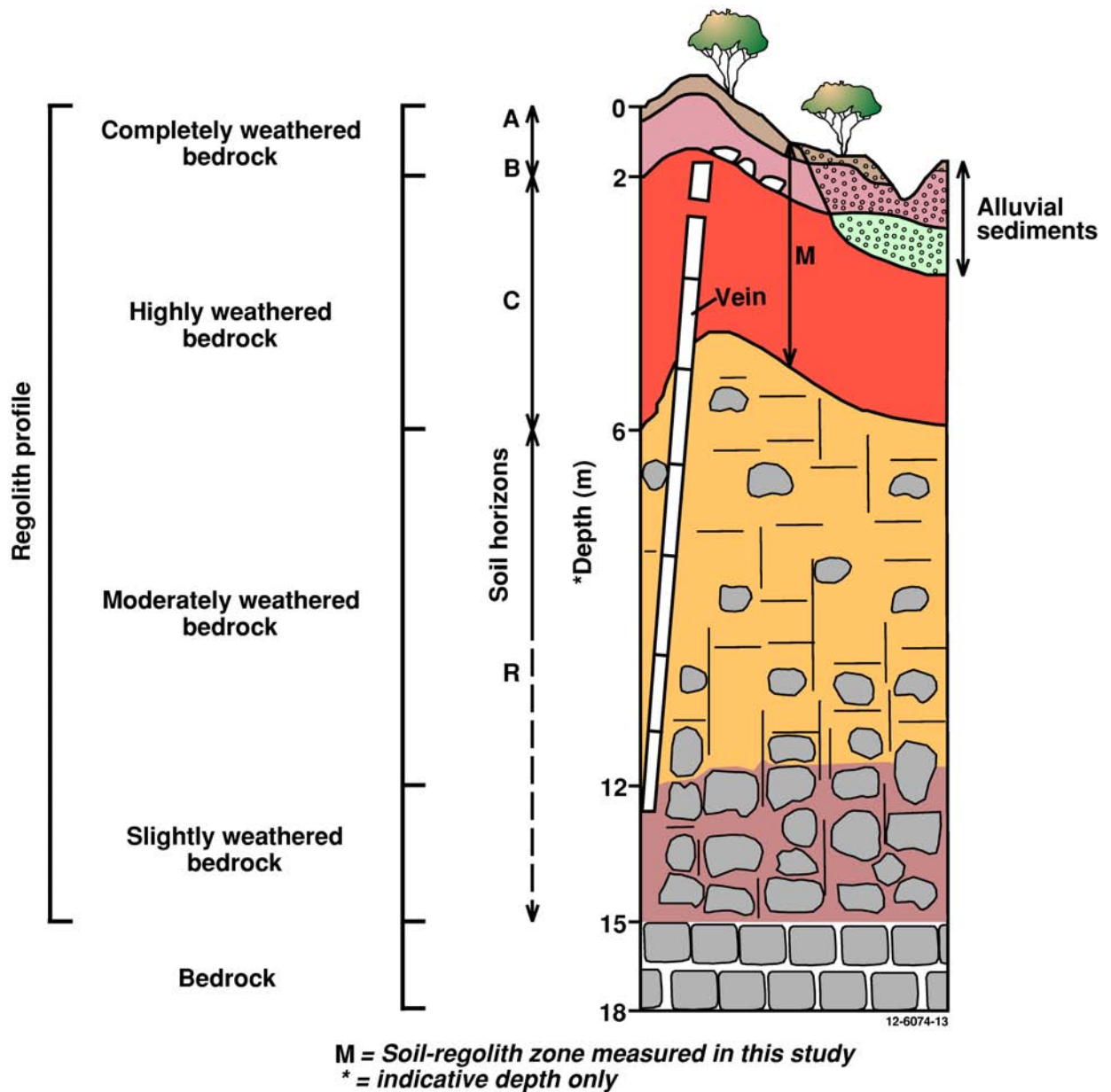
Figure 30 Diagrammatic soil-regolith profile and the interval measured in this study.

Regolith thickness is largely controlled by processes leading to weathering and accumulation and erosion or removal processes. The concept of dynamic equilibrium was proposed in landscapes where the rates of soil removal and accumulation are balanced, leading to uniform soil thickness (Gilbert, 1877; Hack, 1960). Changes in the relative rates of accumulation and removal would lead to either thickening or thinning of the soil. Jahn (1968) used the term denudational balance to describe the interplay of removal processes (e.g. mass movement, slope wash and surface deflation) and soil formation processes in controlling soil thickness. Carson and Kirkby (1972) describe the concept of weathering and transported

limited slopes and associated regolith thickness. Where transport processes are more active than weathering processes, the slope is termed weathering-limited, and maintains or creates a shallow regolith. Conversely, transport-limited slopes are those in which weathering processes are more active than removal processes, leading to the development of deeper regolith. The soil thickness model of Johnson (1985) emphasised the factors controlling addition and removal processes. Johnson's model defined soil thickness as the interplay of processes leading to profile deepening (i.e. weathering and leaching), building up (i.e. organic matter and aeolian dust, slope wash) and removals (i.e. mass wasting, erosion, leaching). Profile deepening,

building-up and removal are controlled by bedrock type including mineralogy and structure; climate, particularly rainfall and temperature; aeolian inputs; topography with control on geomorphic process and water movement; biota including vegetation and organisms; and age, which incorporates soil-landscape history to present (Figure 31). Controls on regolith thickness and the degree to which they influence weathering depth will invariably change over differing spatial and temporal scales. The temporal component is significant in Australia where the nature and thickness of the regolith in many parts of the continent reflects palaeo-weathering and geomorphic processes that have since been modified by contemporary Earth surface processes. In this context, dynamic equilibrium or a steady state regolith depth is likely to be relatively rare due to the dynamic nature of Earth surface processes. Therefore models that predict regolith thickness in the Australian landscape need to incorporate the dual influences of contemporary and palaeo-environmental controls on weathering depth.

Thickness and characteristics of regolith strongly influences groundwater interactions and subsoil water movement, water storage and nutrient availability. The regolith thus has an important bearing on land use, and the viability of land-based industries dependent on rooting depth, e.g. agriculture and forestry. Regolith thickness and composition are also factors in the amplification of earthquake ground shaking, and hence important in predicting earthquake impact (McPherson, 2011). From a mineral exploration perspective, the surface geochemical expression of buried deposits is often linked to the nature and thickness of the regolith cover. Information on the depth and composition of the regolith is particularly useful in exploring for minerals in the deeply weathered landscapes that typify much of the Australian continent. Given its importance, it is surprising that there is a dearth of specific depth information incorporated in most regolith mapping, which is probably best explained by the need for suitable density and often deep drilling for mapping by traditional methods. Existing regolith maps over the Australian continent vary in terms of their mapping scale and approach in compilation, and Australia possesses no consistently compiled national regolith

mapping at scales finer than 1:2,500,000. Where existing, maps are polygon based and do not describe regolith thickness and other properties in a spatially continuous manner.

Information on regolith thickness is mainly sourced from soil-regolith maps and drilling. Most soil maps, however, are restricted to the A and upper B horizons, and so only "capture" the near contemporary overprint of the regolith profile. In contrast, regolith maps are typically underpinned by a stronger focus on landscape ageing processes to develop conceptual models of regolith evolution. However, both traditionally-based mapping approaches are limited by the number of often sparsely distributed site-specific depth observations and laboratory data, which rarely goes to beyond 2 m in depth. Drill logs derived from mineral, groundwater and stratigraphic explorations can be useful additional sources of regolith information, although these are often difficult to use due to a lack of standardised terminology or coring methods.

Newly emerging mapping methods based on digital soil mapping (DSM) approaches offer the prospect of increased efficiencies compared to traditional forms of mapping. Typically DSM gives mapping outputs that are geographic information system (GIS)-ready, are spatially explicit being raster based, and importantly, give estimates of uncertainty required for understanding reliability—especially important when involved in environmental simulation and decision support. McBratney et al. (2003) gives a comprehensive overview of DSM approaches. These approaches involve establishing relationships—usually statistical—between the soil property to be mapped (i.e. the target variable) and predictor datasets (i.e. environmental covariates) to build statistical predictive models (so-called environmental correlation). There are three main approaches used in DSM, those that are: (i) statistically-based; (ii) deterministic, process-based; or (iii) expert knowledge-based or heuristic (Hengl and Reuter, 2009). The selection of approach is not prescriptive and is based on a number of factors, including availability and quality of computing resources, type of predictor and supporting datasets, level of local soil-landscape expert knowledge, and the competency of the practitioner.

Factors affecting soil - regolith thickness
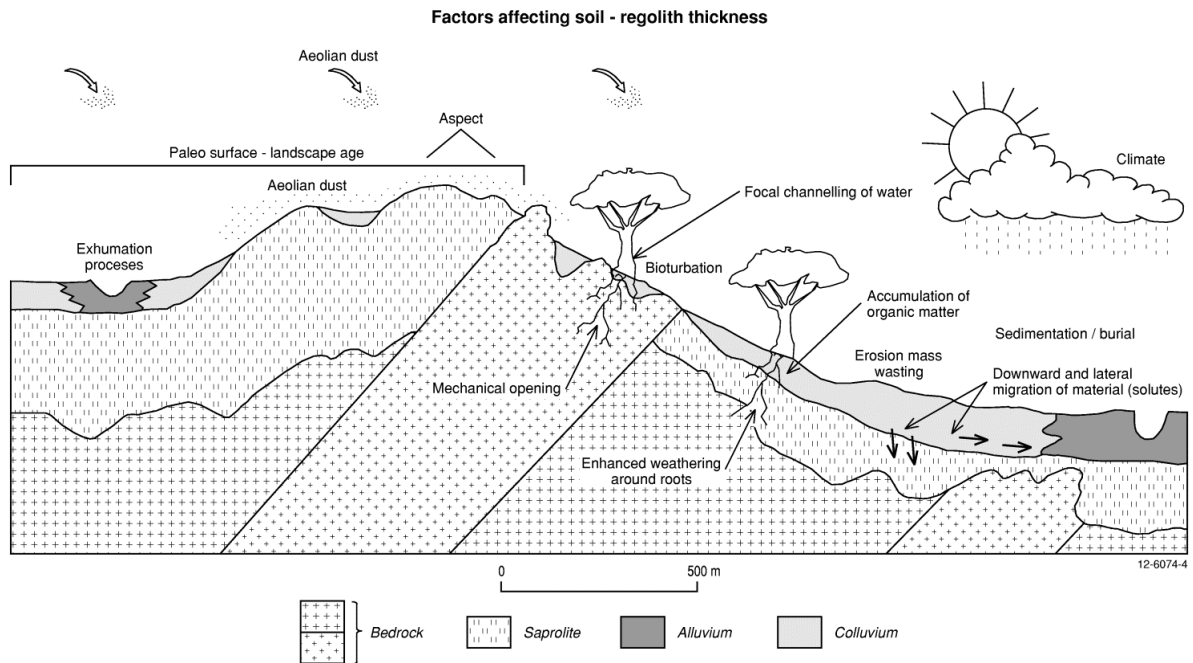
Figure 31 Factors affecting regolith development or thickness. Diagram based largely on the Johnson's model that defined soil thickness as the interplay of processes leading to profile deepening, building up and removals. In addition long term landscape evolution is an important consideration in the model.

A number of studies describe using DSM to map soil and/or regolith depth, including Gessler et al. (1995) and McKenzie and Ryan (1999) where they applied a simple linear relationship between topographic wetness and soil thickness. Tesfa et al. (2009) modelled soil depth from topographic and land cover attributes using generalised additive and random forests models. Bui et al. (2006) and Sekhar et al. (2009) used environmental correlation methods to predict soil thickness in Australia and India, respectively. McKenzie and Gallant (2007) used a combination of two terrain indices including Multi-Resolution Valley Bottom Flatness index (MrVBF) (Gallant and Dowling, 2003) and terrain wetness index (TWI) (Wilson and Gallant, 2000) to partition the landscape into erosional and depositional areas to predict soil thickness. Shafique et al. (2011) used topographic attributes to predict the thickness of valley fill deposits in northern Pakistan. Landscape regression models have been used to predict the thickness of soil horizons to a depth of 1 m in the Hunter Valley region of New South Wales in Australia (Gastaldi et al., 2012).

Here we build on these studies and describe a statistically-based piecewise linear regression modelling approach to predict regolith thickness in the Mt Lofty Ranges in South Australia, an area covering

largely erosional landforms underlain by variably weathered and partly covered (colluvial and alluvial sediments) bedrock. Our approach is based on establishing statistical relationships between regolith thickness measurements from legacy datasets (including drilling) and new targeted drilling, and a selection of commonly available environmental covariates relating to geology, terrain, weathering history and climate. The new drilling and site observations (e.g. road and railway exposures) accounted for approximately half of all the site values used to build the statistical model. These new sites mainly recorded deeper depths compared with existing soil site descriptions which focused largely on solum depth or where the soils are relatively shallow the "C" horizon depth.

4.2 Methods and materials

4.2.1 Study area

The study area covering 128,000 ha lies in the central Mt Lofty Ranges near Adelaide, South Australia (Figure 32). The area has a Mediterranean climate with cool winters and generally warm to hot, dry summers. There is a strong orographic influence on rainfall distribution with higher elevations (> 700 m) along the western flank of

the ranges receiving 800–1100 mm/yr, diminishing rapidly eastwards to 350–500 mm/yr along the lower elevation, eastern boundary of the study area. The town of Mt Barker has an annual average rainfall of 766 mm compared to the town of Callington, 17 km to the east, which has approximately 380 mm of rainfall (Bureau of Meteorology—www.bom.gov.au). The area was largely cleared of native vegetation for grazing (sheep and cattle) and crops by the early 1900s. Prior to clearing, land cover consisted largely of a mosaic of closed and open Eucalyptus woodland. Where communities of remnant vegetation are preserved, their distribution and type is strongly influenced by soil fertility and rainfall (Lange, 1976).

The geology is divided into rocks of Proterozoic, Cambrian and Cenozoic age. The Proterozoic rocks include metamorphosed gneiss and schist associated with the Barossa Basement Complex (> 900 Ma), and more recent Neoproterozoic sediments (Preiss, 1987). The latter occur mainly on the western side of the study area and include feldspathic sandstones, siltstones, quartzites and dolomites. These sediments have been folded and metamorphosed to low grade phyllites and high-grade gneisses. Feldspathic meta-sandstones and meta-siltstones of the Cambrian Kanmantoo Group are typically highly micaceous (i.e. biotite and muscovite-rich) and contain fine grained quartz and feldspar. Both pre and syn-tectonic granitoid intrusive bodies and high-grade basement units occur throughout the area (Daily et al., 1976).
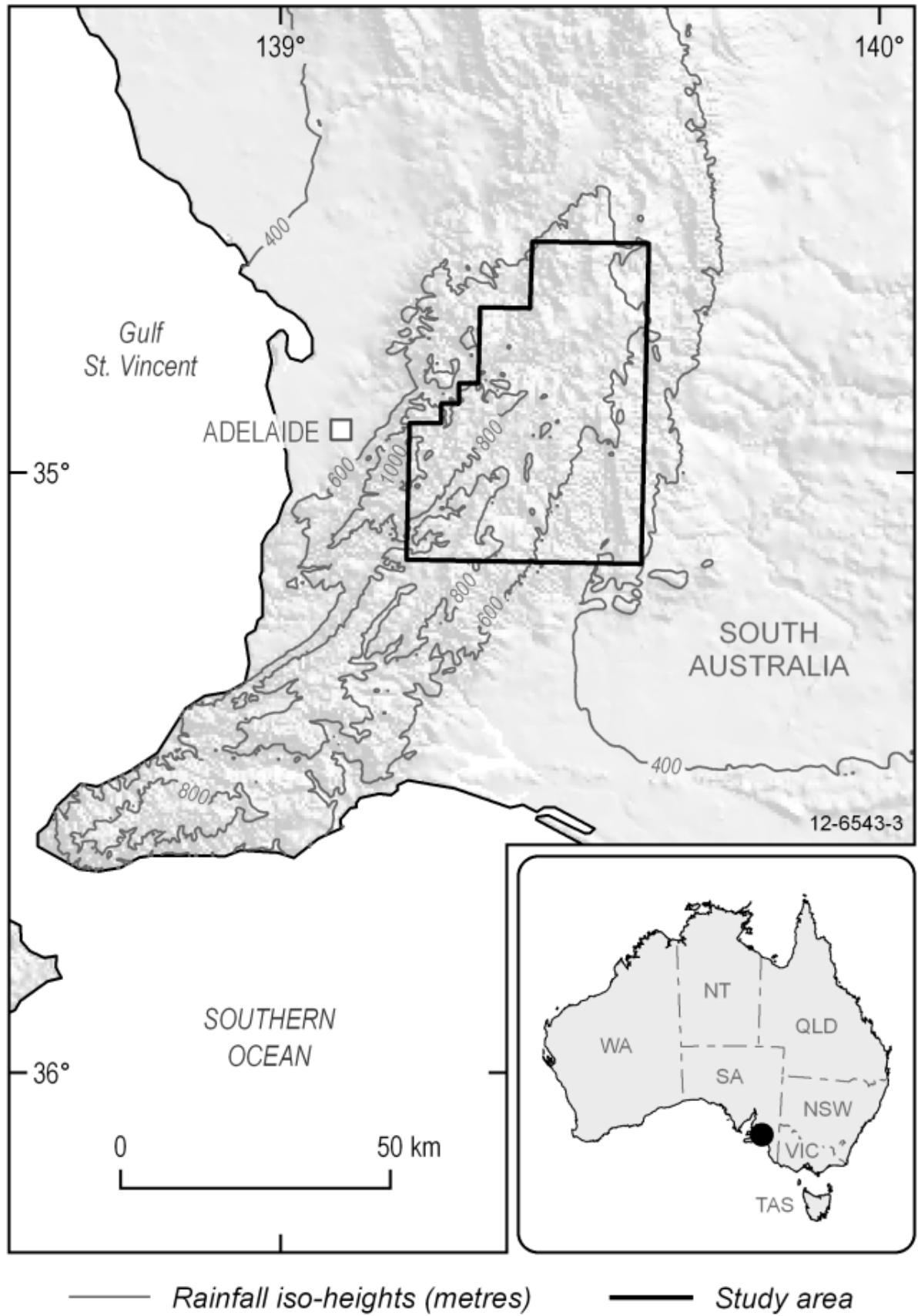
Figure 32 Study area (128,000 ha) with hill shaded DEM and annual rainfall isohyets.

4.2.2 Landforms and landscape history

Landforms range from low relief erosional and depositional plains to steep hills (90–300 m relief) and escarpments. The most elevated and deeply-incised landscapes occur on the western side of the study area. Mt Torrens, Mt Barker and Mt Charles form prominent hills in the central uplands. A major drainage divide along the central western part of the study area separates streams flowing east into the Bremer River to the Southern Ocean from those flowing west into the Gulf of St Vincent. Some of the most striking landforms in the study area include a series of north–south oriented scarps (Figure 33), which are associated with tectonic uplift that formed the Mt Lofty Ranges. Two major tectonic phases are recognised: the first was during the mid Eocene–early Miocene (43 to 14 Ma), and the second after approximately 5 Ma (Tokarev et al., 1998). Uplift along major geological structures is on-going (Bourman et al., 1999).

A distinctive feature of the Mt Lofty Ranges is the partial preservation of a palaeo-surface, deep weathering and associated "lateritic" profile development commonly referred to as a "summit surface" (Twidale, 1976). The surface has a mosaic distribution governed by a complicated geomorphological, weathering and neotectonic history. The origin and age of the surface is contended in the literature: Woolnough (1927) and Stephens (1946) described the surface as an uplifted peneplain with a uniform lateritic cap that has been partially dissected by erosion. However, Daily et al. (1976) and Twidale (1976) have argued that the surface dates back to the Mesozoic and that it has changed little except for stripping to its current extent. Finally, Bourman (1993; 2007) and Milnes et al. (1985) propose that the distribution of regolith materials including those associated with the summit surface is in response to the integrated processes of leaching, erosion, reworking and continuous weathering since the Mesozoic. Bourman (2007) also argues that the ferricrete, mottled and bleached zones commonly associated with a typical "lateritic" profile might evolve independently, reflecting local environmental controls.
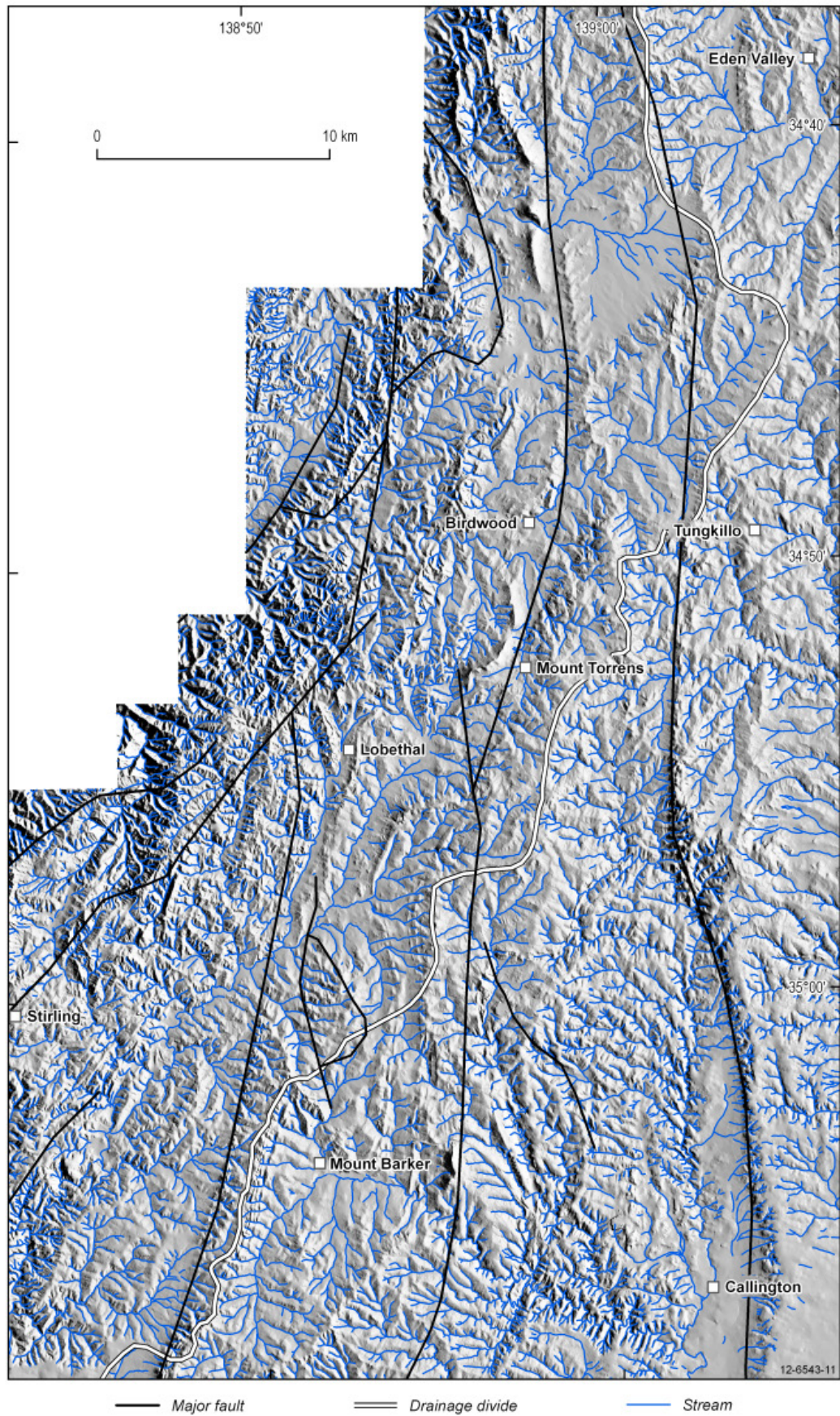
Figure 33 Hill shaded DEM showing major towns, fault scarps, streams and drainage divide.

4.2.3 Site data (the target variable)

We used three methods of acquiring regolith thickness data. Firstly, field measurements were recorded at road cuttings, erosion gullies, streams, and obtained from existing drill hole and legacy soil survey data. Secondly, a drilling program was undertaken using a tapered hollow tube (60 mm diameter) percussion rig to extract regolith cores. Coring areas were selected using expert knowledge of the study area's soil-landscapes. Coring sites within these areas were chosen based on toposequences to capture local landscape variability. Typically, each coring area contained a cluster of four to six coring sites within an 800 m radius. Coring focused on depositional or low relief parts of the landscape as these zones were generally under-sampled with the first method. The third method of collection involved a desktop collation of legacy data from data archives (e.g. soil survey, mineral and groundwater exploration drilling).

In the field, the lower contact of the regolith zone was based on field site characteristics, including hardness and preservation of primary bedrock fabric and minerals. The A, B and C horizons were identified based on pedological criteria (National Committee on Soil and Terrain, 2009) (Figure 34). The C horizon (weathered saprolite) was generally relatively soft and could be broken or powdered by hand. Most of the primary bedrock minerals in this horizon were weathered to clays with the exception of quartz and muscovite. Mottling was also common and typically the original bedrock fabric was visible. These structural and mineral characteristics contrasted with moderately and slightly weathered bedrock, which were considerably harder and contained well-preserved primary bedrock fabric and minerals. The depth to drilling refusal was also recorded and generally corresponded to the depth of moderately or slightly weathered bedrock. We did not core to deeper than 8 m.

A total of 714 site observations from all sources described above were used for training and testing the model.

4.2.4 Environmental covariates

Environmental covariates correlate spatially to either soil forming factors (e.g. slope, parent material) or some other expression of soil properties (e.g. surface colour). The soil forming factors are described in Jenny (1941) through the following formula

$$S = f (c; o; r; p; t…):$$

In this, "S" stands for the soil in its current state, which is a function of ("f") factor "c", which equates to the influence of climate; "o", organisms, "r", relief, "p" parent material, and "t", time, in soil formation. (The "…" allows for discovery of additional factors.)

GIS grid-based environmental covariate datasets were selected that conceptually represented the factors deemed important in soil and regolith formation in study area. The classes of predictor environmental covariates used in the model generation are briefly discussed below, with a full listing with key references presented in Table 9.

4.2.4.1 Geology, surface geochemistry

The parent material theme was based on the 1:250,000 scale geology mapping reclassified according to consolidated (bedrock) and unconsolidated materials (e.g. colluvium and alluvium). Further sub-division was based on silica content, textural and compositional criteria. Airborne gamma-ray spectrometric GIS grids with a ground resolution of 50 m from 200 and 100 m flight-line surveys were accessed from Geoscience Australia. Airborne gamma-ray spectrometric data measures the surface concentration of three gamma-ray emitting elements including potassium (K), thorium (Th), and uranium (U). The distribution of these radio-elements varies in response to bedrock type and secondary weathering or pedological processes.
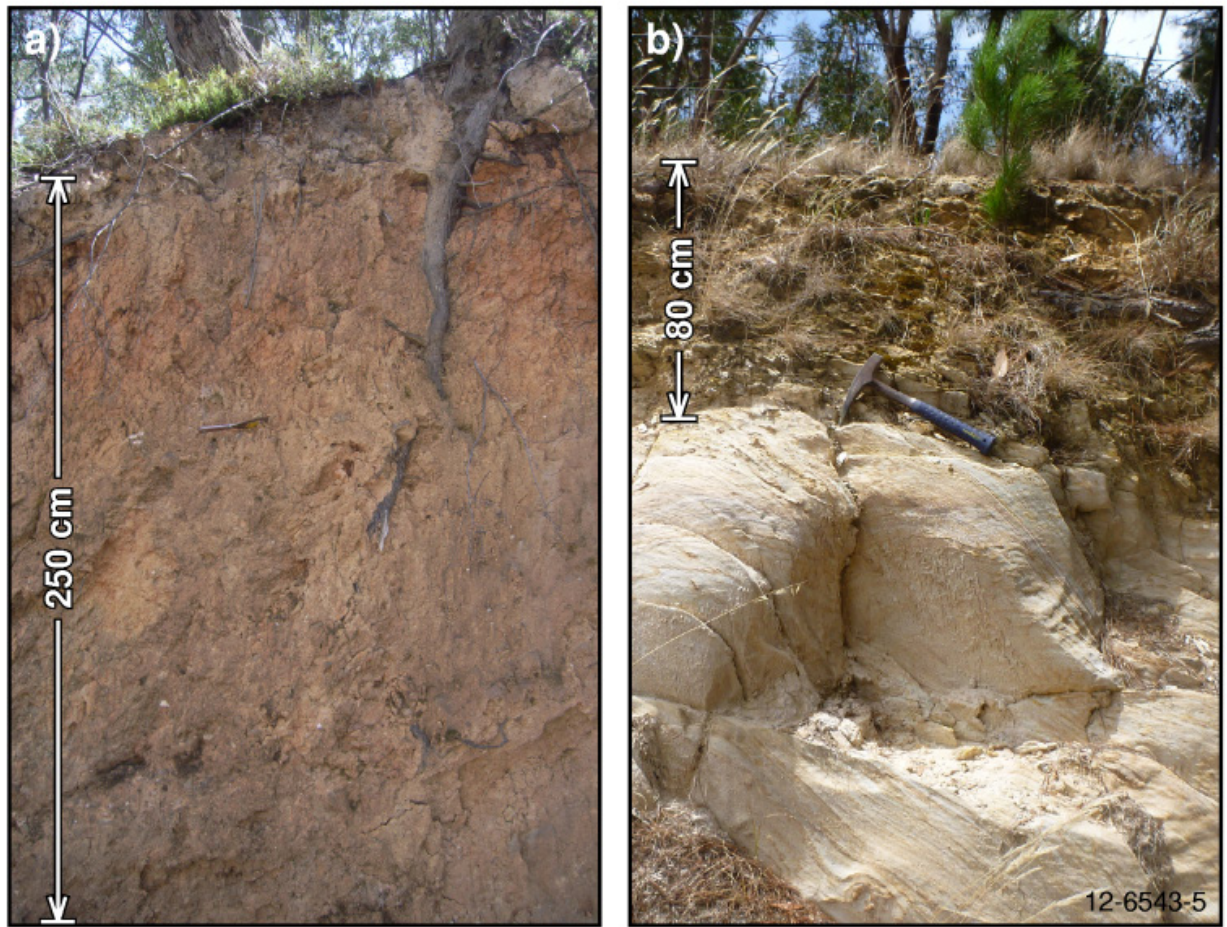
Figure 34 Representative regolith profiles. a—Highly weathered bedrock with a ferruginous earthy fabric. Basal contact not seen. b—Relatively shallow profile with G-pick indicating the highly weathered bedrock contact.

Table 9 Environmental covariate predictive variables used in the regolith depth model, their contributions, and key references and sources.

Theme	No.	Covariate	Description	Pedogenic/geomorphic contribution and key soil forming factors (c=climate; o=organisms, r=relief, p=parent material, and t=time)	Source data / reference
Geology, surface geochemistry	1	Geology	Re-classification of mapping units based on silica content and texture	Geochemistry, structure, resistance to weathering (p)	Geoscience Australia, 1:100,000 scale mapping
	2	Radiometric potassium (%)	Airborne gamma-ray spectrometry derived from radio elemental K %	Soil depth and freshness of bedrock exposure (p, t)	Geoscience Australia
	3	Radiometric thorium (ppm)	Airborne gamma-ray spectrometry derived from radio elemental [208]Thallium to infer Th ppm	Soil depth and degree of weathering (p, t)	Geoscience Australia
	4	Radiometric Uranium (ppm)	Airborne gamma-ray spectrometry derived from radio elemental [214]Bismuth to infer U ppm	Soil depth and degree of weathering (p, t)	Geoscience Australia
	5	Total radiometric count	Airborne total count. Airborne gamma-ray spectrometry :weighted total of K, eTh and eU	Freshness and degree of weathering (p, t)	Geoscience Australia
	6	Ratio potassium/thorium	Ratio of airborne Potassium / Thorium	Freshness and degree of weathering (p, t)	Geoscience Australia
	7	Weathering Intensity Index	Index representing intensity of weathering, derived by incorporating radiometric Thorium and Potassium, and terrain attributes	Landscape weathering history (t)	Geoscience Australia. Wilford (2012)
Terrain, landform	8	Elevation	Digital elevation model, generated from 5 and 10 m contours, spot heights, and with drainage enforcement	Climate, temperature, rainfall; vegetation (o, r)	ANUDEM Hutchinson (1993)
	9	Multi-resolution Valley Bottom Flatness (MrVBF)	An index that applies slope and elevation to define locally low-lying landscape zones, i.e. valley bottoms, from other zones	Zones of deposition and erosion (r)	Gallant and Dowling (2003)
	10	Aspect	Orientation of the line of steepest decent, measured in degrees clockwise from north.	Diurnal heating and cooling; vegetation type; local rainfall; surface heating/cooling (o)	10 m DEM; Wilson and Gallant (2000)
	11	Relief	Elevation range within a 250 m radius giving an index of rates of change	Rates of erosion and deposition; vegetation types (r, o)	10 m DEM
	12	Slope	Rate of elevation fall	Surface flow acceleration; rates of mass wasting (r, o)	10 m DEM
	13	Profile Curvature	Curvature of the surface in the downslope direction	Surface flow acceleration; areas erosion/deposition rates; colluvial development (r)	10 m DEM

Theme	No.	Covariate	Description	Pedogenic/geomorphic contribution and key soil forming factors (c=climate; o=organisms, r=relief, p=parent material, and t=time)	Source data / reference
	14	Plan Curvature	Curvature of the surface in the across slope direction	Converging/divergent surface flows; areas of erosion/deposition in interfluves (r)	10 m DEM
	15	Wetness Index (SAGA version)	Soil-water flow accumulation, combining specific catchment area and slope angle	Zones of wetting or saturation in the landscape (r, o)	10m DEM Hengl and Reuter, (2009)
	16	Convergence	Localised index of land surface convergence/divergence	Surface and subsoil water flow direction; water accumulation (r)	10m DEM
	17	Slope length	Based on flow accumulation and slope steepness	Water flow, areas of accumulation and erosion	10m DEM Hengl and Reuterv(2009)
	18	Topographic position index	Calculates local elevation differences based on kernel sizes. We use a radius of 300m (ie TIP300)	Hill slope facets (r)	10m DEM Jenness, (2006)
Climate	19	Mean annual radiation	Annual mean radiation. The mean of all the monthly radiation surfaces.	Soil temperate, evaporation rates and weathering rates (c, o)	Xu and Hutchinson(2011)
	20	Mean annual precipitation	Mean annual precipitation. Sum of all monthly average precipitation surfaces.	Soil wetness; weathering rates (c, o)	Xu and Hutchinson (2011)
	21	Mean annual temperature	Mean temperature. Mean of all monthly average temperatures.	Soil temperature, weathering rates (c, o)	Xu and Hutchinson (2011)
	22	P-E	Precipitation minus potential evaporation.	Annual water deficit, weathering rates (c, o)	Xu and Hutchinson (2011)
	23	Prescott Index	Prescott Index or leaching index	Water balance, weathering rates (c, o)	CSIRO Prescott (1948)
	24	Annual mean moisture index	Annual mean moisture index based on all monthly moisture values	Water balance, weathering rates (c, o)	Xu and Hutchinson (2011)
	25	Highest month radiation	The highest solar radiation of any monthly radiation	Soil temperate, water balance, weathering rates (c, o)	Xu and Hutchinson (2011)
	26	Lowest period radiation	The lowest solar radiation of any monthly radiation	Soil temperate, water balance, weathering rates (c, o)	Xu and Hutchinson (2011)
	27	Precipitation of the wettest month	The highest precipitation of any monthly precipitation	Water balance, weathering rates (c, o)	Xu and Hutchinson(2011)
	28	Precipitation of driest month	The lowest precipitation of any monthly precipitation	Water balance, weathering rates (c, o)	Xu and Hutchinson (2011)
	29	Annual mean radiation	The mean of all monthly radiation surfaces	Water balance, weathering rates (c, o)	Xu and Hutchinson (2011)

4.2.4.2 Terrain, landform

A digital elevation model (DEM) GIS grid was constructed from 5 and 10 m contours, spot heights and drainage using the ANUDEM method (Hutchinson, 1993). The DEM was interpolated to a 10 m ground resolution and used to generate terrain surfaces using a combination of ESRI ArcMap® and SAGA (System for Automated Geoscientific Analyses) GIS software. The terrain surfaces included slope and slope length to relate to slope stability and thickness, MrVBF for deposition zones and TWI for zones of water accumulation.

4.2.4.3 Climate

GIS grids of climate with a ground resolution of 50 m were generated using the ANUCLIM program (Xu and Hutchinson, 2011). The ANUCLIM model interpolates as series of climatic grids based on long term weather station observations (daily records and monthly averages) and a 9 arc-second (~ 270 m) resolution DEM (Hutchinson et al., 2008). The grids generated include the Prescott Index that relates to weathering rates and leaching intensity, and various other surfaces corresponding to rainfall, evaporation and temperature.

4.2.5 Regolith depth modelling approach

We apply an environmental correlation approach that uses the Cubist data mining algorithm (www.rulequest.com) to establish predictive relations between regolith thickness and the environmental covariates. Cubist has been used effectively to predict a range of soil characteristics based on environmental correlation (Bui et al., 2006; Henderson et al., 2005). The Cubist rules based model structure consists of a conditional component—or piecewise function—acting as a decision tree, coupled with multiple linear regression models. Continuous and categorical environmental covariates can be used in the decision tree to split the data into more homogeneous sub-regions. The decision tree structure is based on recursive partitioning of the prediction variable to minimise the standard deviation across all potential splits (Henderson et al., 2005). The conditional component defines the nodes of sub-models, which consist of linear regression models. Models are explicitly expressed, and an example of a sub-model is

presented below showing (1) the conditional and (2) linear regression components:

1. If (conditional statement – decision tree splits)
   Relief < a
2. Gamma-ray K > b
3. Lithology = (n, m, p)
   Then (linear model)
   Property = $c_1 *$ rainfall + $c_2 *$ slope + $c_3 *$ gamma K

Being explicitly expressed, rules can be evaluated with the benefit of expert knowledge.

The Cubist model is evaluated by randomly sub-dividing the data into training and testing datasets. For this, a split of 75:25% training: testing datasets was used. Using the training data, a map of the residuals of the predicted depths (i.e., predicted values minus the training values) was created by punctual local ordinary kriging using an exponential model (Webster and Oliver, 2001) with VESPER software (Minasny et al., 2005). The kriged residual map was added to the predicted regolith depth map for final map evaluation. The final map quality was assessed in terms of R^2 and root mean square error (RMSE) (Voltz and Webster, 1990) using the withheld 25% of test data.

4.3 Results and discussion

4.3.1 Statistical model

The piecewise linear regression model was evaluated using 75:25% training and testing subsets of the thickness field data with 29 environmental covariate GIS grid layers (Table 9). Site depth values ranged from 0 to 700 cm with a mean and median of 125 cm and 60 cm, respectively (Figure 35). The total depth drill was 700 cm so in places this underestimated the total thickness of the regolith. The training dataset produced a correlation of $R^2 = 0.70$ with a root mean square error (RMSE) of 92.54 cm. The 25% out-of-sample test data retained for model evaluation produced a R^2 correlation of 0.64 and RMSE of 112.89 cm, and we consider this a more meaningful test of mapping accuracy as it shows the "true" independent validation. The final depth prediction surface has a grid cell resolution of 10 m (Figure 36). The model with residual variogram adjustment improved the R^2 correlation to 0.66 with a RMSE of 109.37 cm. Adding back the residuals corrected for the overall underestimation of model versus actual

values in the dataset. However the geostatistical residual map introduced depth values away from the point observations, and the patterns that were not consistent with our conceptual understanding of the underlying pedogenic controls influencing regolith thickness. The inconsistencies in the residual patterns were attributed to the uneven spatial distribution of observations, and hence the patterns considered more a geostatistical artefact. For this reason we did not include the geostatistical residuals in the final model prediction (Figure 36). In the future, weighting the residual grid with a topographic covariate (e.g. MrVBF) so that landscape process is "built into" the residual prediction may give improvements to reliability.
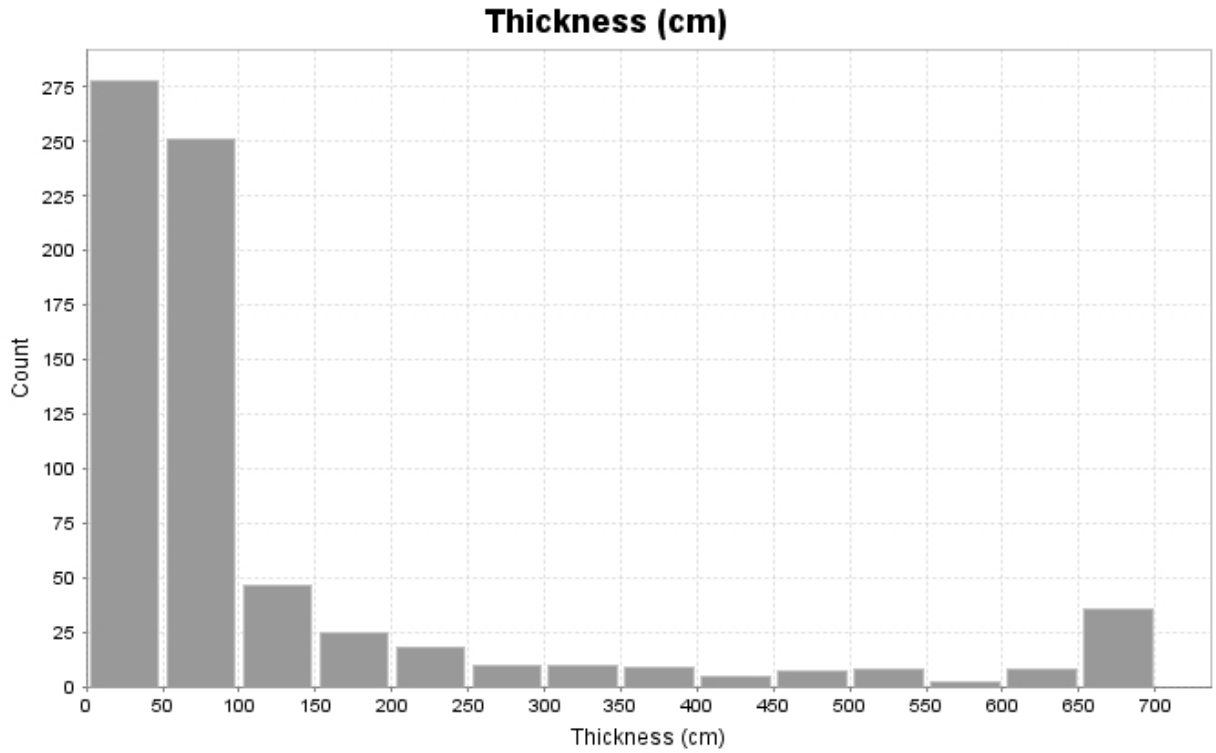
Figure 35 Distribution of site depth values used to establish relationships between regolith depth and environmental covariates.
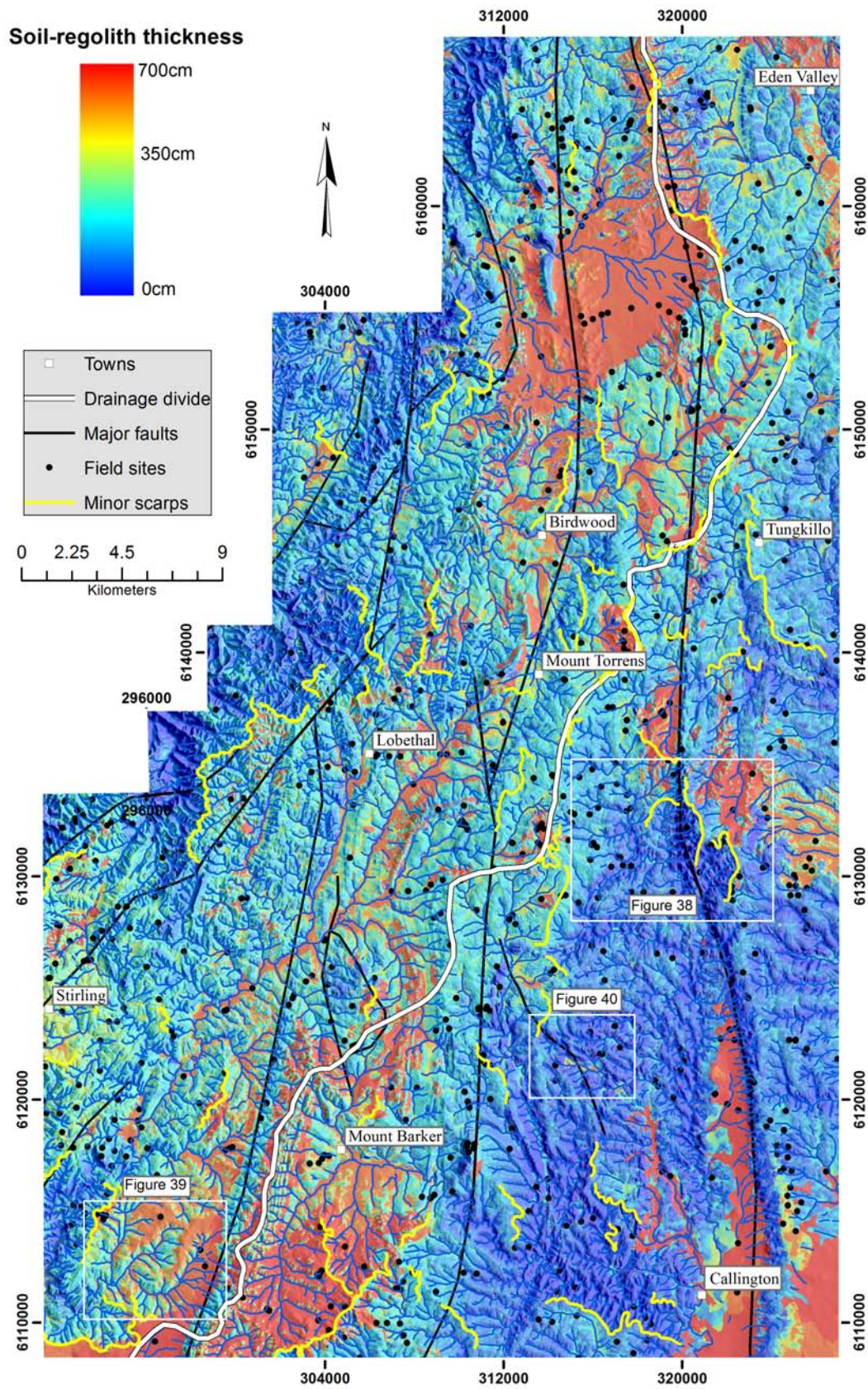
Figure 36 Regolith thickness model overlain on a hillshaded DEM. Morpho-tectonic and topographic features highlighted.

4.3.2 Environmental covariates and weathering processes

The environmental covariates as predictor variables are used in the model to define regions where individual regression models apply, and in the linear regression models themselves. The contribution of the environmental covariates within this model framework are summarised in Figure 37. The use of covariates in the model is broadly consistent with our conceptual understanding of the factors that control regolith depth, and which involve the interplay between physical, chemical and biological processes (Figure 31 and Table 1). Weathering intensity index (WII) and geology (geol) have a first order control or regional control on regolith thickness. The WII is a geochemical index based on airborne derived estimates of K, Th and U (Wilford, 2012). Highly leached and weathered landscape surfaces tend to have low K and elevated Th and U due to scavenging and retention of these elements by Fe-oxides and clays in the regolith profile. Other studies have demonstrated that ratios of K and Th can be used to quantify chemical weathering and erosion processes (Carrier et al., 2006). In this study elevated WII values were effective in delineating relict, highly weathered and chemically leached landscapes associated with summit surfaces. As such, the WII

provided a surrogate for time in Jenny's soil forming formula, and importantly, enabled the model to split palaeo-landforms from contemporary landforms. We expected the bedrock type would have a strong control on regolith thickness since most depths were recorded in the saprolith zone of the weathering profile. Preferential deeper weathering of more argillaceous sedimentary bedrock compared to highly siliceous bedrock was also observed in the field. To a lesser extent MrVBF, Wetness Index, aspect, annual mean temperature and highest monthly radiation are used in defining sub-regions. MrVBF and Wetness Index are important in identifying landscape accumulation zones (e.g. colluvial and alluvial deposition), or where water accumulates leading to hydrolysis and enhanced weathering. Aspect influences soil moisture and solar radiation, and therefore biological activity. Temperature and solar radiation influence weathering directly by affecting the rates of chemical reactions and indirectly through the influence on biological activity. These climatic surfaces separated the cooler, more highly weathered western side of the study area from similar landforms in the drier eastern side that were less weathered. Solar radiation was also found to be an important covariate for predicting topsoil and subsoil thickness due to the influence of heating and subsequent increased weathering rates (Bui et al., 2006; Minasny and McBratney,1999).
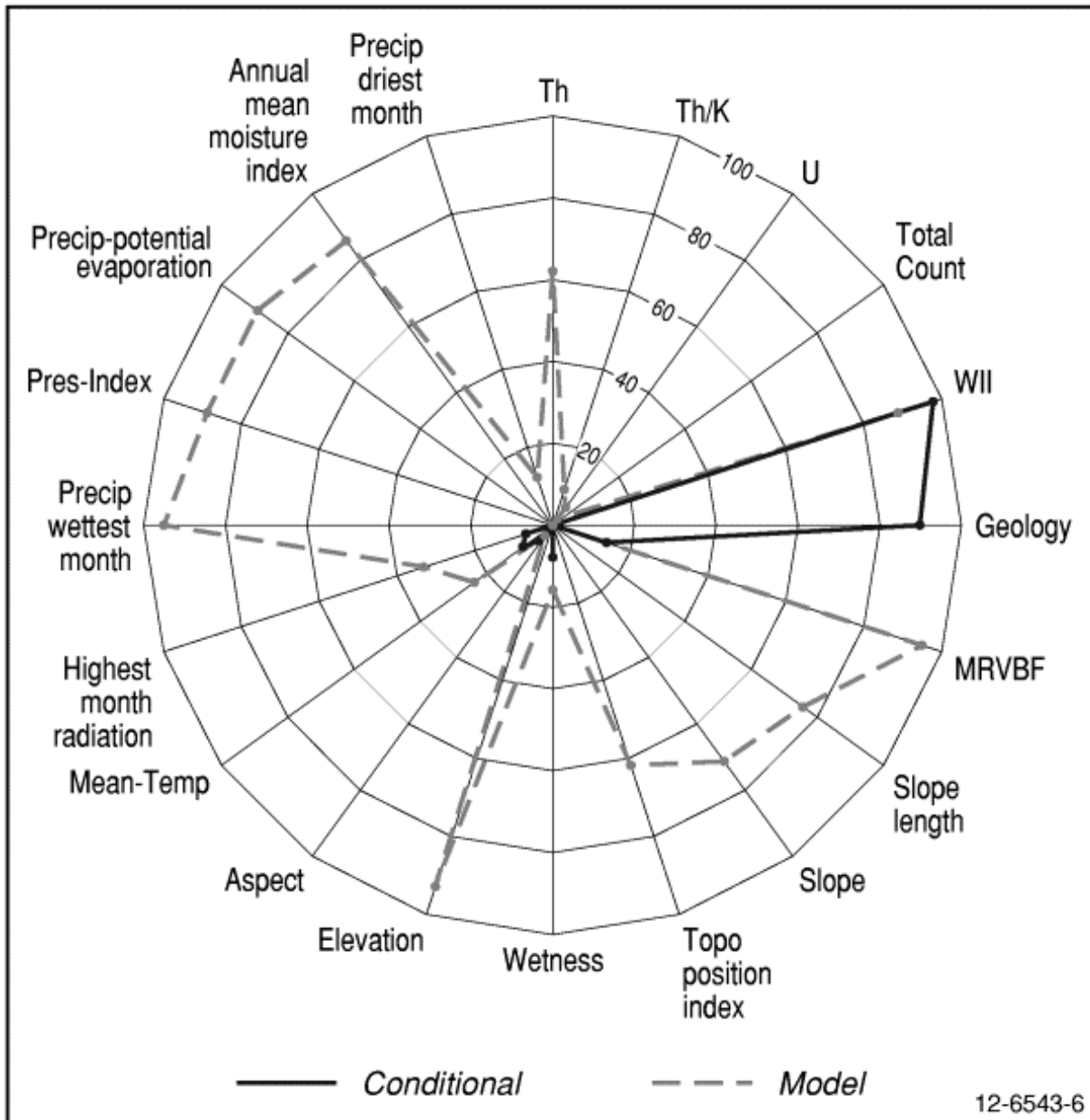
Figure 37 Use of individual covariates in the conditional (solid line) and linear regression(dashed line) components of the regolith model.
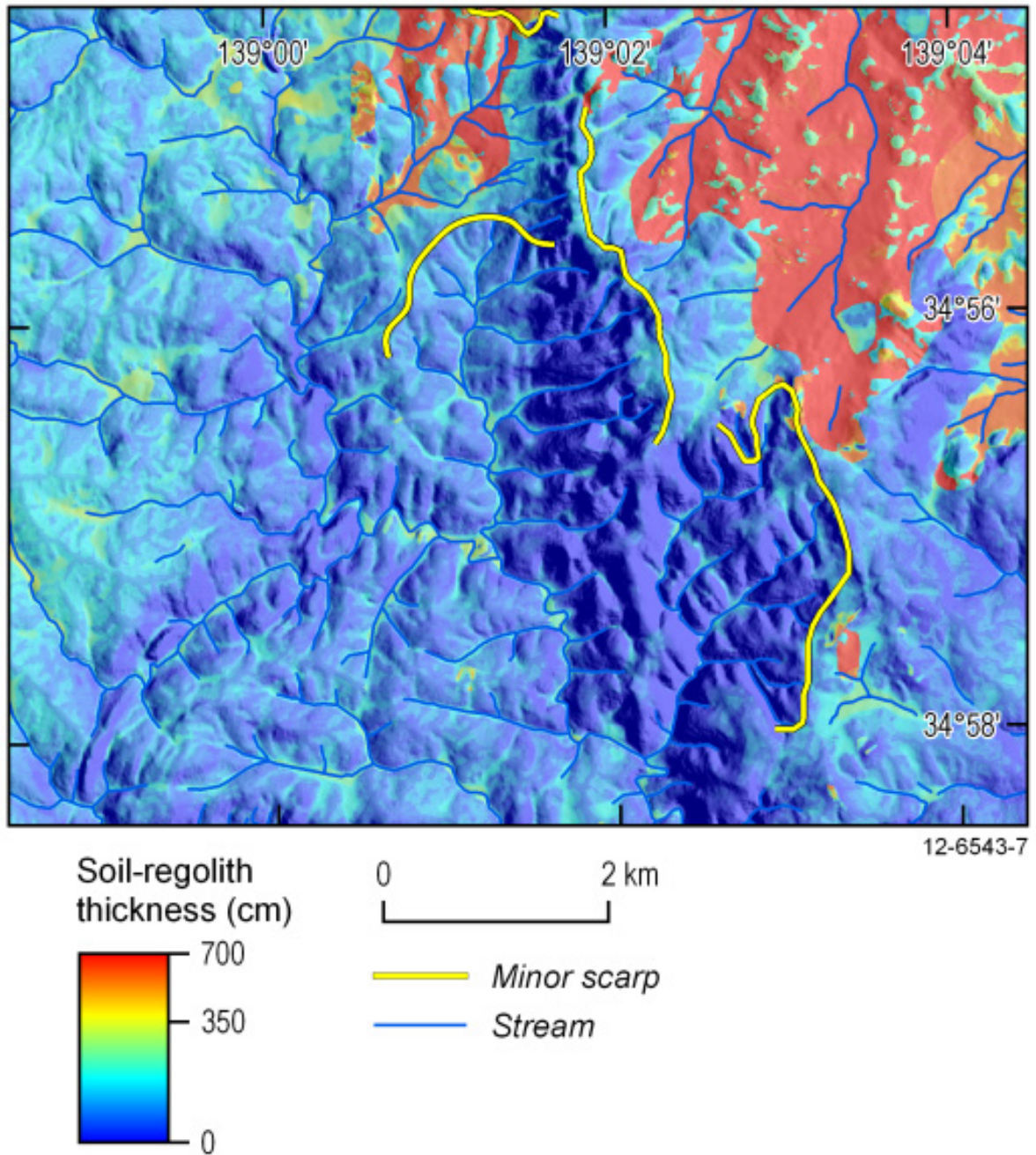
Figure 38 Minor erosional scarps commonly mark a significant boundary between thicker regolith above the scarp and less weathered and shallow regolith below.

The most important environmental covariates used in the regression component of the model consisted of climatic and terrain variables (Figure 37). The climate covariates largely reflect the moisture regime and the degree of hydrolysis and leaching within and beneath the solum. These covariates included precipitation during the wettest month, the Prescott Index, precipitation minus potential evaporation, and annual mean moisture index. The Prescott Index is a water balance model where high values reflect relatively high rainfall, low evaporation and overall greater leaching of soils (Table 9). Precipitation and moisture index covariates were also found to be important in estimating solum thickness (Bui et al., 2006). Terrain covariates including MrVBF, TPI300 and slope (Table 9) described variation of regolith depth associated at the more local, hillslope scale as these express patterns of water infiltration, and soil loss and deposition. The importance of elevation in the regression model component reflects influence on temperature and rainfall. With 73% usage in the regression model, slope length relates to patterns of soil re-distribution.
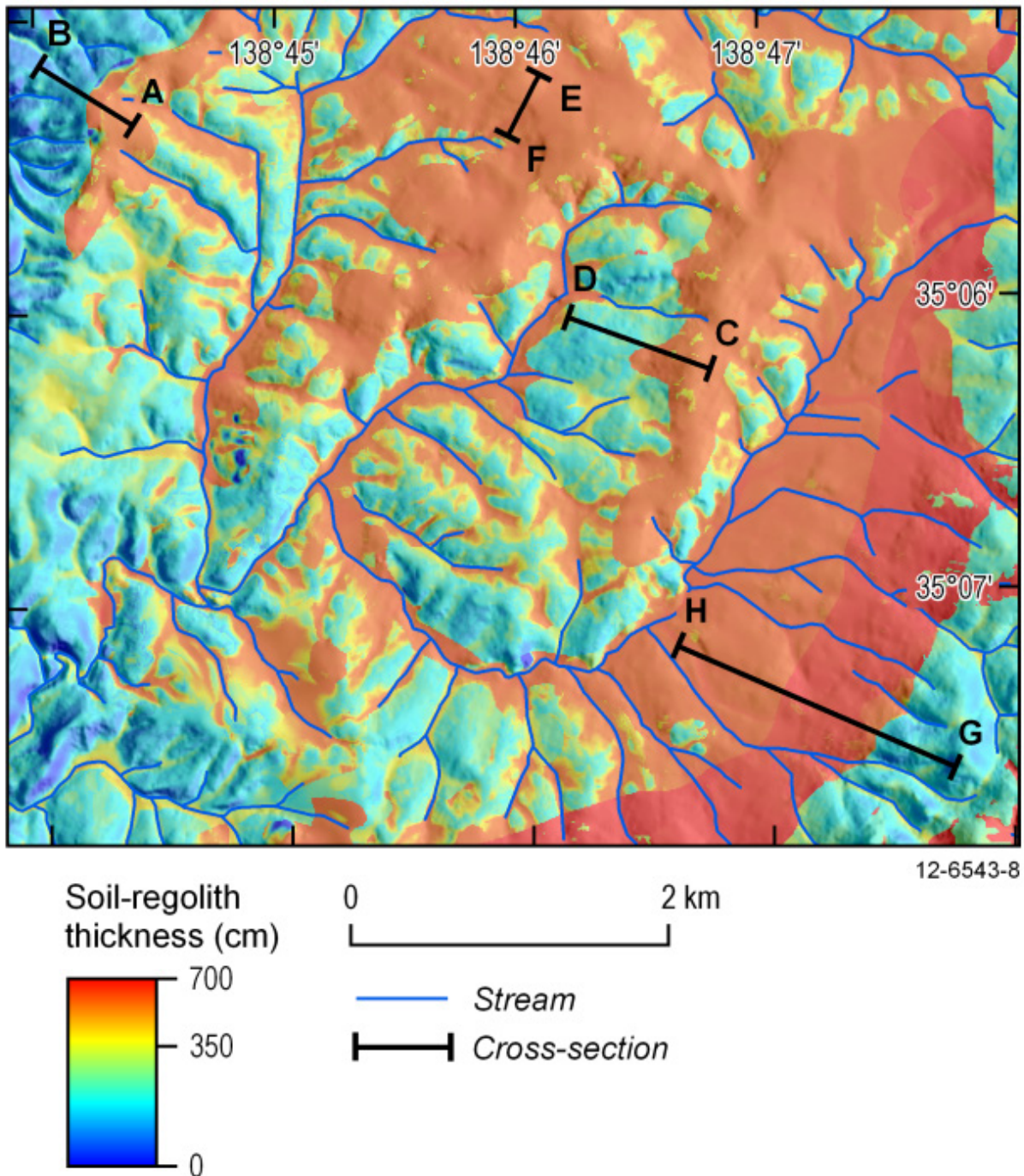
Figure 39 Toposequences within the highly weathered palaeo-landscapes.

Slope length and slope (steepness) are also key components used in the universal soil loss equation to model soil erosion processes (Renard et al., 1994). The remaining environmental covariates that were found to not contribute to the models significantly either did not correlate with regolith depth, or were redundant due to strong correlation with other environmental covariates used. A notable absence in the model covariates is curvature (plan and profile). Other studies (Heimsath et al., 2002; Tesfa et al., 2009) have shown curvature to be an important component in predicting soil thickness with deeper soils associated with concave areas. The difference in usage might be explained by (i) these investigations are predicting over relatively shallow depths where surface morphological controls are more important (ii) palaeo-landscape

components or a similar relict feature that exerted a first order control on soil-regolith thickness in our study were absent in the other studies, and (iii) curvature was made redundant due to correlations with other covariates (e.g. TPI, MrVBF and TWI).

4.3.3 Thickness model thematic map interpretation

Spatial patterns and depth ranges as shown in the resulting regolith depth map (Figure 36) are broadly consistent with our conceptual understanding of the regolith variability and landscape evolution. The model highlights deep weathering south of Mt Barker, immediately east of Mt Torrens and between Eden Valley and Birdwood (Figure 36). This is consistent with known areas of partially preserved palaeo-surface landforms and associated deep Cenozoic weathering profiles. The distribution of the palaeo-surface is controlled by several major north–south trending fault scarps and minor erosional scarps that are presently working back to remove the older landforms. There is a strong relationship between these structural controls and the distribution of regolith thickness (Figure 36 and Figure 38). The model also identifies thicker regolith associated with colluvial and alluvial fans along the base of Bremer fault scarp.

Delineation of the palaeo-surface is a critical component of the model not only because the weathering is deeper but also because the distribution of toposequences of regolith thickness within these landforms differs when compared to more youthful landscapes.

Palaeo-surface toposequences often show greater regolith depths on hill crests and upper hill slopes compared to valley floors (Figure 39: catenas within highly weathered palaeo-landscapes: sections A–B and C–D), which tend to be shallower; this is an expression of incision of the palaeo-surface, and exposure of less weathered bedrock in the valley floor. Where the incision is weak (e.g. started more recently), the highly weathered upper and lower landscapes are preserved in situ (Figure 39: sections E and F). The upper hill crest tends to be flat or bevelled and erosional scarps can

form the boundary between the upper weathered materials and the less weathered lower slopes. In places the typical toposequence association is reversed with weathering depth increasing down slope from the hill crest to the valley floor (Figure 39: sections G and H). The abrupt change in regolith depth along the G-H toposequence might indicate a bedrock boundary or faulting (see faults shown on Figure 36). Within the palaeo-surface landscape this relationship is associated with prominent hills and ridges, and serves to highlight the high degree of local variability within these older landscapes. It suggests that local relief (quite significant in places) coupled with a long weathering and erosional history and bedrock heterogeneity has led to considerable lateral variability in regolith depth. In this context the dynamic and on-going weathering, erosion and deposition model of landscape evolution proposed by Milnes et al. (1985) and Bourman (1993) best explains the distributions of regolith depths identified here. On more youthful landscapes the association of increasing regolith depth from crest to valley floor is the most common toposequence relationship. Within these landscapes bedrock weathering is generally shallow and most of the regolith variations reflect thickening associated with colluvial footslopes and the alluvial valley floor (Figure 40; sections A and B).

4.3.4 Model strengths and weaknesses

Despite the complex weathering and tectonic history of the study area, the Cubist model was able to explain approximately 64% of the recorded regolith depths within the out-of-sample evaluation test data. The strength of the correlation reported in this study is consistent with other studies attempting to predict soil depth in upland landscapes, e.g. Tesfa et al. (2009) and Sekhar et al. (2009). The results presented here are an improvement on regolith depth estimates from existing, traditionally-based soil mapping of the study area (Soil and Land Information, 2002). For example, this mapping only indicates the depth of hard bedrock within 1.5 m of the ground surface, and being polygon mapping, is not spatially explicit inside the polygon mapping unit.
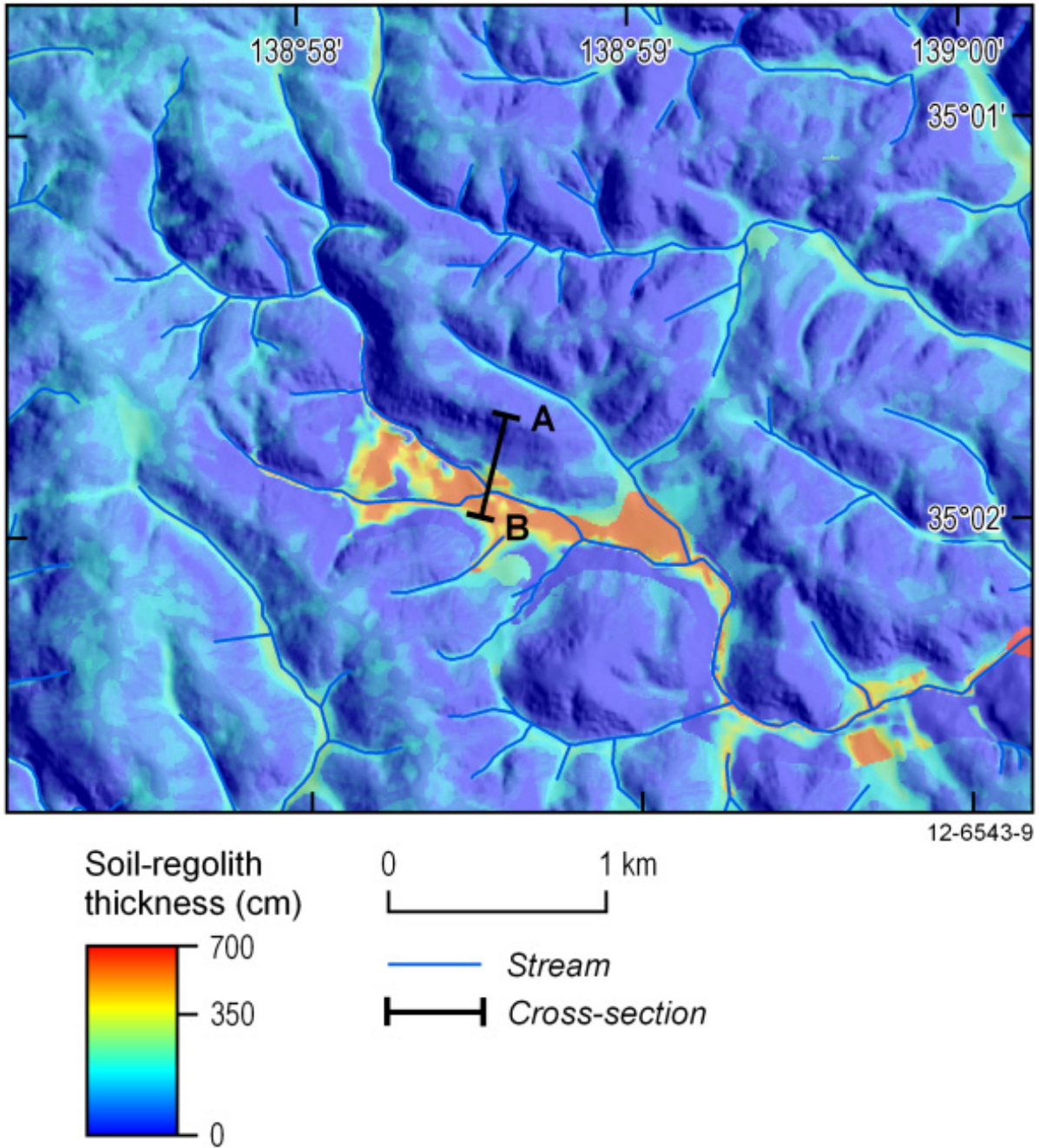
Figure 40 Typical toposequence associated with less weathered erosional landscapes.
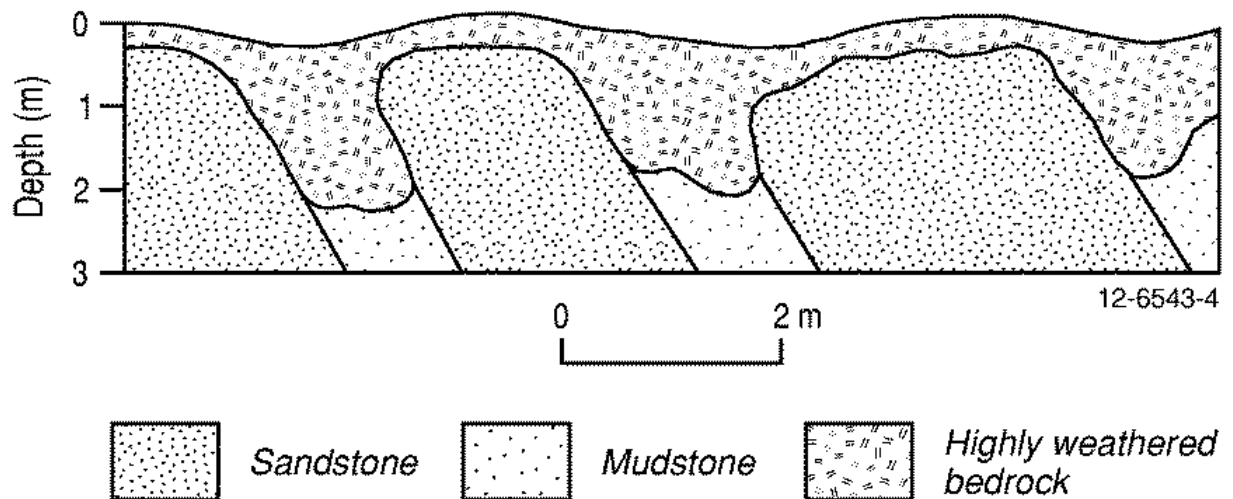
Figure 41 Regolith thickness variations reflecting local scale lithological controls.

The study area has a complex geomorphic and weathering history, which translates to an involved set of relationships at the local topo-sequence scale. The Cubist model hierarchy appears to be well suited to recognising both regional and local hill slope controls on regolith thickness. The WII together with geology and MrVBF (delineating valley floors and hills), and to a lesser extent the temperature climate covariates, have a first order control on weathering depth. This first order sub-division (regional scale) is critical in effectively modelling regolith variation at finer scales, which are based on topographic and climatic covariates. This contribution of terrain attributes at the local scale is plausible because of the strong topographic control on hill slope processes and weathering depth. However the strong contribution of the climatic attributes at this scale is surprising, and may reflect the strong climatic gradients across the study area. Furthermore, this may imply that the same climate gradients have existed for a long time.

The model proved weakest at predicting shallow depth. Extraction of actual and predicted on the 25% test data with depths < 1 m, recorded an R^2 value of 0.19. That the shallower depth ranges were difficult to resolve is not surprising due to the highly variable range of depth to bedrock noted, e.g. at road cuttings. For example, it was common to see depth to bedrock in the range 0.3–2 m within a horizontal distance of a few metres (Figure 41). This variability largely reflects local differences in bedrock mineralogy and physical characteristics including particle size and litho-structure (e.g. fractures, jointing, faulting and bedding). Furthermore, and compounding this, the resolution of the environmental datasets used (≥ 10 m ground resolution) are not sufficient to express these local, fine scale differences in the model. Phillips et al. (2005) demonstrated the importance of fine scale controls to regolith thickness. They showed that the primary controls on regolith thickness are related to litho-structural variability (e.g. lithological types and structural resistance associated with fractures and bedding) and the point-centred pedological influences of trees. Similar to our findings, those authors did not find a correlation between terrain attributes and the depth variations found in relatively shallow regolith cover.

4.4 Conclusions

We have applied a piecewise linear regression digital soil mapping approach using commonly available environmental covariates (geology, geochemistry, terrain and climate) to predict regolith depth to 8 m in a 128,000 ha study area in the central Mt. Lofty Ranges, South Australia. With a ground grid spacing of 10 m, the resulting map is suitable for local, landscape scale modelling and decision support. We note that the model honours much of our conceptual understanding of the complex weathering history of the study area landscape, and with an R^2 estimate of 0.64 for precision of prediction, the approach shows promise. However, the model yielded unreliable results (R^2 = 0.19) for shallow soils (< 1 m), we believe reflecting the fine scale bedrock controls on weathering depth that were not resolvable given the ground resolution of the

environmental covariates used (≥10 m). Overall however, this mapping result is encouraging and is a significant advance over traditional regolith mapping methods that are laborious and costly, hampering regolith mapping to date. With local adaptation, this approach leads the way towards a nationally consistent Australian regolith thickness map that will play an important part in future landscape scale environmental simulation modelling and decision support.

Acknowledgements

Chapter 5

Using airborne geophysics to define
the 3D distribution and landscape evolution
of Quaternary valley-fill deposits around the
Jamestown area, South Australia

5   Using airborne geophysics to define the 3D distribution and landscape evolution of Quaternary valley-fill deposits around the Jamestown area, South Australia

Quaternary valley-fill consisting of water and debris flow deposits found in the Jamestown area of South Australia. The sediments consist mostly of clay, silt and fine sand with local gravels and cobbles. The nature, age and thickness of these deposits are described within a landscape evolution conceptual framework.

Summary

The combined analysis of airborne electromagnetics (AEM), airborne gamma-ray spectrometry (AGRS), magnetics and a digital elevation model with ground-based calibration, has enabled construction of a 3D architectural and landscape evolution model of valley fill deposits around the township of Jamestown in South Australia. The valley fill sediments consist of traction, suspension and debris-flow deposits that range in age (OSL dating) from 102 ka (±12) to the present day. A sediment isopach map generated from the AEM dataset reveals the 3D structure of the valley-fill deposits. The sediments are up to 40 m thick within asymmetrical valleys and are the result of colluvial fan, floodplain and sheet-wash processes. The sediments fine upwards with a higher proportion of coarser bed load deposits toward the base and fine sand, silt and clay towards the top of the sequence. A strong linear correlation between airborne K response and soil texture allowed the percentage of surface silt to be modelled over the depositional landforms. The sediments are thought to have been derived by a combination of aeolian dust accessions, and weathering and erosion of bedrock materials within the catchment. Older drainage lines reflected in the distribution of relatively closely spaced and well connected 'magnetic channels' differ markedly from present day streams that are largely ephemeral and interrupted. This is thought to reflect a change in local hydrology and associated geomorphic processes from relatively high to lower energy conditions as the valley alluviated. These hydrological changes are likely to be associated with a drying climate, lower recharge and runoff.

5.1 Introduction

Airborne and ground-based electromagnetic (EM) geophysical data are becoming increasingly important in providing scientific information to assist natural resource management issues, particularly in relation to groundwater and near-surface water and soil salinity. Electromagnetic methods are also used to generate 3D electrical conductivity maps of regolith and bedrock materials (Lane et al., 2000). The main factors influencing conductivity are the salinity of the pore fluids, and the porosity and composition of the materials (i.e. regolith and bedrock mineralogy). When EM data are calibrated with drilling (lithological and conductivity logging) and surface mapping (e.g. soil–landscape and geomorphological maps) they can be used to develop 3D hydrogeological frameworks that explain the distribution of salt, regolith and bedrock materials. In depositional landscapes the framework is usually in the form of a spatially explicit sedimentological model. These models provide an improved understanding of the distribution of salts and their mobilisation pathways that can be used to target salinity remediation actions (Lawrie et al. 2000; Lane et al. 2001; Munday et al., 2004).

Airborne EM (AEM) interpretations are generally combined with other geophysical datasets, such as airborne magnetics and gamma-ray spectrometry.

These datasets provide complementary information on regolith and bedrock properties to help describe or constrain the 3D hydrological framework. Gunn and Dentith (1997) demonstrated how magnetics could be used to map bedrock alteration and weathering where these processes have either depleted or enriched the magnetic content of the original bedrock. Dauth (1997) used magnetic imagery to identify maghemite-rich and other ferruginous weathering products. Mackey et al. (2000) showed the application of airborne magnetics in delineating maghemite-filled palaeochannels. In contrast, airborne gamma-ray spectrometry (AGRS) is essentially a surface geochemical mapping technique that shows the distribution of the radioelements potassium (K), thorium (Th) and uranium (U) in regolith and bedrock. The distribution of these radioelements has been used to map regolith and bedrock types and understand weathering and geomorphic processes (Bierwirth, 1996; Cook et al., 1996; Dickson and Scott, 1997; Wilford et al., 1997; Pickup and Marks, 2000).

This paper demonstrates how the combined interpretation of AEM, magnetics, AGRS and a digital elevation model (DEM) in conjunction with ground-based studies involving drillhole interpretation, regolith geochemistry and mineralogy, laser grainsize analysis and optically stimulated luminescence (OSL) dating are used to construct a 3D distribution and regolith–landscape model of valley-fill deposits in the Jamestown region. The regolith and sedimentological

model developed in this paper provides insights into how the landscape has evolved through time as well as providing a hydrological framework to better understand salinity and groundwater processes. The landscape evolution component is described here while groundwater salinity aspects are discussed by Cresswell and Herczeg (2004) and Wilford (2004b). The methodology used to reconstruct the sedimentological evolution of the valley-fill deposits in the Jamestown area has the potential to be used in other locations where similar datasets are available or where new multidisciplinary projects are being planned.

5.1.1 Location, vegetation and climate

The study area is in the Northern Agricultural District of South Australia 190 km due north of Adelaide. The townships of Jamestown and Caltowie are in the northern half of the study area at an elevation of ~460m above sea-level (Figure 42).

The region has cool wet winters and hot dry summers. The Jamestown area has an average annual rainfall of ~555 mm and a mean maximum temperature of 22.8^{0}C. Annual evaporation exceeds annual rainfall (weather statistics for the Bundaleer Forest Reserve http://www.bom.gov.au/climate/averages/tables/cw_021008.shtml4). The native vegetation prior to farming in the 1800s probably consisted of open savannah (Cooper 1978). Vegetation along valley floors and adjacent alluvial and colluvial slopes (Stephens et al., 1945) was dominated by grasses, including *Danthonia semi-annularis* (wallaby grass), *Lomandra dura* (iron grass) and *Themeda triandra* (kangaroo grass). Elevated sites with better drainage probably supported a woody cover with a grassy understorey. Woody species included *Casuarina stricta* (sheoak) Acacia spp. (wattle) and *Eucalyptus odorata* of mallee habit (Stephens et al., 1945; Henschke et al., 1994). Most of the native vegetation has been cleared to support farming including cropping (wheat, lucerne, field peas) and sheep grazing. Pine plantations are also important providing timber for local milling operations.

5.1.2 Geology, geomorphology and soils

Bedrock in the area consists of Neoproterozoic siltstone, dolomite, sandstone, quartzite, limestone, tillite, feldspathic sandstone, pyrite shale and calcareous siltstone and sandstone (Mirams, 1964) (Figure 43). These rocks form part of the Umberatana and Burra

Groups that underwent major deformation, and contact and regional metamorphism associated with the Delamerian Orogeny (Preiss, 1987). Phyllite and hornfels rock textures are common. The overall structural trend is north–south with anticlinal and synclinal folds visible on the hill-shaded DEM (Figure 44).

Erosional landforms largely reflect differential erosion processes with resistant rocks (e.g. quartzite and siliceous tillites) forming prominent bedrock ridges with associated steep slopes. These ridges rise 80–150m above the surrounding colluvial slopes and alluvial floodplains. The highest relief is associated with ridges on either side of the Belalie and Bundaleer north–south-trending valleys (Figure 44). The valleys are partially filled with a series of coalescing alluvial and colluvial fans that receive sediments from the surrounding hills. The fans form a series of broad lobes radiating from the base of low hills and ridges. Gradients on these fans are low, with slopes of 0.2–3.0 degrees. Downslope the fans inter-digitate with floodplain sediments along the main axes of the valleys. Softer and preferentially weathered siltstone and carbonate-rich rock occur beneath the valley axes. In places low-angle pediments occur between the ridges and lower colluvial/alluvial slopes. Pediments are common in the upper parts of the Caltowie catchment where they consist of a thin mantle of sediments overlying bedrock.

Thomas et al. (2007) described a regionally repeating east-facing toposequence of the Belalie valley. A typical toposequence of hillslopes in the district comprises: shallow calcareous sandy loams with red clay subsoils associated with steep bedrock slopes; moderately deep loams to sandy loams with red clay sub-soils on low relief rises; and deep loams, sandy loams and silty loams developed on colluvial and alluvial sediments (Stephens et al., 1945; Department of Water, Land and Biodiversity Conservation, 2002). Soils associated with the sediments exhibit both gradational and texture contrast profiles. Some soils are saline with surface salinity associated with waterlogging following periods of higher than average rainfall (Henschke, et al., 1994). Salt-induced scalds and associated soil erosion, locally referred to as 'magnesia patches,' also occur in some upland landscapes. Salt scalds have been mapped in the Caltowie and Bundaleer catchments (Department of Water, Land and Biodiversity Conservation, 2002).

5.2 Data and Methods

The AGRS, magnetics and digital elevation data were acquired over a survey area of ~28 km east–west and 35 km north–south. The AEM survey was restricted to the northern half of the study area (Figure 42).

5.2.1 Airborne gamma-ray spectrometry

AGRS data were collected by Fugro Airborne Surveys during June–August 2002 using a flight-line spacing of 100 m and a nominal terrain clearance of 60 m using an Exploranium GR-820 spectrometer. Gamma-rays were detected using a 50.3L NaI (T1) crystal pack across 256 channels.
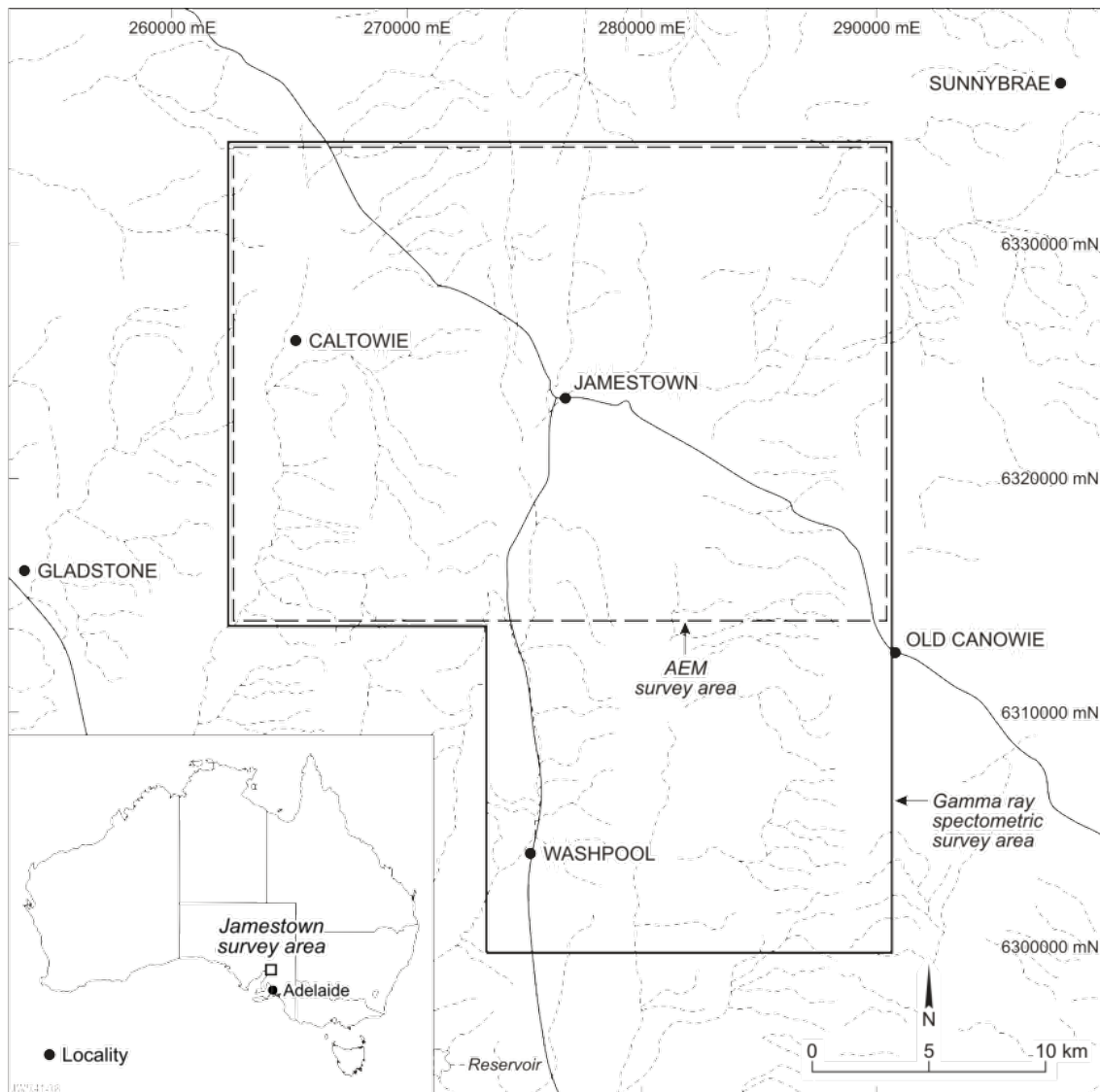
Figure 42 Location of study area and geophysical surveys.

AGRS measures the natural radiation from potassium (K), thorium (Th) and uranium (U) in the upper 30 cm of the Earth's surface. Gamma-ray survey therefore provides near-surface geochemical information of bedrock and regolith materials. Potassium is measured directly from the decay of 40K. Thorium and U are inferred from daughter elements associated with distinctive isotopic emissions from 208Tl and 214Bi in their respective decay chains, so they are usually expressed in equivalent parts per million eU and eTh. Potassium is more abundant and is expressed as a percentage. A series of data processing and calibration steps were then performed including NASVD noise reduction or spectral smoothing (Minty, 1997), cosmic,

aircraft and radon background removal, stripping and height corrections [see Fugro Airborne Surveys (2002a) for detail descriptions of flight-acquisition and data-processing steps]. The flight-line data were micro-levelled for each band and a minimum curvature algorithm was applied to produce grids with 20 m cell size. A median filter was used to remove high-frequency noise (speckling) in each of the gamma-ray channels.

AGRS grids were displayed either as single pseudo-coloured images with red to blue colours relating to high and low gamma-ray emissions respectively, or as three-band colour composite images (ternary images) with K in red, eTh in green and eU in blue (Figure 45). Images were enhanced with ER Mapper software and integrated as raster images within the 3D modelling environment of GOCAD software.

Quaternary
- Alluvial and colluvial silt, sand and minor gravel

Miocene-Pliocene
- Ferruginous pebbly gravels and sandstone

Neoproterozoic
- Black shale and dolomitic siltstone
- Dolomite, siltstone, sandstone dolomitic limestone
- Limestone or dolomite
- Mudstone, siltstone and shale
- Quartzite and interbedded sandstones
- Sandstone and minor siltstone
- Siltstone, dolomitic siltstone, minor sandstone and pyrite
- Tillite, quartzite and siltstone

Figure 43 Major lithological and regolith units.

5.2.2 Magnetics

Airborne magnetics data were collected at the same time as the gamma-ray data by Fugro Airborne Surveys using a Geometrics G856 magnetometer. The magnetometer recorded signals at ~7 m intervals along each flight-line with a sensitivity of 0.001 nT. A line-spline algorithm was used to produce gridded magnetic data with 20 m cell size resolution for enhancement and display in ER Mapper and later modelling and integration with other datasets using ArcGIS and GOCAD software. First-vertical and horizontal derivatives of the magnetics were produced to highlight near-surface geological and regolith features. These derivatives highlight the rate of change in the vertical and horizontal planes of the magnetic image, respectively.
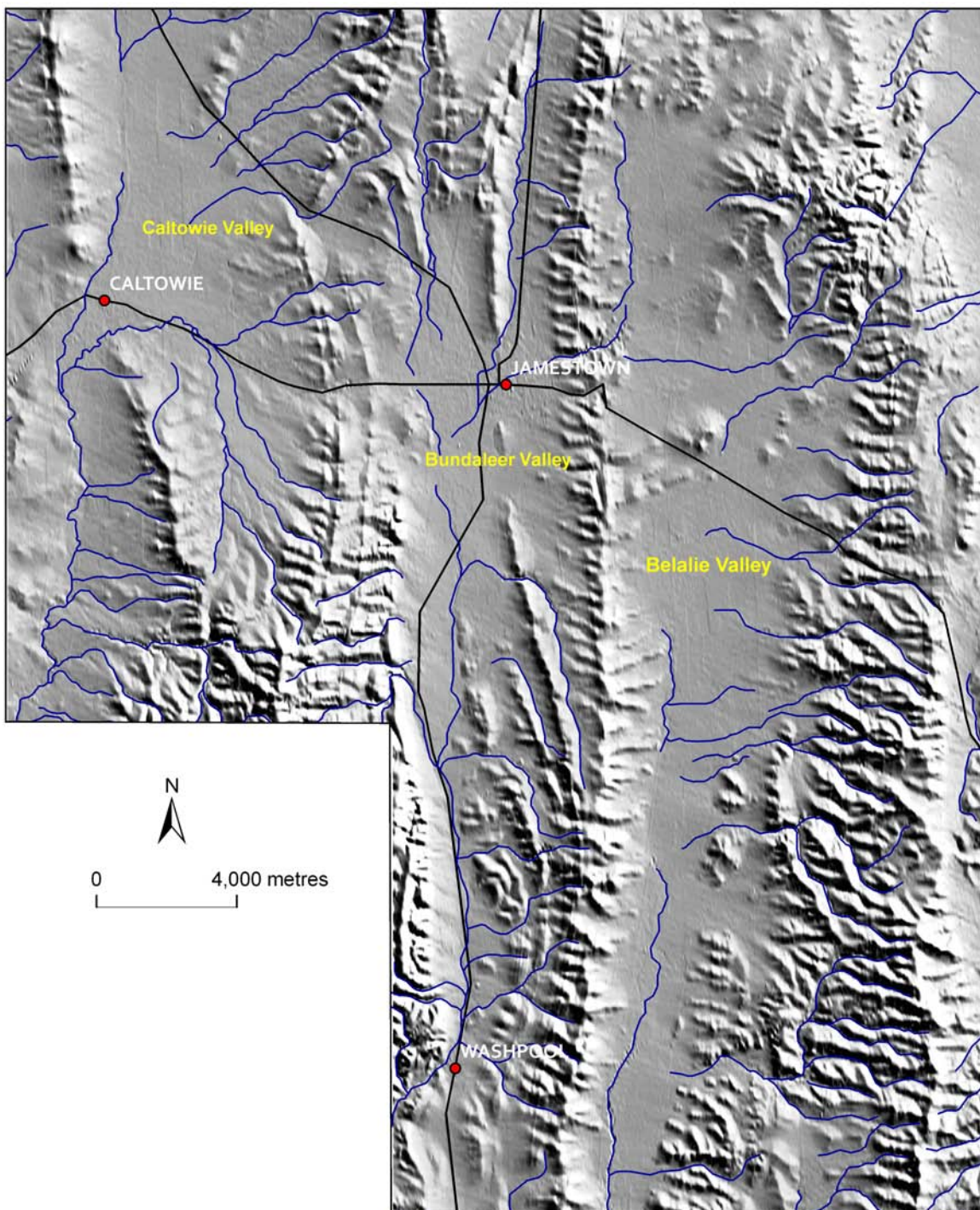
Figure 44 Hill-shaded DEM with roads, towns and surface drainage.

5.2.3 Digital elevation model

Instrumentation on the aircraft that collected gamma-ray and magnetic data including a radar altimeter (flying height above the ground), GPS locations and known altitude (flying height ASL) were used to construct a DEM. Elevation measurements were collected at 60 m intervals along each flight-line (100 m apart). Tie-line levelling and further micro-levelling along each flight-line produced the final levelled DEM. A line-spline algorithm was used to produce a final 20 m cell size DEM grid (Fugro Airborne Surveys 2002a).
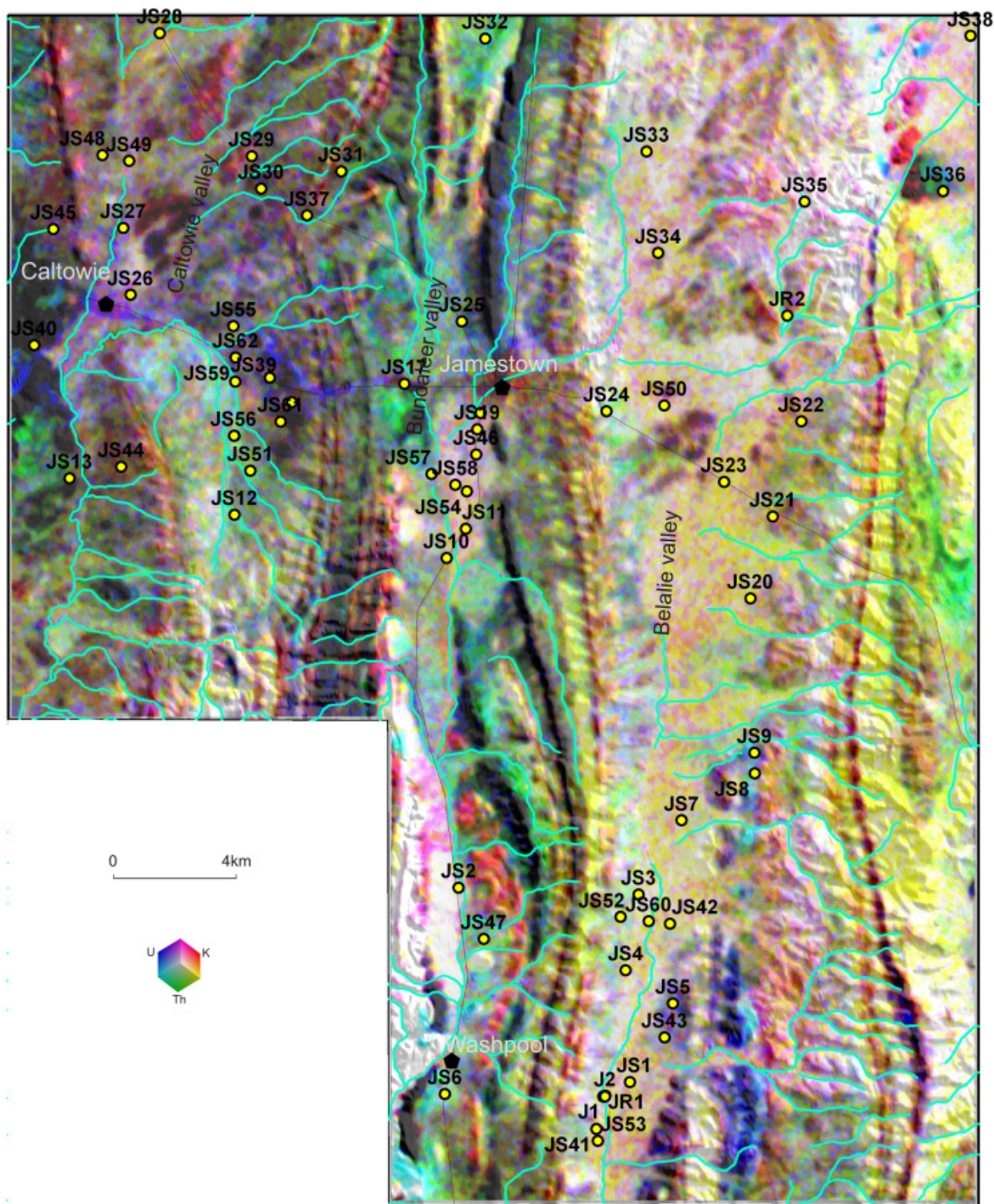
Figure 45 Ternary gamma-ray spectrometric image with K in red, eTh in green and eU in blue. Field sample locations including soil (JS), rock (J1) and OSL (J1, J2) sites.

The DEM was processed to derive a series of surfaces that described major geomorphological, structural and hydrological characteristics. These surfaces or attributes include slope, aspect, elevation and hill-shaded relief, catchments and drainage lines. In addition, the DEM plays an important role in landscape visualisation. For example, combining the DEM with airborne gamma-ray spectrometry images to produce 3D perspective images facilitated the visualisation and understanding of the relationships between gamma-ray responses and surface morphology.

5.2.4 Airborne EM

AEM measures the electrical properties of the subsurface, potentially down to 200 m below the surface. Fugro Airborne Surveys (2002b) flew the Jamestown survey with the TEMPESTTM system between 22 and 27 July 2002. A total of 1404 line km was flown with a flight-line spacing of 400 m. Specifications of the TEMPEST AEM System are described by Lane et al. (1999). A bicubic polynomial gridding routine was used to generate 80 m grid cells from the 400 m flight-line data (i.e. 1/5 the line-spacing). Acquisition parameters and processing steps involved in the TEMPEST system are described in Fugro Airborne Surveys (2002b).

To enable easier interpretation, the processed AEM window amplitude data were inverted to determine the subsurface electrical conductivity. This was done using the conductivity depth imaging (CDI) method calculated using EMFlow software (Macnae et al., 1998). The method assumes the Earth consists of uniformly conductive horizontal layers. Each observation along the flight-lines is transformed or inverted separately, and the derived conductivities are then stitched together to form the 3D subsurface conductivity distribution. The derived conductivity distributions were used to generate interval conductivity images (slices) at 5 m depth increments below the surface. Electrical conductivity depth information was also imported into the GOCAD 3D modelling software.

5.3 Ground-based analysis

5.3.1 Drillhole information

Existing groundwater records and drill log descriptions in the area provided insights into the subsurface

distribution of regolith materials within the valley systems and were used to interpret the AEM dataset. Thirty two drillhole logs were re-interpreted and classified into a consistent and comparable set of descriptions. Transported and in situ weathered materials were recognised. Within these classes further subdivision was made based largely on the degree of bedrock weathering. The regolith classes used to describe the drillholes are shown in Table 10.

5.3.2 Texture, geochemical and mineralogical soil analysis

To assess the relationships between AGRS imagery and soil properties 41 surface soil samples were collected from the colluvial and alluvial valley-fill sediments. Soil properties were not evaluated over the erosional landscapes. Samples of 300–400 g were taken from the top 30 cm of the soil and air-dried for texture, geochemical and mineralogical analysis. The 0–30 cm sample interval corresponds to the materials sensed by the AGRS survey (Minty, 1997). To ensure representative field site collections a sample stratification approach was developed. This involved using a slope threshold of 1.5^0 to separate erosional and depositional landforms. The ternary AGRS image was then used to ensure samples were collected over a representative range of radioelement responses (Figure 45).

Table 10 Regolith subdivisions.

Transported regolith
Alluvial and colluvial clay, silt and minor gravel
Alluvial clay/silt and minor gravel
Colluvial clay/silt and minor gravel
***In situ* regolith**
Residual clay
Highly weathered saprolite (typically high clay content)
Mottled saprolite
Moderately weathered bedrock
Saprock (bedrock structure and mineralogy largely unchanged)
Saprock to fresh bedrock

Soil textures were assessed using a Malvern Mastersizer 2000 particle size analyser. The particle analysis method uses laser diffraction to measure grainsizes from 0.02 to 2000 μm. Major- and trace-element compositions of soil samples were determined using inductively coupled plasma mass spectrometry (ICP-MS). The mineralogy of selected soils was determined by powder X-ray diffractometry (XRD). Commercial quantitative analysis software

(SIROQUANT) was used to determine wt% mineral compositions and clay mineralogy. Standard linear regression correlation methods were then applied to assess whether correlations existed between AGRS response and soil properties.

5.3.3 Optically Stimulated Luminescence (OSL) dating

Valley sediments were dated using the OSL method, which measures stored ionising radiation within quartz and feldspar grains. The amount of stored energy accumulates over time according to the concentration of radioactive elements in the sample. Because sunlight resets the luminescence signal, the time since the soil was exposed at the surface can be determined in the range 0–3 Ma. Two samples were taken at the southern end of the Bundaleer valley system where a 15–20 m-deep gully has been eroded into the sedimentary sequence. The first sample (J1) was collected 50 cm above the bedrock contact and the second (J2) 2.2 m below the surface (Figure 45).

OSL dating was undertaken using methods and instrumentation described in detail in Olley et al. (2004). Samples were prepared using standard procedures (Aitken, 1998) designed to isolate pure extracts of 180–212 mm light-safe quartz grains. Single-grain OSL measurements were made using a Risø TL/OSL DA-15 instrument (Bøtter-Jensen et al., 2000) and by applying the modified single-aliquot regenerative-dose protocol of Olley et al. (2004), which incorporates an infrared wash prior to each OSL readout. Approximately 90% of responsive grains from sample J1 had dose–response curves that saturated at between 150 and 200 Gy and before reaching the natural dose. For this sample therefore, the burial dose has been calculated based on just the small proportion of grains which had dose–response curves exceeding the natural dose ('supergrains': Yoshida et al., 2000). Although this sample size was small (just six grains), all grains had doses with overlapping uncertainties, suggesting that they come from a single well-bleached population.

5.3.4 3D model construction

A 3D model of the Jamestown area was generated by incorporating airborne geophysical datasets with drill logs and DEM attributes using GOCAD software. The 3D model was defined by two bounding surfaces that define the regolith package or 'regolith envelope.' The upper bounding surface is defined by the DEM and the lower surface from the base of the conductor determined from the CDI inversions of the AEM data. Variations within the regolith envelope are described using drillhole logs, AEM-derived conductivity slices and volumes, and AGRS and magnetic imagery. The benefits of creating 3D displays with these types of datasets are described in more detail by Lane et al. (1999) and Wilford (1999).

5.4 RESULTS

5.4.1 AGRS analysis

Bedrock and alluvial and colluvial sediments in the study area show a high degree of radioelement variability. Low bedrock emissions in K, eTh and eU are associated with quartzite, quartzose sediments (sandstone and siltstone) and some dolomites. High gamma-ray emissions are associated with mainly micaceous and feldspathic sandstone and siltstone (white and reddish hues: Figure 45, 2 km north of Washpool). Valley-fill colluvial and alluvial sediments, which are the primary focus of this investigation, exhibit ranges of 0.8–5% K, 7–12 ppm eTh and 1–2.6 ppm eU. The higher values of these ranges are associated with active fan deposits over the southern end of the Bundaleer valley (Figure 45). Notably, high K concentrations also correspond to alluvial sediments in the Belalie and central part of the Bundaleer valleys.

5.4.2 Mineralogy and Geochemistry

XRD mineralogy results on selected samples including weathered bedrock and surface alluvial soils are presented in Table 11. Sediments consist of quartz, kaolinite, microcline/orthoclase, mica/illite (K mica and clay), albite (Na plagioclase) and carbonate. The weathered bedrock contains similar assemblages with the exception of kaolinite which was not detected, and in addition magnesium carbonate (dolomite/ankerite) and chlorite. Chlorite is common in low to medium-temperature metamorphic rocks, and so its presence is not unexpected.

Table 11 XRD mineralogy of soil and bedrock materials in weight percentage.

Sample Label	Quartz	Albite	Microcline/ Orthoclase	Mica/Illite	Kaolin	Anatase	Calcite	Dolomite/ Ankerite	Hematite	Goethite	Maghemite	Smectite	Halite	Chlorite
JS59	60	5	3.7	6.8	21	0.3	2.7	-	-	-	-	-	-	-
JS60	53	10	3.3	23	10	-	-	-	-	-	-	-	-	-
JR1	35	13	1	26	-	-	12	4.4	-	-	-	-	-	8.3
JS61	72	5.1	1.9	8	12	0.2	-	-	0.6	-	?	-	-	-
JS62	57	12.0	3.6	12	15	-	0.1	-	0.4	-	-	-	-	-
Mag1	56	8.5	2.8	14	13	-	4.7	-	0.6	-	yes	-	0.7	-
Mag2	29	9	2	13	14	-	32	-	0.7	-	yes	0.8	-	-

? indicates possibly present but not confirmed   S = sediment R = rock   Mag = channel sediment and magnetic gravels
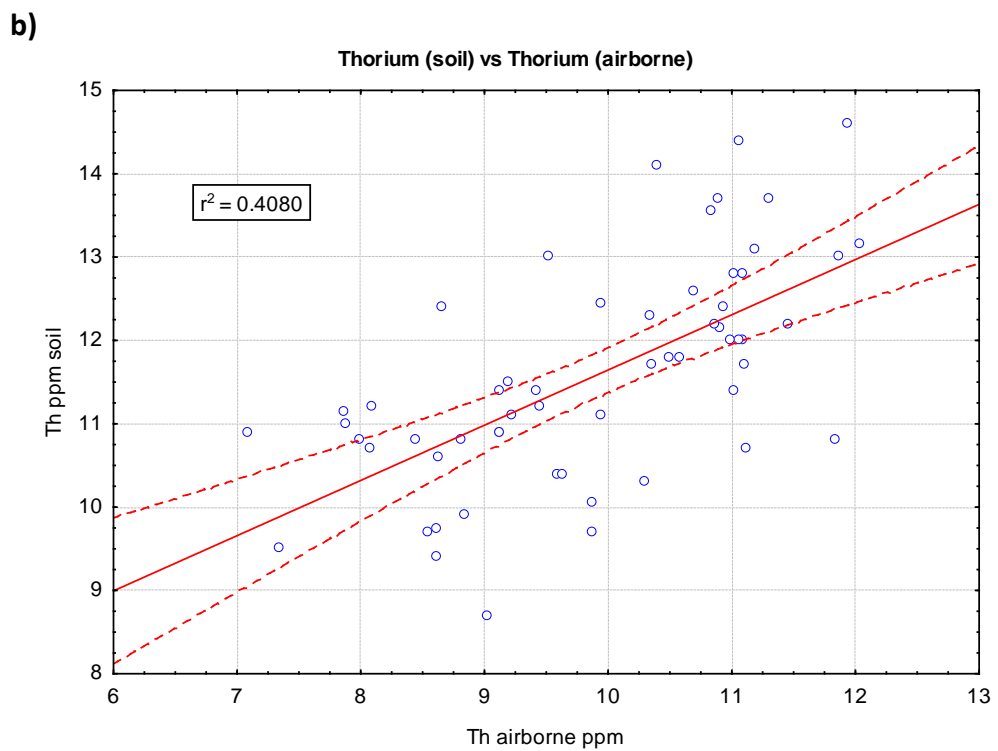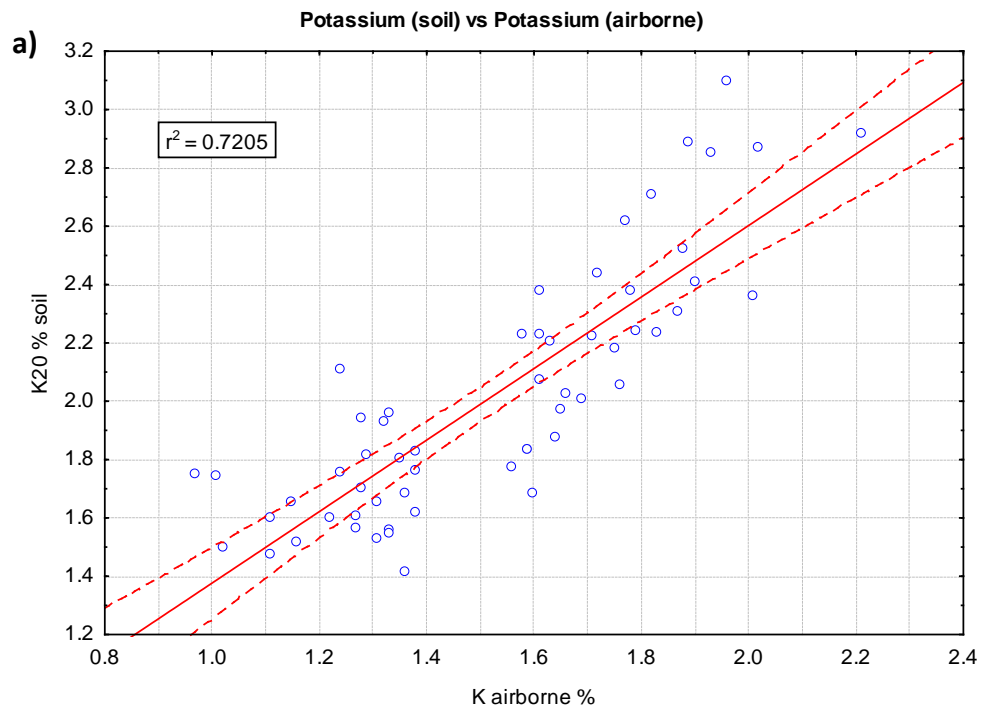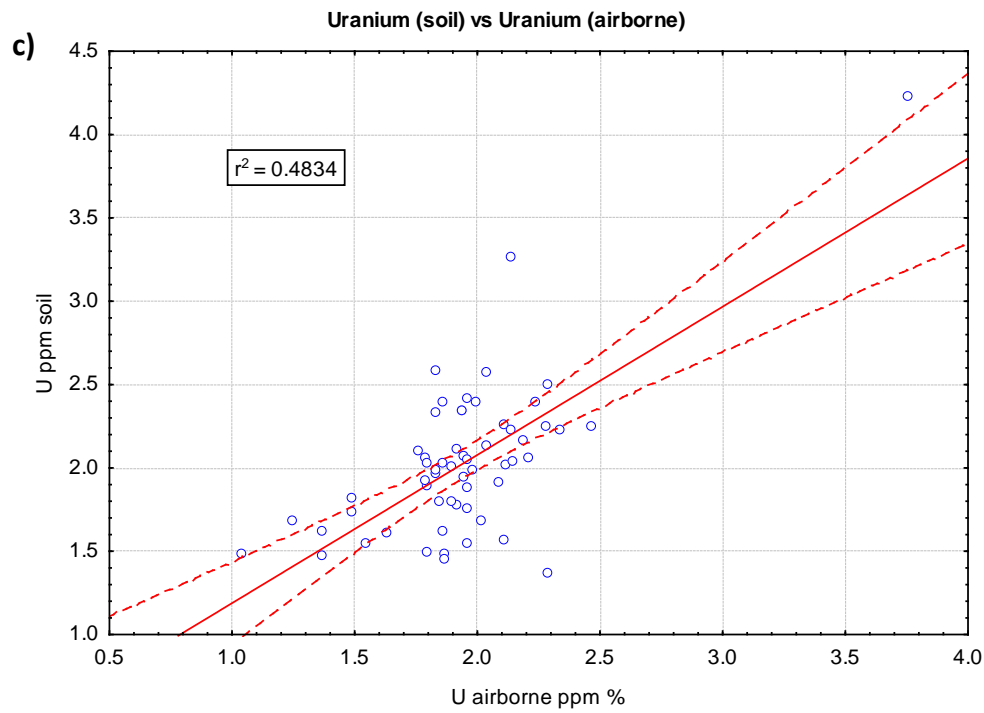
Figure 46 Correlations between airborne radioelement values and soil geochemistry.
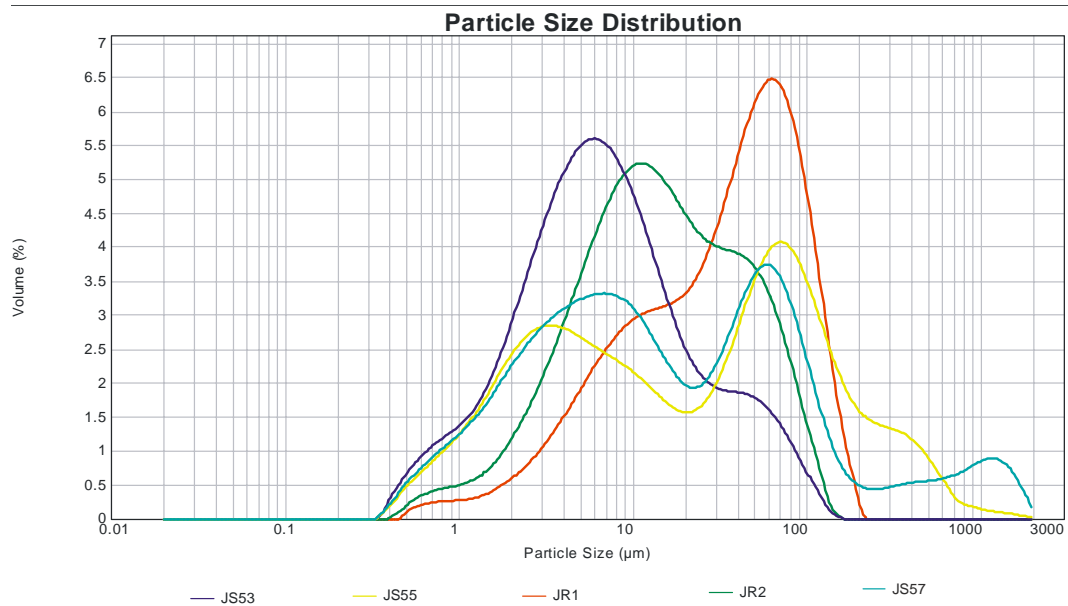
Figure 47 Laser grainsize distributions for representative surface soils. JS53, high silt content corresponding to high K; JS55, low silt content corresponding to low K; JR1, JR2, weathered bedrock; JS57, soils on pediments.

a)

b)
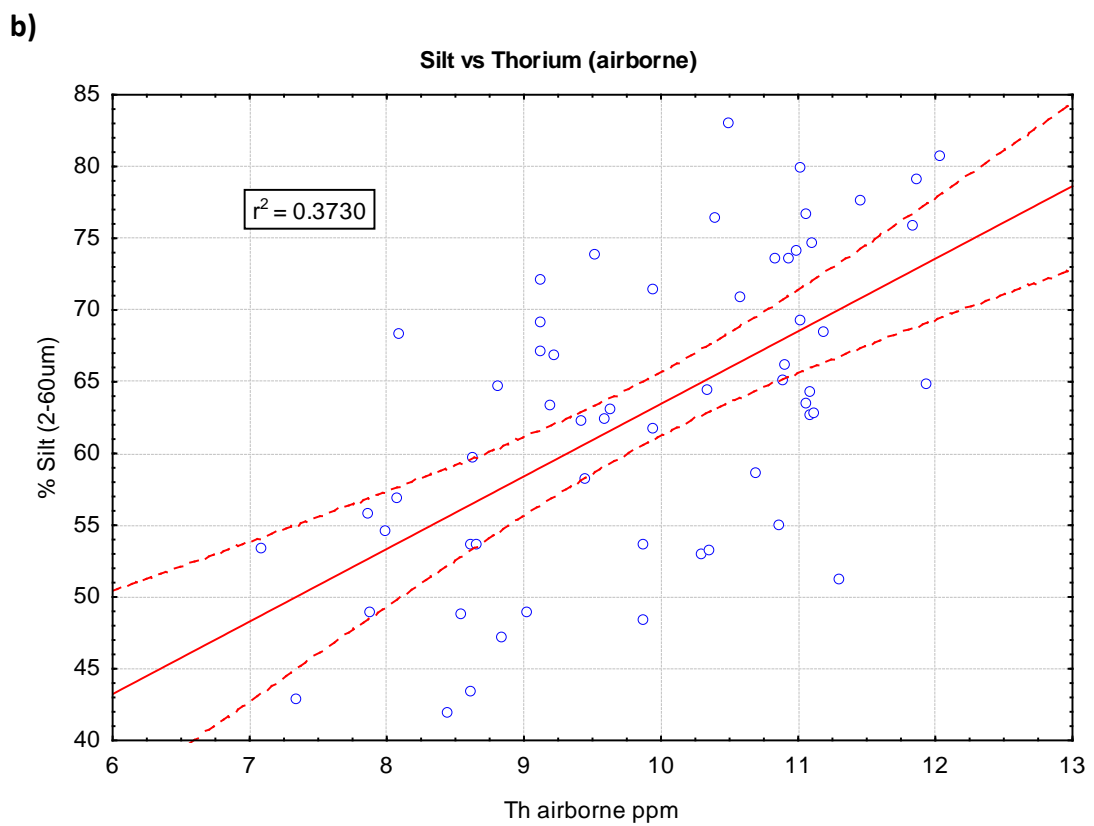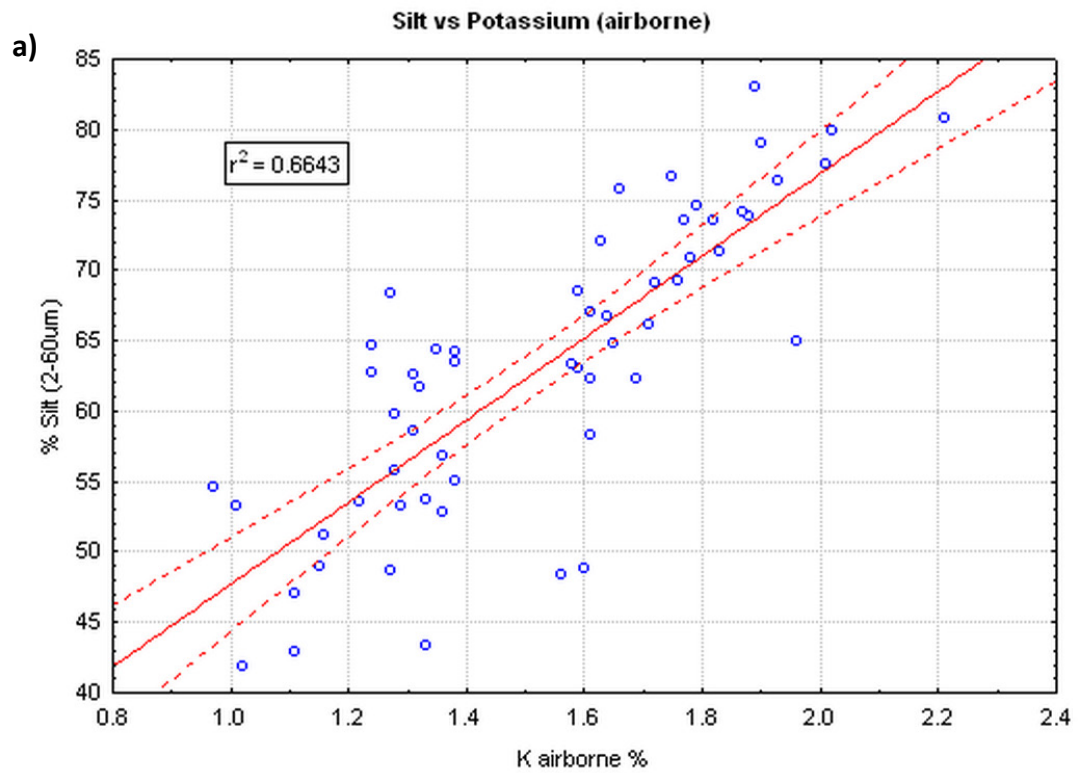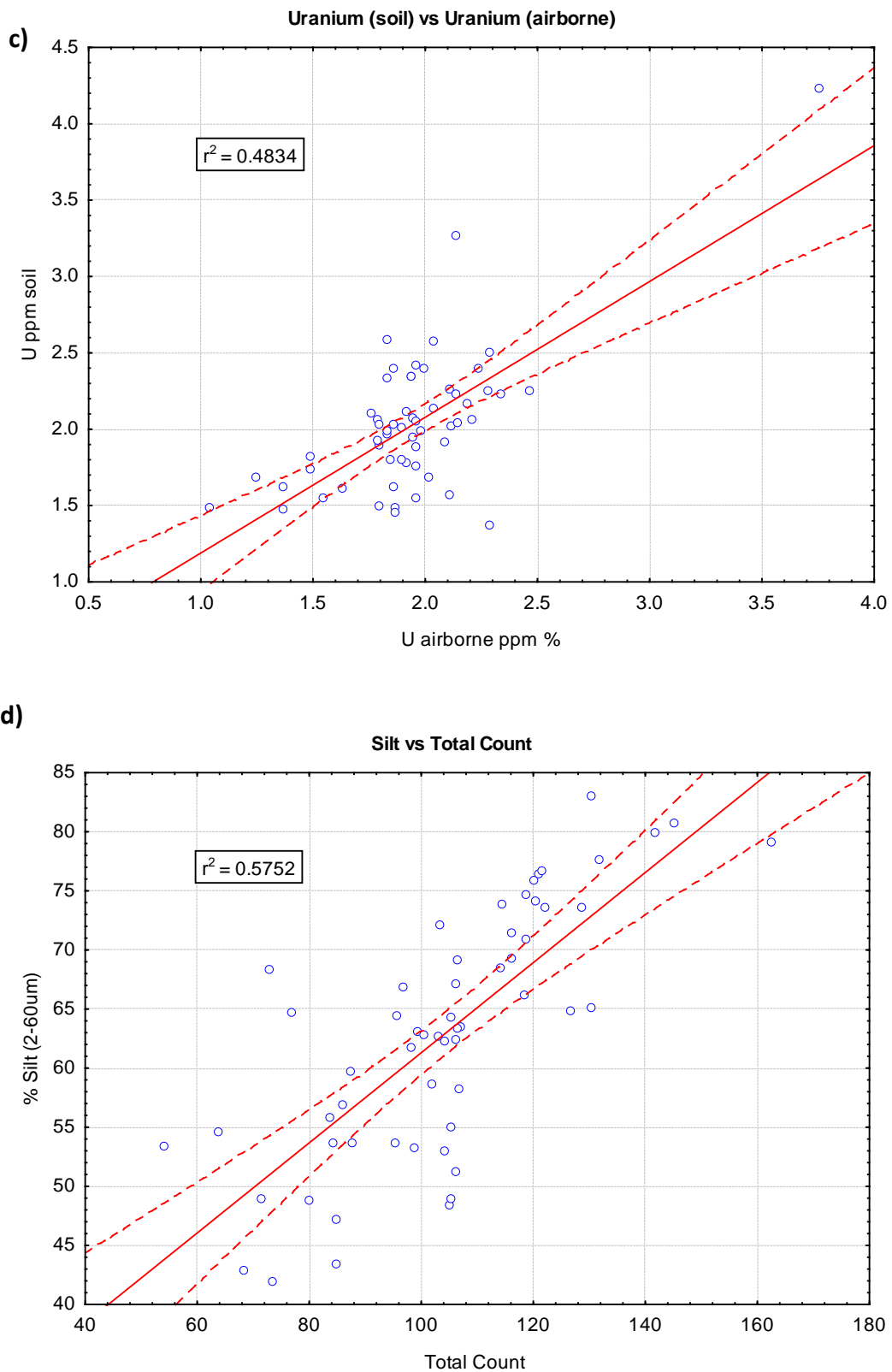
Figure 48 Correlations between radioelement concentrations and percentage silt content: (a) potassium; (b) thorium; (c) uranium; (d) total count.

Potassium concentrations derived by AGRS are well correlated (R^2 = 0.72) to K concentration measured using ICP-MS in the soils from the alluvial and colluvial slopes (Figure 46a). Thorium and U are poorly correlated when comparing airborne and surface soil geochemistry with R^2 = 0.40 and 0.48, respectively (Figure 46b, c). Airborne K, eTh and eU concentrations were generally lower than ICP-MS values.

5.4.3 Soil Texture and Radioelements

Soil textures were classified according to McDonald et al. (1994) where clay is defined as <2 μm, silt 2–60 μm and sand 60–2000 μm. Fifty-eight samples were used in the analysis and linear relationships were based on the Pearson correlation method. Laser grainsize distributions for representative regolith materials are shown in Figure 47. A highly significant correlation was found between airborne K and percentage silt (Figure 48a: R^2 = 0.66; p-test 50.0001), whereas eTh and eU were less correlated (Figure 48b, c: R^2 < 0.40,). Significant correlations were also found between total count and silt (Figure 48d: R^2 = 0.57; p-test < 0.0001). Correlations (not shown) between airborne radioelement concentrations with clay and sand size distributions were poor (R^2 < 0.2). The regression line equation for the AGRS K vs silt concentration was then used to generate a prediction of surface silt within each of the three major catchments. This relationship is specific to the alluvial soils, and therefore soils over erosional landforms were masked out from the final silt prediction map (Figure 49).

5.5 3D regolith distribution and sedimentary facies

5.5.1 AEM analysis

The highest conductivities as shown by the AEM CDIs, correlate to the upper 20 m of regolith and are associated with mainly valley sediments (Figure 50). Relatively high (>50 mS/m) conductivities in the valley materials are likely to relate to the higher porosity and associated moisture/salinity content of the sediments compared with the underlying bedrock. The restricted nature of the alluvial sediments in the Belalie valley and colluvial sediments in the Caltowie valley are particularly well resolved in the 10–15 m CDI (Figure 50). At depths >40 m the conductivities are generally low and reflect resistive bedrock. Weak AEM conductors at 30 m or

greater depths follow the major north–south bedrock structural trend of the area and may relate to either conductive basement rocks (e.g. pyritic units) or preferential weathering of specific bedrock units.

There is generally a good correlation (R^2 = 0.64) between the sediment–bedrock boundary interpreted from drill logs and the base of the main conductivity bulge (~50 mS/m) in the AEM data (Figure 51). Therefore, the base of the conductor provides a generalised surface that approximates to the shape of the valley floor prior to infilling. The base of conductor surface was further constrained by a zero sediment thickness line that marks the contact between erosional and deposition landforms. The line representing that contact was generated using a slope threshold derived from the DEM that assumes slopes <1.5^0 largely corresponded to alluvial/colluvial landforms and slopes >1.5^0 are associated with erosional landforms (e.g. rises, low hills and hills). Also, several deep AEM conductive spikes were manually clipped and deleted from the 3D model. These features are likely to relate to conductive basement rocks and zones of deep in situ weathering. The modified surface was then subtracted from the DEM to generate sediment isopachs. These surfaces were visualised using the 3D GOCAD environment. However, it should be noted that the correlation between the sediment–bedrock boundary and the base conductor was based on a filtered subset of the drillholes. Owing to the fuzzy nature and relative poor resolution of the AEM dataset, drillholes that were located near to the erosional – depositional boundary were not used in the analysis.

The thickest sediments are generally found in the Belalie and Bundaleer valleys, whereas sediments in the Caltowie valley are thinner with pediments occurring over the upper parts of the catchment (Figure 52).

5.5.2 Sediment Composition and Fabrics

The valley sediments are generally reddish-orange with a fine-grained earthy fabric (Figure 53b). In places diffuse reddish-yellow mottling occurs towards the base of the sequence. Numerous gravelly inter-beds are present throughout the sequence, but are more common and thicker towards the base. The texture of the matrix materials becomes progressively finer towards the top of the sequence (i.e. higher proportion of silt and clay).
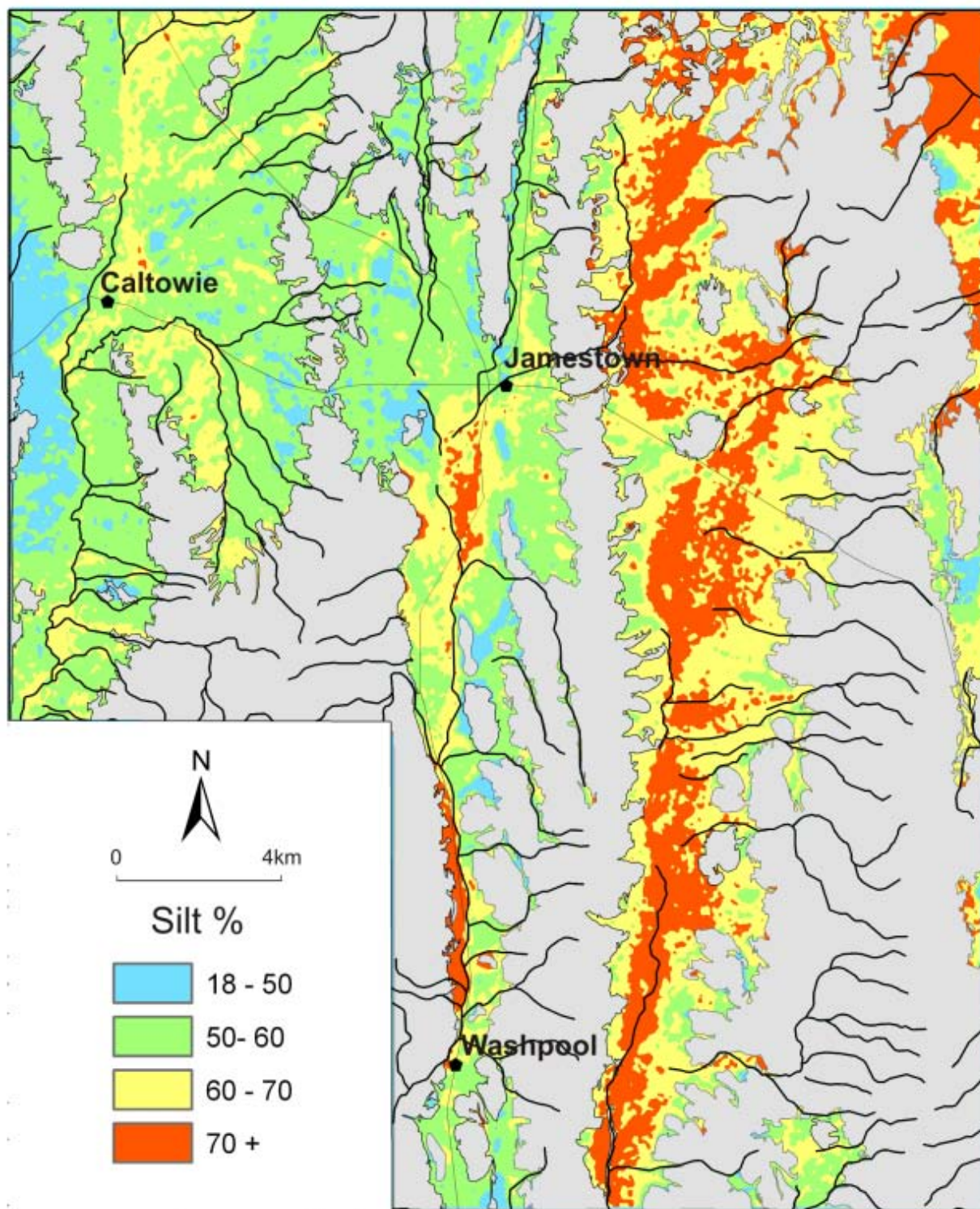
Figure 49 Modelled surface silt distribution for the Belalie, Bundaleer and Caltowie valley systems.

Three main depositional facies are recognised: debris flow, bedload and suspension load (Figure 53c, d). Debris or mudflow deposits are overall fine grained and locally poorly sorted with larger clasts including gravel and cobbles floating in an earthy clay and silt matrix. In places, cut and fill structures within these poorly sorted sediments suggest later reworking of debris-flow deposits by channel erosion and deposition. The clasts include moderately and highly weathered saprolite, quartz, ferruginous saprolite and maghemite gravels and coarse sand (Figure 53c). Debris-flow deposits are likely to be associated with sediments derived from coalescing alluvial and colluvial fans. Bedload deposits consist of discontinuous clast-supported gravel lenses and thin beds that are more laterally extensive than the coarser gravel deposits. The clasts are typically imbricated and consist of subrounded gravel and coarse sand-size saprolite fragments (some of which are magnetic) and quartz pebbles. The channel deposits have a largely random vertical and lateral distribution. These characteristics together with the interwoven channel patterns seen in the airborne magnetic imagery (Figure 54) suggest the channels formed a braided stream network, or perhaps individually stacked channels at various locations and depths. In places fining-upward sequences are observed, grading from clast supported gravel and coarse sand to silt and clay. This reflects a transition from a high-discharge flow regime to one with lower discharge and energy. The silts and clays were probably deposited from suspension during the late stages of a flood event. The suspension deposits are typically interspersed with thin beds of sand and minor gravel.
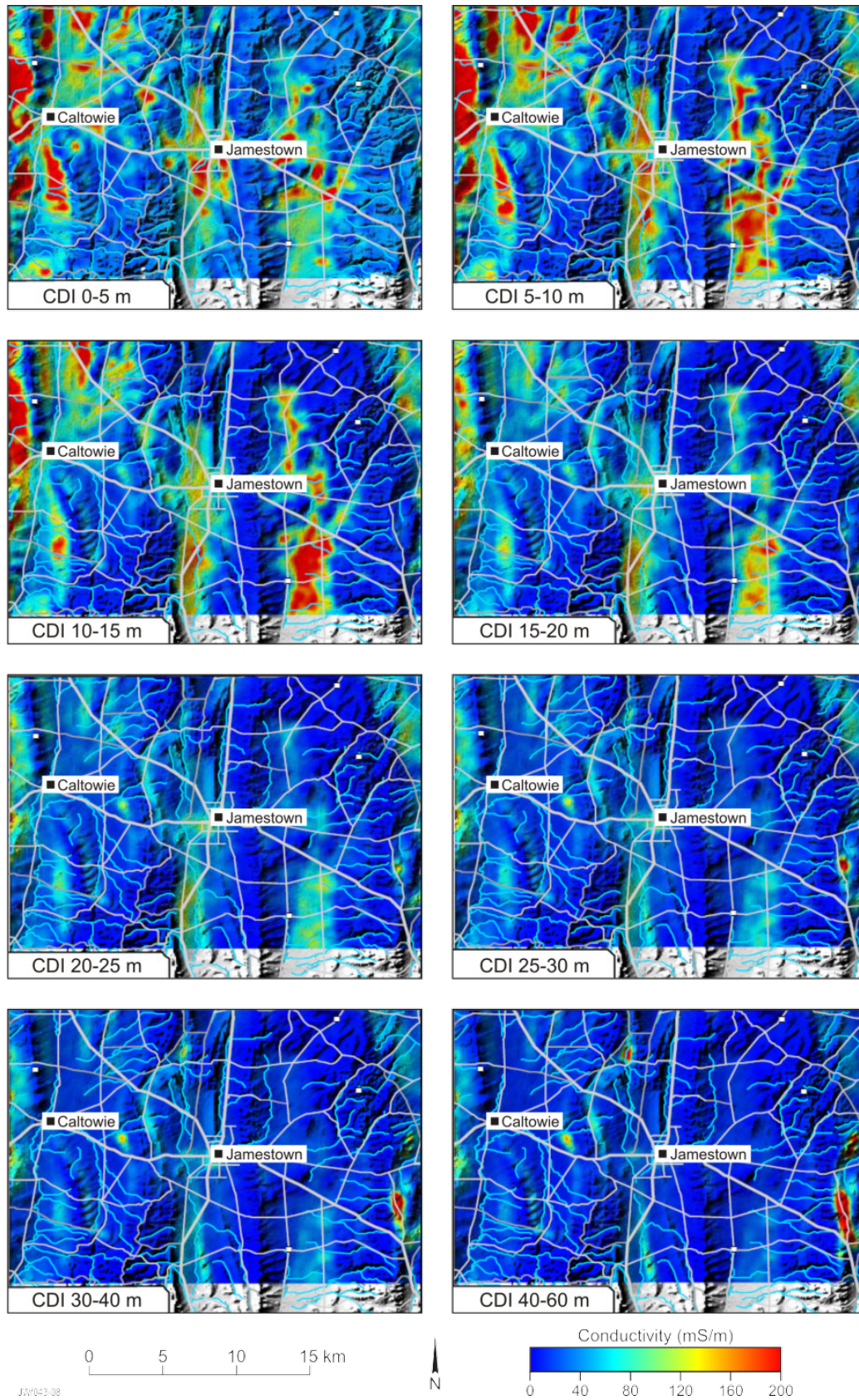
Figure 50 Conductivity depth image (CDI) slices with hill-shaded DEM and drainage attributes added. Conductivity scale from 0 to 200 mS/m in all images.
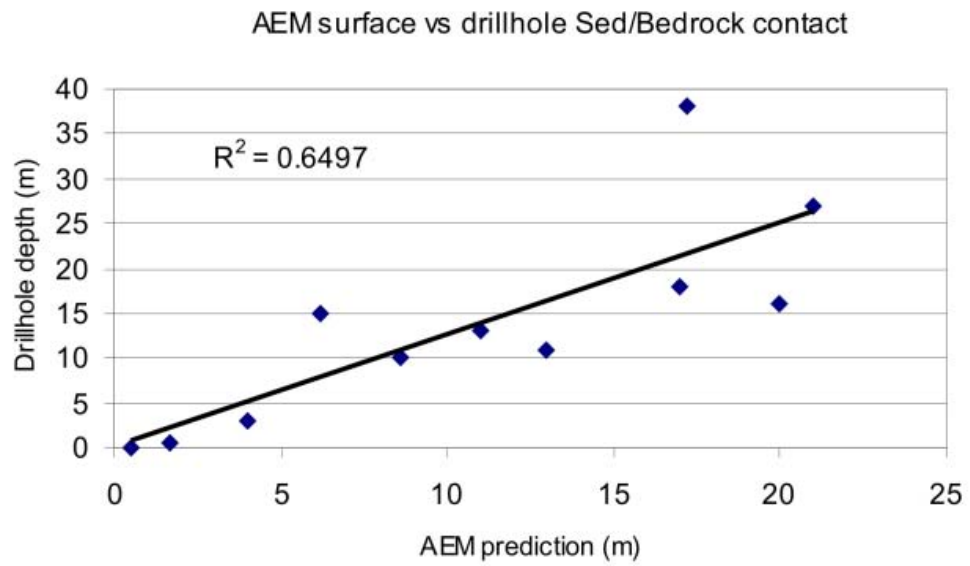
Figure 51 Correlations between the base of the bulge AEM conductor (~50 mS/m) and the depth of the bedrock/sediment contact (based on selected drillholes).
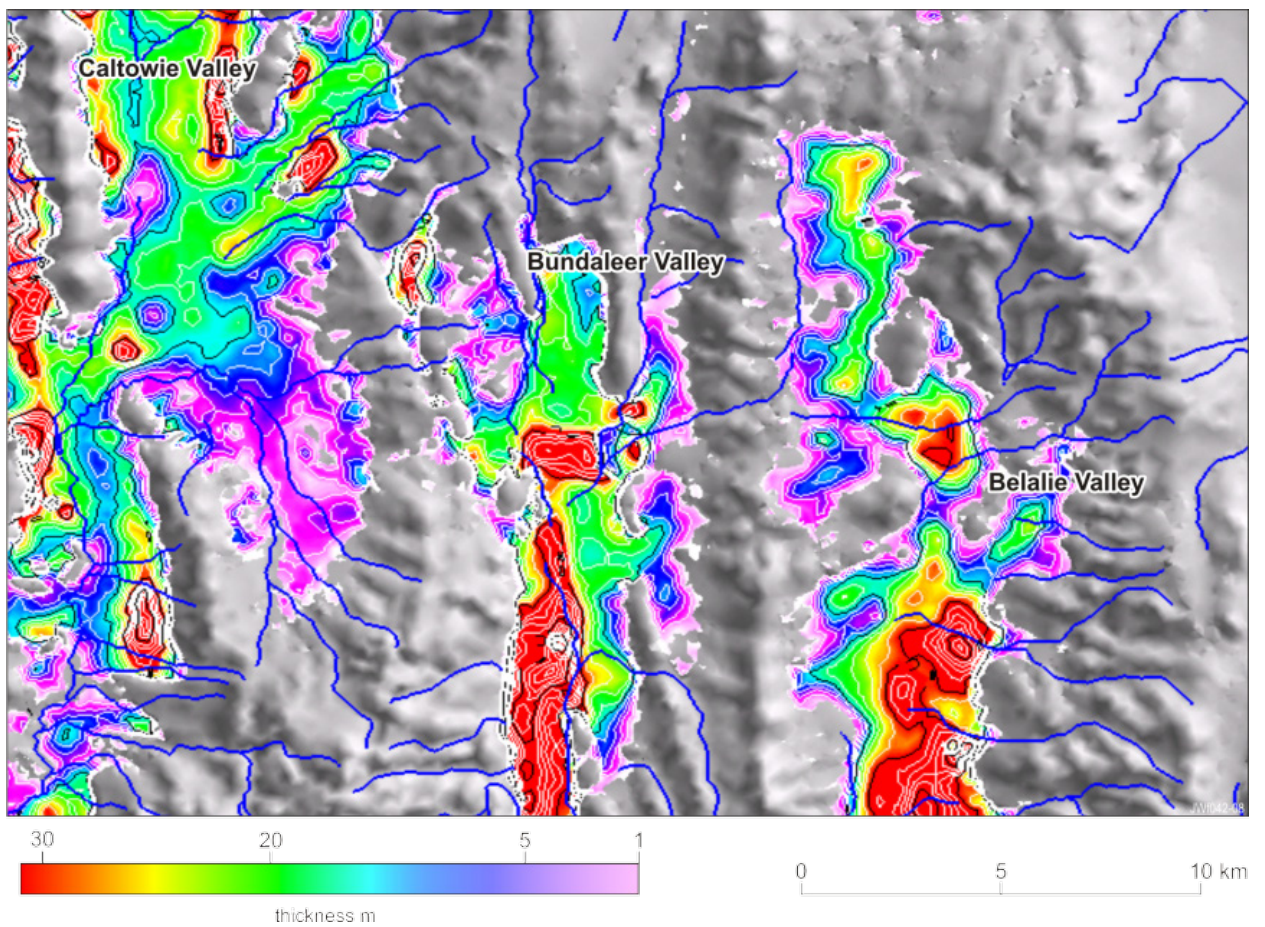
Figure 52 Sediment isopach based on the AEM dataset.
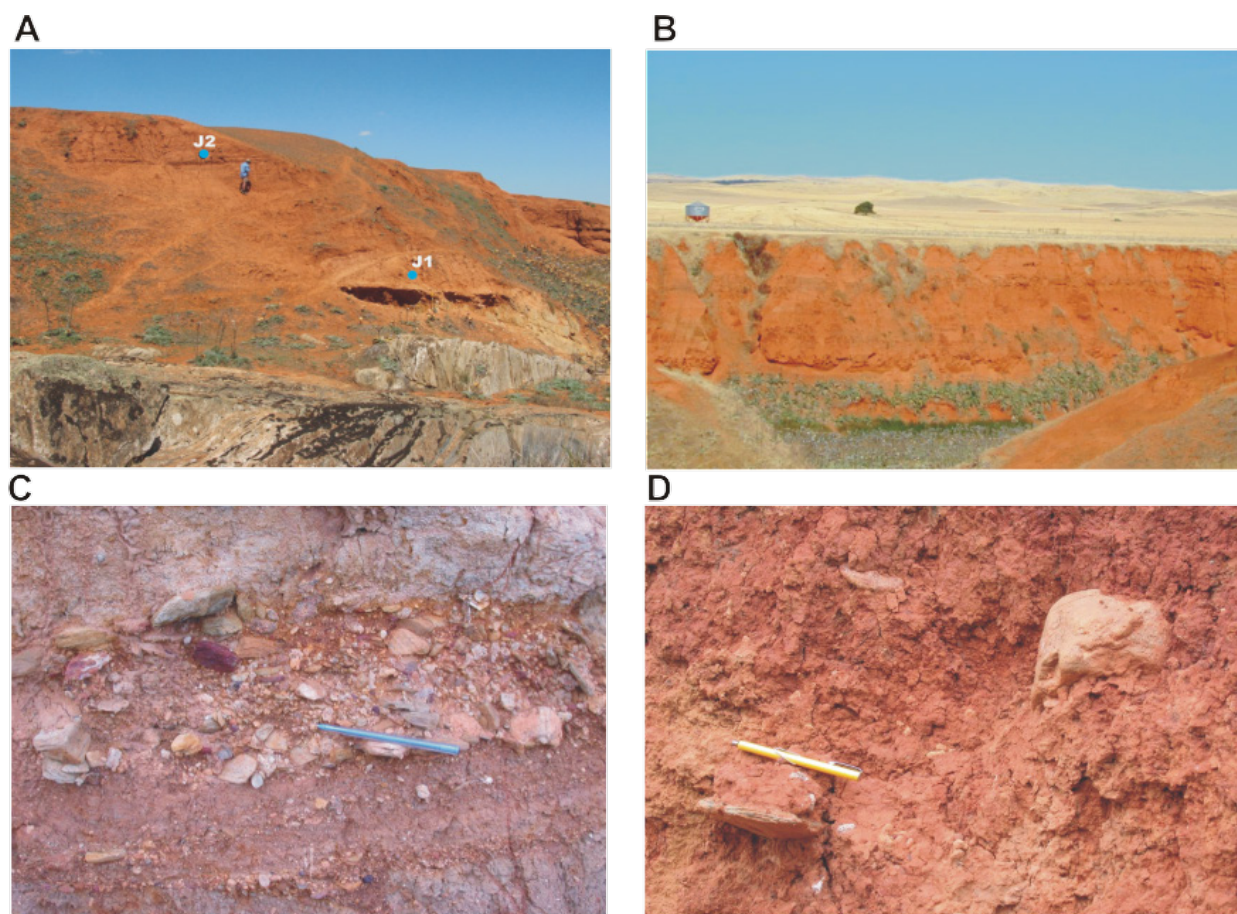
Figure 53 (a) Location of OSL samples in the Belalie Valley. (b) Gully incision (~12 m) exposing red earthy alluvial fill. (c) Bedload deposits. (d) Debris-flow deposits. Pen for scale in (c, d) is ~12 cm long.

Pedogenic and groundwater carbonates occur throughout the valley-fill deposits. Carbonates occur in the soils and sediments as irregular nodules, platy sheets, powdery deposits and as cast features associated with roots and worm burrows. Fluctuating water-tables and drying at the surface favours the precipitation of carbonate in the near-surface. Groundwater carbonates form more massive, nodular to sheet-like structures compared with pedogenic carbonate.

5.5.3 Drainage analysis

The magnetic imagery highlights major north–south bedrock structures in the study area (Figure 54). However, more striking are short-wavelength and low-amplitude magnetic anomalies in the image. These features are associated with 'magnetic' channels that have intricate dendritic to subparallel drainage patterns. The first vertical and horizontal derivatives of

magnetics were effective in highlighting these magnetic drainage features. The horizontal derivative is shown in Figure 54.

These 'magnetic' channels coincide with near-surface (51 m) and buried (up to 40 m) bedload deposits. The magnetic materials in these deposits consist of ferruginised lithic granules and coarse sand-size lithic fragments. Drainage patterns are dendritic or rilled where they drain from steep ridges. The magnetic response is caused by maghemite (Fe_2O_3, γ-Fe_2O_3) associated with these sediments (Table 11).

5.5.4 Age of sediments

The sediments are of Late Pleistocene to Holocene age based on OSL dating. The shallowest sample collected 2.2 m below the surface soil gave an age of 30 +-3 ka. The second 0.5 m above the sediment/saprolite contact gave an age of 102 + 12 ka (Figure 53a).
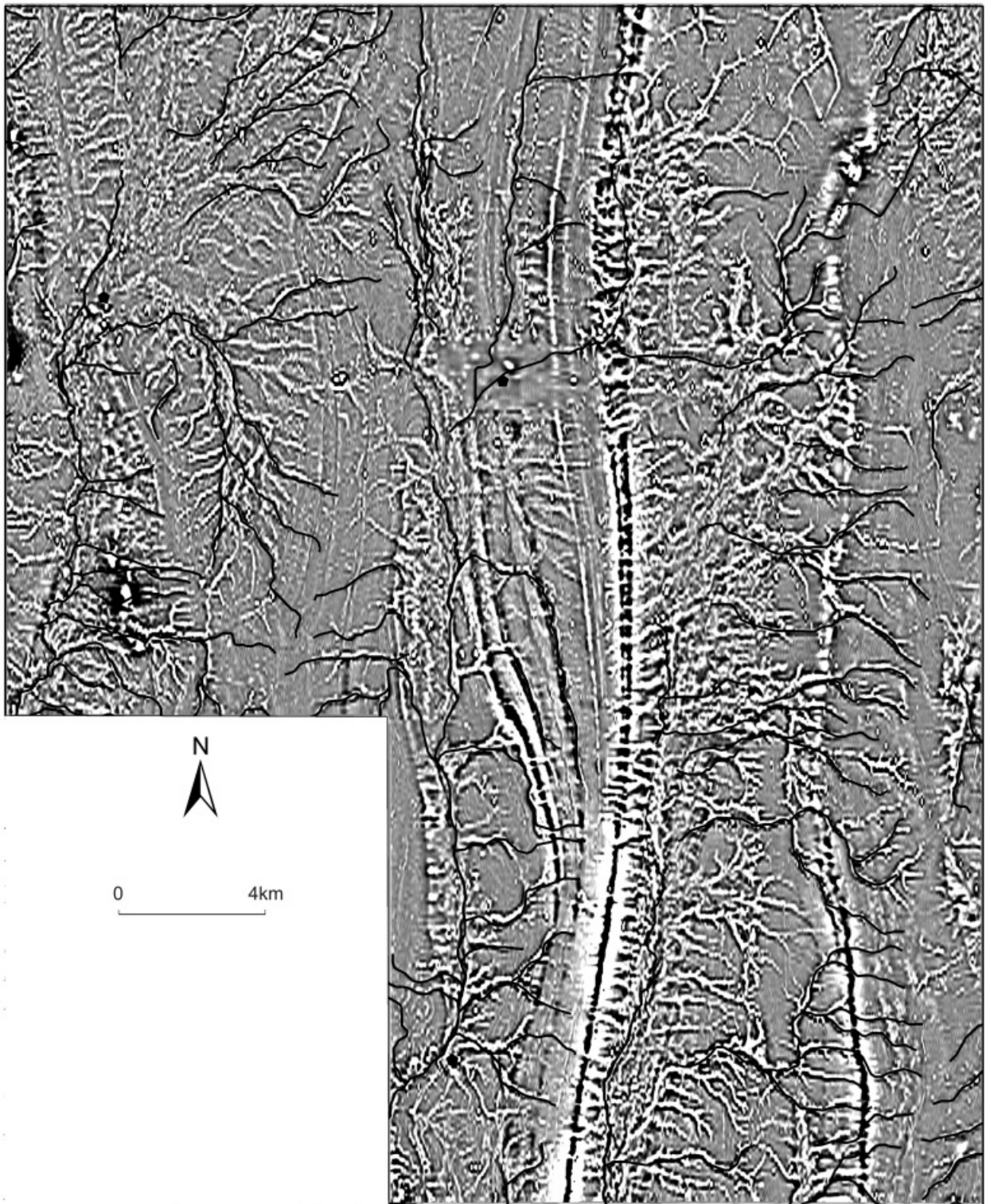
Figure 54 Horizontal derivative of the magnetics highlighting 'magnetic channels.' Present-day rivers shown in black.

5.6 Discussion

Integration and analysis of geophysical, DEM and ground-based measurements have provided new insights into the 3D distribution and composition of valley-fill deposits in the Jamestown area. In most places a sharp conductivity contrast between sediment and underlying bedrock has enabled the construction of a sediment isopach map (Figure 52). The overall concave shape of the buried valley floors is consistent with the confining ridges that separate each of the valley systems. Detailed hydrological studies in the area (Cresswell and Herczeg, 2004) have demonstrated that the higher conductivities in the sediments relate to their relatively high porosities and pore-fluid salinities compared with the underlying bedrock. The valley structure revealed by the AEM survey is only approximate due to the inability to separate highly weathered bedrock and conductive basement rocks from conductive sediments. However, these conductivity relationships have been used effectively in other studies (Worrall et al. 1998) where boundaries between resistive basement rocks from more conductive saprolite and overlying sediments have been delineated to provide a 3D framework for mineral exploration in deeply weathered terrains.

The inferred depositional boundary defined by the AEM, although a good approximation of the sediment–bedrock interface, does not reflect the actual shape of the valley at any one point in time. Erosional and depositional processes will change the shape of the valley over time; what the AEM boundary shows is the net result of these processes. Furthermore, local-scale textural variations within the sediments (i.e. channel gravels vs silt and clay) are not resolved by the AEM data.

The valley sediments have an earthy fabric and consist of silt and clay with numerous, generally thin, gravel beds. The thickest sediments (up to 40 m) and highest AEM conductivities, with the exception of some colluvial footslopes in the Caltowie catchment, occur in the Belalie, and Bundaleer valleys. The Caltowie valley has generally a thinner cover of sediment and is correspondingly less conductive than the other two catchments. OSL dating of sediment in the Belalie valley indicates a Late Pleistocene age (102–30 ka). The sediments are therefore mostly older than the Late Quaternary (33–17 ka) valley-fill deposits described in the Flinders Ranges of South Australia (Chor et al.

2003), and are younger than much thicker (up to 250 m) Cenozoic sediments associated with the Walloway Basin ~25 km north of the study area (Alley and Lindsay, 1995). Lignitic shales (Eocene) occur in the basal Cenozoic sequence of the Walloway Basin whereas no lignitic shales have been found in the Jamestown area. Nor is there any indication of a major discontinuity in the sedimentary sequence to suggest the presence of older Cenozoic materials.

Sediment ages and thicknesses allow estimation of the rates of aggradation. The basal and upper sediment dates indicate an aggradation rate of 0.073 + 0.006 mm/a and 0.078 + 0.007 mm/a, respectively. These rates assume continuous deposition. In reality, rates would have varied through time depending on factors such as climate (e.g. runoff, slope stability) and shifting areas of sedimentation within the floodplain.

A characteristic feature of the valley-fill deposits is their overall uniform oxidation and earthy fabric, although in places what appears to be a buried paleosols are preserved in the alluvial sequence. They correlate with a sharp fabric change in the sediments, with weakly developed columnar and prismatic structures overlain by horizontally layered sediments. These structures may reflect partial truncation of the B horizon, which is then buried by alluvial sediment. If these are paleosols, then they are not well developed, which could reflect the fact that the rate of deposition was either greater or similar to the rate of soil development. For example, the time required to develop distinct horizon differentiation in alluvial soils is in the order of ~15 000–30 000 years (Walker and Coventry 1976; Chen 1997). This period would equate to ~1–2 m of sedimentation in the Jamestown valleys.

The valleys (particularly the Belalie) show distinct profile asymmetry, with gentle slopes east of the main channel and short steep valley slopes on the western side (Figure 44, Figure 55). The asymmetry is likely to reflect bedrock structure. The area underlain by a series of anticlinal and synclinal strata with younger synclinal rocks corresponding to the valley floor. The folding is asymmetrical with generally steeper east-facing slopes and shallower dipping west-facing slopes. In the Belalie valley most of the sediment is sourced from the eastern part of the catchment thereby constraining the main stream to the western side of the valley. The position of the main stream is likely to have changed little as the valley alluviated. This

conclusion is supported by the concentration of subsurface 'magnetic' channels along the western edge of the valley floodplain (Figure 54).

5.6.1 Sediment distribution and origin

Surface soil textures in the three catchments can be broadly described as silt loams. The positive correlation between AGRS K and silt content has allowed more precise spatial prediction of surface soil textures (Figure 48, Figure 49). The Belalie and Bundaleer catchments have a higher proportion of silt compared with the Caltowie catchment, which contains a higher percentage of fine sand. This type of specific soils information highlights the potential use of AGRS spectrometry in improving existing soil maps within the study area.

Based on XRD results (Table 11), the high AGRS K concentrations that relate to finer textured soils (Figure 47 (JS53), Figure 48a) are associated with silt-size mica (muscovite) and illite grains, whereas, low K soil samples have a higher proportion of quartz. The latter soils tend to be bimodal with fine sandy quartz having a distinct modal peak around 70 mm (Figure 47, JS55). The airborne gamma-ray spectrometry total count also correlates with silt content (Figure 48d). This is likely to reflect the proportion of surface quartz that has low gamma-ray emissions. Silty soils have a relatively low percentage of quartz compared with sandy soils. Poor correlations between eTh and eU with soil texture may reflect the fact that these elements are associated with a range of grainsizes. Airborne eTh and eU values poorly correlate with soil geochemistry. This might reflect noise in the airborne data due to the low concentrations of these elements (eTh average 9.9 ppm, eU average 1.9 ppm) in the depositional landscapes. For example, a strong correlation between air and ground eTh and eU values was described in the Wheatbelt of Western Australia (Taylor et al., 2002), although surface concentrations of these elements were relatively high (eTh average 33 ppm; eU average 3.35 ppm).
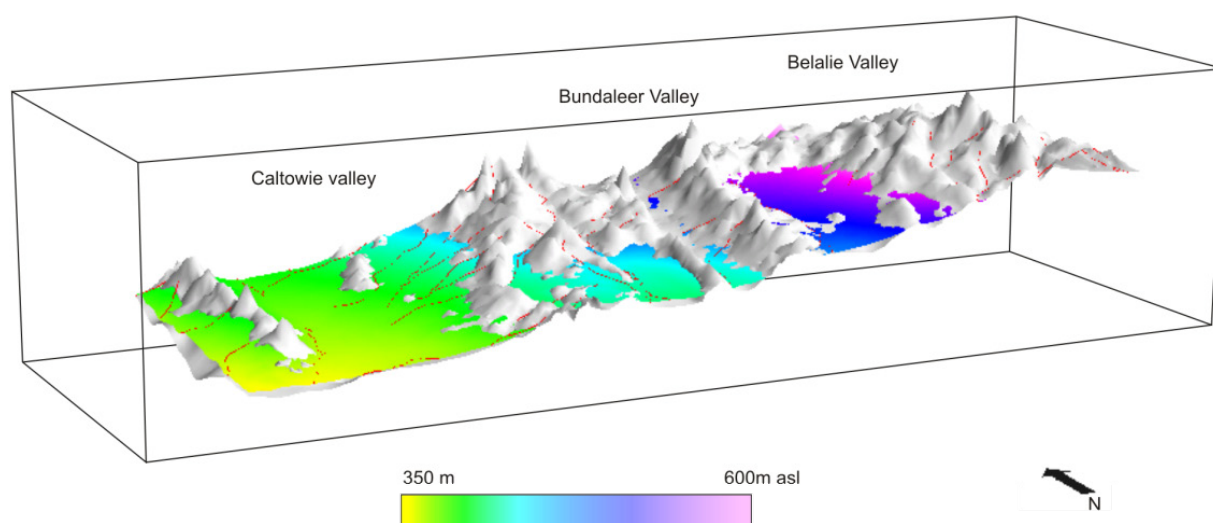
Figure 55 East–west cross-section through the northern part of the study area. Colour according to elevation height for valley basins.

The very high silt content of the alluvial soils may reflect a contribution from aeolian dust. Aeolian dust materials have been recognised as a major source of sediment in similar Quaternary valley-fill deposits in the Flinders Ranges of South Australia (Williams et al., 2001). Aeolian dust forms extensive deposits that have been well documented in southern Australia (Butler 1982; Chartres et al. 1988; Williams et al. 2001). In addition, major dune-building episodes during the Quaternary have been recorded as dust peaks in samples recorded from the Tasman Sea (Hesse 1994) when the climate was drier and cooler. Differentiating aeolian dust from locally derived material can be difficult particularly where bioturbation processes have mixed materials from different sources. A sharp discontinuity between soils and weathered bedrock can be suggestive of aeolian dust accumulations as well as textural and geochemical (i.e. trace-element

chemistry) differences between the soils and underlying parent material. Aeolian dust particle sizes generally fall within the range 0.2–60 μm.

In the Jamestown area an overlap between the particle size distributions of the surface soils from the Belalie and Bundaleer valleys and those of weathered outcropping siltstone and shale makes it difficult to isolate an aeolian component with a high degree of certainty. However, on closer examination there are subtle but significant differences between these two materials. The surface alluvial soils have a modal peak centred at 5 μm (Figure 47, JS53) compared with the coarser bedrock textures centred around 10 and 85 μm (Figure 47, JR1 and JR2). The soils are well sorted with a fine sand and clay tail. This distribution closely matches with the 2–23 μm range of interpreted aeolian-derived dust recorded in valley sediments in the Flinders Ranges of South Australia (Chor et al., 2003). The Jamestown valley sediments are likely to reflect the accumulation and reworking of aeolian dust together with locally sourced weathered bedrock materials. Further research using trace-element geochemistry of the sediments and weathered bedrock might provide additional constraints on whether the materials are largely locally derived or exotic. Chor et al. (2003) showed that the trace elements Zr, Ti, Th, La, Ce, Y, Cr and Nd are enriched in the aeolian material compared with the underlying bedrock. However, the range of lithological types and associated geochemical variability in the Jamestown area may make this type of analysis problematic.

Soils in the upper part of the Caltowie catchment have a bimodal distribution with a distinct peak at 70 mm and broader peak at 3.5 μm (Figure 47, JS57). The highest modal distribution is associated with the 70 mm peak and suggests a relatively high bedrock component for the sediments. This might reflect the fact that sediment, particularly in the upper parts of the catchment, is generally thin with bedrock at or close to the surface. Aeolian dust deposits may have been reworked to lower areas in the catchment in response to potentially higher geomorphic activity rates compared with the other catchments. The modelled silt map (Figure 47) shows concentrations of finer textured sediments near to the township of Caltowie suggest the possible reworking and translocation of finer materials to lower parts of the catchment.

5.6.1.1 Origin of magnetic channels

The widespread distribution of magnetic channels within the alluvial valleys is difficult to explain from only a single primary bedrock source. Based on XRD analysis and field observations the magnetic channel sediments consist of goethitic–hematitic iron oxides (relatively non-magnetic) that have been altered to maghemite (Fe_2O_3) and accumulated in the sediments as ferruginous granules. Similar maghemite drainage patterns have been recorded in other locations where they have provided information on the nature of the paleodrainage and hydrological characteristics (Mackey et al., 2000; Gibson and Wilford, 2002; English et al., 2004). Maghemite can form in the near-surface environment as a result of several different processes (Raison 1979; Stolz et al., 1986; Anand and Gilkes, 1987; Butler, 1992) including: (i) heating (above 200^0C) from bush fires and lightning strikes that convert goethite to maghemite; (ii) favourable biological processes can precipitate magnetic iron oxide crystals; (iii) repeated oxidation and reduction cycles of iron oxides within the regolith; and (iv) dehydration of lepidocrocite (also called hydrohematite) a common oxide–hydroxide mineral. Whatever their origin the magnetic channels are an important element in explanations of landscape evolution in the area.

5.6.1.2 Drainage evolution

There is evidence of drainage diversion in the upper part of the Belalie catchment where the river that once flowed southwards has been captured and diverted into the Bundaleer valley catchment 3 km east of Jamestown (Figure 56). The distribution of channel gravels indicated by the magnetic imagery and AEM depth slices both suggest that the original river flowed south (Figure 50; 5–10 m slice; Figure 54). The river diversion probably reflects infilling of the Belalie valley to a point where the ridge separating the Belalie and Bundaleer valleys was overtopped. Streams above this point then began to flow westward and have now incised 3–4 m into the bedrock ridge that once separated the Bundaleer and Belalie valleys. As a result, a new catchment divide and associated wind-gap developed ~6 km east of Jamestown (Figure 56).

Change in the distribution and pattern of streams as indicated by the largely buried magnetic channels to the present-day drainage is likely to reflect changes in hydrology as the valley alluviated. The present-day

drainage is widely spaced and interrupted, which suggests significant recharge into the underlying sediments (Figure 44). The magnetic channels, in contrast, form discrete and relatively closely spaced drainage lines with a high degree of complexity along the main valley axis (Figure 54). Many of the magnetic channels, particularly the headwater streams, show concordance with ephemerally active and inactive drainage lines inferred from the DEM (A on Figure 57). Most of the flow lines generated from the DEM show areas where channelised flow would occur if there was sufficient runoff. Where the sediments are thicker the

correlation between the surface-generated streams (i.e. derived from the DEM) and the 'magnetic channels' is less obvious (B on Figure 57). Here the control of topography on stream position is lost as the channels migrate across the floodplain in response to changing base-levels. In places the magnetic image has a blurred or diffuse response along the main axial part of the valley floor. This might be due to the accumulation of non-magnetic clays and silts that would have the effect of diffusing the 'magnetic channel' signature.
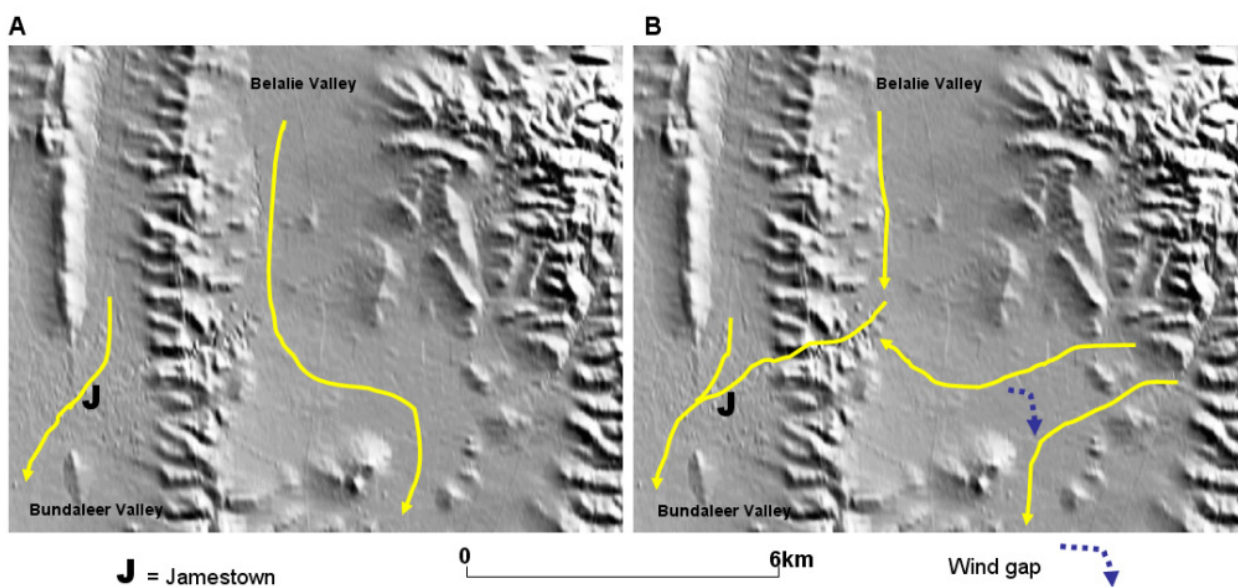
Figure 56 (a) Original drainage based on the magnetic drainage lines and AEM defined channel. (b) Diverted drainage developed as a result of infilling the upper part of the Belalie valley. Surface drainage now flows into the Bundaleer valley.
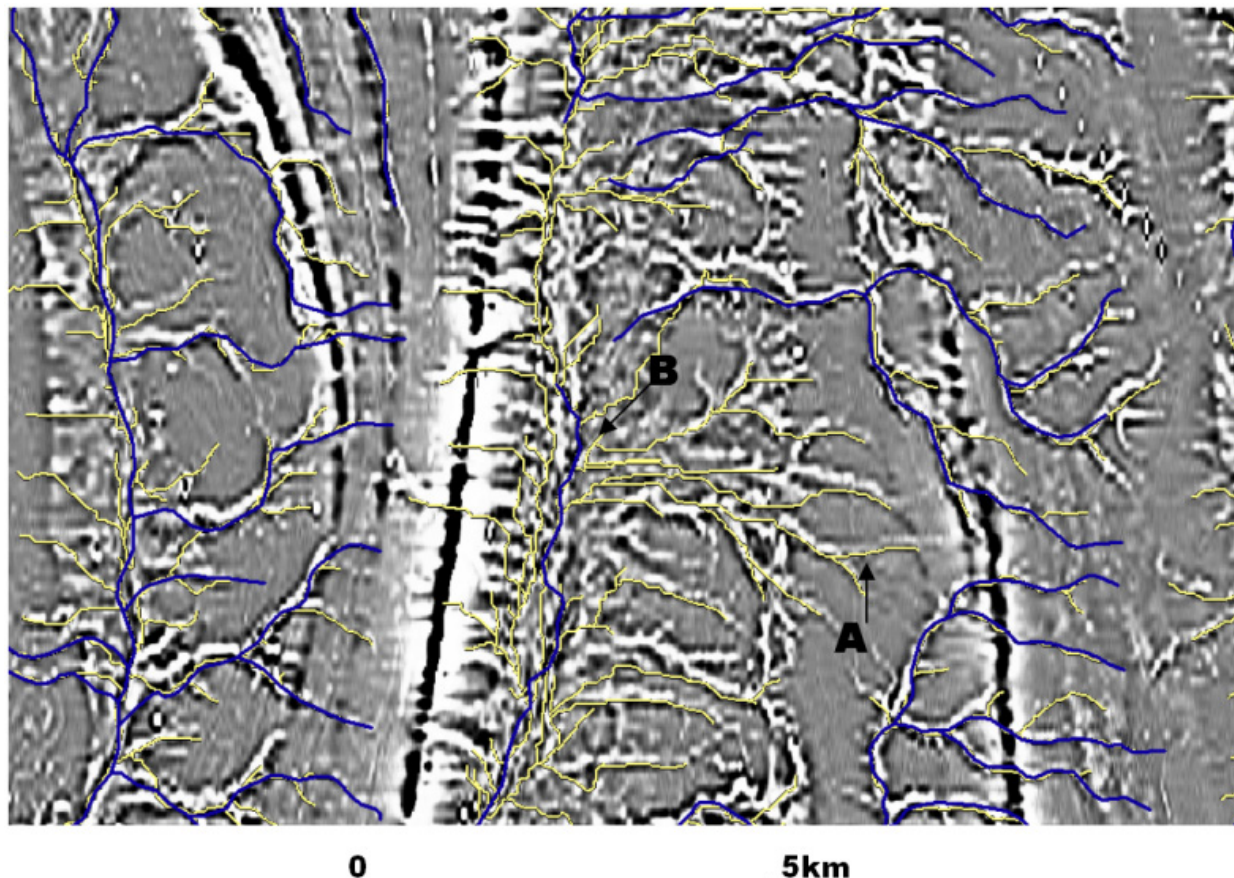
Figure 57 Subset of the magnetic image highlighting 'magnetic channels.' Present-day rivers (black) and DEM derived drainage lines (light grey). A, topographic control on stream position; B, stream position related to

topography.

Drill log descriptions (Henschke et al. 2004) indicated that the lower two-thirds of the valley fill has a higher proportion of coarse-grained sediments and more frequent gravel layers. The dominance of gravel deposits in the basal part of the sequence may reflect streams with relatively steeper gradients and correspondingly higher energies. These gravel deposits form dendritic and subparallel channel patterns. The paleodrainage lines identified in the magnetics correlate with zones of high conductivity, particularly in the 0–20 m depth range. The gravel beds probably act as pathways for preferential groundwater flow through the valley sediments. Relatively high conductivities reflected in the AEM probably correspond to saline waters in the gravel layers.

The upper part of the alluvial sequence is generally finer textured with a higher proportion of silt and clay. Surface silt distribution (Figure 49) is associated with low-angle sheetflood fans and broad low-gradient floodplains. This suggests lower-energy environments with suspension deposits of silt and clay becoming more important as stream gradients became shallower during alluviation.

There is thus a shift from relatively high-energy bedload and debris-flow deposits at the base of the sequence to lower-energy suspension deposits toward the top. This might reflect an overall lowering of stream gradients during alluviation and/or a change in climate with lower discharge, in particular episodic flood events. Similar textural trends are present in Quaternary valley-fill materials in the Flinders Ranges (Chor et al., 2003). There aeolian dust accumulation within the catchment is thought to be pivotal in providing an increased supply of fine-grained sediment, and reducing hillslope runoff primarily through increased infiltration, in the transition from bedload to suspension deposition. Similar process may also have occurred in the Jamestown area.
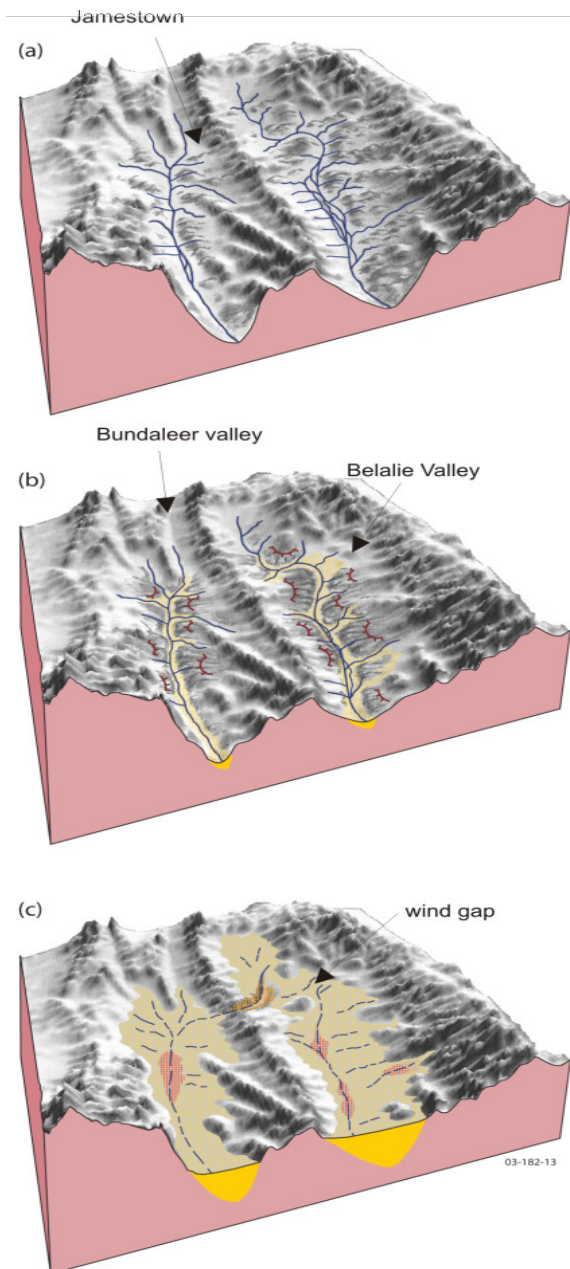
Figure 58 Regolith–landscape model for valley deposits highlighting major hydrological and geomorphological processes. Incised valleys with well-developed rill drainage associated with steep bedrock slopes. (a) Valleys begin to infill with alluvial and colluvial sediments. Remobilisation of aeolian dust into the valley deposits. Sediments generally poorly sorted consisting mostly of silt, clay and local channel gravels (some magnetic). (b) Sediments drown the main valley floors. Valley gradients and stream energy reduced. The ridge separating the Belalie and Bundaleer valleys is breached east of Jamestown. Headwater streams that once flowed south are diverted west into the Bundaleer catchment. (c) In response to increased recharge into the sediments and an overall drying climate channelised flow is significantly reduced. Interrupted drainages develop.

In summary, a landscape model highlighting significant stages in landscape development and associated hydrological and geomorphological processes is summarised in Figure 58. In the Late Pleistocene the Jamestown area consisted of incised valleys separated by prominent bedrock ridges. Most of the streams were bedrock floored with well developed rill drainage on steep bedrock slopes. At a later stage (Figure 58b) a combination of aeolian dust (predominantly silt size) and locally derived materials were eroded from the catchments and deposited on the valley floors in the form of debris-flow and floodplain deposits. Gravels and coarse sand were deposited in stream channels. The maghemite associated with these sediments allows surface and subsurface channels to be delineated. As the valleys aggraded the ridge separating the Belalie and Bundaleer valleys was breached. This created a wind-gap and diverted the upper tributaries of the Bundaleer catchment into the Belalie catchment. With aggradation, stream gradients and energy were reduced (Figure 58c). Channelised flow was reduced in response to the drying climate and possibly more effective vertical recharge across the valley deposits. This has led to the interrupted nature of the present-day streams.

5.7 Conclusions

An interpretation of AGRS, magnetics, DEM and AEM data combined with ground-based studies has been used to build a 3D model of Quaternary valley-fill deposits in the Jamestown area of South Australia. The AEM provides constraints on the distribution and thickness of valley sediments, the magnetics provides insights into the distribution of buried stream channels, and the AGRS imagery when appropriately stratified by landforms (e.g. partitioning erosional and depositional landscapes) is able to map specific soil properties (e.g. soil mineralogy and texture). The latter highlights the potential of AGRS imagery to update existing soil maps in the area.

The sediments are up to 40 m thick and were deposited during the Late Pleistocene to the present day. The paleolandscape had significantly more relief prior to alluvation. Bedload, suspension and debris-flow facies are present in the sedimentary sequence. The clay and fine silt fractions of the valley fill have been derived from the local weathering of siltstone and mudstone in the catchments and from reworking

of aeolian dust deposits that were probably deposited under dryer climatic condition than at the present day.

This type of integrated analysis has led to an improved understanding of the sedimentological and hydrological characteristics of valley-fill deposits in the Jamestown area and how these processes have changed through time. This information has the potential to be used to develop more robust hydrological and soil-landscape models for the area.

5.8 Acknowledgements

Chapter 6

Discussion and conclusions

6 Discussion and conclusions

Four case studies have been presented that describe digital regolith mapping approaches underpinned by quantitative and geostatistical analysis to predict regolith attributes from national through to local scales. These investigations included a continent wide prediction of weathering intensity using a step-wise multiple regression based model using airborne gamma-ray imagery and terrain relief; a national prediction of near-surface secondary carbonate using environmental correlation and regolith geochemistry; a prediction of soil-regolith thickness over the Mt Lofty Ranges in central South Australia using environmental correlation, drilling and legacy data; and finally a 3D regolith-landscape evolution model of valley-fill deposits based on dataset integration, regression analysis and optically stimulated luminescence dating. These investigations have been written as individual research papers with separate discussions and conclusions. In this final discussion I link these investigations and describe more broadly the application of digital regolith mapping (DRM) in Australia and future research directions.

Digital regolith mapping approaches described in this thesis differ markedly from traditional methods used to compile regolith maps over Australia. Traditional regolith maps are largely based on a soil-landscape methodology as discussed in the introduction, with hand drawn regolith-landform units based on the interpretation of aerial photographs and supplementary datasets including, for example, gamma-ray imagery and Landsat TM. Regolith mapping approaches described in this thesis mirror to a large extent recent developments in geostatistical analysis and modelling of soil properties as reviewed by McBratney et al. (2003). The principle difference between this work and digital soil mapping (DSM) are that DSM describes the upper 1-1.5 metres of weathered material, whereas DRM is describing a zone that is often considerably deeper (i.e. base of the weathering front). However, clearly the two disciplines overlap and there are benefits in integration. For example, extending soil mapping over the Mt Lofty Ranges to include modelling of highly weathered

bedrock and sediments up to a depth of 7 m as described in Chapter 4 is likely to broaden the utility of the existing soil maps. Extending mapping beyond the solum (A and B horizons) would better support land capability assessment for deep rooted crops and trees (i.e. forestry), assessment of soil fertility, and near-surface hydrology and water quality (i.e. regolith salt stores – Fitzpatrick, 2008).

The nature of the predictive target variable and the context in which the results are interpreted differ between the two disciplines. Digital soil mapping approaches are largely concerned with predicting soil properties such as pH, texture, CEC's and organic carbon to support the agriculture sector and natural resource management. In contrast, regolith mapping links closely into a landscape evolution framework where both present and palaeo geomorphic and weathering processes are used to explain the nature of the regolith. Regolith-landform maps were initially compiled to support mineral exploration in deeply weathered terrains but more recently have been used for natural resource management, particularly hydrology and associated land salinisation issues.

The degree of weathering is a key attribute of regolith-landform maps and is the reason why the weathering intensity model was developed. Weathering intensity (Chapter 2) is a critical component of the regolith in terms of understanding weathering and geomorphic processes operating across a range of spatial and temporal landscape scales. Changes in weathering intensity are likely to correspond to changes in the physical, chemical and biological characteristics of the regolith, as the bedrock weathers to secondary mineral constituents. The weathering intensity prediction was shown to be consistent with our current understanding of landscape processes, preservation of weathered surfaces and tectonic controls on weathering and erosional processes across many parts of the Australian continent (Chapter 2). However, a potential limitation of the index is its reliance on radioelements (K, eTh and eU) as the principle predictive covariates. Where gamma-ray data was not available or where the surface bedrock has little or no gamma-ray emissions, relief is used to predict weathering intensity. In places this led to edge effects in the prediction grid where the gamma-ray model differed from that of the relief based model. This was particularly evident over the Nullarbor Plain which straddles the southern edge of

Western Australia and South Australia (Figure 12a). These artefacts were not present in the carbonate prediction study due to the large number of environmental covariates used in the model (Chapter 3; Figure 25a). Therefore, the inclusion of additional environmental covariates is likely to improve the weathering intensity model.

In chapter 2 it was postulated that the weathering intensity index would be a good proxy for regolith depth. This was borne out in the Mt Lofty Ranges study (Chapter 3) where weathering intensity, climate, landforms and geology were the principal covariates used in predicting regolith. Weathering intensity and weathering depth are strongly linked, and both will reflect present and palaeo-weathering and geomorphic processes. The landscape complexity described in the Mt Lofty Ranges investigation, where landscape and weathering processes date back to at least the Paleogene, is not uncommon. In most upland regions of Australia we see areas of active erosion and relatively thin profile development juxtaposed with partially preserved relict, deeply weathered landforms that reflect much older weathering and geomorphic processes. Therefore, models predicting regolith depth and weathering intensity are likely to have broad application in these types of upland landscapes, albeit the specific covariates and rules of the Mt Lofty depth model will likely change in other regions with different climate, landscape histories and bedrock types.

6.1 Site data and gaps in environmental covariates

Quantitative DRM requires quantitative site information to establish statistical relationships for spatial prediction and modelling. This highlights three keys issues with DRM. Firstly, most legacy regolith site data are qualitative and are therefore difficult to use in DRM; secondly, in most cases we only see the upper part of the regolith profile in the field; and, thirdly our environmental covariates are strongly biased in measuring surface properties with limited capacity to measure regolith variability at depth.

The Regolith Terrain Mapping (RTMAP) database (Pain et al., 2000) is the principal source of regolith site information recorded and maintained nationally. Most of the regolith descriptions recorded in RTMAP are qualitative which thereby restricts its use in

quantitative analysis and prediction. In places, detailed geochemical, mineralogical, ground-based spectral profiles (e.g. Portable Infrared Mineral Analyser - PIMA) and textural measurements are recorded, but these are rare. To a lesser extent soil site databases are in a similar situation. However, this is changing rapidly with quantitative methods, such as spectral soil analysis (e.g. diffuse reflectance spectroscopy within the visible, near-infrared and mid-infrared) providing a wealth of information for specific modelling of soil properties (McBratney et al., 2006; Masakazu and Shibusawa, 2013; Reeves, 2010). Regolith surveys need to follow a similar path to support future quantitative prediction of regolith materials. This issue of site data quality was avoided when modelling secondary regolith carbonate by using analytically measured calcium from the National Geochemical Survey of Australia database. Other disciplines, such as civil engineering, where quantitative methods are used to assess substrate strength and weathering depth might also be useful alternative sources of quantitative information for DRM. Synergies and approaches in describing the weathered mantle from different disciplines are discussed by Ehlen (2005).

Regolith profiles are rarely completely observed in the field. Road cuttings, gullies, quarries and pits provide useful information, but rarely do we see the entire profile. Drill logs, where available, can provide constraints on weathering depth but these logs are typically difficult to interpret. This issue was particularly relevant in modelling regolith depth over the Mt Lofty Ranges in SA (Chapter 4). Improved cost effective methods for measuring regolith depth would greatly assist future studies in predicting weathering depth.

Finally, many of the covariates used in both soil and regolith mapping reflect surface or near surface characteristics (Figure 59). These covariates are appropriate for soil mapping but are less effective for mapping the characteristics of the regolith where weathering profiles typically extend 5 or more metres below the surface. Multi-spectral imagery and gamma-ray spectrometry sense the surface or near-surface. Vegetation, mineralogy and geochemistry once calibrated can be used to infer features at or near to the surface but these relationships are increasingly tenuous at greater depths. Surface morphology and associated terrain indices (i.e. Multi-Scale Valley Flatness Index, topographic wetness index – McKenzie

and Gallant, 2007) can provide some constraints on depositional thickness in a relative sense. However over an extensive depositional plain, surface morphology is unlikely to tell if the bedrock is two or one hundred metres below the surface. However, airborne electromagnetics (AEM) can be effective in mapping the depth of weathering. Worrall et al. (1998) were able the map the saprock contact over deeply weathered terrains in the Kalgoorlie region of Western Australia using AEM data. Interestingly, the amplitude of the weathering front as mapped by AEM greatly exceeded that of the surface topography. Local variations in weathering depth are likely to reflect bedrock type, grainsize, fabric and structural characteristics including bedding orientation, fracturing and faulting. Airborne electromagnetic data used in the Jamestown study (Chapter 5) were able to delineate regolith depth because of a strong conductivity contrast between the regolith and underlying basement bedrock. However, AEM datasets are confined to relatively small areas, the depth of

sensing is highly dependent on the conductivity of the upper surface, and conductivity gradients imaged by AEM will not necessarily correspond to zones within the regolith.

The Mt Lofty Study (Chapter 4), Jamestown Study (Chapter 5) and the investigation by Worrall et al. (1998) serves to illustrate the high degree of weathering depth variability. Most of our current predictive covariates do not have sufficient resolution to resolve near-surface changes that are reflecting local changes in lithology and bedrock structure as illustrated by the weathering depth prediction over the largely erosional landscapes of the Mt Lofty Ranges in South Australia (Chapter 4). Furthermore, there are significant gaps in our covariates datasets to map broader weathering patterns over the 5-50 m depth range with perhaps the exception of AEM (Figure 59). Many of the sensors over this depth range have limited depth of penetration, resolution or are expensive to acquire, particularly over large areas.
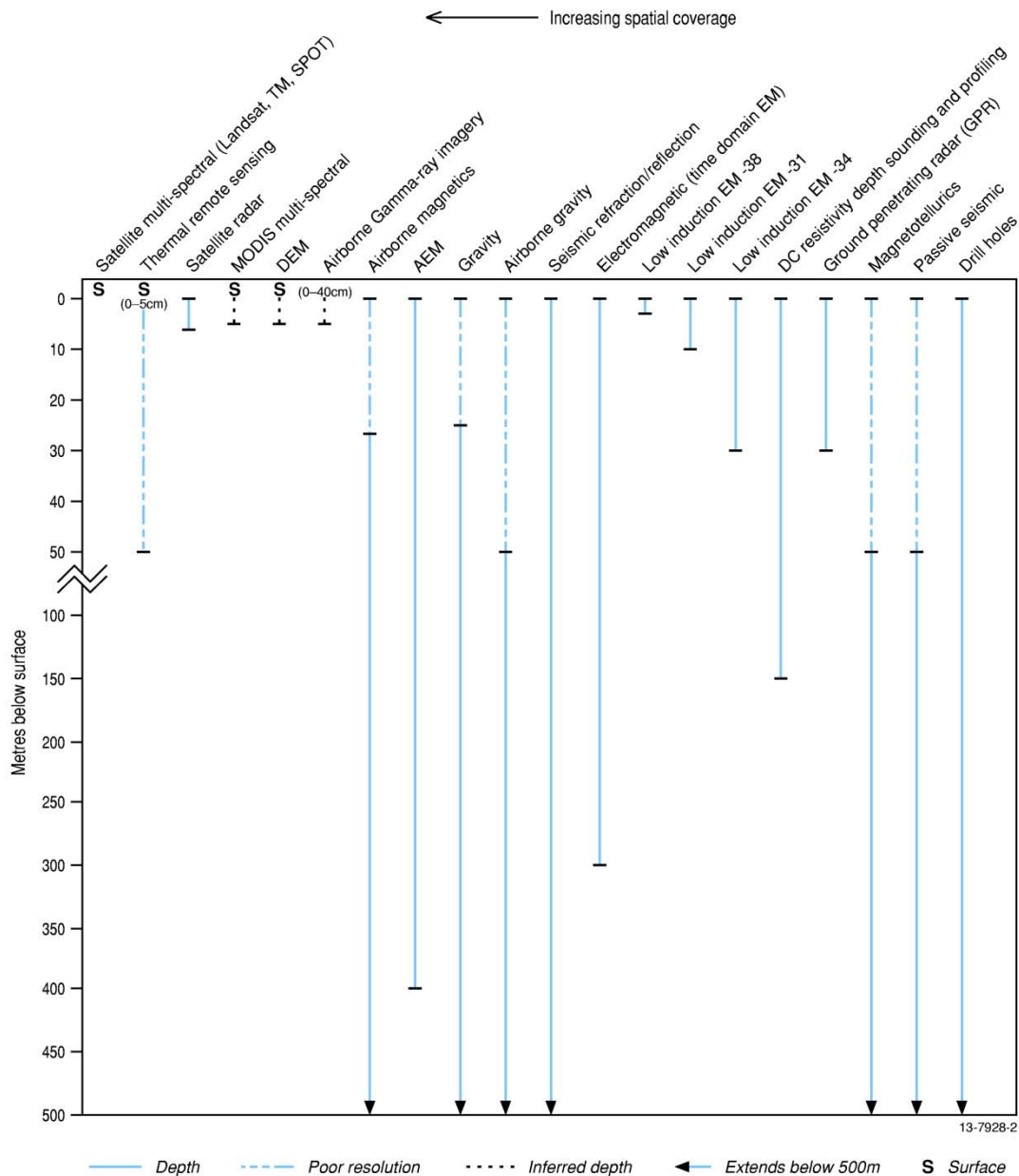
Figure 59 Indicative depths measured by different sensors. Depths represent average conditions. For example in hyper-dry sandy environments radar can penetrate 100m below the surface – depths reported here are based on typical substrate materials. The inferred depth indicates relative depth information based on surrogacy e.g. DEM can be used to infer relative depth based on relief and landscape position. Poor resolution relates to sensors that image over that interval but which have limited spatial resolution over that depth.

6.2 Process understanding and reliability

An advantage of DRM is its cost effectiveness compared to traditional regolith-landform mapping, particularly when predicting regolith attributes at the national scale. This is illustrated by the weathering intensity prediction and the continent wide prediction of secondary carbonate. DRM also provides a set of tools to integrate and analyse large numbers of covariate datasets at both local and national scales that would not be possible using conventional mapping approaches.

All the DRM studies discussed in this thesis have the ability to be updated or revised where new site or environmental datasets become available. However, a potential trap of using a data driven approach is deriving a model with stated correlation or uncertainty without any real understanding of the environmental

factors that underpin the prediction or how the model prediction fits into the broader conceptual framework of regolith formation and landscape evolution. One approach as described in the Jamestown study (Chapter 5) is to combine quantitative and qualitative analysis to build a conceptual model of recent landscape evolution.

Digital regolith mapping approaches have the potential to be used as a powerful knowledge exploration tool. Modelling regolith depth (Chapter 4) and soil calcium carbonate (Chapter 5) used covariates that were consistent with our current conceptual knowledge of the factors that control weathering depth and the accumulation and retention of secondary carbonate in the landscape. Digital regolith mapping is therefore a useful approach for testing conceptual models of regolith and landscape evolution. However, differences between the model and our conceptual understanding can lead to new insights into the controls on regolith development.

Knowledge on the interactions between weathering, geomorphic processes, geology, climate, biota and time with weathering products is used in palaeo-environmental interpretation and landscape evolution reconstruction. Furthermore, residual weathering features provide insights into environmental change, relative ages of exposed surfaces, palaeosurfaces and sediments (Turkington et al., 2005). Digital regolith mapping approaches have the potential to explore or test conceptual models that explain the distribution and nature of regolith materials which will in turn lead to more robust regolith evolution models, and palaeo-environmental models to better assess potential changes caused by climate change and other impacts. There is considerable scope for this type of analysis since compared with the geological sciences, genetic models for regolith development are still being discussed and continue to evolve (Taylor and Eggleton, 2001).

Our preconceived genetic models of regolith formation can bias datasets used in conventional regolith mapping and the latter interpretations drawn from those maps (Hill 1995). Hill (1995) gives the example where the underlying bedrock lithology was used as a basis for subdividing regolith units within a study area. The map was then used to demonstrate the close relationships between regolith materials and bedrock type. Preconceived models of regolith and landscape development can influence the way we interpret field

observations and how we map regolith units (Taylor and Eggleton, 2001). These issues are in part addressed in DRM where the covariates usually have equal weight or importance, and correlations are based on statistical relationships.

In DRM the robustness of the regolith prediction will reflect the strength of the correlations between the site measurements and the environmental covariates used in the model. However, statistical correlations are only telling you about the accuracy of the model which may or may not be an accurate assessment of its actual distribution. For example if the site data does not adequately sample the environmental factors that control the distribution of the target variable (i.e. regolith property) then it is possible to get a statistically robust model with poor prediction reliability. Knowledge of landscape processes and field work to assess and validate model predictions are critical. Post field validation of mapping units is built into traditional soil survey (Dent and Young, 1981), this component is even more important in DRM when models are generated from legacy site datasets without prior fieldwork and landscape context.

6.3 Future work

Through digital mapping approaches we are likely to see greater convergence between the two disciplines of soil and regolith mapping as we aim to develop a more holistic understanding of processes and nature of materials operating within the whole regolith or critical zone. Information on A-B soil characteristics has been a focus of soil mapping but information on the C horizon and below is becoming increasingly important (Lin, 2010; Fitzpatrick et al., 1996; Brantley et al., 2007). In addition with increased focus on mapping the physical, and bio-geochemical properties of the weathered zone rather than classification types, the distinctions between soil and regolith become less important since they are all part of the weathered zone.

Digital soil mapping is well advanced in quantitative description of the upper part of the regolith profile with a set of attributes to support agricultural productivity, sustainability and environmental management (i.e. climate change, land use). A global digital soil map at 100 m resolution is currently being compiled as part of The GlobalSoilMap project (GlobalSoilMap Science Committee, 2011; http://www.globalsoilmap.net/). The

map will show the global distribution of key soil properties to a depth of 2 m unless restricted by bedrock or an indurated layer. These soil properties include; total profile depth, plant exploitable depth, organic carbon, pH, sand, silt, clay, gravel, effective cation exchange capacity (ECEC), bulk density of fine earth fraction, bulk density of the whole soil and available water capacity. Such a project highlights the gap between development and implementation of DSM compared with DRM. Detail coverage of traditional regolith maps nationally is at best patchy let alone a global map of specific regolith properties.

From a mineral perspective the importance of mapping the thickness and nature of the regolith needs to be put into the context of the recent decline of mineral exploration success in Australia. Most of the current discoveries have been in areas of outcropping rock. Even in landscapes with relatively shallow cover (<30 m) the regolith is seen as an impediment to exploration and have been largely under explored. A national and coordinated geoscience research strategy called 'Searching The Deep Earth' (www.science.org.au/policy/uncover.html) seeks to significantly enhance the discovery of hidden mineral wealth in Australia. The strategy includes four main research themes including Characterising the Australian cover; Investigating Australia's lithospheric architecture; Resolving the 4D geodynamic and metallogenic evolution of Australia, and Characterising and detecting the distal foot prints of ore deposits. The age, physical and chemical characteristics of the regolith have direct input into research themes one and four. Integration and modelling of geoscientific datasets using DRM approaches are likely to be important in facilitating an understanding of regolith-landscape processes and mapping regolith attributes to support these research themes. Regolith depth is arguably the most fundamental regolith attribute that

is amenable to mapping by DRM. Depth in this context includes both weathering depth and depth through sedimentary rock to older more prospective basement lithologies (e.g. Mesozoic sediment over Proterozoic rock). Other desirable regolith properties include; texture, geochemical composition (e.g. Fe, Al Si, Mg, K), hydraulic properties including permeability and porosity, bulk density, age and weathering intensity. Also important would be knowledge of whether the regolith is locally derived (in-situ) or transported including vectors of transport (i.e. provenance of sediment). Some of these properties have been dealt with in this thesis but there is considerable scope to build and expand the framework being developed through the GlobalSoilMap project.

The methodology used to predict regolith depth (Chapter 4) is currently being expanded Australia wide using national drillhole databases to extract weathering depth. In addition, environmental correlation used to model near-surface secondary carbonate (Chapter 3) is being used to model a spectrum of other major and trace element concentrations as recorded by the NGSA.

Knowledge of the regolith and associated chemical, biological and physical processes occurring within it has direct relevance to many activities or disciplines including environmental management, natural hazard mitigation, agricultural sustainability, civil engineering and mineral exploration. Digital regolith mapping has the potential to model specific attributes tailored to support these activities as well as providing a knowledge discovery tool to better understand the complex interactions and processes occurring within the weathered zone. Critical steps to ensure future success of DRM in Australia are addressing gaps in our covariate datasets and the acquisition of key quantitative site attributes.

References

References

Adbelouas, A., Lutze, W., Gong, E., Nuttal, E.H., Strietelmeier, B.A., Travis, B.J., 2000. Biological reduction of uranium in groundwater and subsurface soil. Science Total Environment. 250, 21–35.

Acworth, R.I., 1987. The development of crystalline basement aquifers in a tropical environment. Quarterly Journal of Engineering Geology 20, 265–272.

Ahnert, F., 1987. Process-response models of denudation at different spatial scales. Catena Supplement 10, 21–50.

Aitken M.J., 1998. An introduction to optical dating: the dating of Quaternary sediments by the use of photon-stimulated luminescence. Oxford University Press, Oxford.

Alley N.F., Lindsay J.M., 1995. Walloway Basin. In: Drexel J. F., Preiss W. V. (eds), The Geology of South Australia, Volume 2, The Phanerozoic, Geological Survey of South Australia Bulletin 54, 198–199.

Anand R. R., Gilkes R. J., 1987. Variation in the properties of iron oxides within individual specimens of lateritic duricrust. Australian Journal of Soil Research 25, 287–302.

Anand, R.R., Pain, M., 2002. Regolith geology of the Yilgarn Craton, Western Australia: implications for exploration, Australian Journal of Earth Sciences 49,(1),3-162.

Arakel, A.V., 1986. Evolution of calcrete in palaeodrainages of the Lake Napperby area, Central Australia. Palaeogeography, Palaeoclimatology, Palaeoecology 54, 283-303.

Atkinson, G., 1993. Soil materials, a layer based approach to soil description and classification, Catena, 20, 411-418.

Belton, D.X., Brown, R.W., Kohn, B.P., Fink, D., Farley, K.A., 2004. Quantitative resolution of the debate over antiquity of the central Australian landscape: implications for the tectonics and geomorphic stability of cratonic interiors. Earth and Planetary Science Letters 219, 21–34.

Beven, K.J., Kirkby, M.J., 1979. A physically based, variable contributing area model of basin hydrology. Hydrological Sciences Bulletin 24, 1.

Bierwirth, P., 1996. Investigation of airborne gamma-ray images as a rapid mapping tool for soil and land degradation: Wagga Wagga, NSW. Australian Geological Survey Organisation, Record, 1996/22.

Blewett, R. (ed), 2012. Shaping a Nation - A Geology of Australia, ANU press, Canberra.

Bøtter-Jensen L., Bulur E., Duller G. A. T., Murray A. S., 2000. Advances in luminescence instrument systems. Radiation Measurements 32, 523–528.

Bourman, R.P., 2007. Deep regolith weathering on the summit surface of the Southern Mount Lofty Ranges, South Australia: a contribution to the 'Laterite' debate. Geographical Research 45, (3), 291–299.

Bourman, R.P., 1993. Models of ferricrete genesis: evidence from southeastern Australia. Zeitschrift für Geomorphologie 37, 77–101.

Bourman, R.P., Belperio, A.P., Murray-Wallace, C.V., Cann, J.H., 1999. A last interglacial embayment fill at Normanville, South Australia, and its neotectonic implications. Transactions of the Royal Society of South Australia 123, 1–15.

Brantley .S.L., Goldhaber, M.B., Ragnarsdotttir, K.V., 2007. Crossing disciplines and scales to understand the critical zone, Elements, 3, 307-314.

Brantley, S.L., White, T.S., White, A.F., Sparks, D., Richter, D., Pregitzer, K., Derry, L., Chorover, J., Chadwick, O, April, R., Anderson, R., 2006. Frontiers in exploration of the critical zone, An NSF-sponsored Workshop, National Science Foundation, 30.

Breiman, L., 1996. Bagging predictors. Machine Learning 24, (2), 123-140. doi:10.1007/BF00058655.

Brown, A.V., Cooper, R.A., Corbett, K.D., Daily, B., Green, G.R., Grindley, G.W., Jago, J., Laird, M.G., VandenBerg, A.H.M., Vidal, G., Webby, B.D., Wilkinson, H.E., 1982. Late Proterozoic to Devonian Sequences of Southeastern Australia, Antarctica and New Zealand and their correlation. Special Publication, No. 9. Geological Society of Australia, Inc. 103.

Bui, E.N., 2007. A review of digital soil mapping in Australia In: P. Lagacherie, A.B. McBratney, M. Voltz (eds.), Digital Soil Mapping, an Introductory Perspective. Developments in Soil Science 31. Elsevier, Amsterdam, 3–24.

References

Bui, E.N., Henderson, B.L., Viergever, K., 2006. Knowledge discovery from models of soil properties developed through data mining. Ecological Modelling 191, 431–446.

Bui, E., Henderson, B., Viergever, K., 2009. Using knowledge discovery with data mining from the Australian Soil Resource Information System database to inform soil carbon mapping in Australia. Global Biogeochemical. Cycles, 23, GB4033, doi:10.1029/2009GB003506.

Bui, E.N., Loeppert, R. H., Wilding, L, P., 1990. Carbonate phases in calcareous soils of the Western USA. Soil Science Society of America Journal 54, 39-45.

Bui, E.N., Moran, C.J., 2003. A strategy to fill gaps in soil survey over large spatial extents: an example from the Murray-Darling basin of Australia. Geoderma 111, 21-14. doi: 10.1016/S0016-7061(02)00238-0.

Butt, C.R., Horwitz, R.C., Mann, A.W., 1977. Uranium Occurrences in Calcrete and Associated Sediments in Western Australia. CSIRO Division of Mineralogy, Report FP 16, Floreat Park, WA.

Butt, C. R. M., Lintern, M. J., Anand, R. R., 2000. Evolution of regoliths and landscapes in deeply weathered terrain – implications for geochemical exploration. Ore Geology Reviews 16, 167–183.

Butt, CRM, Scott KM, Cornelius, M and Robertson, IDM, 2008.Regolith sampling for geochemical exploration, In Regolith Science, Scott and Pain (ed),CSIRO publishing, Victoria.

Butler, B.E., 1956. Parna – an aeolian clay. Australian Journal of Sciences 18, 145-151.

Butler, B.E., Blackburn, G., Bowler, J.M., Lawrence, C.R., Newell, J.W., Pels, S., 1973. A geomorphic map of the Riverine Plain of south-eastern Australia, Australian National University Press, 39pp.

Butler B. E., 1982. The location of aeolian dust mantles in southeastern Australia. In: Wasson R. J. ed. Quaternary dust mantles of China, New Zealand and Australia, Australian National University, Canberra, 141–144pp.

Butler R. F., 1992. Paleomagnetism: magnetic domains to geologic terranes. Blackwell Scientific, Boston.

Capo, R.C., Chadwick, O.A., 1999. Sources of strontium and calcium in desert soil and calcrete. Earth and Planetary Science Letters 170 (1-2), 61-72.

Caritat, P. de, Bloch, J., Hutcheon, I., 1994. LPNORM: a linear programming normative analysis code. Computers and Geosciences, 20, 313-347.

Caritat, P. de., Cooper, M., 2011. National Geochemical Survey of Australia: The Geochemical Atlas of Australia. Geoscience Australia Record, 2011/20 (2 Volumes + Dataset), 557 pp. Available at: https://www.ga.gov.au/products/servlet/controller?event=GEOCAT_DETAILS&catno=71973

Caritat, P. de, Cooper, M., Lech, M., McPherson, A., Thun, C., 2009. National Geochemical Survey of Australia: Sample Preparation Manual. Geoscience Australia Record, 2009/08, 28 pp. Available at: https://www.ga.gov.au/products/servlet/controller?event=GEOCAT_DETAILS&catno=68657

Caritat, P. de, Cooper, M., Pappas, W., Thun, C., Webber, E., 2010. National Geochemical Survey of Australia: Analytical Methods Manual. Geoscience Australia Record, 2010/15, 22 pp. Available at: https://www.ga.gov.au/products/servlet/controller?event=GEOCAT_DETAILS&catno=70369

Caritat, P. de, Cooper, M., Wilford, J., 2011. The pH of Australian soils: field results from a national survey. Soil Research, 49, 173-182.

Carrier, F., Bourdon, B., Pili, E., Truffert, C., Wyns, R., 2006. Airborne gamma-ray spectrometry to quantify chemical erosion processes. Journal of Geochemical Exploration 88, 266–270.

Carson, M.A., Kirkby, M.J., 1972. Hillslope Form and Process. Cambridge University Press, Cambridge, 475pp.

Cattle, S.R., Meakin, S.N., Ruszkowski, P., Cameron, R.G., 2003. Using radiometric data to identify aeolian additions to topsoil of the Hillston district, western NSW. Australian Journal of Soil Research 41, 1439–1456.

Cerling, T. E., 1984. The stable isotopic composition of modern soil carbonate and its relationship to climate. Earth and Planetary Science Letters, 71(2), 229-240.

Chan, R.A., 1986. The Regolith Terrain Map of Australia 1:5 000 000, BMR Record, Canberra, 1986/27. (Map http://www.ga.gov.au/meta/ANZCW0703002403.html).

Chan, R.A, 1998. Bathurst regolith-landforms, in: Watkins, J.J and Pogson, D.J., (Compilers), Bathurst New South Wales Explanatory Notes, 1:250 000 Geological Series, Sheet SI55-8, second edition. Geological survey of New South Wales, 311–328.

Chan, L.S., Wong, P.W., Chen, Q.F., 2007. Abundances of radioelements (K, U, Th) in weathered igneous rocks in Hong Kong. Journal of Geophysics and Engineering 4, 85–292.

References

Chartres, C. J., Chivas A. R., Walker P. H., 1988. The effect of aeolian accessions on soil development on granitic rocks in southeastern Australia. Oxygen-isotope, mineralogical and geo-chemical evidence for aeolian deposition. Australian Journal of Soil Research 26, 17–31.

Chen, X. Y., 1997., Quaternary sedimentation, parna, landforms, and soil landscapes of the Wagga Wagga 1:100 000 map sheet, south-eastern Australia, Australian Journal of Soil Research 35, 643–668.

Chen, X.Y., Lintern, M.J., Roach, I.C., 2002. Calcrete: Characteristics, Distribution and Use in Mineral Exploration. Cooperative Research Centre for Landscape Environments and Mineral Exploration (CRC LEME), Canberra, Australia. 160pp.

Cherry, D.P., Wilkinson, H.E., 1994. Bendigo and part of Mitiamo 1:100,000 map geological report. Geological Survey of Victoria, Report 99, 80.

Chiquet, A., Michard, A., Nahon, D., Hamelin, B., 1999. Atmospheric input vs in situ weathering in the genesis of calcretes: An Sr isotope study at Gálvez (Central Spain). Geochimica et Cosmochimica Acta 63 (3-4), 311-323.

Chittleborough, D.J., 1991. Indices of weathering for soils and paleosols formed on silicate rocks. Australian Journal of Earth Sciences 38, 115–120.

Chor, C., Nitschke, N., Williams, M., 2003. Ice, wind and water: Late Quaternary valley-fills and aeolian dust deposits in arid South Australia. In: Roach I. C. ed. Advances in regolith, CRC LEME, Bentley70–73.

Christian, C. S., Stewart,. 1953. General report on survey of Katherine-Darwin region, 1946. CSIRO Land Research Series 1. CSIRO, Australia.

Cook, S.E., Corner, R.J., Grealish, G., Gessler, P.E., Chartres, C.J., 1996. A rule-based system to map soil properties. Soil Science Society of America Journal, 60, 1893-1900.

Cook, S.E., Corner, R.J., Groves, P.R., Grealish, G.J., 1996. Use of airborne gamma-radiometric data for soil mapping. Australian Journal of Soil Research 34, 183–194.

Cooper, L., 1978. Jamestown—a photographic study. Corporation of Jamestown.

Cooper, M., Caritat, P. de, Burton, G., Fidler, R., Green, G., House, E., Strickland, C., Tang, J., Wygralak, A.S., 2010. National Geochemical Survey of Australia: Field Data. Geoscience Australia Record, 2010/18, 93 pp. Available at: https://www.ga.gov.au/products/servlet/controller?event=GEOCAT_DETAILS&catno=70478

Coram, J. E., Dyson, P. R., Houlder, P. A., Evans,W. R., 2000. Australian Groundwater Flow Systems contributing to Dryland Salinity. Report by the Bureau of Rural Sciences for the Dryland Salinity Theme of the National Land and Water Resources Audit. Canberra.

Craig, M.A., 2001. Regolith mapping for geochemical exploration in the Yilgarn Craton, Western Australia, In Geochemical exploration for gold and nickel in the Yilgarn Craton, Western Australia; Geochemistry - Exploration, Environment, Analysis (November 2001), 383-390.

Craig, M. A., Wilford, J., 1995. Leonora Regolith Landforms Image Map. Australian Geological Survey Organisation, 1:250 000 Regolith Landforms Map.

Cresswell, R. G., Herczeg A. L., 2004. Groundwater flow systems and salinity in the valleys around Jamestown, South Australia: geochemical and isotopic constraints. CSIRO Land and Water Technical Report 30/04.

Curtis, C.D., 1976. Chemistry of rock weathering: fundamental reactions and controls. In: Derbyshire, E. (ed.), Geomorphology and Climate. Wiley, London, 25–57pp.

Daily, B., Firman, J.B., Forbes, B.G., Lindsay, J.M., 1976. Geology. In: Twidale, C.R.T., Tyler, M.J., Webb, B.P. (eds.), Natural History of the Adelaide Region. Royal Society of South Australia.

Dalrymple, J. B., Blong, R.J., Conacher, A.J., 1968. A hypothetical nine unit landvsurface model, Zeitschrift für Geomorphologie, 12, 60–76.

Dart, R.C., Barovich, K, M., Chittleborough, D. J., Hill, S.M., 2007. Calcium in regolith carbonates of central and southern Australia: Its source and implications for the global carbon cycle. Palaeogeography, Palaeoclimatology, Palaeoecology 249, 322-334.

Dauth, C. 1997., Airborne magnetic, radiometric and satellite imagery for regolith mapping in the Yilgarn Craton of Western Australia. Exploration Geophysics 28, 199–203.

Dent, D,L., Munday, T.J., Brodie, R.C., Lawrie, K.C., 2002. Implications for salinity and land management—Honeysuckle Creek Victoria: a preliminary interpretation of high-resolution airborne geophysical data, In Phillips and Ely (eds.), Victoria Undercover: Benalla 2002 Conference Proceedings and Field Guide: Collaborative Geoscience in Northern Victoria, CSIRO Exploration and Mining (2002), 223–233.

Dent, D., Young, A. 1981. Soil survey and land evaluation. London, George Allen and Unwin.

References

Department of Water, Land and Biodiversity Conservation 2002. Central Districts Land Resource Information (CD). Department of Water, Land and Biodiversity Conservation, South Australia, Soil and Land Information Group.

Dickson, B.L and Scott, K,M., 1997., Interpretation of aerial gamma-ray surveys-adding the geochemical factors. AGSO Journal of Australian Geology and Geophysics, 17(2), 201–216.

Drexel, J.F., Preiss, W.V. (Eds.), 1995. The Geology of South Australia Vol. 2, The Phanerozoic, Bulletin 54. South Australia Geological Survey.

Duval, J. S., 1990. Modern aerial gamma-ray spectrometry and a regional potassium map of the conterminous United States. In: Darnley, A.G., Garrett, R.G. (eds.) International Geochemical Mapping, Journal of Geochemical Exploration 39, 249–253.

Eggleton, R.A., 1998. Weathering. In: Eggleton, R.A. (ed.), The State of the Regolith: Geological Society of Australia Special Publication 20, pp. 126–140.

Eggleton, R.A. (Ed.), 2001. The Regolith Glossary: Surficial Geology, Soils and Landscapes. National Capital Printing, Canberra.

van Egmond, F.M., Loonstra, E.H., Limburg, J., 2010. Gamma ray sensor for topsoil mapping: the mole. In: Viscarra Rossel, R.A., McBratney, A.B., Minasny, B. (eds.), Proximal Soil Sensing: Progress in soil science, Vol 1. Springer.

Ehlen, J., 2005. Above the weathering front: contrasting approaches to the study and classification of weathered mantle. Geomorphology 67, 7–21.

English, P., Richardson, P., Glove,r M., Cresswell, H, Gallant, J., 2004. Interpreting airborne geophysics as an adjunct to hydro-logical investigations for salinity management: Honeysuckle Creek Catchment, Victoria. CSIRO Land and Water Technical Report 18/04.

Erbe, P., Schuler, U., Wicharuck, S., Rangubpit, W., Stahr, K., Herrmann, L., 2010. Creating soil degradation maps using gamma-ray signatures. 19th World Congress of Soil Science, Soil Solutions for a Changing World, 1–6 August, Brisbane, Australia.

Evans, W.R., 1998. What does Boorowa tell us? Salt stores and groundwater dynamics in a dryland salinity environment. In: Weaver, T.R., Lawrence, C.R. (Eds.), Groundwater: Sustainable Solutions. Proceedings of the IAH International Groundwater Conference, University of Melbourne, (8–13), 267–274.

Fitzpatrick, R.W., 1988. Iron compounds as indicators of pedogenic processes: Examples from the southern hemisphere, in: Stucki, J.W. Goodman, B.A., Schwertmann, U. (eds.) Iron in Soil and Clay Minerals, NATO ASI Ser. C. Vol. 217, D. Reidel, Dordrecht, Holland, pp. 351-389.

Fitzpatrick, R.W., Merry, R.H., 2000. Pedogenic carbonate pools and climate change in Australia, In: Lal, R., Kimble, J.M., Eswaran, H., Stewart, B.A. (eds.), Global Climate Change and Pedogenic Carbonates, CRC Press, Boca Raton, FL., 105-120.

Fugro Airborne Surveys 2002a. Acquisition and processing technical report: Jamestown and Angas–Bremer Airborne Surveys. Airborne magnetic, gamma-ray and elevation surveys (prepared by S. Murphy and L. Stenning). Bureau of Rural Sciences FAS JOB # 1545.

Fugro Airborne Surveys 2002b. Acquisition and processing technical report: Jamestown and Angas–Bremer Plains Airborne Surveys. TEMPEST Geophysical Surveys (prepared by M Owens and L. Stenning). Bureau of Rural Sciences FAS JOB # 1544.

Galbraith, J.H., Saunders, D.F., 1983. Rock classification by characteristics of aerial gamma ray measurements. Journal of Geochemical Exploration 18, 49–73.

Gale, S.J., 1992. Long-term landscape evolution in Australia. Earth Surface Processes and Landforms 17, 323–343.

Gallant, J.C., 2011, 3 Second SRTM Derived Digital Elevation Model (DEM) version 1.0 Geoscience Australia – metadata : http://www.ga.gov.au/meta/ANZCW0703014182.html

Gallant, J.C., Dowling, T.D., 2003. A multi-resolution index of valley bottom flatness for mapping depositional areas. Water Resources Research 39, 1347–1360.

Gallant, J.C., Wilson, J.P., 1996. TAPES-G: a grid-based terrain analysis program for the environmental sciences. Computers and Geosciences 22, 713-722.

Gastaldi, G., Minasny, B., McBratney, A.B., 2012. Mapping the occurrence and thickness of soil horizons within soil profiles. In: Minasny, Malone, McBratney (eds.), Digital Soil Assessments and Beyond. Taylor and Francis Group, London. ISBN: 978-0-415-62155-7, 145–148.

George, R.J., Conacher, A.J., 1993. Interaction between perched and saprolite aquifers on a small, salt affected and deeply weathered hillslope. Earth Surface Processes and Landforms. 18, 91–108.

References

Gessler, P.E., Moore, I.D., McKenzie, N.J., Ryan, P.J., 1995. Soil-landscape modelling and spatial prediction of soil attributes. International Journal of Geographical Information Systems 9 (4), 421–432.

Gibson, D., 2003. A new regolith/geology/landform mapping framework for hydrogeological investigations in the Angas Bremer Plains area, SA, Advances in regolith (ed) I.C. Roach, Proceedings of the CRC LEME regional regolith Symposia, Perth.

Gibson D. L., Wilford J., 2002. Aspects of regolith and landscape of the Strathbogie–Caniambo–Dookie area. In: Phillips G. N. and Ely K. S. eds. Victoria Undercover: Benalla 2002 Conference Proceedings and Field Guide: Collaborative Geoscience in Northern Victoria, CSIRO Publishing, Collingwood, 235–247.

Gilbert, G.K., 1877. Report on the geology of the Henry Mountains. U.S. Geographical and Geological Survey of the Rocky Mountain Region, Washington, D.C.

Globalsoilmap Science Committee. 2011. Specifications Version 1 GlobalSoilMap.net products.

Goudie, A.S., 1996. Organic agency in calcrete development, Journal of Arid Environments 32, (2), 103-110.

Gray, D.R., 1997. Tectonics of the southeastern Australian Lachlan Fold Belt: structural and thermal aspects. In: Burg, J.P., Ford, M. (eds.), Orogeny Through Time: Geological Society Special Publication 121, 149–177.

Greenman, D.J., Rose, A.W., Washington, J.W., Dobos, R.R., Ciolkosz, E.J., 1999. Geochemistry of radium in soils of Eastern United States. Applied Geochemistry 14, 365–385.

Grunwald, S., 2009. Multi-criteria characterization of recent digital soil mapping and modeling approaches. Geoderma 152, 195–207.

Gunn P. J., Dentith M. C., 1997. Magnetic responses associated with mineral deposits. AGSO Journal of Australian Geology and Geophysics 17, 145–155.

Hack, J.T., 1960. Interpretation of erosional topography in humid temperate regions. American Journal of Science 258-A, 80–97.

Hall, G.F., Olson, G.C., 1991. Predicting Variability of Soils from Landscape Models, in Spatial Variabilities of Soils and Landforms, M. J. Mausbach., L. P. Wilding (ed.), Soil Science Society of America.

Hall, J.A.S., Maschmedt, D.J., Billing, N.B., 2009. The Soils of Southern Australia. The South Australian Land and Book series, Volume1: Geological Survey of South Australia, Bulletin 56, (1), Department of Water, Land and Biodiversity Conservation, Government of South Australia.

Harriss, R.C., Adams, J.A.S., 1966. Geochemical and mineralogical studies on the weathering of granitic rocks. American Journal of Science 246, 146–173.

Harrison, J.B.J., Hendrickx, J.M.H., Muldavin, E., McMahon, D., Wardell, J., 2003. Biological and climate controls on calcium carbonate precipitation in a small first order drainage basin, Sevilleta long term ecological research site, New Mexico. USA, XVI INQUA Congress Reno, Nevada, Geological Society of America Abstracts: https://gsa.confex.com/gsa/inqu/finalprogram/abstract_55929.htm.

Hays., 1967. Land surfaces and laterites in the north of the Northern Territory. In Jennings, J.N and Mabbutt, J.A. (eds) Landform Studies from Australia and New Guinea. Australian National University press. Canberra, 182-210.

Heimsath, A.M., Chappell, J., Spooner, N.A., Questiaux, D.G., 2002. Creeping soil. Geology 30, 111–114.

Henderson, B.L., Bui, E.N., Moran, C.J., Simon, D.A.P., 2005. Australia-wide predictions of soil properties using decision trees. Geoderma 124, 383-398.

Hengl, T., 2009. A pratical guide to geostatistical mapping, EUR 22904 EN Scientific and technical research series, Office for official Publications of the European communities, Luxembourg, ISBN: 978-92-79-06904-8.

Hengl, T., Reuter, H.I., 2009. Geomorphometry: Concepts, Software, Applications. Elsevier, Amsterdam.

Henschke C., Jone G., Cresswell R,. 2004. Groundwater investigations on valley fills, Jamestown, South Australia. Bureau of Rural Sciences Technical Report September 2004.

Henschke, C. J., McCarthy, D. G., Richardson, S. B., Evans, T. D., 1994. Investigation and management of dryland salinity in a catchment at Jamestown in the mid north of South Australia. Primary Industries South Australia Technical Paper 35.

Hesse, P. P., 1994. The record of continental dust from Australia in Tasman Sea sediments. Quaternary Science Reviews 13, 257–272. LANE R. LEEMING P., OWENS M. and TRIGGS D. 1999. Undercover assignment for Tempest. Preview 82, 17–21.

Hesse, P.P., McTainsh, G.H., 2003. Australian dust deposits; modern processes and the Quaternary record. Quaternary Science Reviews 22, 2007-2035.

References

Hill, S.M., McQueen, K.G., Foster, K.A. 1999. Regolith carbonate accumulations in western and central NSW: Characteristics and potential use as an exploration sampling medium. In: Taylor, G.M., Pain, C.F., (eds) New Approaches to an Old Continent. Regolith '98 Proceedings, pp. 191-208 CRC LEME, Perth.

Houlder, D., Hutchinson, M., Nix, H., McMahon, J., 1999. ANUCLIM version 5.0. User Guide. Centre for Resource and Environmental Studies. The Australian National University, Canberra.

Hutchinson, M.F., 1989. A new method for gridding elevation and stream line data with automatic removal of spurious pits. Journal of Hydrology. 106, 211-232.

Hutchinson, M.F., 1993. Development of a continent wide DEM with applications to terrain and climate analysis. In: Goodchild, M.F., et al. (Ed.), Environmental Modeling with GIS. Oxford University Press, New York, 392–399pp.

Hutchinson, M., Stein, J., Stein, J., Anderson, H., Tickle, P., 2008. GEODATA 9 second DEM and D8: Digital Elevation Model Version 3 and Flow Direction Grid - Gridded Elevation and Drainage Data Source scale 1:250 000. User Guide. (Fenner School of Environment and Society, the Australian National University and Geoscience Australia, Australian Government. Available at: https://www.ga.gov.au/image_cache/GA11644.pdf

IAEA, 2003. Guidelines for Radioelement Mapping Using Gamma-Ray Spectrometry Data. IAEA-TECDOC-1363, IAEA, Vienna.

Isbell, R.F., 1996. The Australian Soil Classification. CSIRO Publishing, Canberra.

Isbell, R.F., Gillman, G., 1973. Studies on some deep sandy soils in Cape York Peninsula, north Queensland. 1. Morphological and chemical characteristics. Australian Journal of Experimental Agriculture and Animal Husbandry 13 (60), 81–88.

Isbell, R.F., McDonald, W.S., Ashton, L.J., 1997. Concepts and Rationale of the Australian Soil Classification. CSIRO Land and Water, Australia

Jahn, A., 1968. Denudational balance of slopes. Geographica Polonica 13, 9–29.

Jenkin, J.J., Dyson, P.R., 1983. Groundwater and salinisation near Bendigo, Victoria. In: Knight, M.J., Minty, E.J., Smith, R.B. (eds.), Collected Case Histories in Engineering Geology, Hydrogeology, Environmental Geology, Geological Society of Australia Special Publication, 11. Engineering Geology Specialist Group, pp. 229–257.

Jenness, J., 2006. Topographic Position Index (tpi_jen.avx) extension for ArcView 3.x, v. 1.3a.

Jenness Enterprises (Available at: http://www.jennessent.com/arcview/tpi.htm).

Jenny, H., 1941., Factors of Soil Formation-A System of Quantitative Pedology. McGraw Hill Book Co., New York.

Johnson, D.L., 1985. Soil thickness processes. Catena 6, 29–40 (Suppl.). Natural History of the Adelaide Region. Royal Society of South Australia, Inc., Adelaide.

Johnston, C.D., McArthur, W.M., Peck, A.J., 1980. Distribution of soluble salts and water in soils of the Manjimup Woodchip Licence area, Western Australia. CSIRO Australia, Division of Land Resources Management Technical Paper 5, p. 129.

Joyce, E.B., 2003. Western volcanic plains, Victoria, advances in regolith. In: Roach, I.C. (Ed.), Proceedings of the CRC LEME Regional regolith Symposia, 1–5.

Joyce, E.B., Webb, J.A., Dahlhaus, P.G., Grimes, K.G., Hill, S.M., Kotsonis, A., Martin, M.M., Neilson, J.L., Orr, M.L., Peterson, J.A., Rosengren, N.J., Rowan, J.N., Rowe, R.K., Sargeant, I., Stone, T., Smith, B.L., White, S., 2003. Geomorphology: the evolution of Victorian landscapes. In: Birch, W.D. (ed.), Geology of Victoria: Geological Society of Australia Special Publication 23, 533–561.

Kahle, C.F., 1977. Origin of subaerial Holocene calcareous crust: Role of algae, fungi, and sparmicritisation: Sedimentology 24, 413-435.

Keywood, M.D., Chivas, A.R., Fifield, L.K., Cresswell, R.G., Ayers, G.P., 1997. The accession of chloride to the western half of the Australian continent. Australian Journal of Soil Research 35:1177-1189.

Klappa, C.F., 1980. Rhizoliths in terrestrial carbonates: classification, recognition, genesis and significance. Sedimentology, 27:613-629.

Koons, R.D., Helmke, P.A., Jackson, M.L., 1980. Association of trace elements with iron oxides during rock weathering. Soil Science Society of America Journal 44, 155–159.

Krishnaswami, S., 1999. Thorium. In: Marshall, C.P., Fairbridge, R.W. (eds.), Encyclopedia of Geochemistry. Kluwer Academic Publishers, London, 630pp.

Land and Soil Spatial Data for Southern South Australia –GIS CD. 2007. Department of Water, Land and Biodiversity Conservation, SA Government.

References

Lagacherie, P., McBratney, A.B., Voltz, M. (eds.), 2007. Digital soil mapping — an introductory perspective. : Developments in Soil Science, Vol. 31. Elsevier, Amsterdam. Lahti, M., Jones, D.G., 2003. Environmental applications of airborne radiometric surveys. First Break 21, 35–42.

Langmuir, D., Herman, J.S., 1980. The mobility of thorium in natural waters at low temperatures. Geochimica et Cosmochimica Acta 44, 1753–1766.

Laffan, S.W., Lees, B, G., 2004. Predicting regolith properties using environmental correlation: a comparison of spatially global and spatially local approaches, Geoderma, 120, 241-258.

Lagacherie,P., McBratney, A.B., 2007. Chapter 1. Spatial soil information systems and spatial soil inference systems: perspectives for Digital Soil Mapping. In: P. Lagacherie, A.B. McBratney and M. Voltz (Eds.), Digital Soil Mapping, an introductory perspective. Developments in soil science, vol. 31. Elsevier, Amsterdam, pp. 3–24.

Lal, R., Kimble, J.M., 2000. Pedogenic carbonates and the global carbon cycle, in: Lal, R., Kimble, J.M., Eswaran, H., Stewart, B.A. (Eds.), Global Climate Change and Pedogenic Carbonates, CRC Press, Boca Raton, FL., pp. 1-14.

Lane, P.W., 2002. Generalized linear models in soil science. European Journal of Soil Science 53, 241-251.

Lane, R., Green A., Golding C., Owers M., Pik P., Plunkett C., Sattel D. and Thorn B. 2000. An example of 3D conductivity mapping using the TEMPEST airborne electromagnetic system. Exploration Geophysics 31, 162–172.

Lane, R., Heislers D. and McDonald P. 2001 Filling in the gaps— validation and integration of airborne EM data with surface and subsurface observations for catchment management: an example from Bendigo, Victoria, Australia. Exploration Geophysics 32, 205–215.

Lawrie K. C., Munday T. J., Dent D. L., Gibson D. L., Brodie R. C., Wilford J., Reilly N. S., Chan R. A., 2000. A 'Geological Systems' approach to understanding the processes involved in land and water salinisation in areas of complex regolith—the Gilmore Project, central-west NSW. AGSO Research Newsletter 32, 26–32.

Lawrie, KC, Tan, K.P, Clarke, JC, Munday, T.J, Fitzpatrick, A, Brodie, RS, Apps, H, Halas, L, Cullen, K, Pain, CF, Kuske, TJ, Cahill, K., Davis, A 2010, Using the SkyTEM time domain airborne electromagnetics (AEM) system to map aquifer systems and salinity hazard in the Ord Valley, Western Australia, Geoscience Australia Professional Opinion 2010/01.

Lawrie, K. C., Wilford, J., Gibson, D., Pain, C., Roberts, L., Coram, J., Halas, L., Apps, H., Fitzpatrick, A., Tan, K. P., Sorenson, C. James, J., Tate, S., 2004. Regolith constraints on modeling salt movements in upland landscapes in the Murray-Darling Basin. In Roach, I (ed.) CRC LEME Regional Regolith Symposia, 2004, 193-197.

Lin, H. 2010. Earth's Critical Zone and hydropedology: concepts, characteristics, and advances. Hydrological Earth Systems Science 14. Available at: www.hydrol-earth-syst-sci.net/14/25/2010.

Lintern,M.J., Butt, C.R.M., 1993. Pedogenic carbonate: an important sampling medium for gold exploration in semi-arid areas, Exploration Research News, CSIRO Australia, Division of Exploration Geoscience, 7 (1993), 7–11pp.

Lintern, M.J.; Sheard, M.J., Chivas, A.R., 2006. The source of pedogenic carbonate associated with gold-calcrete anomalies in the western Gawler Craton, South Australia. Chemical Geology, 235,(3-4), 299-324.

Lowry, D.C., 1970. Geology of the Western Australian part of the Eucla Basin. Geological Survey of Western Australia, Bulletin 122.

Lymburner, L., Tan, P., Norman, M., Thackway, R., Lewis, A., Thankappan, M., Randall, R., Islam, A., Senarath, U., 2011. The National Dynamic Land Cover Dataset-Technical Report, Geoscience Australia Record 2011/31. Available at: https://www.ga.gov.au/products/servlet/controller?event=GEOCAT_DETAILS&catno=71069

Mackey T., Lawrie K., Wilkes P., Munday T., De Souza Kovacs N., Chan R., Gibson D., Chartres C. and Evans R. 2000. Paleochannels near West Wyalong, New South Wales: a case study in delineation and modelling using aeromagnetics. Exploration Geophysics 31, 1–7.

Macnae J. C., King A., Stolz N., Osmakoff A. and Blaha A. 1998. Fast AEM data processing and inversion. Exploration Geophysics 29, 157–162.

Mann, A.W., Horwitz, R.C., 1979. Groundwater calcrete deposits in Australia: some observations from Western Australia. Journal of the Geological Society of Australia 26:293-303.

Martelet, G., Drufin, S., Tourliere, B., Saby, N., Perrin, J.,Deparis, J., Prognon, F., Jolivet, C., Ratié, C., Arrouays, D., 2013. Regional Regolith Parameter Prediction Using the Proxy of Airborne Gamma Ray Spectrometry.

Vadose Zone Journal 12, 4. doi:10.2136/vzj2013.01.0003

Martz, L.W., de Jong, E., 1990. Natural radionuclides in the soils of a small agricultural basin in the Canadian Prairies and their association with topography, soil properties and erosion. Catena 17, 85–96.

Massart, D.L., Vandeginste, B.G.M., Deming, S.M., Michotte, Y., Kaufman, L., 1996. Chemometrics: a Textbook. Elsevier, Amsterdam.

McBratney, A.B.; M.L. Mendonça Santos, B. Minasny., 2003. "On digital soil mapping". Geoderma, 117 (1–2), 3–52. doi:10.1016/S0016-7061(03)00223-4.

McDonald, R,C., Isbell, R.F., Speight, J.G., Walker, J., Hopkins, M., 1990. Australian Soil and Land Survey Field Handbook, 2nd edn. Inkarta Press, Melbourne.

McKenzie, N.J., Austin, M.P., 1993. A quantitative Australian approach to medium and small scale surveys based on soil stratigraphy and environmental correlation. Geoderma 57, 329-355.

McKenzie, N., Gallant, J., 2007. Chapter 24. Digital Soil Mapping with improved environmental predictors and models of pedogenesis. In: P. Lagacherie, A.B. McBratney and M. Voltz (Eds.), Digital Soil Mapping, an introductory perspective. Developments in Soil Science, 31. Elsevier, Amsterdam, 327–352

McKenzie, N.J., Grundy, M, J., 2008. Approaches to land resource survey, In Guidelines for Surveying Soil and Land Resources (Ed) McKenzie, N,J., Grundy, M,J., Webster, R and Ringrose-Voase, A,J.CSIRO Publishing, Collingwood, Victoria Australia.

McKenzie, N., Isbell, R., Jacquier, D., Brown, K., 2004. Australian Soils and Landscapes: An Illustrated Compendium, CSIRO Publishing, Australia, ISBN: 9780643069589.

McKenzie, N., Jacquier, D.W., Isbell, R., Brown, K., 2004. Australian Soils and Landscapes — an Illustrated Compendium. CSIRO Publishing, Melbourne.

McKenzie, N.J., Jacquier, D., Isbell, R., Katharine, B., 2004. Australian soils and landscapes: An illustrated compendium, CSIRO publishing, Collingwood, Victoria.

McKenzie, N.J., Ryan, P.J., 1999. Spatial prediction of soil properties using environmental correlation. Geoderma, 89, 67-94.

McPherson, A.A., 2011. Development of the Australian National Regolith Site Classification Map, Geoscience Australia, Canberra, Record. down load at: https://www.ga.gov.au/ products/servlet/controller?event=GEOCAT_DETAILS&catno=65240.

McQueen, K.G., Hill, S.M., Foster, K.A. 1999. The nature and distribution of regolith carbonate accumulations in southeastern Australia and their potential as a sampling medium in geochemical exploration. Journal of Geochemical Exploration 67, 67-82.

McQueen K.G., 2006. Calcrete geochemistry in the Cobar-Girilambone region, New South Wales. Cooperative Research Centre for Landscape Environments and Mineral Exploration Open File Report 200, 27pp.

Melton, M.A., 1965. Debris-covered hillslopes of the southern Arizona desert — consideration of their stability and sediment contribution. Journal of Geology 73, 715–729.

Mernagh, T., Miezitis, Y., 2008. A review of the geochemical processes controlling the distribution of thorium in the Earth's crust and Australia's thorium resources. Geoscience Australia, Record 2008/05, Canberra.

Merrill, G.P., 1897. A treatise on rocks, rock-weathering and Soils, Macmillan, New York.

Miller, C.R., James, N.P., Bone, Y., 2012. Prolonged carbonate diagenesis under an evolving late Cenozoic climate; Nullarbor Plain, southern Australia, Sedimentary Geology, 261-262, 15 June 2012, 33-49.

Milne, G., 1935. Some suggested units of classification and mapping particularly for East African soils. Soil Research 4,183-198.

Milnes, A.R., Bourman, R.P., Northcote, K.H., 1985. Field relationships of ferricretes and weathered zones in southern South Australia: A contribution to 'laterite' studies in Australia. Australian Journal of Soil Resources 23, 441–465.

Milnes, A.R., Hutton, J.T.,1983. Calcretes in Australia, in: Soils: An Australian viewpoint, Division of Soils, CSIRO, Melbourne, 119-162.

Minasny, B., McBratney, A.B., 1999. A rudimentary mechanistic model for soil production and landscape development. Geoderma 90, 3–21.

Minasny, B., McBratney, A.B., 2002. The neuro-m method for fitting neural network parametric pedotransfer functions. Soil Science Society of America Journal. 66, 352-361.

Minasny , B., McBratney, A.B., McKenzie, N.J and Grundy, M.J., 2008. Predicting soil properties using pedotransfer functions and environment correlation, In Guidelines for surveying soil and land resources, 2nd edition, (Editors: McKenzie, Grundy, Webster and Ringrose-Vose) CSIRO Publishing, Melbourne.

Minasny, B., McBratney, A.B., Whelan, B.M., 2005. VESPER Version 1.62. Australian Centre for Precision Agriculture, McMillan Building A05, The University of Sydney, NSW 2006 (http://www.usyd.edu.au/su/agric/acpa).

Minasny, B. and McBratney, A. B. 2010. Methodologies for Global Soil Mapping. In: BOETTINGER, J., HOWELL, D., MOORE, A., HARTEMINK, A. and KIENAST-BROWN, S. (eds.) Digital Soil Mapping. Springer Netherlands.

Minty, B.R.S., 1997. Fundamentals of airborne gamma-ray spectrometry. AGSO Journal of Australian Geology and Geophysics 17, 39–50.

Minty, B., Franklin, R., Milligan, P., Richardson, L.M., Wilford, J., 2009. New radiometric map of Australia. Exploration Geophysics 40 (4), 325–333.

Mirams, R. C. 1964. Burra 1:250 000 geological map sheet SI 54–5. Geological Survey of South Australia, Adelaide.

Monger, H.C., Daugherty, L.A., Lindemann, W.C., Liddell, C.M., 1991. Microbial precipitation of pedogenic calcite. Geology 19(10), 997-1000.

Monger, H.C., Gallegos, R.A., 2000. Biotic and abiotic processes and rates of pedogenic carbonate accumulation in the southwestern United States—relationship to atmospheric CO2 sequestration, in: Lal, R., Kimble, J.M., Eswaran, H., Stewart, B.A. (Eds.), Global Climate Change and Pedogenic Carbonates, CRC Press, Boca Raton, FL., pp. 273-289.

Moore, J.D., Gessler, P.E., Nielsen, G.A., Peterson, G.A., 1993. Soil attribute prediction using terrain analysis. Soil Science Society of America Journal, 57, 443-452.

Moore, D.M., Lees, B.G., Davey, S.M., 1991. A new method for predicting vegetation distributions using decision tree analysis in a geographic information system. Environmental Management 15, 59-71.

Mulcahy, M.J., 1967. Landscapes, laterites and soils in southwestern Australia. In Jennings, J.N and Mabbutt, J.A. (eds) Landform Studies from Australia and New Guinea. Australian National University press. Canberra, 211-230.

Munday, T., 2004. Application of Airborne Geophysical Techniques to Salinity Issues in the Riverland, South Australia. DWLBC Report 2004/ 3. 71p.

Munday T. J., Hill A., Wilson T., Hopkins B., Telfer A., White G., Green A., 2004. Combining geology and geophysics to develop a hydrogeologic framework for salt interception in the Loxton Sands aquifer, central Murray Basin, Australia. CRC LEME Open-file Report 180.

Naiman, Z., Quade, J., Patchett, P.J., 2000. Isotopic evidence for eolian recycling of pedogenic carbonate and variations in carbonate dust sources throughout the Southwest United States. Geochimica et Cosmochimica Acta 64 (18), 3099-3109.

National Committee on Soil and Terrain, 2009. Australian soil and land survey field handbook. Australian Soil and Land Survey Handbook Series; No. 1, 3rd ed. CSIRO Publishing, Collingwood, Victoria.

Nesbitt, H.W., Young, G.M., 1982. Early Proterozoic climates and plate motions inferred from major element chemistry of lutites. Nature 299, 715–717.

Northcote, K.H., Beckmann, G.G., Bettenay, E., Churchward, H.M., Van Dijk, D.C., Dimmock, G.M., Hubble, G.D., Isbell, R.F., McArthur, W.M., Murtha, G.G., Nicolls, K.D., Paton, T.R., Thompson, C.H., Webb, A.A., Wright, M.J., 1960-1968. Atlas of Australian Soils, Sheets 1 to 10. With explanatory data (CSIRO Aust. and Melbourne University Press: Melbourne).

Odeh, I.O.A., McBratney, A.B., Chittleborough, D.J., 1994. Spatial prediction of soil properties from landform attributes derived from a digital elevation model. Geoderma 63, 197-214.

Olley J. M., Pietsch T. and Roberts R. G. 2004. Optical dating of Holocene sediments from a variety of geomorphic settings using single grains of quartz. Geomorphology 60, 337–358.

Ollier, C.D., 1965. Some features of granitic weathering in Australia. Zeit f. Geomorph. 9, 285–304.

Ollier, C., 1984, Weathering. (Ed. K.M Clayton), 2nd ed. Longman, London.

Ollier, C., and Pain, C., 1996. Regolith, Soils and Landforms, John Wiley and Sons, Chichester.

Ollier, C.D., 2001. Evolution of the Australian landscape. Mar. Freshwater Res. 52, 13–23. Ollier, C.D., Pain, C.F., 1996. Regolith, Soils and Landforms. John Wiley and Sons Ltd, Chichester.

Pain, C, F., 2001. Regolith description and mapping, In, Regolith geology and geomorphology (Ed: Taylor, G and Eggleton, R.A), John Wiley and Sons; Chichester.

Pain C F., 2008. Regolith description and mapping, In; Regolith Science. Scott and Pain (ed), CSIRO publishing, Victoria.

References

Pain, C., Chan, R., Craig, M., Gibson, D., Kilgour, P., Wilford, J., 2001. RTMAP regolith database field book and users guide. CRC LEME Report 138.

Pain, C., Kilgour P., 2003. Regolith mapping – a discussion. In Advances in regolith (ED) Ian Roach, Proceedings of the CRC LEME Regional regolith Symposia, Perth.

Pain, C.F., Ollier, C.D., 1996. Regolith stratigraphy: principles and problems. AGSO Journal of Australian Geology and Geophysics 16 (3), 197–202.

Pain, C.F., Pillans, B.J., Roach, I.C., Worrall, L., Wilford, J.R., 2012. Old, flat and red—Australia's distinctive landscape, In Shaping a Nation - A Geology of Australia, Edited by Richard Blewett, ANU press, Canberra

Parker, A., 1970. An index of weathering for silicate rocks. Geological Magazine 107, 501–504.

Peverill, K.I., Sparrow, L.A., Reuter, D.J., (eds) 2001. Soil analysis an interpretation manual, CSIRO publishing, Collingwood, Victoria. ISBN: 064306376 5

Phillips, J.D., Marion, D.A., Luckow, K., Adams, K.R., 2005. Nonequilibrium regolith thickness in the Ouachita Mountains. Journal of Geology 113, 325–340.

Pickup, G., Marks, A., 2000. Identifying large scale erosion and deposition processes from airborne gamma radiometrics and digital elevation models in a weathered landscape. Earth Processes and Landforms 25, 535–557.

Pillans, B., 2001. Regolith through time, In: Regolith geology and geomorphology (Ed: Taylor, G and Eggleton, R.A), John Wiley and Sons; Chichester.

Pillans, B., 2005. Geochronology of the Australian regolith. In: Anand, R.R., de Broekert, P. (Eds.), Regolith-Landscape Evolution Across Australia. CRC LEME, Perth, 41–61.

Preiss, W.V., (compiler), 1987. The Adelaide Geosyncline–Late Proterozoic stratigraphy, sedimentation, palaeontology and tectonics. South Australian Geological Survey, Bulletin, 53.

Prescott, J. A., 1948. A climatic index for the leaching factor in soil formation. Journal of Soil Science. 1, 9-19.

Price, J.R., Velbel, M.A., 2003. Chemical weathering indices applied to weathering profiles developed on heterogeneous felsic metamorphic parent rocks. Chemical Geology 202, 3–4, 397–416.

Quade, J., Chivas, A.R., McCulloch, M.T., 1995. Strontium and carbon isotope tracers and the origins of soil carbonate in South Australia and Victoria. Palaeogeography, Palaeoclimatology, Palaeoecology 113, 103-117.

Raison R. J. 1979. Modification of the soil environment by vegetation fires, with particular reference to nitrogen transformations: a review. Plant and Soil 51, 73–108.

Rawlins, B.G., Lark, R.M., Webster, R., 2007. Understanding airborne radiometric survey signals across part of eastern England. Earth Surface Processes and Landforms 32 (10), 1503–1515.

Rawlins, B.G., Marchant, B.P., Smyth, D., Scheib, C., Lark, R.M., Jordan, C., 2009. Airborne radiometric survey data and a DTM as covariates for regional scale mapping of soil organic carbon across Northern Ireland. European Journal of Soil Science 60 (1), 44–54.

Raymond, O.L. (editor), 2012. Surface Geology of Australia data package 2012 edition [Digital Dataset] Geoscience Australia, Commonwealth of Australia, Canberra. Available at: https://www.ga.gov.au/products/servlet/controller?event=GEOCAT_DETAILS&catno=74855

Reeves, J. B., 2010. Near-versus mid-infrared diffuse reflectance spectroscopy for soil analysis emphasizing carbon and laboratory versus on-site analysis: Where are we and what needs to be done?, Geoderma, 158, 1-2, 3-14.

Renard, K.G., Laflen, J.M., Foster, G.R., KcCool, D.K., 1994. The Revised Universal Soil Loss Equation, In: Lal, R. (Ed.), Soil Erosion Research Methods, Second edition. Soil and Water Conservation Society and St Lucie Press, 105–124.

Roberts, L., Wilford, J., Field, J., Greene, R., 2002. High resolution ground based gamma ray spectrometry and electromagnetics to assess regolith properties, Boorowa, NSW. In: Roach, I. (Ed.), Regolith and Landscapes in Eastern Australia, 136. CRC LEME.

Robertson, I.D.M., Craig, M.A., Anand, R.R., 2006. Atlas of regolith materials of the Northern Territory. Cooperative Research Centre for Landscape Environments and Mineral Exploration, Perth, Australia Open File Report 196.

Ryan, P.J., McKenzie, N.J., O'Connell, D., Loughhead, A.N., Leppert, P.M., Jacquier, D., Ashton, L.U., 2000. Integrating forest soils information across scales: spatial prediction of soil properties under Australian forests. Forest Ecology and Management 138, 139–157.

Sadlier, S.B., Gilkes, R.J., 1976. Development of bauxite in relation to parent material near Jarrahdale, Western Australia. J. Geol. Soc. Aust. 23, 333–344.

References

Sandiford, M., Quigley, M., de Broekert, P., Jakica, S., 2009. Tectonic framework for the Cainozoic cratonic basins of Australia. Australian Journal of Earth Sciences 56, S5–S18.

Schaetzl, R.J., Anderson, S., 2005. Soils: Genesis and Geomorphology. Cambridge University Press, United Kingdom.

Scheepers, R., Rozendaal, A., 1993. Redistribution and fractionation of U, Th and rare-earth elements during weathering of subalkaline granites in SW Cape Province, South Africa. Journal of African Earth Sciences. 17, 41–50.

Schlesinger, W. H., Pilmanis, A. M. 1998. Plant-soil interactions in deserts. Biogeochemistry, 42(1-2), 169-187.

Schoeneberger, P.J., Wysocki, D.A., Benham, E.C., Broderson, W.D., 2002. Fieldbook for Describing and Sampling Soils, 2nd ed. Natural Resources Conservation Service, National Soil Survey Center, Lincoln, NE, USA. environmental variables in an anthropogenic landscape, a case study in the Western Ghats of Kerala, India. Catena 79 (1), 27–38.

Selby, M.J., 1982. Hillslope Materials and Processes. Oxford University Press, Oxford. Stewart, A.J., Blake, D.H., Ollie, C.D., 1986. Cambrian river terraces and ridgetops in Central Australia: oldest persisting landforms? Science 233, 753–761.

Shafique, M., van der Meijde, M., Rossiter, D.G., 2011. Geophysical and remote sensing-based approach to model regolith thickness in a data-sparse environment. Catena 87, 11–19.

Skidmore, A.K., Watford, F., Luckananurug, P., Ryan, P.J., 1996. An operational GIS expert system for mapping forest soils. Photogrammetric engineering and remote Sensing 62, 501-511.

Soil and Land Information, 2002. Atlas of Key Soil and Landscape Attributes of the Agricultural Districts of South Australia. SaLI Group, The Department of Water, Land and Biodiversity Conservation, Adelaide, South Australia, Adelaide, Australia.

Specht, R.L., 1981. Major vegetation formations in Australia. In: Keast, A. ed. Ecological Biogeography of Australia. The Hague, Dr. W. Junk bv Publishers. 163 - 297.

Stephens, C.G., 1946. Pedogenesis following the dissection of lateritic regions in southern Australia. Council for Scientific and Industrial Research, Bull. No. 206.

Stephens C. G., Herriot R. I., Downes R. G., Langford-Smith T. 1945. A soil, land-use and erosion survey of part of Country Victoria, South Australia, Council for Scientific and Industrial Research Bulletin 188.

Stevens, N.C., 1965. The Volcanic rocks of the southern part of the main range, SE Queensland. Proceeding of the Royal Society of Queensland 77, 37-52.

Stolz J. F., Chang S-B. R., Kirschvink, J. L., 1986. Magnetotactic bacteria and single-domain magnetite in hemipelagic sediments. Nature 321, 849–951.

Summerfield, M.A., 1991. Global Geomorphology: an Introduction to the Study of Landforms. Longman Wiley, London, p. 537.

Taboada, T., Cortizas, A.M., Garcia, C., Garcia-Rodeja, E., 2006. Uranium and thorium in weathering and pedogenetic profiles developed on granitic rocks from NW Spain. Science of the Total Environment, 356, 192–206.

Tan, P., Lymburner, L., Thankappan, M., Lewis, A., 2009. 'Mapping Broadacre Cropping Practices Using Modis Time Series: Harnessing the Data Explosion', in International Workshop on Impact of Climate Change on Agriculture, Ahmedabad, India.

Taylor, G., Eggleton, R.A., 2001. Regolith Geology and Geomorphology: Nature and Process. John Wiley and Sons.

Taylor, G., Eggleton, R.A., Foster, L.D., Tilley, D.B., Le Gleuher, M., Morgan, C., 2008. Nature of the Weipa Bauxite deposits, northern Australia. Australian Journal of Earth Sciences 55, S45–S70.

Taylor, G., Roach, I.C., 2005. Monaro Region, New South Wales. In: Anand, R.R. and Broekert, P. de, (Eds) Regolith Landscape Evolution Across Australia, A Compilation of Regolith Landscape Case Studies With Regolith Landscape Evolution Models. CRC LEME, ISBN 1 921039302, Perth.

Taylor, M.J., Smettem, K., Pracilio, G., Verboom, W.H., 2002. Investigation of the relationships between soil properties and high resolution radiometrics, central eastern Wheat belt, Western Australia. Exploration Geophysics 33, 95–102.

Tesfa, K.T., Tarboton, D.G., Chandler, D.G., McNamara, J.P., 2009. Modeling soil depth from topographic and land cover attributes. Water Resources Research 45.

Thomas M., Fitzpatrick R. W., Cannon M. E. and McThompson, J., 2007. Soil patterns along a hillslope in the Belalie Valley, Midnorth, South Australia. CSIRO Land and Water Science Report 33/07. Online 5http://www.clw.csiro.au/publications/ science/2007/4

References

Thomas, M., Fitzpatrick, R.W., Heinson, G.S., 2009. An expert system to predict intricate saline—sodic subsoil patterns in upland South Australia. Australian Journal of Soil Research 47, 602–612.

Tokarev, V., Sandiford, M., Gostin, V.A., 1998. Landscape evolution in the Mt Lofty Ranges: implications for regolith development. In: Taylor, G., Pain, C. (Eds.), Regolith '98, New Approaches to an Old Continent, CRC LEME, 3rd Austustralian. Regolith Conference, Kalgoorlie, WA, Proceedings, 127–134.

Tsykin, E.N., Slessar, G.C., 1985. Estimation of salt storage in the deep lateritic soils of the Darling Plateau, Western Australia. Australian. Journal of Soil Research. 23, 533–541.

Turkington, A., Phillips, J., Campbell, S., 2005. Weathering and landscape evolution, In Weathering and Landscape Evolution, Proceedings of the 35th Binghamton Symposium in Geomorphology (Ed: A Turkington, J Phillipos and S Campbell), Special issue, Geomorphology 67.

Twidale, C.R., 1976. Geomorphological evolution. In: Twidale, C.R., Tyler, M.J., Webb, B.P. (Eds.), Natural History of the Adelaide Region. Royal Society of South Australia, 43–59.

Viscarra Rossel, R. A., 2011. Fine-resolution multiscale mapping of clay minerals in Australian soils measured with near infrared spectra Journal of Geophysical Research: Earth Surface, Volume 116, Issue F4.

Viscarra Rossel, R. A., Bui, E. N., de Caritat, P., and McKenzie, N. J., 2010. Mapping iron oxides and the color of Australian soil using visible–near-infrared reflectance spectra, Journal of Geophysical. Research., 115, F04031.

Voltz, M., Webster, R., 1990. A comparison of kriging, cubic splines and classification for predicting soil properties from sample information. Journal of Soil Science 41, 473–490.

Walker P. H., Coventry, R. J., 1976. Soil profile development in some alluvial deposits of eastern New South Wales. Australian Journal of Soil Research 14, 305–317.

Walker, G, Gilfedder, M, Evans, R, Dyson P., Stuaffacher, M., 2003. Groundwater Flow Systems Framework – Essential Tools for Planning Salinity Management, MDBC publication ISBN 1

Wedepohl, K.H. (Ed.), 1969. Handbook of Geochemistry, Vol II-5. Springer Verlag, Berlin.

Webster, R., Oliver, M.A., 1990. Statistical Methods in Soil and Land Resource Survey. Oxford Univ. Press, Oxford.

Webster, R., Oliver, M.A., 2001. Geostatistics for Environmental Scientists. John Wiley and Sons, Chichester, England.

Wilford, J.R., 1995. Airborne gamma-ray spectrometry as a tool for assessing relative landscape activity and weathering development of regolith, including soils. AGSO Research Newsletter 22, 12–14.

Wilford, J. 1999. Scientific visualisation and 3D modelling applications for mineral exploration and environmental management. AGSO Research Newsletter 31.

Wilford, J., 2002. Regolith-landform characteristics, evolution and implications for exploration over the Selwyn region, Mt Isa. Open file report 131, CRC LEME, Perth.

Wilford, J. R., 2004a. Regolith-landforms and salt stores in the Angas-Bremer Hills. CRC LEME Open File Report 177. CRC LEME 100pp.

Wilford J.R., 2004b. 3D regolith architecture of the Jamestown area—implications for salinity. CRC LEME Open-File Report 178, Perth.

Wilford, J., 2012. A weathering intensity index for the Australian continent using airborne gamma-ray spectrometry and digital terrain analysis. Geoderma, 183-184, 124-142.

Wilford, J. R., Bierworth, P. N. and Craig, M. A. 1997. Application of airborne gamma-ray spectrometry in soil/regolith mapping and applied geomorphology. AGSO Journal of Australian Geology and Geophysics 17(2), 201–216.

Wilford, J., Butrovski, D., 2000. Customised regolith maps incorporate hydrologic modelled attributes for geochemical exploration, AGSO Research Newsletter.

Wilford, J., Minty, B., 2007. The use of airborne gamma-ray imagery for mapping soils and understanding landscape processes. In: Lagacherie, P., McBratney, A.B., Voltz, M. (Eds.), Digital Soil Mapping an Introductory Perspective. : Developments in Soil Science, 31. Elsevier.

Wilford, J., Smitt, C., Cox, J., Walker, G., submitted for publication. Relationships between regolith thickness, rainfall and salt mobilisation in the central Mt Lofty Ranges, South Australia with implications for salinity management. Exploration Geophysics.

Wilkinson, M.T., Richards, P.J., Humphreys, G.S., 2009. Breaking ground: pedological, geological, and ecological implications of soil bioturbation. Earth Science Reviews 97 (1–4), 257–272.

Williams, M., Prescott J. R., Adamson D., Cock B., Walker K., Gell, P., 2001. The enigma of a late Pleistocene wetland in the Flinders Ranges, South Australia. Quaternary International 83–85, 129–144.

Wilson, J.P., Gallant, J.C., 2000. Digital terrain analysis. In: Wilson, J.P., Gallant, J.C. (Eds.), Terrain Analysis: Principles and Applications. John Wiley and Sons Inc., New York.

Woolnough, W.G., 1927. The duricrust of Australia. Journal of the Royal Society of New South Wales 61, 24–53.

Worrall, L., Green, A., Munday, T., 1998. Beyond bump finding—airborne electromagnetics for mineral exploration in regolith dominated terrains. Exploration Geophysics 29, 199–203.

Wright, M.J. 1984. Red-brown hardpans and associated soils in Transactions of The Royal Society of South Australia. 107, 252-254.

Xu, T., Hutchinson, M., 2011. ANUCLIM Version 6.1 User Guide. Fenner School of Environment and Society, Australian National University, Canberra. Available at: http://fennerschool.anu.edu.au/files/panel/447/anuclim61_user_guide.pdf

Yoshida, H., Roberts R. G., Olley J. M., Laslett G. M., Galbraith, R. F., 2000. Extending the age range of optical dating using single 'supergrains' of quartz. Radiation Measurements, 32, 439–446.

Appendices

Appendix A Related papers

A.1 National datasets support natural resource management

John Wilford, Allan Nicholson[1] and Greg Summerell[1]

[1]NSW Department of the environment

An understanding of hydrological processes is vital when addressing issues such as water availability, water quality and ecological management, particularly when groundwater-dependent ecosystems are involved. Consideration of water sustainability within the context of climate change, population growth and socioeconomic development requires holistic and more sophisticated water management approaches. It is against this background that a Hydrogeological-Landscape framework for more effective management of natural resources has been developed. The frame work is used to divide the landscape into areas that have similar hydrological characteristics. The use of the term *Hydrogeological* highlights the importance of geology to hydrologic processes, whereas the use of the term *Landscape* highlights the importance of landform sand regolith (or the weathered material above bedrock).

A.1.1 The Hydrogeological-Landscape framework

The Hydrogeological-Landscape framework (HGL) builds on the groundwater flow system (Coram 1998; Walker et al 2003) framework that was developed approximately 10 years ago– primarily to assist in the management of groundwater salinity. The Hydrogeological-Landscape framework is a broad, all encompassing entity which accommodates all forms of water flow (surface, interflow and groundwater flow). Hydrogeological-Landscape Units

(HGLU) integrate information on lithology, bedrock structure, regolith (including soils), landforms, climate (including rainfall, seasonality, evaporation) and vegetation (figure 1). These components all influence, to greater or lesser degrees, the recharge, transmission, storage and discharge characteristics of a particular hydrological system. The HGL concept has been developed for upland erosional landscapes (such as where hill slopes have a major control on water movement) as documented here; however, it also has the potential to be applied to depositional settings.

Hydrogeological-Landscape frameworks are compiled over a range of spatial scales ranging from landscape facets that may describe, for example, local changes along a hill slope through to regional systems spanning hundreds of kilometres. This multi-scale approach addresses the fact that both hydrologic systems and management strategies are intrinsically linked across different scales. For example, most local flow systems are nested within larger ones and most local land management strategies ideally need to be integrated into regional programs and goals. Different datasets or criteria are used in defining the HGL units across these different spatial scales. At the broadest scale major bedrock types, structural and architectural elements (such as a flat lying sedimentary unit or a fractured granite), landform and climatic characteristics are used. Whereas at local scales regolith/soil type and thickness, morphology (hill slope: steepness, curvature and length) and lithostructure (for example, lithologies, fabrics and structures) are used. The latter components assert local controls on water movement and storage and, therefore, provide spatially-explicit information on hydrological processes to support farm-scale management strategies.
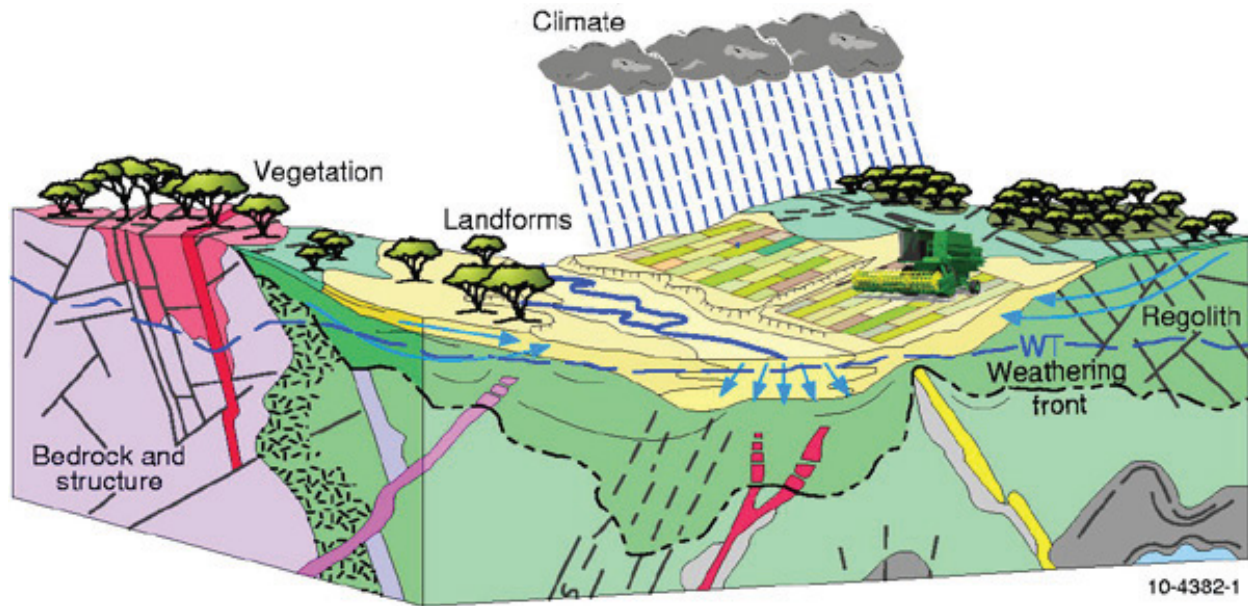
Figure 1. Factors influencing surface and groundwater movement and storage.

A.1.1.1 Key elements of the framework

Some of the key elements in building a HGL framework included bedrock type, regolith and landform. Geological attributes are derived from state and national scale geological maps (*AusGeo News 93*), whereas regolith and landform components are derived mainly from modelling of gamma-ray radioelement imagery and digital terrain analysis. Emissions of gamma-rays from Earth's surface will largely reflect the geochemistry of bedrock as well as weathering processes and regolith materials. The gamma-ray imagery together with terrain relief has been used to predict the degree to which the landscape has been weathered (Wilford 2010). This approach enables delineation of regolith and bedrock-controlled hydrological systems which typically have very different porosity and permeability characteristics (figure 2). The gamma-ray data uses the new radioelement map of Australia (*AusGeo News 92*) which enables quantitative assessment of the distribution of potassium, equivalent thorium and equivalent uranium in exposed bedrock and regolith. Landforms, slope facets, valley constrictions and seepage zones are derived from a range of digital terrain process techniques including topographic wetness index (TWI), the UPNESS index from the Fuzzy Landscape Analysis Geographic Information System (FLAG) model (Summerell et al 2005) and a multi

resolution index of valley bottom flatness (MRVBF: Gallant and Dowling 2003).

A.1.1.2 Central West Catchment HGL map

The Hydrogeological-Landscape map of the Central West Catchment in New South Wales (figure 3) illustrates how this new framework is providing key baseline information for managing water quality in the catchment. The Central West Catchment, which is about 1.5 million hectares in area, is a north-west draining subdivision of the Darling

River system and includes the Macquarie and Lachlan rivers. The region falls within the jurisdiction of the Central West Catchment Management Authority which provided financial support for the HGL mapping in the catchment. Hydrological characteristics within the Central West Catchment are highly variable, reflecting a diversity of climate, geology, vegetation, landform and regolith. The development of the regolith in the catchment varies greatly and typifies many erosional landscapes in Australia where older and more recent landscapes are juxtaposed. Some of the thickest regolith in the catchment is associated with partially preserved palaeo-surfaces that reflect weathering during the Paleogene or older.
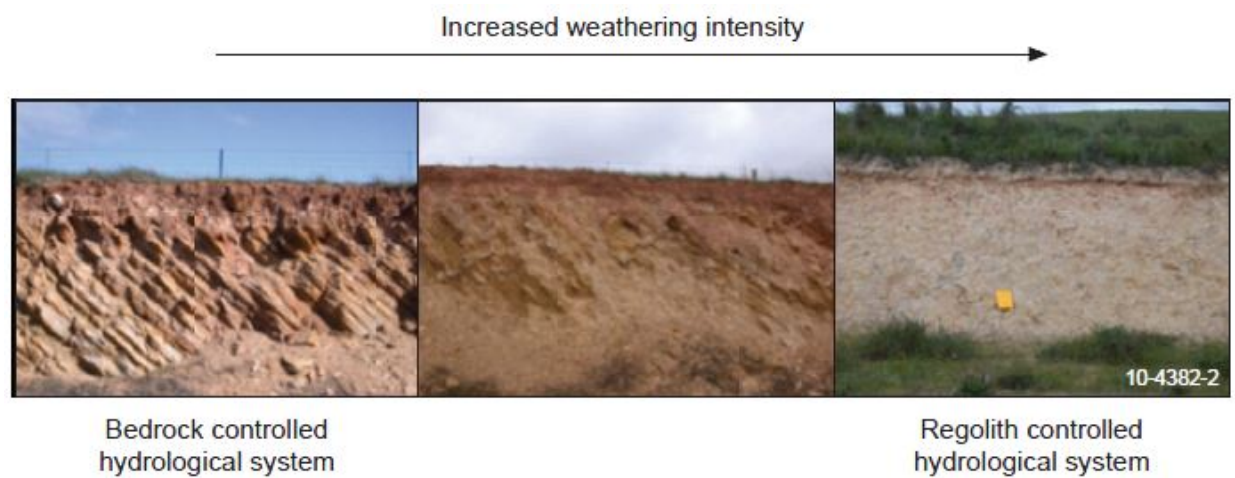
Figure 2. Transition from bedrock to regolith-controlled hydrological systems with increasing weathering intensity from fractured bedrock (left) to residual clay (right).

The palaeo-surfaces are mainly preserved along the south, southwest catchment divide (around Molong, Orange), and in lower parts of the catchment where the rates of erosion are relatively low (around Dubbo and lower reaches of the Cudegong River). Many of these deeply weathered landscapes are associated with sluggish groundwater flow systems, waterlogging and salt scalding. This HGL map delineates areas with similar hydrological characteristics across different landscape scales. The multi-scaled structure of the HGL framework allows for a broad assessment of recharge, discharge and water quality characteristics over the whole catchment, as well as targeting specific sub-catchments for on-ground actions (for example, targeting high salt producing sub-catchments). Each HGL unit is linked to a conceptual hydrological cross section which describes surface, inter-flow and groundwater flow characteristics, as well as management approaches for specific parts of the landscape. Such options might include the location of interception plantings to control recharge for salinity management. The HGL framework can be used to support a range of land use, remedial re-vegetation intervention and engineering strategies for salinity management or other natural resource management activities. The combination of climatic attributes, weathering intensity and geology within the HGL framework enables predictions of salt storage and export within different parts of the catchment. The HGL approach also has applications in the urban environment where it can be used to better understand salinity processes effecting infrastructure and water quality. Although the HGL concept has mainly been used for addressing land and water quality associated with salinity to date, the framework was originally developed to assist with a broad range of natural resource management issues. The New South Wales Department of Environment, Climate Change and Water is currently using or assessing the HGL approach for a number of different natural resource management applications including assessment of:

- soil degradation—sodicity, acidity, acid sulphate soils, and soil erosion
- soil carbon
- surface and groundwater interaction in the landscape
- biodiversity and vegetation
- landscape processes with non-floodplain wetlands such as hanging swamps.

The HGL approach is currently being assessed for application in other catchments in New South Wales and has the potential to be developed as a national framework.
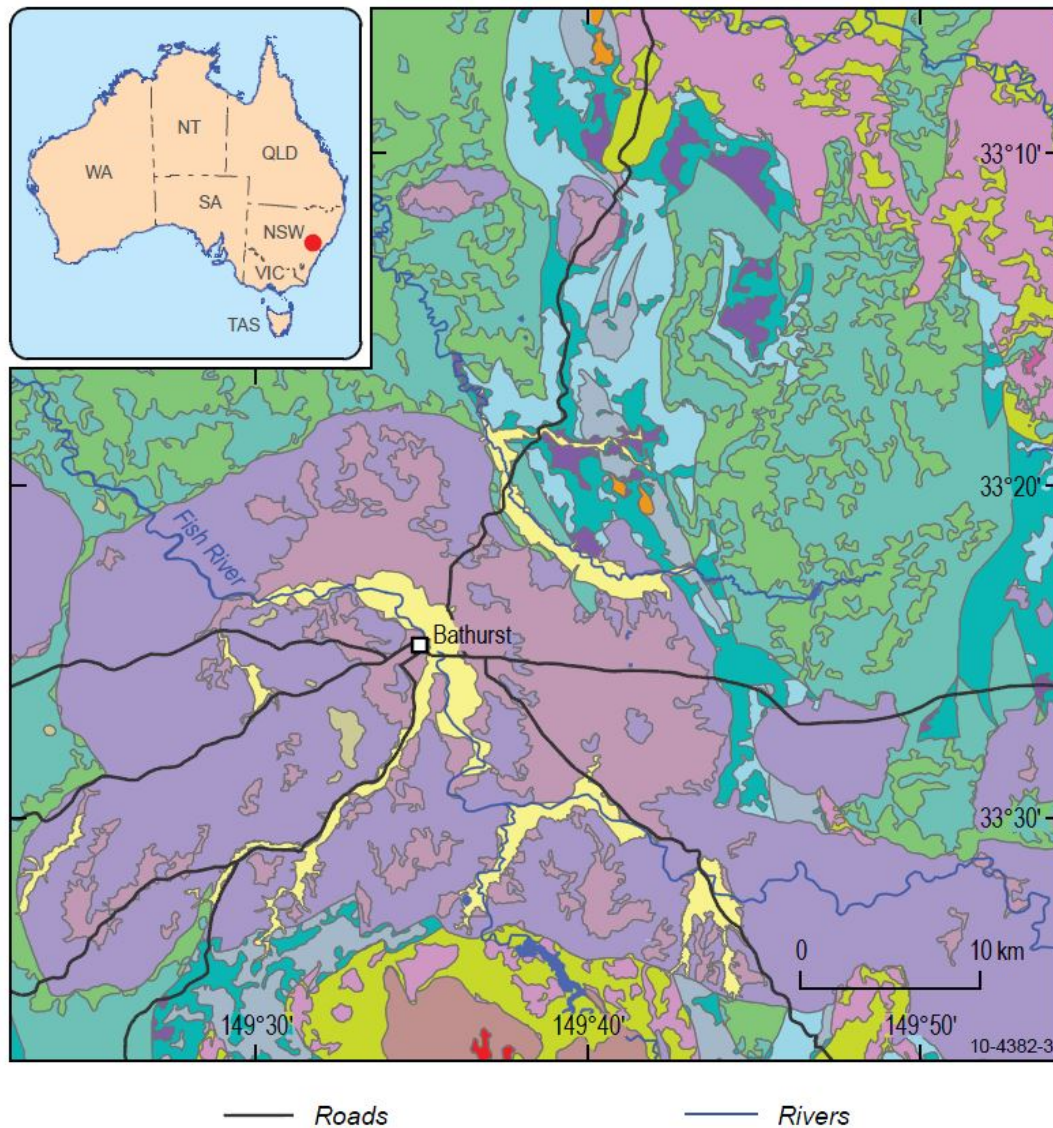
Figure 3. Part of the Central West Catchment Hydrogeological-Landscape (HGL) map. The colours represent areas with similar recharge, transmission, storage and discharge characteristics.

References

Coram, J., 1998. National Classification of Catchments for land and river salinity control: A catalogue of groundwater systems responsible for dryland salinity in Australia. Rural Industries Research and Development Corporation, Canberra. Publication No 98/78.

Walker G, Gilfedder M, Evans R, Dyson P., Stuaffacher, M., 2003. Groundwater Flow Systems Framework–Essential Tools for Planning Salinity Management. Murray Darling Basin Commission.

Summerell, G.K, Vaze J, Tuteja N.K, Grayson, R.B, Beale, G., Dowling, T.I., 2005. Delineating the major landforms of catchments using an objective hydrological terrain analysis method. Water Resources Research, 41.

Gallant, J.C., Dowling, T.I., 2003. A multi-resolution index of valley bottom flatness for mapping depositional areas. Water Resources Research, 39(12), 1347–60.

A.2 Weathering intensity map of the Australian continent

John Wilford

Published : AusGeo News March 2011 Issue No. 101

A.2.1 New framework provides new insights into an old continent

A recent study by Geoscience Australia scientists has integrated and modelled geoscientific datasets to generate a weathering intensity index for the Australian continent. Weathering intensity is a fundamental characteristic of the regolith, the often discontinuous and highly variable layer of weathered bedrock and sediments that overlies fresh bedrock at depth. The weathering intensity index has broad applications for a range of natural resource management, environmental, mineral exploration and engineering issues.

Regolith materials cover over 85 per cent of the Australian continent and range from thin, skeletal, soils over slightly weathered bedrock through to very highly weathered bedrock at depths of more than 100 metres below the surface. Important geological and biochemical cycles operate within the regolith zone, including groundwater systems and nutrient cycles involving carbon, nitrogen, oxygen, phosphorus and sulfur, and all elements necessary for life and the biomass. Biogeochemical cycles within this zone are complex and occur across diverse spatial and temporal scales. Northern hemisphere researchers use the term 'critical zone' to describe this life-sustaining environment. Critical zone research involves integrated studies of water with soil, air and biota in the near-surface terrestrial environment (Lin 2010).

http://www.ga.gov.au/servlet/BigObjFileManager?big objid=GA19210

A.2.2 The regolith and weathering intensity

The degree to which the regolith is weathered (or its weathering intensity) is intrinsically linked to the factors involved in soil formation including parent material, climate, topography, biota and time. These processes operate within, and are characteristic of, the critical zone. Typically there is a correlation between the degree of weathering intensity and the degree of soil development. With changes in weathering intensity we see changes in the geochemical and physical features of rocks, ranging from essentially unweathered parent materials through to intensely weathered and leached regolith where all traits of the original protolith (original unweathered rock) is overprinted or lost altogether. These relationships are summarized in figure 1. An example of these changes is the generation of clays; depending on the parent material and climatic conditions, clays are formed by combining alumina, hydroxide ions and silica. Generally, the amount of clay produced increases as weathering intensity increases and two-layer clays transition to more stable one-layer clays. Since clays have an extremely high surface area and are able to retain water, minerals and nutrients, they are favoured sites for chemical reactions and biological activity in soil.
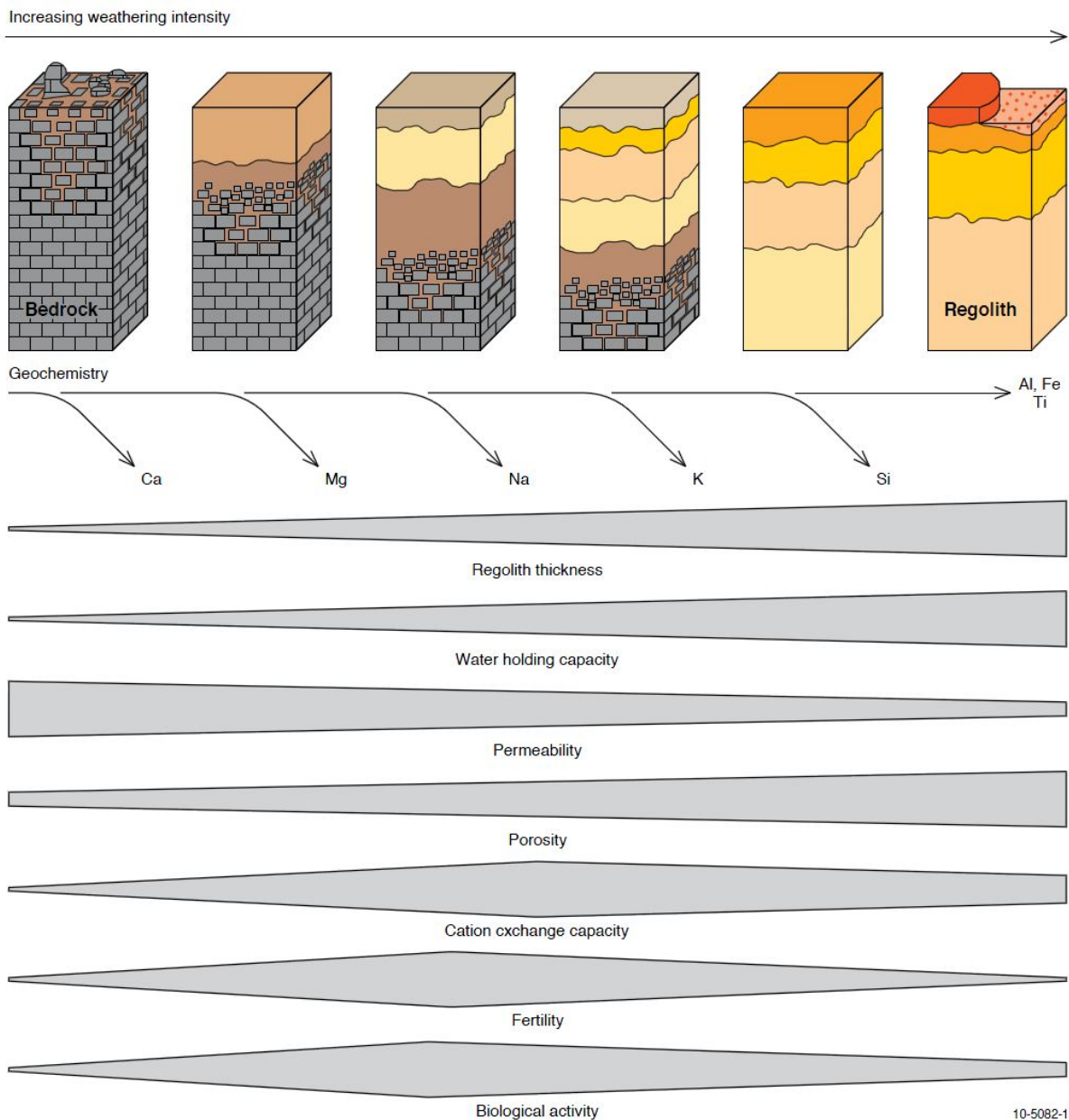
Figure 1. Physical, chemical and biological changes associated with increasing weathering intensity. The trends (shown left to right) are generalised and will change in response to bedrock type and climate. Evolving regolith materials are stylistic and shown in warm hues.

Geochemical indices have been used to quantify and measure the degree of weathering intensity based on the relative proportions of stable versus mobile elements measured from regolith samples that have been collected down a weathering profile. As weathering intensity increases, soluble elements such as potassium, sodium and calcium are lost in solution while the more stable oxides and resistate minerals (such as zircon) are retained in the regolith. However, a limitation of this approach is that they are single-point/single profile measurements and consequently do not inform on spatial weathering variations across a landscape. This limitation has been addressed in the new study which integrates and models two national geoscientific datasets to generate a prediction of weathering intensity across the surface of the continent as a whole.

A.2.3 Building a weathering intensity model for Australia

http://www.ga.gov.au/servlet/BigObjFileManager?big
objid=GA19216

The national weathering intensity prediction has been developed using airborne gamma-ray spectrometric data from Geoscience Australia's Radiometric Map of Australia and NASA's 90 metre resolution Shuttle Radar Topography Mission (SRTM) elevation data (see Related articles/websites). Airborne gamma-ray spectrometry effectively measures the distribution of three radioelements-potassium, thorium and uranium- in surface bedrock and soil. Most gamma-rays measured at airborne survey heights emanate from the uppermost 30 to 40 centimetres of soil and rock. Variations in concentrations of these radioelements largely relate to changes in the mineralogy and geochemistry of rock and regolith materials. Distributions of these elements change as the primary minerals in the rock weather to secondary components including clay minerals and oxides. Potassium abundance is measured directly as gamma-rays emitted when potassium (^{40}K) decays to argon (^{40}Ar). Uranium and thorium abundances are derived indirectly by measuring gamma-ray emissions associated with the daughter radionuclides bismuth (^{214}Bi) and thallium (^{208}Tl) respectively. As a result they are expressed as equivalent concentrations of uranium and thorium.

The SRTM elevation data provide digital terrain attributes, such as slope or relief, which are useful because they can indicate geomorphic processes. Areas where bedrock outcrops are relatively unweathered can be conspicuous, whilst in other areas, the relative rates of soil removal verses accumulation (that is, denudation balance) can be depicted.

For generation of the national weathering intensity index, the degree of bedrock weathering was assessed using a six-level, field-based classification scheme. Level 1 describes largely unweathered landscapes with a high proportion of fresh bedrock exposed at the surface, whilst level 6 relates to areas where bedrock is completely weathered to secondary minerals (such as clays and oxides: see Figure 2.) Over 300 classified field sites were used to establish regression model relationships between the degree of weathering

intensity and the environmental covariates (the total count of the three radioelements) and a terrain relief image derived from the elevation model data. A forward stepwise regression model approach resulted in a strong correlation (R^2 = .86) between the environmental covariates and weathering intensity observed in the field.


1

2

3

4

5

6

Figure 2. Pictorial representation of regolith profiles for the 6 level classification scheme. 1- largely unweathered landscapes with a high proportion of exposed bedrock, 2- slightly weathered bedrock, 3- moderately weathered bedrock still retaining primary bedrock fabric and structure, 4- moderately to highly weathered bedrock most primary minerals weathered to clays and oxides, 5- highly weathered bedrock most primary bedrock fabric lost and 6- completely weathered bedrock consisting of resistant mineral such as quartz and secondary clays and oxides. http://www.ga.gov.au/servlet/BigObjFileManager?bigobjid =GA19236

Some rock types contain few or no gamma-emitting radioelements, for example, highly siliceous sandstones or ultramafic rock. Where such materials are exposed at the landscape surface the radioelement distribution obviously cannot be used to predict the degree of weathering. In these cases, a terrain attribute such as relief is used to estimate weathering intensity based on the assumption that those

landscapes with high relief are likely to have or maintain thin soil and slightly weathered bedrock. In contrast, low relief landscapes are likely to accumulate and preserve weathered materials (that is, paleo-surfaces) with correspondingly higher weathering intensities. Rocks and sediments with low radioelement emissions are identified using the total count or dose channel of the gamma-ray dataset. For materials emitting low levels of gamma-rays a second regression model has been generated with predictions based solely on terrain relief. The two regression models were subsequently combined to generate the final weathering intensity prediction. Details of the approach are provided in Wilford (2012).

A.2.4 The index and soil property predictions

The weathering intensity index has broad application in understanding weathering and geomorphic processes across a range of spatial and temporal landscape scales. The index can pinpoint highly weathered paleo-surfaces, assess chemical and physical denudation processes, and map the relative rates of regolith formation and its removal through erosion across different landscapes (Figure 3 and 4). Calibration of, or linking the weathering intensity model with observed physical, chemical and biological changes within the regolith has the potential to improve our understanding of biogeochemical processes within the critical zone and across large areas, including soil-water interactions and nutrient cycling. The index also has the potential to be used in combination with other environmental covariates in a range of soil property predictions including texture, chemical composition, depth, fertility, pH, porosity and permeability.

10-5082-3

Weathering Intensity Index

Intensely weathered

Slightly weathered
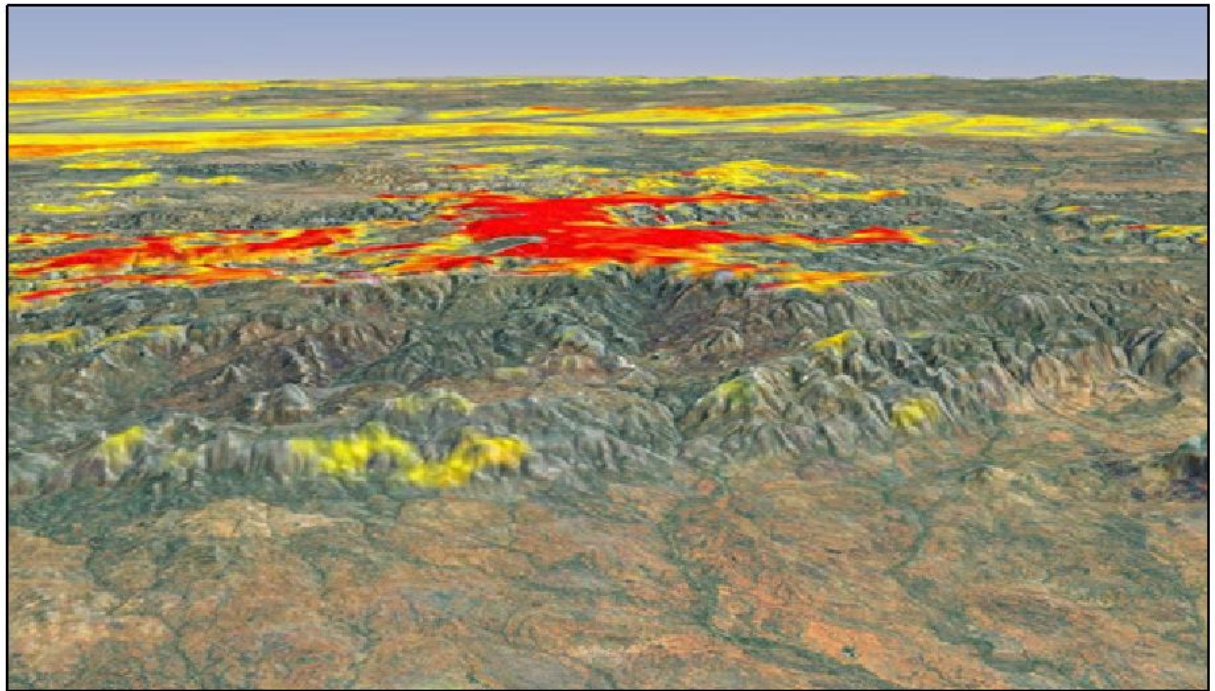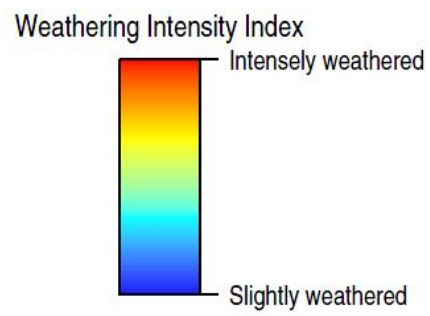
Figure 3. Weathering intensity model from a 3D landscape perspective, showing highly weathered Proterozoic granites and Jurassic sandstones over the southern half of the Mt Isa Inlier. Only moderately to highly weathered bedrock is shown.
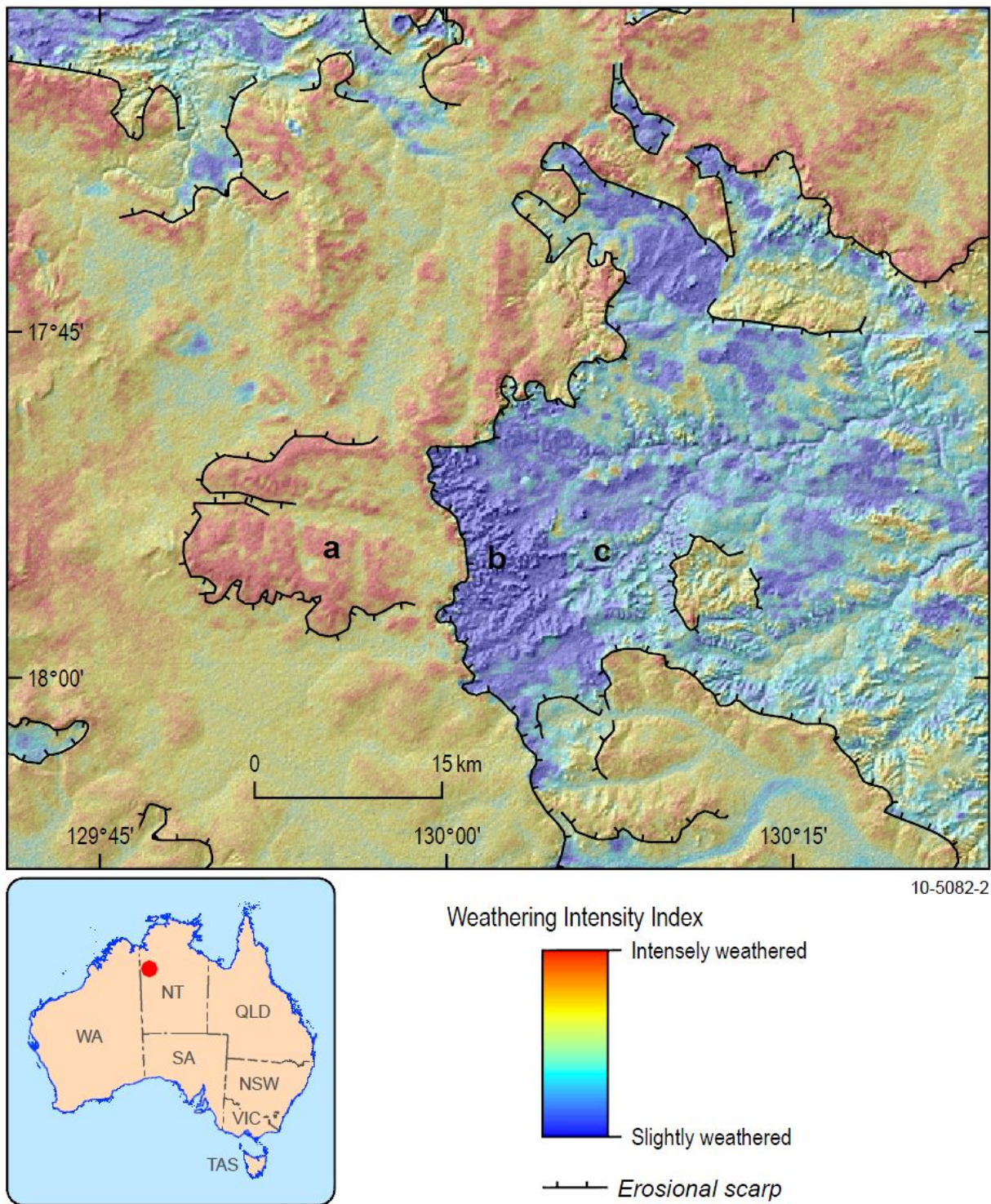
Figure 4. The weathering intensity index has the potential to encapsulate landscape evolution in the context of surface age, weathering, and geomorphic processes, and the associated physical and chemical characteristics of the regolith. In this example landscape denudation is largely controlled through a series of retreating erosional scarps. The oldest surface and more intensely weathered regolith occur above the scarp (a) and least weathered materials are exposed at the base of the scarp (b). Surface age increases down-slope and away of the edge of the scarp (c).

The latter two properties are important for understanding the way in which solutes move through groundwater and the interflow pathways within the regolith and the consequent hydropedological processes and characteristics within different landscapes. The weathering intensity index is currently being integrated with other datasets to develop an improved hydrogeological framework to assist in improved salinity and groundwater management (*AusGeo News* 97). Correlations are expected when using the weathering index for broad-scale ecological studies where biological processes are underpinned by soil fertility and water availability. The index is therefore likely to be useful in mapping and modelling plant types and/or for predicting the distribution of plant communities as well as assisting a more general understanding of the interrelationships between regolith, climate (present and palaeo) and vegetation at local, regional or continental scales.

References

Lin H. 2010. Earth's Critical Zone and hydropedology: concepts, characteristics, and advances. Hydrological Earth Systems Science 14. Available at: www.hydrol-earth-syst-sci.net/14/25/2010.

Wilford, J., 2012. A weathering intensity index for the Australian continent using airborne gamma-ray spectrometry and digital terrain analysis. Geoderma, 183-184, 124-142.